AGENCY FOR INTERNATIONAL DEVELOPMENT
WASHINGTON, D. C. 20523

BIBLIOGRAPHIC INPUT SHEET

FOR AID USE ONLY
0128

1. SUBJECT CLASSIFICATION

A. PRIMARY
Agriculture — AP12-0000-0000

B. SECONDARY
Drainage and irrigation

2. TITLE AND SUBTITLE
Flow in sand-bed channels

3. AUTHOR(S)
Mahmood, Khalid

4. DOCUMENT DATE
1971

5. NUMBER OF PAGES
293p.

6. ARC NUMBER
ARC 627.52.M215

7. REFERENCE ORGANIZATION NAME AND ADDRESS
Colo.State

8. SUPPLEMENTARY NOTES (Sponsoring Organization, Publishers, Availability)
(in Water management tech.rpt.no.11)

9. ABSTRACT

10. CONTROL NUMBER
PN-RAA-077

11. PRICE OF DOCUMENT

12. DESCRIPTORS
Alluvial deposits
Flow resistance
Flumes
Kinetic viscosity

13. PROJECT NUMBER

14. CONTRACT NUMBER
CSD-2162 Res.

15. TYPE OF DOCUMENT

AID 890-1 (4-74)

FLOW IN SAND-BED CHANNELS

Water Management Technical Report No. 11

by

Khalid Mahmood

Prepared under support of

United States Agency for International Development
Contract No. AID/csd-2162
Water Management Research
in Arid and Sub-Humid Lands of the
Less Developed Countries

Colorado State University

Fort Collins, Colorado

February 1971

CED70-71KM30

Reports published previously in this series are listed below. Copies can be obtained by contacting Mrs. Mary Fox, Engineering Research Center, Colorado State University, Fort Collins, Colorado 80521. The prices noted are effective as long as supplies last. After the supply of reports is exhausted, xerox copies can be provided at 10 cents per page.

No.	Title	Author	No. of Pages	Cost
1	Bibliography with Annotations on Water Diversion, Conveyance, and Application for Irrigation and Drainage, CER69-70KM3, Sept. '69.	K. Mahmood A.G. Mercer E.V. Richardson	165	$3.00
2	Organization of Water Management for Agricultural Production in West Pakistan (a Progress Report) ID70-71-1, May 1970	P.O. Foss J.A. Straayer R. Dildine A. Dwyer R. Schmidt	148	$3.00
3	Dye Dilution Method of Discharge Measurement, CER70-71WSL-EVR47, January 1971	W.S. Liang E.V. Richardson	36	$3.00
4	Water Management in West Pakistan, MISC-T-70-71RFS43 May, 1970	Robert Schmidt	167	$3.00
5	The Economics of Water Use, An Inquiry into the Economic Behavior of Farmers in West Pakistan, MISC-D-70-71DW44 March, 1971	Debebe Worku	176	$3.00
6	Pakistan Government and Administration: A Comprehensive Bibliography, ID70-71GNJ17, March, 1971	Garth N. Jones	114	$3.00
7	The Effect of Data Limitations on the Application of Systems Analysis to Water Resources Planning in Developing Countries, CED70-71LG35 May, 1971	Luis E. Garcia-Martinez	225	$3.00

No.	Title	Author	No. of Pages	Cost
8	The Problem of Under-Irrigation in West Pakistan: Research Studies and Needs, ID 70-71GNJ-RLA19	G. N. Jones R. L. Anderson	53	$3.00
9	Check-Drop-Energy Dissipator Structures in Irrigation Systems, AER 70-71, GVS-VTS-WRW3, May 1971	G. V. Skogerboe V. T. Somorey W. R. Walker	180	$3.00
10	Maximum Water Delivery in Irrigation	J. H. Duke, Jr.	213	$3.00

ABSTRACT

FLOW IN SAND-BED CHANNELS

The flow of water in sand-bed channels has been studied to formulate resistance and transport functions for a given depth, energy gradient and bed-material. The study was based on the flume data obtained at Colorado State University by the U.S. Geological Survey from 1956 to 1961, forty-three canal sections from West Pakistan and 112 river sections from the Rio Grande, New Mexico.

It was found, that in sand-bed channels with general bed-movement the sand boundary always behaves as hydrodynamically rough. For width-depth ratios varying from 3 to 60 the wall-correction applied to the smooth walled sand-bed flumes was found to over-correct so that the resulting characteristics of the resistance to flow became dependent on the width-depth ratio. For these reasons, it is concluded that the flow in sand-bed channels with width-depth ratios greater than 3 should be analysed on the basis of the average depth without using the wall correction and without applying a smooth to rough transition function. In plane sand-bed flows the grain roughness is related to D_{84} of the bed-material.

The sand-size bed-material samples from the Rio Grande and West Pakistan canals exhibit a lognormal particle size distribution in the 10th to 90th percentile size range. This distribution is convenient for the engineering computations of equilibrium flows in sand-bed channels.

In the sand-bed channels, because of the local non-uniformity of flow it is not possible to represent the mean vertical velocity distribution by the observations on a single vertical. A mean velocity profile for sand-bed channels is proposed which has a logarithmic velocity

distribution in the inner layer based on an "effective shear velocity." The value of von Karman's κ in the outer layer of the flow in sand-bed flumes was analysed and it was found to be related to parameters which represent the total sediment load as well as the bed forms.

It was also found that a single resistance function cannot be used to analyse the flow over all the bed configurations. Therefore, separate resistance functions were developed for the upper regime, the lower regime and the transition zone. These functions predict the average velocity in sand-bed flumes and canals within 15 percent for most of the data used.

The bed-material transport function in sand-bed channels was developed in terms of the mean velocity distribution developed in this study and a reference concentration related to the Shields' grain shear parameter and the fall velocity-shear velocity ratio. The prediction of the size distribution of the bed-material transport from this function was found to be in accord with the observed gradation in flumes over the whole range of transport and bed forms.

Khalid Mahmood
Civil Engineering Department
Colorado State University
Fort Collins, Colorado, 80521
February, 1971

ACKNOWLEDGEMENTS

The writer expresses his sincerest gratitude to his major professor, Dr. D. B. Simons, for the stimulating guidance and encouragement provided by him throughout the course of this study. Dr. E. V. Richardson both as a member of the writer's graduate committee and as a personal advisor has been a source of inspiration and counsel. Doctors S. A. Schumm and A. G. Mercer, members of the graduate committee have been helpful throughout the writer's program. The writer expresses his sincerest appreciation for their help.

The original draft of this dissertation was individually reviewed by Dr. Simons and other members of the writer's graduate committee. For the suggestions arising out of these reviews and for the generous gift of their time, the writer wishes to thank all of them.

Thanks are also due to Dr. Fazal H. Chaudhry for reviewing the portions of the original draft concerning the turbulent flow and the two-phase flow and to Mr. Ikram ul Haque, a fellow graduate student for many general discussions relating to this study. Doctors C. F. Nordin, Jr., and R. E. Rathbun of U. S. Geological Survey helped the writer by their discussions at various stages of the analysis and by providing some useful references.

The writer has worked in the West Pakistan Irrigation Department since 1955. This study would not have been possible but for the professional training and the experience gained by the writer during his long association with that department. To the West Pakistan Irrigation Department and to his many friends and fellow engineers in Pakistan, the writer expresses his indebtedness for the encouragement and stimulation provided by them during all these years.

The writer acknowledges the continuous support and motivation he has received from his father. He also acknowledges the indulgence of his wife Safia and his children Zeba, Asma, Kausar and Umar throughout the course of his academic program at Colorado State University.

The financial support for this study was partially provided by the Tipton and Kalmbach Graduate Fellowship at C.S.U. and partially by the United States Agency for International Development. The funds for the computer analysis were mostly provided by the Colorado State University from its unsponsored research grants.

TABLE OF CONTENTS

Chapter		Page
	LIST OF TABLES	x
	LIST OF FIGURES	xii
	LIST OF SYMBOLS	xvi
I	INTRODUCTION	1
II	DATA USED	5
	Laboratory Data	5
	Field Data	7
III	TURBULENT FLOW IN RIGID BOUNDARY CHANNELS	10
	Regions of Velocity Distribution in Turbulent Flows	12
	Turbulence Characteristics of Inner and Outer Layers	15
	Effect of Boundary Roughness on Turbulent Flow	16
	Effect of Roughness Shape and Concentration	17
	Vortices Generated at Roughness Elements	19
	Origin for Velocity Profiles on Rough Boundaries	20
	A Velocity Distribution Equation for Inner Layer in Flow Over Large Roughness Elements	22
IV	TURBULENT FLOW IN SAND-BED CHANNELS	24
	Effect of Bed Forms	24
	Plane-Bed Form in Sand-Bed Channels	26
	Effect of Sediment Suspension	28
	Sediment Suspensions as Two-Phase Flow	32
	Effect of Contact Load	34
	Effect of Bed Porosity	36

TABLE OF CONTENTS - Continued

Chapter		Page
V	PROPERTIES OF NATURAL SAND-MIXTURES	39
	Properties of Individual Particles	39
	Variation of Particle Properties in Natural Sand-Mixtures	40
	Size Classes for Sand Mixtures	41
	Size Distribution Indices for Sand Mixtures	43
	Some Reported Characteristics of Natural Sand-Mixtures	43
	Processes Yielding Lognormal Distribution	46
	Processes Involved in Generating Natural Sands	47
	Relative Importance of Mechanical Wear and Hydraulic Sorting	49
	Advantages of Lognormal Distribution for Natural Sands	51
	Analysis of Data for Size Distribution of Bed-Material Sand-Mixtures	52
VI	ANALYSIS FOR von KARMAN'S κ IN FLUME RUNS	56
	Analysis of κ for Flume Data	58
	Parameters Studied	61
	Prediction of κ	68
	Statistical Analysis	71
VII	RESISTANCE FUNCTION FOR PLANE SAND-BED FLOWS	77
	Correction for Side-Wall Friction	81
	Effect of Unequal Velocities in Wall and Bed Regions on Wall Correction	82
	Resistance Function for Smooth Flumes	85
	Analysis of Plane Sand-Bed Runs	86

TABLE OF CONTENTS - Continued

Chapter		Page
	Equivalent Roughness Size	89
	Validity of the Wall Correction	90
	Smooth to Rough Flow Transition	91
	Resistance Function for Plane Sand-Beds	92
VIII	RESISTANCE FUNCTION IN SAND-BED CHANNELS	95
	Velocity Profiles in Sand-Bed Channels	97
	Prediction of the Regimes of Flow	104
	Resistance Functions	107
	Summary	111
IX	TRANSPORT FUNCTION FOR SAND-BED CHANNELS	113
	General Form of Transport Function	116
	Variation of Concentration in The Vertical	118
	Evaluation of the Suspended Load	122
	Evaluation of the Bed Load	125
	Evaluation of the Reference Concentration	126
	Transport Function	127
X	APPLICATIONS OF THE RESISTANCE AND TRANSPORT FUNCTIONS	130
	Resistance Function	130
	Transport Function	136
XI	SUMMARY AND CONCLUSIONS	145
	Recommendations for Future Study	148
	REFERENCES	151
	APPENDICES	159
	FIGURES	184
	TABLES	253

LIST OF TABLES

Table		Page
2-1	WEST PAKISTAN CANALS	254
7-1	VALUES OF FRICTION FACTOR f VERSUS R/f BASED ON TRACY AND LESTER (1961)	255
7-2	SIZE DISTRIBUTION OF SANDS	256
7-3	VARIATION OF ξ WITH ROUGHNESS REYNOLDS NUMBER R_{ks}, FOR PLANE-BED RUNS	257
7-4	VARIATION OF ξ WITH ASPECT RATIO, FOR PLANE-BED RUNS	257
7-5	SUMMARY OF ξ VALUES AND RELATED PARAMETERS FOR PLANE-BED RUNS $(k_s = D_{84})$	258
7-6	COMPARISON OF OBSERVED AND PREDICTED VALUES OF f FOR PLANE-BED RUNS	259
8-1	SEPARATION OF BED FORMS FOR THE FLUME DATA	260
9-1	VARIATION OF RELATIVE CONCENTRATION $C\eta/C\eta_a$	261
10-1	VALUES OF $A1 = \ln(\frac{33.35}{\eta_{ks}})$	262
10-2	VALUES OF $A2 = (\frac{\eta_a}{1-z})\{(\frac{.15}{\eta_a})^{1-z} - 1\}$	263
10-3	VALUES OF $B = \eta_a\{\frac{(\frac{.15}{\eta_a})^{1-z}\ln(.15) - \ln(\eta_a)}{(1-z)} - \frac{(\frac{.15}{\eta_a})^{1-z} - 1}{(1-z)^2}\}$	263
10-4	VALUES OF $C_1 = \ln[\frac{1}{.15}(\frac{5.0}{\eta_{ks}})^{\frac{1}{Ae}}]$	264
10-5	VALUES OF $D = (\frac{\eta_a}{.85})^z$	264

LIST OF TABLES - Continued

Table		Page
10-6	VALUES OF $b_1 = \eta_a \ln \left(\frac{33.35\eta_a}{\eta_{ks}}\right)$	265
10-7	VALUES OF $I = \int_{.15}^{1.0} \left(\frac{1-\eta}{\eta}\right)^z d\eta$ AND $J = \int_{.15}^{1.0} \left(\frac{1-\eta}{\eta}\right)^z \ln \eta \cdot d\eta$	266
10-8	COMPUTATION OF TRANSPORT PARAMETER G FOR RIO GRANDE AT ALBUQUERQUE, N. M. OBSERVATION DATED MARCH 26, 1954	267

LIST OF FIGURES

Figure		Page
4-1	Prediction of bed form in sand-bed channels (after Simons and Richardson, 1966)	186
5-1	Normalized lognormal plot of bed-material size distribution in Rio Grande at Albuquerque and Bernalillo, N.M. (112 samples)	187
5-2	Normalized lognormal plot of bed-material size distribution in West Pakistan canals (327 samples)	188
6-1	Velocity profile in Run 6-32 - plane bed	189
6-2	Velocity profile in Run 5-05 - ripple bed	190
6-3	Velocity profile in Run 5-17 - ripple bed	191
6-4	Velocity profile in Run 10-58 - dune bed	192
6-5	Velocity profile in Run 10-91 - dune bed	193
6-6	Velocity profile in Run 9-01 - dune bed	194
6-7	Velocity profile in Run 2-08 - dune bed	195
6-8	Velocity profile in Run 4-15 - dune bed	196
6-9	Velocity profile in Run 4-29 - plane bed	197
6-10	Velocity profile in Run 7-12 - plane bed	198
6-11	Velocity profile in Run 4-30 - transition bed	199
6-12	Velocity profile in Run 6-39 - standing wave	200
6-13	Velocity profile in Run 10-68 - standing wave	201
6-14	Velocity profile in Run 5-45 - antidune	202
6-15	Variation of Karman's Kappa (213 runs)	203
6-16	Variation of Karman's Kappa (213 runs)	204
6-17	Kappa predicted by Shimoura's equation (213 runs)	205
6-18	Kappa predicted by Shimoura's equation (213 runs)	206
6-19	Variation of Karman's Kappa (213 runs)	207

LIST OF FIGURES - Continued

Figure		Page
6-20	Variation of Karman's Kappa (213 runs)	208
6-21	Variation of Karman's Kappa (213 runs)	209
6-22	Variation of Karman's Kappa (213 runs)	210
6-23	Variation of Karman's Kappa (213 runs)	211
6-24	Variation of Karman's Kappa with Froude number (148 runs)	212
6-25	Variation of Karman's Kappa with Froude number (213 runs)	213
6-26	Variation of Karman's Kappa with prediction parameter (148 runs)	214
6-27	Variation of Karman's Kappa with prediction parameter (213 runs)	215
6-28	Variation of von Karman's Kappa with Froude no. (Sayre-Albertson Data - 1963)	216
7-1	f versus R/f for smooth flumes based on Tracy-Lester's equation (1961)	217
7-2	Variation of ξ with aspect ratio - plane bed runs without wall correction ($ks = D_{84}$)	218
7-3	Variation of ξ with aspect ratio - plane bed runs with wall correction (based on Tracy-Lester smooth flume equation) [$ks = D_{84}$]	219
7-4	Variation of ξ with R_{ks} - plane bed runs without wall correction ($ks = D_{84}$)	220
7-5	Variation of ξ with R_{ks} - plane bed runs with wall correction (based on Tracy-Lester smooth flume equation) [$ks = D_{84}$]	221
8-1	Variation of total roughness in flume data	222
8-2	Comparison of average velocity profile for Atchaflaya River at Simmesport from 500 observations (Toffaleti, 1963) and from Eqns. (8-6) & (8-7)	223

LIST OF FIGURES - Continued

Figure		Page
8-3	Limits of P_{max} for upper and lower regime bed forms (flume data)	224
8-4	$V/\Delta U_{*o}$ versus shear parameter $1/S$ for the flume and West Pakistan canals data	225
8-5	Separation of flow regime - upper range points	226
8-6	Separation of flow regime - lower range points	227
8-7	Separation of flow regime - intermediate range points	228
8-8	Loci of solution points in intermediate range	229
8-9	Resistance curves for upper and lower $P_{max} - D_{50}$ range	230
8-10	Resistance curves for intermediate $P_{max} - D_{50}$ range	231
8-11	Predicted versus observed velocities for analysis based on resistance curves (Flume, Barton-Lin and West Pakistan Canals Data)	232
8-12	Percentage error in predicted velocity versus aspect ratio of section (Flume, Barton-Lin and West Pakistan Canals Data)	233
8-13	Percentage error in predicted velocity versus roughness Reynolds number (Flume, Barton-Lin and West Pakistan Canals Data)	234
9-1	Relation between total bed-material load transport and transport parameter G for flume runs (315 runs)	235
9-2	Relation between total bed-material load transport and transport parameter G for upper and middle range flume runs (203 runs)	236
9-3	Relation between total bed-material load transport and transport parameter G for lower range flume runs (112 runs)	237
9-4	Relation between total bed-material load transport and transport parameter G for flume runs (315 runs) and Rio Grande data 112 sections	238

LIST OF FIGURES - Continued

Figure		Page
9-5	Transport function for sand-bed channels	239
9-6	Comparison of observed and predicted gradation of total bed-material load (bed material D_{50} = 0.19 mm, σ = 1.30)	240
9-7	Comparison of observed and predicted gradation of total bed-material load (bed material D_{50} = 0.27 mm , σ = 1.56)	241
9-8	Comparison of observed and predicted gradation of total bed-material load (bed material D_{50} = 0.28 mm, σ = 1.67)	242
9-9	Comparison of observed and predicted gradation of total bed-material load (bed material D_{50} = 0.45 mm, σ = 1.60)	243
9-10	Comparison of observed and predicted gradation of total bed-material load (bed material D_{50} = 0.93 mm, σ = 1.54)	244
10-1	A1 versus η_{ks}	245
10-2	A2 versus η_a for different z values	246
10-3	B versus η_a for different z values	247
10-4	C_1 versus η_{ks} for different Ae values	248
10-5	$\mathcal{D}$ versus η_a for different z values	249
10-6	b_1 versus η_a for different values of η_{ks}	250
10-7	Integrals I and J versus z	251
10-8	Bed-material and bed-material load size distribution for Rio Grande at Albuquerque, N. M. (observation dated March 26, 1954)	252

LIST OF SYMBOLS

Symbol	Definition	Dimensions
a, a_1, a_2, a_3, b	Constants	
A	Coefficient in logarithmic velocity equation, $A = 1/\kappa$	
A_o	Universal value of A for $\kappa = 0.40$, $A_o = 2.5$	
$A1$	A component of transport parameter G, $A1 = \ln\left(\frac{33.35}{\eta_{ks}}\right)$	
$A2$	A component of transport parameter G, $A2 = \left(\frac{\eta_a}{1-z}\right)\left\{\left(\frac{.15}{\eta_a}\right)^{1-z} - 1\right\}$	
A_b, A_w	Component of the area of cross section of the flow associated with bed and wall, respectively	L^2
Ae	Ratio of shear velocity U_{*o} to effective shear velocity U_{*oe}	
A	A component of transport parameter G, $A = A1 \cdot A2$ for $z \neq 1$ and $A = \eta_a \ln\left(\frac{5.00}{\eta_{ks}\eta_a}\right)$ for $z = 1$	
b_1	A component of transport parameter G $b_1 = \eta_a \ln(33.35\ \eta_a/\eta_{ks})$	
B	Additive term in logarithmic velocity distribution as $\frac{u_y}{U_{*o}} = A \ln\left(\frac{y}{d}\right) + B$	
B_2	A constant depending on η_1, $B_2 = \kappa_o(1 + \ln \eta_1 - \eta_1)$	

Symbol	Definition	Dimensions
B	A component of transport parameter G $$B = \eta_a \cdot \left\{ \frac{\left(\frac{.15}{\eta_a}\right)^{1-z} \cdot \ln(.15) - \ln(\eta_a)}{(1-z)} - \frac{\left(\frac{.15}{\eta_a}\right)^{1-z} - 1}{(1-z)^2} \right\},$$ for $z \neq 1$ and $$B = \frac{1}{2}\eta_a \left\{ (\ln \cdot (0.15\ \eta_a) \ln\left(\frac{0.15}{\eta_a}\right) \right\}, \text{for } z = 1$$	
c	Local concentration of sediment as weight of sediment per unit weight of sediment-water mixture	
c_v	Local concentration of sediment in volume of sediment per unit volume of sediment-water mixture	
C_b	Mean concentration of the bed-material in the reference bed-layer measured in weight of sediment per unit volume of sediment-water mixture	$\frac{F}{L^3}$
C_D	Drag coefficient	
C_{η_a}, C_y	Time-averaged concentration of sediment in weight of sediment per unit volume of the sediment-water mixture at elevation η_a and y above the mean bed elevation, respectively	$\frac{F}{L^3}$
C_t	Average concentration of total sediment transport in a flow section by weight of sediment per unit weight of sediment-water discharge	
C_v, C_o	Average volumetric concentration of sediment load in a flow section or a vertical measured as volume of sediment transported per unit volume of sediment-water discharge and maximum possible value of C_v, respectively	
C_1	A component of transport parameter $$G,\ C_1 = \ln\left\{\frac{1}{.15}\left(\frac{5.0}{\eta_{ks}}\right)^{\frac{1}{Ae}}\right\}$$	

LIST OF SYMBOLS - Continued

Symbol	Definition	Dimensions
$C/\sqrt{g}$	Chezy's dimensionless resistance coefficient	
C	A component of transport parameter G, $C = C_1 \mathcal{D}$	
d	Average depth of flow	L
d_ℓ	Local depth of flow	L
D, D_{84}	Fall diameter of bed-material. The subscript where used refers to the percentile in cumulative size distribution of the sediment mixture	L
D_i	Geometric mean size of the ith fraction of bed-material	
D_n	Nominal diameter of sediment particle	L
$\mathcal{D}$	A component of transport parameter G, $\mathcal{D} = (\frac{\eta_a}{0.85})^z$	
e	Distance of the origin for y in the logarithmic velocity distribution below the mean bed elevation	L
f	Darcy-Weisbach resistance factor	
$f[a,b]$	A function of variables a and b. In general, functional dependence of any quantity on a number of variables is indicated by square brackets enclosing those variables	
f_b, f_w	Value of f relating to the segment of flow associated with the bed and the wall, respectively	
f_{b1}, f_{bo}	Value of f_b corresponding to the assumption of equal average velocities in wall and bed segments and corresponding to actual average velocities in these segments, respectively	
f_{gi}	Fraction of bed-material discharge in the ith size fraction	

Symbol	Definition	Dimensions
$F_Y(y)$	Value of the distribution function of random variable Y at $Y = y$	
F_1	A function of bed-material transport variables, $F_1 = g_t/C_b$	$\frac{L^2}{T}$
F	Froude number of flow, $V/\sqrt{gd}$	
g	Gravitational acceleration	$\frac{L^2}{T}$
$g_1[a,b]$	A function relating κ and κ_o as $\kappa = \kappa_o\, g_1[a, b]$	
g_{bi}, g_{si}	Part of g_i moving as bed-load and suspended load, respectively	$\frac{F}{LT}$
g_i	Bed-material transport rate corresponding to the ith size fraction in weight per unit width per unit time	$\frac{F}{LT}$
g_t	Total bed-material discharge per unit width, $g_t = \sum_{i=1}^{n} g_i$	$\frac{F}{LT}$
g_{tb}, g_{ts}	Part of g_t moving as bed and suspended load, respectively	$\frac{F}{LT}$
g_x, g_y	Component of g along X and Y direction, respectively	
G	Transport parameter	$\frac{F}{LT}$
i	Index of summation	
$I(\eta)$	Indicator function, $I(\eta) = 1$ for $0.8 < \eta < 1$ and $I(\eta) = 0$ for all other values of η	
I	A component of transport parameter G, $I = \int_{.15}^{1} \left(\frac{1-\eta}{\eta}\right)^z d\eta$	

LIST OF SYMBOLS - Continued

Symbol	Definition	Dimensions
J	A component of transport parameter G, $J = \int_{0.15}^{1} \left(\frac{1-\eta}{\eta}\right)^{z} \ln[\eta]\, d\eta$	
k	Physical height of roughness element above smooth boundary to which it is attached	L
k_a	Absolute roughness as in $\frac{1}{\sqrt{f}} = 2.03 \log\left(\frac{d}{k_a}\right)$	L
kr	A function representing roughness shape, size, arrangement, etc.	
ks	Equivalent roughness in terms of Nikuradse's sand. For open channel flow the equivalence is in terms of Nikuradse's sand and Keulegan's velocity equation	L
ℓ_f, ℓ_s	Mixing length for fluid and solid phase, respectively	L
$\ln(a)$	Natural logarithm of a	
L	Length along the stream	L
m_1, m_2, m_3, m_4	Sample estimates of parameter μ_y of a lognormally distributed variate	
n	(1) number of fractions representing equal proportions of the cumulative size distribution of the bed-material (2) size of a random sample from a population (in Appendix B)	
n_o	Porosity of the sand-bed	
p	Pressure intensity	$\frac{F}{L^2}$
P	Stream power, $P = \tau_o V$	$\frac{F}{LT}$

LIST OF SYMBOLS - Continued

Symbol	Definition	Dimensions
P_{max}	Maximum stream power $P_{max} = \tau_o \cdot 2.5\, U_{*o} \ln\left(\frac{12.27d}{D_{84}}\right)$	$\frac{F}{LT}$
q	Unit discharge, $q = \frac{Q}{W}$	$\frac{L^2}{T}$
Q	Total discharge in a flow section	$\frac{L^3}{T}$
Q_b , Q_w	Total discharge in bed and wall segment of a flow section, respectively	$\frac{L^3}{T}$
R	Hydraulic radius of a flow section	L
R_b, R_w	Component of R associated with bed and wall, respectively	L
R_x, R_y	Component of force per unit volume due to interaction between sediment and water phase along X and Y direction, respectively (in Appendix A)	$\frac{F}{L^3}$
R	Reynolds number of flow, $R = \frac{4dV}{\nu}$	
R_{ks}	Roughness Reynolds number $R_{ks} = \frac{U_{*o}\, ks}{\nu}$	
s_1	Reciprocal of aspect ratio of a channel section, $s_1 = d/W$	
s_1^2, s_2^2, s_3^2, s_4^2	Sample estimates of parameter σ_y^2 of a lognormally distributed variate	
S	Energy gradient	
S_s	Specific gravity of sand	
S	Shields' grain shear parameter, $S = \frac{\rho U_{*oe}^2}{(\gamma_s - \gamma_f) D_{50}}$	
t	Time	

LIST OF SYMBOLS - Continued

Symbol	Definition	Dimensions
T_f	Parameter representing the effect of suspended sediment on κ $T_f = (1 + \frac{30(\rho_s - \rho_f)}{\rho_f} \frac{V w_{16} C_v}{U_{*o}^2})$	
u	Velocity along X-direction	$\frac{L}{T}$
u', v', p', ρ'	Fluctuating component of u, v, p and ρ, respectively	$\frac{L}{T}$
$\bar{u}, \bar{v}, \bar{p}, \bar{\rho}$	Time averaged value of u, v, p and ρ, respectively	$\frac{L}{T}$
u_f, u_s	Value of u for water and sediment phase, respectively	$\frac{L}{T}$
u_{max}	Maximum velocity at the edge of a boundary layer or at the free surface of open channel flow without the surface cut-back	$\frac{L}{T}$
u_y, u_η	Value of u at elevation y and η, respectively	$\frac{L}{T}$
$u_{\eta p}$	Value of u_η for flow on plane rigid boundary with sand grain roughness	$\frac{L}{T}$
$(u_2 - u_1)$	Difference in the velocity over one log cycle of a logarithmic velocity profile	$\frac{L}{T}$
U_{*o}	Shear velocity $U_{*o} = \sqrt{gdS}$	$\frac{L}{T}$
U_{*oe}	Effective shear velocity (that shear velocity for the inner layer which would give the same logarithmic velocity profile with origin of y at the mean bed, as is actually observed)	$\frac{L}{T}$
$U_{*o\ell}$	Shear velocity based on local depth, $U_{*o\ell} = \sqrt{gd_\ell S}$	
v	Velocity along Y-direction	$\frac{L}{T}$

LIST OF SYMBOLS - Continued

Symbol	Definition	Dimensions
V	Average velocity of flow in a vertical or in a section	$\frac{L}{T}$
V_w	Average velocity in the segment of flow associated with the wall	$\frac{L}{T}$
V_f	Dimensionless resistance factor in a sand-bed channel, $V_f = V/U_{*o}$	
V_p	Dimensionless resistance factor for flow in a wide rigid boundary open channel flow $V_p = 2.5 \ln (12.27 \frac{d}{D_{84}})$	
w, w_{50}	Terminal fall velocity of a sediment particle and of D_{50}, respectively	$\frac{L}{T}$
W	Water surface width of an open channel section	L
W_o, W_ℓ	Weight of a sediment particle initially and after traveling a distance L, respectively	F
x, y	Coordinate of a point along X and Y direction, respectively	L
x, y, w, z	A value of random variable X, Y, W and Z, respectively (in Appendix B)	
X, Y	Directions of Cartesian coordinates	
X_j	Value of random variable X at jth step of a stochastic process	
X_{q_1}, X_{q_2}	q_1th and q_2th order quantile of random variable X, respectively	
X, Y, W, Z	Random variables (in Appendix B)	
X_{50}, Y_{50}, W_{50}	Median value of random variable X, Y, and W, respectively (in Appendix B)	
z	Rouse number, $z = \frac{w}{k_o U_{*o}}$	

LIST OF SYMBOLS - Continued

Symbols	Definition	Dimensions
α, β	Constants	
α_1	Ratio of average velocity in the wall segment V_w to the mean velocity V in the flow section, $\alpha_1 = \frac{V_w}{V}$	
ΔU_{*o}	A component of U_{*o}, $\Delta U_{*o} = \sqrt{U_{*o}^2 - U_{*oe}^2}$	$\frac{L}{T}$
$\Delta\rho$	Difference in the mass density of sediment and fluid, $(\rho_s - \rho_f)$	$\frac{FT^2}{L^4}$
δ, δ_v	Thickness of boundary layer and viscous sub-layer, respectively	L
ε	Eddy viscosity, $\varepsilon = -\overline{v'\ell'}$	$\frac{L^2}{T}$
$\varepsilon_f, \varepsilon_s$	Eddy viscosity for fluid and sediment phase, respectively	
ε_w	Eddy viscosity associated with wake layer for large roughness elements	$\frac{L^2}{T}$
ε_{log}	Eddy viscosity in flow along smooth wall with logarithmic velocity distribution	$\frac{L^2}{T}$
ε_j	A set of mutually independent variables	
γ_s, γ_f	Specific weight of sediment and fluid, respectively	$\frac{F}{L^3}$
η	Dimensionless distance from the mean bed, $\eta = \frac{y}{d}$	
η_a, η_{ks}	Dimensionless thickness η of bed-layer and dimensionless height of equivalent roughness, respectively	
κ, κ_o	Value of von Karman's "universal" constant for a flow. $\kappa_o = 0.40$	

Symbol	Definition	Dimensions
κ_1, κ_2	Average value of κ determined from outer layer regions of velocity profiles observed in a flow section based on average and local shear velocity, respectively	
κ_3, κ_n	Value of κ determined from a normalized - composite velocity profile for a flow section based on U_{*o}	
λ	Linear concentration of sediment particles, $\lambda = 1/\{(\frac{C_o}{C_v})^{1/3} - 1\}$	
λ_k	Roughness concentration defined as sum of roughness areas normal to the flow per unit area of the boundary	
μ_y, σ_y^2	Parameters of lognormal distribution of random variable X $\{Y = \ln[x]$ and $Y \sim N(\mu_y, \sigma_y^2)\}$	
ν	Kinematic viscosity	$\frac{L^2}{T}$
ν_{q_1}, ν_{q_2}	q_1th and q_2th order quantile of standard normal distribution, respectively (in Appendix B)	
ρ, ρ_f, ρ_s	Mass density of sediment-water mixture, water and sediment, respectively	$\frac{FT^2}{L^4}$
ρ_1	Integral of surface cut-back function, $\rho_1 = \int_0^1 I(\eta)\, a_1 (1 - \frac{\eta}{0.8})^2\, d\eta$	
σ	Gradation of sand-mixture, $\sigma = \frac{1}{2}\{\frac{D_{50}}{D_{16}} + \frac{D_{84}}{D_{50}}\}$	

LIST OF SYMBOLS - Continued

Symbol	Definition	Dimensions
τ, θ	Lower and upper bound of lognormal distribution, respectively (in Appendix B)	
τ_o, τ_c	Boundary shear stress and critical boundary shear stress, respectively	$\frac{F}{L^2}$
τ_{xx}, τ_{xy}	Shear stress on XX plane and YY plane, respectively	$\frac{F}{L^2}$
τ_{xy_s}, τ_{xy_f}	Component of τ_{xy} relating to solid and fluid phase, respectively	$\frac{F}{L^2}$
ξ	A variable in the resistance equation as, $\frac{1}{\sqrt{f}} = 2.03 \log (\xi \frac{R}{ks})$	

CHAPTER I

INTRODUCTION

In the field of natural resources, the problem of flow over sand-bed channels is encountered whenever relative motion between water and an erodible sand boundary exists. Once the threshold conditions for movement of bed-material have been exceeded, the flow involves mutual interaction between the fluid and the boundary. In its entirety, this problem involves time and space non-homogeneous processes of boundary deformation, effect of the boundary on turbulence characteristics of flow, suspension of bed material and the effect of such suspension on dynamics of flow. These processes, which are not adequately understood in themselves, are interrelated. So, even if they were independently understood, the general problem would still be far from solution.

Theories of turbulent liquid flows are at present (1971) in an empirical stage. Certain phenomenological theories, like those of Prandtl, Karman, Taylor and Townsend, are useful in the analysis of problems relating to such flows. The mechanism of turbulence is, however, not fully understood. For description of the vertical velocity distribution in turbulent shear flows, a two-layer model is currently accepted. This divides the turbulent part of the flow into a wall layer and an outer layer. This division also corresponds to the differences in certain turbulence characteristics in the two layers. Flow over a sand-bed imposes conditions for which the clear water turbulent flow theories do not provide an answer. These conditions, which stem mainly from the mutual interaction of flow and the

boundary, create some gross changes in the vertical distribution of velocity. Efforts have been made in the past to explain these changes in terms of the suspension of sand and the phenomenological theories, but an important aspect of flow in sand-bed channels has been neglected in these studies. This aspect is related to the local acceleration over parts of the bed forms. It is difficult to ascertain how much of the gross effects noted in velocity profiles are due to these accelerations and how much are due to the suspension of sand.

The engineer, in general, is concerned with the discharge of water and sediment, size distribution of the transported material, channel geometry and stability of the geometry of the alluvial section. Lateral stability of the section is evaluated by regime theories and dealt with by standard channel stabilization practices. The vertical stability (of the bed) is related to the time scale of the phenomenon. In most cases of engineering interest two-dimensionality and time-homogeniety of the process can be assumed at least as a first step. With these restrictions, the variables of interest reduce to the properties of the fluid and the sand-bed, depth of flow, energy gradient, water discharge, sediment load and size gradation of the transported material. The sediment load is recognized as consisting of an indeterminate fine material component and the determinate bed-material load. For a given sand-bed and fluid, there are four remaining variables, viz., water discharge, bed-material load and its size gradation, depth of flow and energy gradient. Knowing any two of these variables, it should be possible with the help of a resistance and a transport function to determine the two remaining variables. However, the resistance and the transport functions are not always single-valued functions. It is

known that under certain depth-slope combinations, the flow over a sand-bed may result either in an upper regime situation or in a lower regime situation. The former is characterized by both higher velocities and transport rates and the latter by both lower velocities and transport rates. Although, the range of conditions in which a multiplicity of resistance and transport solutions can exist is not known it is in this range that it may be possible to uniquely determine only one of the four variables from the known values of the other three.

The problem of predicting the bed-material transport rates, with a known velocity, depth and bed-material is considerably simpler than that of predicting both the velocity and the transport rate. The reason for this lies in the final regime and turbulence structure of the flow. Both the mean velocity and sediment transport are a consequence of the turbulence structure of the flow. Even though the mechanism of diffusion and transport of the sediment and the liquid may be different, because both are related to the resulting regime of flow and the turbulence structure, they show a good correlation with each other.

Perhaps the greatest obstacle in the understanding of flow over sand-beds is the variety of bed forms that can accompany such flows. The recognition of different bed forms is not new, but the importance of different flow regimes and a differentiation of the resistance and transport phenomena associated with these regimes is an outstanding contribution of recent times. It is understood that it is not possible to define a single resistance or transport function for all of the bed forms.

This dissertation is concerned with the investigation of two-dimensional, time-homogeneous flow of water in sand-bed channels. The object of this study is to derive predictive relations for the discharge of water and the quantity and size gradation of the bed-material transport for the given properties of water, sand-bed, depth and energy gradient. The prediction of the regime of flow and the uniqueness of this regime are important steps in the analysis of flow in sand-bed channels. Therefore, it is also necessary to investigate these aspects of the flow to determine the range of conditions in which the regime can be uniquely predicted. This investigation is primarily based on the recirculating laboratory flume data in which the two-dimensionality and time-homogeniety of the flow phenomena are realized. Some field data from the Rio Grande in New Mexico and the West Pakistan Canals are also used to extend the predictive relations to a wider range of the depth of flow and other conditions.

CHAPTER II

DATA USED

Data available on flow in sand-bed channels are of two types, viz., those obtained under controlled laboratory conditions and those collected in natural rivers and canals. The field data (rivers and canals) are generally characterized by a larger range of depths but a smaller range of other variables. They also suffer from disturbances such as variation of discharge, curved channels, presence of seepage forces etc. Moreover, field observations are not as complete as those made in the laboratory especially for total bed-material transport and the description of bed forms. Experiments with flow over sand-beds in the laboratory have contributed greatly to the description and understanding of the phenomena involved, mainly because of the absence of extraneous disturbances and the opportunity for detailed observations. For these reasons, this study of flow in sand-bed channels is primarily concerned with the laboratory data.

Laboratory Data

The data on which this study is based were collected at Colorado State University by Daryl B. Simons and E. V. Richardson between 1956 and 1961. A compilation of the data and description of the procedures has been published as U.S. Geological Survey Professional Paper No. 462-I (1966), entitled "Summary of Alluvial Channel Data from Flume Experiments, 1956-1961". These data are generally referred to, in this text, as the flume data or the flume runs.

The flume studies were made in two recirculating flumes, one with a nominal width of 2 feet (actual width 1.969 ft) and the other 8 feet

wide. In all, 339 runs were made under equilibrium conditions. The range of bed forms extended from plane bed without movement to chutes and pools. The range of some other variables covered in these runs is given below:

Bed-material	
Median diameter (mm)	0.19 - 0.93
Geometric standard deviation, σ	1.25 - 2.07
Flow	
Mean depth (ft)	0.19 - 1.33
Mean velocity (ft per second)	0.65 - 6.34
Energy gradient (percent)	0.0055 - 1.928
Bed-material discharge (lb per sec per ft width)	up to 12.51
Fine material load concentration (tables 10 and 11 only) (ppm)	up to 63,700

Published data for these runs include all the hydraulic and sediment variables. Some data, such as the complete size distribution analyses of bed material load, have not been published and were obtained from the original records.

In connection with the analysis of plane-bed runs, some intermediate width-depth ratios between those provided by the 2 and 8 foot flume were needed. For this purpose and for testing the resistance function derived in Chapter VIII, flume data reported by Barton and Lin (1955) were also used. The data which are referred to in this text as Barton-Lin data were collected at Colorado A & M College, in a 4 foot wide flume with a sand of 0.18 mm median size and a geometric standard deviation of about 1.25. No other laboratory data were used.

Field Data

As all resistance and transport theories have to be used ultimately under field conditions, it was necessary to include some field data in the analysis. This was done by using 43 canal observations from 3 canals in West Pakistan (West Pakistan WAPDA, 1963). All the selected canals are perennial and known to be stable. The reason for selecting the canals instead of river sections was that these canals are operated with nearly constant discharges for long durations and thus are more likely to be in equilibrium than the river sections. Another reason was that these canal sections are all located in long straight reaches and have nearly constant depths across the sections. A list of the canal sections used is given in Table 2-1 with their hydraulic and sediment variables. The range of variables for these sections is listed below.

Bed-Material	
Median diameter (mm)	0.085 - 0.35
Geometric standard deviation, σ	1.22 - 1.50
Flow	
Average depth (ft)	2.5 - 10.6
Mean velocity (ft per sec)	1.27 - 3.53
Energy gradient (percent)	0.0078 - 0.025

Bed-material transport data are not available for these canals and therefore, they were not used in the formulation of the transport function. In this text these data are referred to as the canal data.

For the transport function, part of the data reported by Nordin and Beverage (1965) for the Rio Grande were also utilized. This comprised 112 observations pertaining to the sites near Bernalillo

and at Albuquerque, New Mexico. Nordin and Beverage have listed all the hydraulic and sediment variables for these sections including bed-material size analyses for each observation. In most of these, however, the slopes have been adopted as averages from other studies. The range of variables involved in these data are given below:

Bed-material	
Median diameter (mm)	0.18 - 0.45
Geometric standard deviation, σ	1.29 - 3.72
Flow	
Mean depth (ft)	0.52 - 4.80
Average velocity (ft per sec)	0.99 - 7.82
Energy gradient (percent)	fairly constant
Albuquerque	0.11
Bernalillo	0.086
Bed-material discharge (lb per sec per ft width)	0.00045 - 10.2

Total sediment loads for these sections had been calculated by the Modified Einstein Procedure, and reported for all sediment sizes as well as for sizes greater than 0.062 mm. In using these data the reported total sediment load in size range greater than 0.062 mm was taken as the observed total bed-material load. This was done for want of a better definition of the indeterminate fine material load for individual observations. These data are referred to in this text as the river data or the Rio Grande data.

The bed-material size distributions of the river data were also used for testing the applicability of lognormal distribution to natural sand-mixtures. Also used for this purpose were all the bed-material

analyses reported for the West Pakistan canals for 1963. These analyses were obtained from the Canal and Headworks Data Observation Program of West Pakistan Water and Power Development Authority (1963).

In this study all the analyses were performed on a digital computer. For this purpose, it was necessary to punch the data used in this investigation on computer cards. For the flume runs, the data punched on cards comprised all the information contained in U. S. Geological Survey Professional Paper No. 462-I, including the velocity profiles. In the case of Barton-Lin and the canal data all the pertinent hydraulic and sediment variables required for the resistance function were punched on cards. The channel cross-sectional data reported for the West Pakistan canals were not included in this as they were not required for the objectives of this study. For the Rio Grande data, all the hydraulic, sediment and transport variables reported by Nordin and Beverage (1965) for the sites near Bernalillo and at Albuquerque were transferred to the computer cards. They also include the bed-material size distribution analyses. To avoid reading of the complete set of data for each phase of the investigation, certain reduced sets of data were produced through the computer. Specifically, these sets pertain to the variables involved in the resistance phase, the transport phase, the bed-material gradation and the κ analysis of the velocity profiles. The master set of punched cards for the complete data and the reduced sets are available at the computer terminal in the Engineering Research Center of the Colorado State University.

CHAPTER III

TURBULENT FLOW IN RIGID BOUNDARY CHANNELS

Flow over sand-bed channels is different from rigid boundary flows in that the interaction between the flow and the boundary is not simply a function of the roughness-height viscous-layer-thickness ratio. In sand-beds, once the general movement has started, the flow and boundary interact in a more complicated manner. Salient features that differentiate flow over sand-beds from rigid boundary flow are as follows:

(i) In sand-bed channels, the flow and boundary shape are interrelated. After general movement of the bed has started, the sand-bed is distorted, giving rise to bed forms. The shape, size and rate of movement of these forms vary with the flow.

(ii) Roughness size represented by the bed forms can be of the same order as the depth of flow in some phases like dunes and anti-dunes. Similar relative roughness sizes are generally not encountered in rigid boundary flows.

(iii) A sand-bed is not impervious. Unlike rigid boundaries, therefore, there is a possibility of flow, however small, penetrating into the bed. Thus, the turbulent fluctuations normal to the flow do not always vanish at the boundary.

(iv) The boundary in the case of sand-beds is moving at both the grain and the bed form scales. Grains rolling at the boundary may introduce additional shear by their rotation and change the turbulence level close to the boundary by their wakes. The movement of bed forms, on the other hand, creates unsteadiness of flow at a vertical due to the changing bed elevation and flow pattern.

(v) At advanced stages of movement, bed-material is thrown up in suspension. The presence of particles in suspension affects the turbulence characteristics of the flow.

(vi) As the bed forms achieve dimensions comparable to the depth (dunes), the flow is no longer uniform. Both the depth and velocity change along the main flow direction and across the section.

The consequence of these differences between rigid boundary and sand-bed flows are not known in detail, but it is apparent that these are too important to be ignored in the analysis of sand-bed flows. Yet, there is no theory of turbulent flow over mobile beds comparable to theories available for rigid boundary turbulent flows; therefore, all analysis of flow over alluvial beds, relies on the rigid boundary turbulent flow theories. Before proceeding with the resistance problem, a brief summary of the theories of turbulent flows will be given, along with a discussion of the effects of the above features on alluvial flows.

Turbulent shear flows that are commonly studied are either the boundary layer flows along plates or symmetrical conduit (pipe, channel) flows. These are similar in their mean flow patterns and distribution of turbulence quantities in the vicinity of the wall. Farther away, however, the boundary layer flows exhibit intermittency of turbulence near the outer edge of the layer. Similar intermittency cannot be experienced in fully developed conduit flow. In exploring the turbulence and mean flow characteristics, the differences between the two kinds of shear flows are not very important. For example, it has been shown by Hama (1954) that the roughness function for fully rough flow

are the same for a given roughness geometry in pipe, channel and zero-pressure gradient boundary layer flows. In open channel flow, if the Froude number of the flow and the size of the bed forms is small, the free surface is nearly plane and fully developed turbulent flow can be approximated by a boundary layer flow with the boundary layer thickness the same as the depth of flow. This would be more nearly so in channels of large width-depth ratio and in the portions of flow away from the banks. However, such a flow would not have intermittency of turbulence at the outer edge of the flow.

Regions of Velocity Distribution in Turbulent Flows

In turbulent boundary layer flow three regions of mean velocity distribution are recognized. There is a very thin region close to the wall, where viscous effects dominate. This is called the viscous sub-layer. This layer is characterized by a constant shear stress equal to τ_o, the boundary shear stress and has a time average thickness of about $5\nu/U_{*o}$, where ν is the kinematic viscosity of the fluid and U_{*o} is the shear velocity $\sqrt{\tau_o/\rho}$. Flow in the viscous sublayer is neither entirely laminar nor steady. It undergoes periodic growth and disintegration, so that the same set of fluid particles is not associated with it at all times. The velocity profile in the viscous sublayer is linear over most of its thickness but departs from linearity almost abruptly near its end.

Beyond the viscous layer and up to about a distance of 0.1 to 0.2 times the boundary layer thickness, is the equilibrium layer. This layer, also called the "inner" layer, has a nearly constant shear stress equal to τ_o, the shear stress at the boundary. Flow in this layer is fully turbulent except in a small transition region close to the viscous

layer. Flow in the fully turbulent region has "similarity" in terms of the shear velocity U_{*o} as the reference velocity and ν/U_{*o} as the reference length. The velocity profile in the inner layer is given by

$$\frac{u_y}{U_{*o}} = A \ln \frac{U_{*o} y}{\nu} + B \tag{3-1}$$

where

u_y is the velocity at distance y from the boundary and

A and B are constant for a given flow.

Outside the inner layer, is the outer layer, the region containing 80 to 90 percent of the depth. Velocity distribution in this layer is given by a velocity defect relationship (Rotta, 1962),

$$\frac{u_{max} - u_y}{U_{*o}} = f\left[\frac{y}{d}, \frac{U_{*o}}{u_{max}}\right] \tag{3-2}$$

derived from dimensional considerations. If this relationship is applied up to the inner layer, an asymptotic form of the velocity defect law is obtained as

$$\frac{u_{max} - u_y}{U_{*o}} = -A \ln \frac{y}{d} + B\left[\frac{U_{*o}}{u_{max}}\right] . \tag{3-3}$$

where

u_{max} is the velocity at the outer edge of the boundary layer and

d is the boundary layer thickness.

Experimental results show that the dependence of B on $\frac{U_{*o}}{u_{max}}$ is weak and is quantitatively not yet known.

The observed velocity profiles in fully developed turbulent boundary layer and conduit flows show a close fit to the logarithmic

velocity profile (Equation 3-1) in the inner layer. However, velocities in the outer layer show systematic departure and the velocity defect law (Equation 3-3) gives an underestimation of velocity. This has sometimes been corrected by the adoption of a parabolic function for the velocity defect law in the outer region (Hama, 1954) or some other correction terms in the logarithmic form of velocity defect law (Hinze 1959, p. 483).

If the flow boundary is not smooth and the protuberances on its surface are not smaller than the viscous sublayer, the flow undergoes a transition from smooth turbulent flow of Equation (3-1) which becomes

$$\frac{u_y}{U_{*o}} = A \ln \left(\frac{yU_{*o}}{\nu}\right) + B[R_{ks}] \tag{3-4}$$

where

$$R_{ks} = \frac{U_{*o}\, ks}{\nu} \quad \text{and}$$

ks is the size of the roughness.

For still larger roughness of the boundary, the flow in the inner layer becomes dependent on the roughness height ks as the reference length and the velocity profile is given by:

$$\frac{u_y}{U_{*o}} = A \ln \left(\frac{y}{ks}\right) + B \tag{3-5}$$

where constant B is now dependent on the type, shape, size variation and concentration of the roughness elements.

Logarithmic velocity profiles given in Equations (3-1) to (3-5) can be derived by theories such as Prandtl's and von Karman's. In Prandtl's mixing length theory, the shear stress is constant and the mixing length increases linearly with distance from the wall, resulting

in Equation (3-1). With von Karman's similarity hypothesis, the mixing length is proportional to the ratio of the first and second derivatives of the local velocity. This combined with a linearly varying shear stress gives a velocity defect law. However, it is not necessary to invoke any of the phenomological theories to derive the log velocity profiles discussed above. Milikan (Hinze 1969, p. 469) has shown that it is possible to derive log velocity profiles entirely on the basis of functional relations and an overlapping region where both the inner and outer laws apply.

Turbulence Characteristics of Inner and Outer Layers

The division of turbulent boundary layers into inner and outer layers is not only convenient for empirical description of observed velocity profiles, but is also supported by the consideration of turbulence characteristics. Townsend (1961) divided the turbulent boundary layer flow into an "inner layer" and an "outer layer". According to him, the inner layer, which is also the constant stress layer, is very nearly in a condition of absolute energy equilibrium and the local production of turbulent energy in it is only slightly more than the local dissipation. This surplus in the inner layer is a major source of turbulent energy in the outer regions of flow. On the other hand, mean flow energy from the outer layer is transferred to the inner layer by the gradient of Reynold's stresses in the outer layer. Measurements of turbulence quantities in the inner and outer layers indicate the diffusion of turbulence energy to the outer layer. The inner and outer layers thus interact, but they have different turbulent-flow mechanisms.

Towards the wall the contribution to the turbulence energy by larger eddies decreases while that by the smaller eddies increases. In the outer layer, the smaller eddies (higher frequencies) are found to be somewhat isotropic and the large scale eddies are elongated along the mean flow direction.

The size of eddies, in the two layers, brings about another distinction between the outer and the inner layers. As the larger eddies in the outer layer are slower to recover from any disturbance, the flow there has a long "memory". Thus, while the conditions in the inner layer are determined by the wall, those in the outer layer are determined by the distribution of wall stress for some considerable distance upstream.

Effect of Boundary Roughness on Turbulent Flow

It has already been stated that if the size of protuberances on a flat plate is not smaller than the viscous sublayer, constant B in Equation (3-5) becomes a function of roughness Reynolds number R_{ks}. Nikuradse's data on pipes, along with other experimental results, shows that for values of R_{ks} greater than about 55, the law of the wall is altered such that, in the inner layer, "similarity" is in terms of some proportion α of the absolute roughness height k and the shear velocity U_{*o}. The boundary then becomes fully rough and velocity distribution in the inner layer becomes,

$$\frac{u_y}{U_{*o}} = A \ln \left(\frac{y}{ks}\right) + B, \quad R_{ks} > 55 \tag{3-6}$$

$ks = \alpha k, \quad \alpha = \alpha$[roughness shape, concentration, etc.]

Physically it is interpreted that the transfer of momentum takes place by action of forces normal to the wall surface, and this transfer may depend weakly or not at all on the fluid viscosity.

Following Clauser (1956) and Hama (1954) the form of Equation (3-4) has been retained, through the whole range of smooth-turbulent to rough-turbulent regime as

$$\frac{u_y}{U_{*o}} = A \ln \frac{U_{*o} y}{\nu} + B - \frac{\Delta u}{U_{*o}} \tag{3-7}$$

where

$$\frac{\Delta u}{U_{*o}} = A \ln \frac{U_{*o} ks}{\nu} + B - B_1 \quad \text{and} \tag{3-8}$$

B, B_1 are constants for a particular roughness shape and concentration.

Experimental data from different types of roughness show that $\frac{\Delta u}{U_{*o}}$ is not a universal function of R_{ks} but for a given roughness type, the function is unique. It is apparent that as long as there is no theoretically derived function for $\frac{\Delta u}{U_{*o}}$, Equation (3-6) may be written with either A, B or ν as a function of R_{ks}. (This will be discussed in greater detail subsequently.)

Effect of Roughness Shape and Concentration

The form of transition from smooth-turbulent to rough-turbulent flow in a resistance diagram (like Moody's) depends on the size distribution of roughness elements. Nikuradse's data, which were collected from densely packed, uniform-sized, sand particles glued to the inside of the pipes, show a more abrupt transition than non-uniform sand roughness. Colebrook and White (1937) explained this in terms of the gradual

exposure of roughness elements in a mixture of non-uniform sizes. The functional relationship of $\frac{\Delta u}{U_{*o}}$ in Equation (3-7) would reflect the manner of transition.

Roughness patterns other than densely packed have also been studied. Some of these investigations are: Schlichting (1936), sperical, hemispherical, conical and cleat type roughness in closed rectangular channel; Chu and Streeter (1940), square threaded grooves in pipes; Albertson and Sayre (1936), cleat roughness in open channel; Koloseus and Davidian (1966), sand particles and cubical elements in open channel; O'Loughlin (1965), cubical elements in closed rectangular channel; Perry et al. (1969), square grooves in boundary layer flow. These investigations bring out some important aspects of roughness concentration and types.

Concentration of roughness elements λ_k, has been defined by Koloseus and Davidian, O'Loughlin and others as the ratio of the sum of projected areas of roughness elements normal to the mean flow, to the total floor area. Ratio of equivalent sand roughness ks (in terms of Nikuradse's roughness) to the physical dimension k of the roughness element gives a dimensionless measure of the roughness offered by a geometry and concentration. From a study of $\frac{ks}{k}$ versus concentration λ_k, Rouse (1965) concluded that to about $\lambda_k = .15$, the resistance varies in direct proportion to the concentration and the maximum resistance occurs at a concentration from .15 to .25 for different geometries. After this optimum concentration, the resistance decreases in all cases, but the pattern and rate of decrease varies with the roughness geometry and arrangement. Reduction of roughness beyond the optimum concentration is explained by mutual interference of the roughness elements.

The "similarity" in the wall layer, in terms of dimensions of roughness element and shear velocity, experienced with discrete roughness elements on a smooth boundary is not valid for certain roughness patterns like narrow grooves cut in the wall. This type of roughness has been studied by Perry et al. (1969) and they term it "k" type roughness in contrast with the usual type, which they call "d" type.

Vortices Generated at Roughness Elements

The effect of roughness elements on the mean flow field around them, goes beyond the shift in the velocity profile predicated by Equation (3-7). Measurements by Schlichting, Jacobs and others (Rotta, 1962), show that a secondary flow in the form of longitudinal vortices is generated behind roughness elements. These vortices counteract the damping effect of viscous forces in the vicinity of the wall. O'Loughlin, (1965) considering the effect of roughness elements, argued that the turbulence produced in the zones of intense shear downstream of the elements, intensifies the mixing or transfer of momentum above that otherwise present in the flow. For a sequence of roughness elements, he called the integrated effect of these elements a "wake layer" of approximately uniform thickness with highly intense turbulence. Outside this wake layer, O'Loughlin considered the turbulence characteristics independent of the nature of the roughness elements. This concept is the same as for flow on a rough wall, where flow in the outer layer is independent of the wall immediately below it.

To derive the mean flow resistance, O'Loughlin (1965) considered an increased turbulent viscosity ε' in the region of flow close to the wall as

$$\varepsilon' = \varepsilon_{log}$$

where

ε_{log} is the eddy viscosity due to smooth wall with logarithmic velocity profile and

ε_w is the increment in eddy viscosity due to enhanced turbulence of the wake layer.

By definition

$$\varepsilon = \frac{\tau}{\rho \cdot \frac{du}{dy}}$$

and for the logarithmic velocity Equation (3-1) in the inner layer

$$\varepsilon_{log} = \frac{U_{*o}\, y}{A}$$

The above approach of increasing the value of ε, to account for the effect of large roughness element on the vertical velocity distribution amounts to a reduction in the value of A. This implies that $\frac{\Delta u}{U_{*o}}$ in Equation (3-7) is made to depend on ε_w also.

Origin for Velocity Profiles on Rough Boundaries

In the case of smooth boundary, the origin for measuring y is uniquely defined. For rough boundaries, except at large distances from the wall compared with the roughness size, the question of origin for measuring y becomes important. Measured with respect to the boundary on which roughness elements are placed or with respect to the mean elevation of the roughness tops, velocity profiles in the inner layer show a systematic deviation from the logarithmic velocity distribution. This can be corrected by selecting a virtual origin for y, some distance e (<k) below the mean elevation of the boundary, by trial and error. In practice, this is done graphically similar to the method used in

determining the reference levels in natural open channel controls or the lower limit of a three parameter lognormal distribution (Aitchison and Brown, 1957).

Assuming that y is measured from the mean bed elevation of the rough boundary, the wall-law can be written as

$$\frac{u_y}{U_{*o}} = A \ \ln \frac{U_{*o}\,(y + e)}{\nu} + B - \frac{\Delta u}{U_{*o}} \quad . \tag{3-9}$$

If the inner law is now considered for fully rough flow with varying roughness arrangements, for which e is unknown and for which coefficient A is not a universal constant, the velocity equation for the fully rough flow can be written as

$$\frac{u_y}{U_{*o}} = A \ \ln \cdot \left(\frac{y + e}{ks}\right) + B \tag{3-10}$$

where

$A = A[kr]$,

kr being some function representing roughness size, shape, arrangement and possibly other factors which may cause A to depart from its universal value and B is a constant.

Equation (3-10) can be rewritten as

$$\frac{u_y}{U_{*o}} = A \ \ln \left(\frac{y + e}{b \cdot ks}\right) \quad . \tag{3-11}$$

Now e, the distance of the origin below the mean bed level, is a function of the roughness size k, its geometry and possible other factors. For Nikuradse roughness, a value of e of $-0.03k$ is reported. Perry and Joubert (1963) reported an average value of e as $0.25k$ for their experiments and $0.2k$ for Moores' experiments, both of which were conducted with boundary layer flow on square bar

type roughness, placed normal to flow. (For groove type "d" roughness, Perry et al. (1969) report that e is not related to the roughness height).

The velocity distribution in the inner layer can now be expressed, using the fact that the displacement e of the origin for logarithmic velocity profiles on fully rough boundaries is related to the height of the roughness element for a "k" type roughness. This is in contrast to some other methods which amend A (like O'Loughlin's), B or ν (Perry et al., 1969) in Equation (3-4) to account for the influence of roughness elements on the boundary.

A Velocity Distribution Equation for Inner Layer in Flow Over Large Roughness Elements

Since the displacement e, of the origin for velocity profiles on rough boundaries is proportional to the height of roughness element, ks and the constant of proportionality depends on the type and concentration of the roughness elements, it is possible to write

$$e = a_1 \, ks$$

where

$$a_1 = a_1[kr] \; .$$

Introducing this value in Equation (3-11) gives

$$\frac{u_y}{U_{*o}} = a_2 A_o \ln\left(\frac{y + a_1 \, ks}{b \, ks}\right) \tag{3-12}$$

where

$$A = a_2 A_o$$

$A_o = 2.5$, is the value of A for $\kappa = 0.40$,

and

$a_2 = a_2[kr]$ as discussed for Equation (3-10). Equation (3-12) can be further simplified to

$$\frac{u_y}{U_{*o}} = a_2\ a_3\ A_o\ \ln\left(\frac{y}{b\ ks}\right) \tag{3-13}$$

where,

$$\frac{y}{b\ ks}\left(1 + \frac{a_1\ ks}{y}\right)$$

is replaced by

$$\left(\frac{y}{b\ ks}\right)^{a_3} .$$

Equation (3-13) can then be written as

$$\frac{u_y}{U_{*oe}} = A_o\ \ln\left(\frac{y}{ks}\right) + B \tag{3-14}$$

where

B is a constant for fully rough flow,

A_o is a universal constant and

$U_{*oe} = U_{*o} \cdot (a_2\ a_3)$ is called the effective shear velocity in the inner layer.

U_{*oe} is that shear velocity, which would give the same log-linear velocity distribution in the inner layer, with the origin assumed at the mean bed elevation, as is actually observed with large roughness elements. It also accounts for any change in A, that occurs due to these elements or other causes. Equation (3-14) will be used in deriving vertical velocity distribution in sand-bed channels, where large roughness elements are present and the turbulence structure close to the boundary is affected by rolling and suspended particles.

CHAPTER IV

TURBULENT FLOW IN SAND-BED CHANNELS

In sand-bed channels, there is an interaction between the flow and the boundary, such that as the flow increases the boundary distorts into bed forms and the boundary material is mixed with the flow, in suspension. The interaction between the flow and the boundary in shallow water flows is well known in open channel hydraulics. This led Exner (Leliavsky, 1955) to combine a simple continuity equation to the bed material and water discharge to yield an equation for approximate bed form shape and growth. Similar but more complex methods have since been applied by Anderson (1953), Kennedy (1961), Mercer (1964), Raudkivi (1966), Gradowczyk (1968), Engelund (1970) and others to predict the stability of the boundary and rate of growth, direction of travel and other aspects of bed forms. The effect of the sand bed on the turbulence characteristics of flow is, however, not dealt with by these theories. In considering gross transport and resistance parameters of sand bed flows, it is necessary to know the differences introduced in the structure of flow from single phase rigid boundary flow. Some of these aspects are discussed in this chapter. A gross measure of the change in turbulence characteristics of flow over sand bed channels is provided by the change noted in the value of von Karman's κ. This change is analysed in Chapter VI for the velocity profiles observed in the flumes.

Effect of Bed Forms

The most important aspect which differentiates sand-bed channels from rigid boundary channels is formation of the bed forms and their

interaction with the flow. When bed shear is less than that corresponding to beginning of movement (e.g., Shields' criterion), sand bed channels are not different from rigid boundary channels, except with regard to the porosity of the bed. Flow resistance is the only aspect involved and can be analysed as for a rigid boundary with similar roughness. As the shear is increased, individual grains start to move and the intensity of movement increases with increasing boundary shear. Soon after this stage, the boundary distorts, giving rise to a sequence of bed forms, which for a given sand, change with increasing shear.

A systematic study of these forms, the conditions of their formation and characteristics of flow resistance and transport associated with individual forms, was one of the objective of the flume studies carried out by Simons and Richardson (1963). They divided the bed forms into two different regimes, lower and upper, with a transition region between. This classification is based on the mode of transport and energy dissipation associated with each regime. A criterion for the prediction of bed forms, from known stream power and median fall diameter, was also given by Simons and Richardson (1966), (Figure 4-1).

The sequence of bed forms occurring on sand beds with increasing stream power is

Lower Regime

- Ripples
- Dunes with ripples superposed
- Dunes

Transition

Upper Regime

- Plane bed
- Antidunes
  - Standing waves
  - Antidunes
  - Breaking antidunes
- Chutes and Pools
- Slug flow

In general the transport increases from lower to upper regime with a possible minor reduction as bed form changes from dunes to a plane bed, while the resistance to flow increases within lower and upper regime in the sequence of bed forms given. In the lower regime, the resistance is much greater than that due to grain roughness. In the transition region, the resistance decreases from dunes to antidunes and is somewhat higher than the grain roughness. In the upper regime, the resistance is nearly the same as for the grain roughness until antidunes start breaking. Breaking antidunes and chutes and pools, may offer greater resistance than some situations in the lower regime, due to energy consumed in surface wave phenomena.

The consequence of the range of bed form, which can occur in a sand bed, is that the boundary roughness is not a property of the sand bed, but depends on both the sand bed and fluid flow.

Plane-Bed Form in Sand-bed Channels

In sand-bed channels, Simons and Richardson (1966) defined the plane bed as "...a bed without elevations or depressions larger than the largest grains of the bed material." The plane-bed condition

occurring with significant movement of bed-material is a distinct form which contains all other features of flow in sand-bed channels except the complex boundary configuration associated with other bed forms. It, therefore, provides an opportunity to study some aspects of flow in sand-bed channels, which cannot be isolated, in the presence of other bed forms.

There is some disagreement about the occurrence of plane sand-bed condition in the lower regime. Mercer (1964) gave one point of view: "In the absence of local bed irregularities appreciable movement can occur without the development of bed undulations, but in the presence of small irregularities, local scour develops immediately downstream and the scoured material is redeposited some distance further on." Chabert and Chauvin (1963), on the other hand, stated a criterion by which for flow of water over sand-beds, plane-bed form may occur when the mean diameter of the bed-material is greater than about 0.6 mm. In the flume data, plane-bed runs in the lower regime, with significant transport of the bed-material were reported for coarse sand only (D_{50} = 0.93 mm). For fine and medium sands, this form was not experienced in the lower regime.

Conditions under which steady plane-bed forms occur in the transition region and the upper regime can vary with the fall diameter and shear, as well as with the scale of the flow system. The range of boundary shear over which the plane-bed form developed under transition and the upper regime conditions in the flumes, are given below:

Median Fall diameter (mm)	Flume	Boundary shear τ_o (lbs per ft^2)	P_{max} (ft lb per sec per ft width)
.18 - .19	8'	.054 - .055	.202 - .299
.27 - .28	8'	.057 - .090	.209 - .416
.32 - .33	2'	.092 - .193	.563 - 1.273
.45 - .47	8'	.106 - .251	.460 - 1.783
.54	2'	.149 - .193	.826 - 1.225[2]

[1] P_{max} is the stream power that would accrue for the same roughness as the bed-material under rigid boundary conditions with the velocity obtained from Keulegan's equation, for fully rough flow in open channels.

[2] Run 5-26 is omitted.

Within the range of depth and slope studied in the flumes, it can be stated that the maximum value as well as the range of P_{max} for which plane bed condition can be achieved increases with increasing fall diameter for a given flume width, but the range of P_{max} for a given sand narrows as the flume width is reduced.

In certain transitions runs, Simons and Richardson (1963) observed that the bed continued to oscillate between washed out dunes and plane bed. However, in general, plane bed under transition and upper regime conditions can be achieved as a stable form. Plane-bed runs are separately analysed in Chapter VII, to evaluate their resistance function.

Effect of Sediment Suspension

Characteristics of turbulent flow discussed in Chapter III are valid for single phase flow of newtonian fluids. In sand-bed channels, the rolling and suspension of sediment particles will change the

flow behavior, even if the bed forms are not present. The effect of suspension of solid particles on the velocity profile has been noted by Vanoni (1946). It was observed by him, and later by Vanoni and Brooks (1957), when comparing velocity profiles in flows with and without suspensions, that the sediment laden flow had a higher velocity at every level and that the velocity gradient was steeper than in the clear water flow. Elata and Ippen (1961) studied the effect of neutrally buoyant particles on the flow. They found that whereas the velocity gradient increased in the region away from the bed, it decreased closer to the bed of the flume. They derived an equation for the velocity profile, which accounted for the effect of concentration on both the Kappa value and the shape of the profile itself.

Though the effect of suspended particles on the velocity profile is not disputed, there is considerable divergence of opinion on the mechanism through which it takes place. Vanoni and Brooks (1963) and Einstein and Chien (1955) believe that the presence of sediment dampens the turbulence and hence reduces eddy viscosity of the flow. Einstein and Chien (1955) proposed a parameter, which is the ratio of the power consumed in keeping the sediment in suspension to the stream power and showed its correlation with the observed Kappa value in flume and river studies. Vanoni and Brooks (1963) found that the Einstein-Chien parameter evaluated for the power required to keep the sediment in suspension over the portion of flow near the bed between $y = .001\ d$ to $.01\ d$, was better correlated with the observed values of Kappa.

The study of Elata and Ippen (1961) was made in a 2 1/2 foot wide, 40 foot long flume, with neutrally buoyant particles of specific

gravity 1.05. Eighty five percent of the particles had diameters between .1 and .155 mm with a uniformity coefficient (D60/D10) of 1.2. The fall velocity of these particles was 0.1 cm/sec in water and volumetric concentrations of 0 to .27 were used. In addition to the general hydraulic and depth measurements, turbulence intensities and spectra in the mean flow direction were also measured for some of the runs. Observations by Elata and Ippen differed from Vanoni's in the sense that the particle concentration was found to reduce the velocity gradient near the bottom of the flume and to increase it (as observed by Vanoni) in the outer region. Also their measurements of $\overline{u'^2}$ showed that its value increased with the concentration instead of decreasing as might be suggested by the hypothesis of dampening of turbulence. Elata and Ippen reasoned that the effect of suspensions was not to dampen the turbulence but to alter the structure of turbulence such that in higher frequencies, the turbulence intensity was increased in the wall-layer and this changed the equilibrium conditions in the outer layer, to result in an increased velocity gradient there.

The value of Kappa was measured by Elata and Ippen, from the tangent to semilogarithmic plot of the velocity profile at the surface. They found that κ thus measured was a function of the linear concentration of particles λ as $\kappa = \kappa_o(1 - .15\lambda)$, where κ_o, the value of von Karman's Kappa in clear water flow, is 0.40. The velocity profile was deduced from their observations as

$$\frac{u_{max} - u_y}{U_{*o}} = \frac{-1}{\kappa_o(1-.15\lambda)} \ln \left(\frac{y}{d} + 0.03\lambda \left(1 - \frac{y}{d}\right)^2\right) \qquad (4\text{-}1)$$

where u_{max} is the maximum velocity at the surface, U_{*o} is the boundary shear velocity, y is the distance from bed and d is the depth of flow.

Hino (1963) developed a theory for turbulent flows with suspended particles. He modified the energy equation for turbulent flow by the inclusion of change in density caused by the suspension. Also by considering that the presence of suspended particles effectively reduces the space available for liquid eddies, he postulated the reduction in turbulent viscous dissipation. He also derived the acceleration balance equation for suspensions to obtain an expression for the mixing length in terms of mixing length of clear water flow, suspension concentration, fall velocity, etc. Incorporating these two concepts in the velocity distribution equation, he integrated the velocity equation and further obtained prediction equations for κ, decay time of eddies, eddy viscosity ε and $\overline{u'^2}$ in terms of the values for clear water flow. Hino applied this to data from Vanoni and Elata and Ippen among others to show the adequacy of his theory. For volumetric concentrations less than 0.01, Hino's equation reduces to Shimura's equation (Hino, 1963) derived from the energy equation for density-varying flow as

$$\frac{1}{\kappa} = \frac{1}{\kappa_o} + \frac{\beta_1(\gamma-1)\, C_v g\, w(d-\delta_v)}{U_{*o}^3(\ln \frac{h}{\delta_v} - 1)} \qquad (4\text{-}2)$$

where

κ and κ_o are the von Karman's Kappa for sediment laden flow and clear water, respectively,

C_v is the average volumetric concentration of sediment in the flow section,

γ_s is the specific weight of the material in suspension,

w is the fall velocity of the material in suspension,

d is the depth of flow,

δ_v is the thickness of the viscous sub-layer,

U_{*o} is the shear velocity and

g is the gravitational acceleration.

Sediment Suspensions as Two-Phase Flow

Flow of solid-water mixtures has also been studied as a two-phase flow problem, in which the interaction of the solid and liquid phases has been considered to a varying degree. A summary of the development of two-phase flow theory is given by Vasiliev (1969). In Appendix A, equations of motion for a two-phase solid water flow are considered and expressions for continuity, concentration and shear are derived for open channel uniform flow. Equation (A-34) gives the shear for these conditions as

$$\tau_{xy} = -\rho\,\overline{u'v'} - (\rho_s - \rho_f)\, u\, w\, c_v \qquad \text{(A-34)}$$

It is not possible to solve this equation on the basis of a phenomenological theory of turbulence (e.g., Prandtl's etc.), because the volumetric concentration c_v is unknown. In one phase turbulent flow in the outer layer the turbulent shear stress is given by

$$\tau_{xy} = -\rho\overline{u'v'} = \tau_o(1 - \frac{y}{d}) .$$

Subscripting the single phase flow as f, Equation (A-34) can be rewritten as

$$\tau_o \left(1 - \frac{y}{d}\right) =$$

$$\tau_{of}\left(1 - \frac{y}{d}\right) - (\rho_s - \rho_f)\, u_y\, w\, c_v$$

Also, in the outer layer

$$\tau_o\left(1 - \frac{y}{d}\right) = \rho\kappa^2 y^2 \left(\frac{du_y}{dy}\right)^2$$

and for small c_v, $\rho \doteq \rho_f$

therefore,

$$\frac{\kappa_o}{\kappa} = \left[1 + \frac{(\rho_s - \rho_f) u_y\, w\, c_v}{\tau_o\left(1 - \frac{y}{d}\right)}\right]^{\frac{1}{2}} \tag{4-3}$$

The average value of κ/κ_o in the outer layer would be the average of the right hand side, over the outer layer. Since u_y and c_v are not known yet, one could replace the local values by average values and a function of the related variables. Thus

$$\frac{\kappa_o}{\kappa} = \left(1 + \frac{(\rho_s - \rho_f)}{\rho_f} \cdot \frac{v \cdot w\, c_v}{U_{*o}^2} \cdot f_1\right)^{1/2} \tag{4-4}$$

where $f_1 = f_1[\bar{u}, \frac{du_y}{dy}, w, c_v, U_{*o}]$. Zagustin and Zagustin (1969), derived a similar form for κ over the whole depth of flow and showed that

$$\frac{\kappa_o}{\kappa} = \sqrt{1 + 96.5 \left(\frac{\rho_s - \rho_f}{\rho_f}\right) \frac{V \cdot w\, c_v}{U_{*o}^2}} \tag{4-5}$$

fits Missouri River and Vanoni's data among others.

All the models of the effect of suspension on the momentum diffusion of flow discussed above, express κ in terms of the flow and sediment concentration parameters. In utilizing the change in κ

for predicting the velocity distribution in flow, the gross resistance of flow or the sediment transport, these parameters are not known *a priori*. Therefore, a prediction of κ cannot be used in formulating a resistance or transport function for flow in sand-bed channels. However, the study of effect of suspensions on turbulent characteristics of flow is important in the context of the theory of turbulent flows in sand-bed channels. For this reason and for eliciting some of the problems involved in defining κ in flow on sand-beds, this subject is dealt with exclusively in Chapter VI.

Effect of Contact Load

In the context of flow over sand-bed channels, the effect of contact load has to be considered at the level of viscous sublayer. In turbulent flow, the absolute thickness of the sublayer is so small that it is generally not possible to make measurements in it. No measurements in viscous sublayers with a rolling grain boundary fully or partly immersed in the viscous layer exist.

In discussing the structure of the inner layer, it has been stated (Chapter III) that in turbulent flow, the reference length for similarity of the flow over a rough boundary is a function of the relative thickness of the viscous sublayer and the roughness size. In the smooth to rough turbulent flow transition, the reference length is a function of the roughness Reynolds number R_{ks}, whereas in the fully rough flow ($R_{ks} > 55$) the reference length is proportional to the roughness size alone. It has also been stated that the viscous sublayer does undergo periodic growths and bursts and that eddies can penetrate into it.

It is easily visualized that when grains on the boundary are moving, additional disturbances in the viscous sublayer are being created by this movement. Depending on the relative size of grains and the sublayer thickness and the intensity of grain movement, the sublayer would be bursting from point to point into turbulent spells more frequently than in the absence of movable grains. Result of this activity would be to decrease the mean thickness of the viscous sublayer. The question about the reference length in the inner layer in such a case cannot be answered directly. Elata and Ippen (1961) in this connection stated: "For flow with a suspension, however, it is doubtful if one can define a laminar sublayer at all".

Apart from the effect on the stability of the viscous sublayer, contact load, by its rotation would also generate additional shear in the boundary. This aspect has been considered by Yano and Daido (1969). Their object was to study and explain the deviation of velocity profiles near the boundary on which the contact load is moving. By considering rotation of a particle and the flow field generated around it, they derived an additional shear term, which was added to the turbulent shear to yield an origin correction (e in Equation 3-10). This term depends on the size, specific weight, rate of transport and angular rotation of the particle. Yano and Daido (1969) studied the velocity profiles in a 30 cm wide flume with spherical particles 7.43 cm in diameter and a specific gravity of 1.44. By introducing some correction (based on other experiments) in the angular velocity of a rolling particle, they were able to show that, with the change in ordinate, a logrithmic profile resulted with a constant $\kappa = 0.40$.

The effect of contact load on flow in sand-bed channels is, therefore, twofold. By influencing the stability of the viscous sub-layer, it alters the roughness of the boundary and by inducing additional shear close to the boundary, it causes a shift in the virtual origin for the logarithmic velocity distribution. Both aspects will be subsequently used in formulating a resistance function for sand-bed channels.

Effect of Bed Porosity

Sand-beds are porous in contrast to rigid boundaries. In natural channels the bed porosity can be important, due to seepage inflows or outflow, in determining the bed form (Simons and Richardson 1963). In flumes, because of the small hydraulic gradients, there can be no tangible net flow through the bed over the flume length. In the dune range, however, because the free surface and the bed form are out of phase, sufficient hydraulic gradients may be experienced over individual bed forms to yield seepage from the upstream slope to the lee slope. (This subsurface flow is perhaps responsible for the difference in the compaction between the two slopes of a dune).

In a plane bed, although there are no local hydraulic gradients imposed on the bed, the porosity can affect the flow close to the wall, in two ways. At an impervious wall, the no slip criterion $(\frac{\partial u}{\partial \eta}|_{\eta=0} \sim 0)$ has to be satisfied at the wall. In porous boundaries the velocity would drop at the boundary, but to a non-zero value. The effective wall surface may therefore be located below the boundary, thereby yielding a larger equivalent roughness size.

Porosity of the wall can also have an effect on the turbulent velocity fluctuations at the wall. For an impervious

boundary these fluctuations have to vanish at the boundary. On a porous boundary they may not vanish, thereby yielding a smaller viscous layer thickness and a higher roughness value. The effect of porosity of the wall on turbulence characteristics of the flow has been studied by Goma and Gelhar (1968). Using an open air circuit, they studied mean velocity and turbulence characteristics of flow through two pipes; one artificially roughened with 1/8" beads and the other lined with an industrial foam of 0.97 porosity and a permeability of $1.3 \times 10^{-6} ft^2$ per sec. Their results show an equivalent roughness size for the porous lining of the same order as the thickness of the lining. They also found that the friction factor instead of becoming independent of the flow Reynolds number, increased with it. For the turbulence characteristics on a porous wall, they found that the turbulence fluctuation $\overline{v'^2}/V$ increased steadily as the wall was approached.

The permeability of sand-beds is much smaller than the one tried by Goma and Gelhar. However, a systematic trend toward decreasing the viscous sublayer thickness and increasing the equivalent sand roughness would be expected on such beds due to the affects of porosity.

Although, it is not yet possible to formulate a theory for turbulent flow in sand-bed channels, some of the differences between rigid boundary and moving sand boundary turbulent flows, reviewed in this discussion, can be qualitatively used in the analysis of flow in sand-bed channels. The concept of different regimes of flow is used in this study, in the formulation of resistance functions by developing different functions for the upper and lower regimes. The influence of bed-porosity and contact load has been shown to increase the

equivalent sand roughness in such channels and to affect the hydro-dynamic roughness of the boundary. This influence is investigated for plane-bed runs in Chapter VII and the results are used in the resistance analysis subsequently made. Influence of large roughness elements in the shape of bed forms and of the contact load has been found to induce a shift in the effective origin of the velocity profile. This is used in Chapter VIII in conjunction with the velocity distribution proposed in Chapter III. The shift in the origin e, the effect of suspension on the turbulent characteristics and the change in eddy viscosity caused by the large roughness elements (bed forms) are all combined in an effective shear velocity in the inner layer, to define a logarithmic velocity distribution based on $\kappa = 0.40$. With this approach, the change of κ value in sand-bed channel flows, needs to be investigated in the outer layer only and this is done in Chapter VI.

CHAPTER V

PROPERTIES OF NATURAL SAND-MIXTURES

In the study of flow and transport phenomena in sand-bed channels, sediment properties enter in two ways. Sediment moving as a contact load determines the shape and angularity of the bed forms, while that moving in suspension effects the turbulence characteristics of flow. Transport of sediment is affected by both the bed forms and the turbulence characteristics of flow. When sediment is moving as a contact load i.e., by rolling or sliding, specific gravity, shape, angularity and size of a particle are the relevant properties affecting the phenomenon. In movement by suspension, the behavior of a particle in a free fall in the fluid also becomes important. A particle in free fall is affected differently by shape, than when it is rolling on the bed. This is particularly connected with the alignment of elongated-flat particles as they are resting on the bed (Lane and Carlson, 1954) and their hydrodynamic stability or instability during free fall (Stringham et al., 1969). If this aspect of the behavior of flat particles is ignored, the relevant properties of a sediment particle are its density, shape, angularity and size.

Properties of Individual Particles

While there is no ambiguity in the definition of density of sand sizes (no flocculation), the shape, angularity and size have been defined variously. Current (1970) definitions for these properties are given in the progress report of the ASCE Sedimentation Committee (1962)

Shape is defined in terms of sphericity, which is the ratio of the surface area of a sphere of the same volume of the particle to the surface area of the particle itself. Wadell's (1933) definition of sphericity is the ratio of the diameter of a circle of the same area as projected by the particle (when resting on its larger face) to the diameter of the smallest circle circumscribing this projection. This is more convenient for sand size particles. In the fall velocity studies of sand grains, the shape is defined by Corey's shape factor $c/\sqrt{ab}$ where a, b and c are respectively the longest, intermediate and shortest mutually perpendicular axes of the particle.

Angularity of a sediment particle is described in terms of its roundness. The roundness of a particle is defined as the ratio of the average radius of curvature of individual edges to the radius of the largest circle that can be inscribed within either the projected area or a cross section of a grain.

Size of sand particles is defined either in terms of the sieve opening diameter through which the particle will just pass or as the sedimentation diameter, which is the diameter of a sphere of the same specific weight and terminal settling velocity as the given particle in the same sedimentation fluid.

Variation of Particle Properties in Natural Sand-Mixtures

Sands found in the beds of natural streams are "product of both heritage and environment" (Pettijohn, 1957). Size, gradation, sphericity, roundness, shape factor and other characteristics of sands are dependent on the lithology and structure of the parent rock as well as on the mechanical and chemical agents acting during transport from

their source of origin and the process of transport. In sands, the lithology and structure of the parent rock becomes less important. The sphericity and roundness of sand sizes are theoretically, mutually independent properties of the particle geometry. In nature, because both the sphericity and the roundness are related to the history of abrasion and transport of the particle, these properties are closely related to each other. Both the sphericity and roundness increase rapidly in the early stages of the particle abrasion but later tend to certain asymptotic values.

Within a single sample of natural sands, the sphericity, roundness and the density do not show much variation. The Corey's shape factor (which is related to the sphericity) is fairly constant around 0.7. The variation of roundness is not as well documented but is generally observed to be about 0.35. The density of particles is fairly uniform and close to that of quartz (2.65). However, the size shows the largest variation of the particle properties within a single sample. Distribution of sizes in a sand sample is usually given either as a frequency or cumulative frequency function of sizes by indicating the fractions of the sample weight in certain size ranges or below certain sizes. The latter method is more common because the frequency distribution curve is dependent on the number of classes selected if such a number is too small.

Size Classes for Sand Mixtures

The original classification of size ranges is due to Udden (Pettijohn, 1957). This classification covered sizes from clay to boulders and as such had to be based on a geometric scale to represent

all size-classes. It used larger units for larger sizes and smaller units for smaller sizes. Udden selected 1 millimeter as the basic scale and derived all other sizes in ratios of 2. This scale had a disadvantage because in well-graded sediments it yielded few classes. The introduction of a $\sqrt{2}$ class interval by Taylor increased the number of size-classes but resulted in odd and irrational sizes. In 1934 Krumbein (1934) proposed his phi-scale to overcome the disadvantage of irrational class limits and mid points. There have been other scales of class limits proposed beside those based on ratios of 2 and $\sqrt{2}$. Somewhat similar to Krumbein's phi-scale, Goncharov (1964) adopted a grouping system in which the classification group number is about twice the logarithm of the average grain size (in microns) of the group. The scale currently accepted in engineering (1971) is the one adopted by the subcommittee on sediment terminology of the American Geophysical Union (1947). This scale which is based on a basic size of 1 mm and a class ratio of 2 is given below:

Scale of Sand and Silt Sizes

Class name	Size limit mm	Size limit microns
Very coarse sand	2-1	2000-1000
Coarse sand	1-1/2	1000-500
Medium sand	1/2-1/4	500-250
Fine sand	1/4-1/8	250-125
Very fine sand	1/8-1/16	125-62
Coarse silt	1/16-1/32	62-31
Medium silt	1/32-1/64	31-16
Fine silt	1/64-1/128	16-8
Very fine silt	1/128-1/256	8-4

Size Distribution Indices for Sand Mixtures

It has long been recognized that the frequency curves of natural sediments are skewed. For such distributions it becomes necessary to specify more than two parameters. In geology, four attributes of measured frequency distributions are frequently used. These are as follows:

(1) Average taken as the median size (50th percentile)

(2) Sorting coefficient as the square root of the ratio of 75th and 25th percentile

$$= \sqrt{D_{75}/D_{25}}$$

(3) Skewness as the ratio of the product of 75th and 25th percentiles to the square of the median size

$$= \frac{D_{75}\ D_{25}}{D_{50}^2}$$

(4) Peakedness or kurtosis measured as

$$\frac{D_{75} - D_{25}}{2(D_{90} - D_{10})}$$

Where D_{75} is the 75th percentile of the measured cumulative size distribution of the sediment sample etc.

Some Reported Characteristics of Natural Sand-Mixtures

Natural sand-mixtures are known to have deficiency of material in certain size ranges depending on their depositional environments. Similarly the modal class in these mixtures falls in a certain well defined size range. For alluvial deposits, the deficiency occurs in 1 - 4 mm size range and the modal class is generally found in 1/8 - 1 mm size range. Different reasons have been adduced in the past for this

phenomenon. In 1914 Udden (Pettijohn, 1957, p. 48) ascribed the deficiency to non-representative sampling. Pettijohn (1957, p. 50) summarized the possible causes of this deficiency by concluding that either such sizes are structurally unstable or that the process of rock disintegration is such that it produces more of certain sizes and less of others. Pettijohn also considered the hypothesis of selective transport, but observed: "Hydraulic considerations might prevent their deposition in some particular place or with certain other sizes but can hardly prevent their deposition everywhere."

Yatsu (1955) studied the grain size frequency curves for the deposits of graded rivers in central Japan. He found that in the case of deposits falling entirely in gravel or sand size ranges, the frequency curves showed only one maximum. For the deposits containing both gravel and sand sizes he found that there were two maxima, one in the sand size range and the other in the gravel size range and one minimum which always fell in 2 - 4 mm size range. Yatsu also observed breaks in the exponential profiles of the river studied by him, which occured when the bed material changed from gravel to sand. He considered the profile of the rivers dependent on the bed material and concluded that the grain size reduction from pebbles (greater than 2 mm size) to sand (less than 2 mm size) is a discontinuous process which rarely produced particles in the range - 4 mm size.

In natural rivers, it becomes difficult to separate a cause from its effects. The river gradient for example is interrelated with the bed and from Yatsu's data it might be argued that the profile is the cause and the change in bed material is its effect. It is probable that the size range of minimum and modal class in natural sand-mixtures is a

result of the chemical and mechanical processes of size reduction as well as the mode of transport. This brings out an area, in which the application of the mode of transport and differential transport of various fractions of a sand-mixture may be important.

Another characteristic of natural sand-mixtures relates to the distribution of sizes within a sample. Some workers like Udden (1914, quoted in Pettijohn, 1957), and Krumbein (1938) came to the conclusion that sediment size frequency follows a lognormal probability distribution Doeglas (1946) on the other hand, found that in the 5-500 micron range, well sorted sediments followed a normal probability distribution. Friedman (1962), after studying some 612 ancient and modern sand samples, concluded that although his samples showed a departure from lognormal distribution in the "tails" as well as in the skewness and kurtosis, the departure was not significant to invalidate the distribution parameters derived from lognormal distributions. In his study, Friedman found an average value of absolute skewness of 0.76 and of kurtosis of 5.31 versus 0.0 and 3.0 for lognormal distributions.

Nordin and Culbertson (1961), in a study of bed-material distribution along the Rio Grande, found that all the distribution curves of the surface-bed-material samples were unimodal and approximated a lognormal distribution. Their study included the reaches above White Rock Canyon where the core samples extended from gravel to sand sizes and were bimodal.

Blench (1952), using river-bed sand data collected by the Natural Research Council of Canada, made a common plot of all data, normalized by dividing with the mean size (circa) of each sample, on log probability

paper. The plot showed that in the cumulative frequency range of 10 to 90 percent the data were lognormally distributed.

An impetus to the adaption of lognormal distribution to particulate matter also came from chemical engineering (grinding processes) and sedimentary petrology. Hatch (1933) pointed out that in the case of non-uniform particulate matter obtained by crushing, chemical precipitation and other means, the frequency of particles by weight is lognormally distributed.

Processes Yielding Lognormal Distribution

The lognormal distribution is so commonly observed in nature that Aitchson and Brown (1957, p.2) state:

"Man has found addition an easier operation than multiplication, and so it is not surprising that an additive law of errors was the first to be formulated. Had man been more adept at multiplication the 'exponential-lognormal', or normal, might have been the derivative distribution".

In general it can be stated that if the processes underlying change are multiplicative the resulting distribution is lognormal just as when the processes are additive, the resulting distribution is normal.

A variate subject to a process of change is said to obey the law of proportionate effect if the change in the variate at any step of the process is a random proportion of the previous value of the variate. Thus if X_j is the value of the variate at j^{th} step and set $\{\varepsilon_j\}$ is mutually independent and also independent of $\{X_j\}$, the process

$$X_j - X_{j-1} = \varepsilon_j X_{j-1}$$

has a proportionate effect. For such a process, assuming that the change at each step is small, it can be shown by the central limit theorem that log X_n is asymptotically normally distributed (See Aitchison and Brown 1957, p. 22)

In the theory of breakage, the proportionate effect can be considered to be operative, if it is assumed that the distribution of sizes at any stage is a function of the ratio of variates at the current and immediately preceding stage. Kolmogoroff (1941), has shown this for a more generalized case. Halmos (1944) and Aitchison and Brown (1957) showed that for such processes the resulting distribution is lognormal. Epstein (1947), assumed a process that is more directly related to the physical breakage, and showed the resultant size distribution of the mixture to be lognormal.

Processes Involved in Generating Natural Sands

The processes involved in the generation of alluvial sediments are more complicated than the simple breakage process assumed by the above mentioned authors. For alluvial sediments, at least two general processes are acting simultaneously; mechanical wear and differential transport.

Mechanical agents working on the particles during transport are mutual impact, abrasion and crushing of the particles. They are defined as "abrasion" due to the mutual rubbing of particles, "impact" due to the collision of particles and "grinding" due to the crushing of smaller particles by larger ones (Krumbein, 1941).

The differential transport of a given mixture merely implies that smaller particles are moved easily and more rapidly than larger particles.

This is of course directly related to the mode of transport. Smaller particles will cover a larger proportion of the distance by suspension, in which case they are traveling at or about the velocity of the surrounding fluid medium. Larger particles, on the other hand, would travel mostly as contact load, which moves at much smaller velocities than the mean velocity of the transporting medium. Even in the case of particles which are moving in suspension, the selectivity of transport for different sizes occurs through the vertical distributions of the concentration of particles and the velocity of flow. In a given flow over a sand-bed the concentration of smaller sizes is more uniformly distributed in the vertical while the larger sizes are more concentrated near the bed. The velocity of flow increases with increasing height above the bed. Thus, among the particles moving in suspension the smaller particles on the whole are transported faster than the larger particles. Therefore, in a given flow, the downstream transport of particles in a sand bed is a function of their size at any stage.

The probability of mechanical wear is dependent on the size of the particle and the presence of other sizes. The product of mechanical wear, in the case of abrasion is "dust" (Krumbein, 1961) and in the case of impact and grinding is both "dust" and larger sizes. Since impact and grinding are of very little importance once the sand size has been reached, the product of mechanical wear in sand sizes can be excluded from resulting size distribution.

In the transport of a given sediment mixture, there always are some particles which are mainly transported by suspension and others which are mainly transported by rolling along the bed. The mean fraction of a step (in space) which a particle travels by

rolling is a function of its size, shape and the hydraulic conditions. Since the chances of abrasion and impact are greater for a particle rolling on the bed than the one in suspension, the probability of mechanical wear of a particle is also dependent on its size.

Processes of mechanical wear and hydraulic sorting can, therefore, be reduced to "processes with proportionate effect" and a theoretical analysis of the asymptotic distribution of the size frequency can be made. This is easier for sand sizes than for the gravel sizes, because the product of mechanical wear in sands can be excluded from consideration. However, evaluation of set c_j is not easy because the hydraulic conditions are implicitly related with the median bed-material size and its dispersion. Also the distributions of suspension and rolling phases of the transport-step of a given size are neither explicit nor the same for other sizes. For example, a discontinuity in the mode of transport occurs when the fine material size range is achieved by a particle. Nevertheless, it is possible to make simplifying assumptions and to relate mechanical wear and hydraulic transport to different powers of the size at any step. The resulting distribution of particle sizes in a mixture is lognormal in such a case.

Relative Importance of Mechanical Wear and Hydraulic Sorting

Sternberg (Lelliavsky, 1955 and Krumbein, 1961) had shown in 1875 that the weight of a pebble decreases exponentially during abrasion. That is, the change in the weight of a particle is proportional to the original weight and the distance travelled by the particle. Thus,

$$W_\ell = W_o e^{-aL}$$

Where W_ℓ is the weight of the particle after traveling a distance L,

W_o is the original weight and a is a coefficient. Sternberg also stated that the gradient of a graded river follows a logarithmic curve. In many natural channels it has been observed that the size reduction of sediments follows an exponential curve as stated by Sternberg's law. (Krumbein, 1941, Rafay, 1964 and others). For a time, it was believed that since the size reduction follows Sternberg's law, the essential mechanism in size and shape change was the one stated by Sternberg.

The mechanical wear of the particles has been studied in tumbling barrels by Daubree (Krumbein, 1941), Wentworth (1919), Schoklitsch (Krumbein, 1941) and others. These experiments showed that for "abrasion", the size, whether typified by weight, volume or length reduces by the Sternberg's relationship, but that the coefficient 'a' is a function of the velocity of movement of the barrel, size distribution of the particles and the kind of rock of the particles. Thiel's experiments (1939) among others also showed that the rate of abrasion of sand is much slower than that of gravels and larger sizes.

It was apparent from tumbling barrel experiments that in sand sizes the rate of wear is too small to explain the size reduction found in natural channels, and that mechanical wear is ineffective as far as the size reduction of sand sizes in natural channels is concerned. The importance of hydraulic sorting in determining the size distribution of alluvial sands was thus established. The effect of transport by suspension on the size distribution was analytically and experimentally studied by Brush (1965). He showed that the size distribution of suspensions at increasing elevation above a bed under active movement changes such that both the median size and geometric standard deviation decrease. Simons et al., (1965) also concluded that in lower regime flows

the median diameter and geometric standard deviation of the transported material are smaller than that of the bed material. (In the upper regime both the parameters approach their values in the bed material).

Advantages of Lognormal Distribution for Natural Sands

There are many advantages in adopting a lognormal distribution to sediment sizes. For example, if a variate is lognormally distributed, then all powers of the variate are also lognormally distributed. This leads to a considerable simplification in the method of analyzing samples for size distribution. Thus in the case of sands if the diameter is lognormally distributed, then the weight of particles is also lognormally distributed, as are all other factors related to some power of the diameter. These include areas projected to the flow (in computing drag), number of particles on the surface, or bed area occupied by different sizes. It is not widely acknowledged that if the percentage of surface area covered by a particular size fraction is assumed to be the same as the percentage of the size fraction in the bed-material sample, then a lognormal distribution is tacitly assumed. Hatch (1933) showed by mathematical analysis and by experiments that with a lognormal distribution the distribution of particle sizes in a mixture can be transferred to the distribution of other properties of the particles. Because of the utility of lognormal distribution in natural sand gradation a brief discussion of three such distributions and of the problem of estimation of their parameters is given in Appendix B.

In the resistance and transport phenomena, the effect of tails of distributions are insignificant if the phenomena are time steady. For example, in the case of resistances to flow, it will be shown that the

grain roughness is related to the 84th percentile. In transport computations, the lower tail is more important because of its greater contribution to the total sediment discharge, than other fractions of equal frequency. However, in natural channels the lower 10 percent of the material is often ignored as the indeterminate fine material load. Thus in the usual analyses of time steady, resistance or transport phenomena, the range of interest of the bed material gradation is from about 10th to 90th percentile. An analysis of bed-material size distribution data was made in this study to test the applicability of lognormal distribution in this cumulative frequency range.

Analysis of Data for Size Distribution of Bed-Material Sand-Mixtures

The data used for studying the size distribution of bed-materials included both river and canal data. For rivers, the bed-material data from Albuquerque and Bernalillo sites on the Rio Grande (Nordin and Beverage, 1965) were selected, and for canals, West Pakistan canal data (West Pakistan Wapda, 1963) were used.

Data reported in all these cases are given as percent finer than standard diameters. For Rio Grande, these diameters vary from .062 to 16 mm increasing in ratios of 2, while for the canals the standard diameters vary from 0.062 to .700 mm increasing in ratios of $\sqrt{2}$. In general these samples do approximate a lognormal distribution in the bulk of the distributions, and also have the usual deviations at the tails.

(i) Normalization of data - Individual samples of bed material can vary from each other for a number of reasons. Surface samples of bed material are affected by the location of the sampling point with respect to the dune, if that happens to be the bed form. Brush (1965)

has shown the mean particle size variation along a dune surface. He concluded that evenly spaced surface samples along the dunes would yield a mean size smaller than that of a core sample.

The constitution of bed material in a natural channel is also dependent on the position of the sampling event in the annual hydrograph. In rivers, the sediment available in the bed depends on the sediment inflow from upstream sections, bank cutting, tributary inflows, etc. Since all these factors are behaving differently at the beginning, middle and the end of the flood season, the bed material varies in both its median size and gradation. For the Rio Grande, Nordin and Culbertson (1961) showed that the median diameters for Bernalillo station for about two-third of a total of 139 observations, fell in the range 0.27 mm - 0.31 mm. This type of variation, but with a large range of median diameters, is also typical of the sand-bed reaches of rivers in West Pakistan. Experience with the sediment samples collected at control structures in West Pakistan in addition indicates a cyclic variation related to the flow hydrograph. Therefore, the canals, which are fed from rivers, are also influenced by the changes in the median diameter and gradation of the transported load in the parent rivers.

In order to obtain a single plot of all the river and the canal data, their bed-material distribution curves were normalized and plotted. The normalization was done by the median size for the location parameter and average quantile standard deviation $[\sigma = \frac{1}{2}(\frac{D_{50}}{D_{16}} + \frac{D_{84}}{D_{50}})]$ for the scale parameter of each sample. The normalized distribution for each sample was made to yield a median size of 1.0 and average (quantile) standard deviation of 1.5.

(ii) Conclusion - The normalized distributions are plotted on log-probability scale for the river data on Figure 5-1 and for the canal data on Figure 5-2. The river data comprise 112 bed-material samples from two similar reaches of a sand bed river (Bernalillo and Albuquerque on the Rio Grande) spread over a period of about 10 years Canal data on the other hand consist of 327 bed-material samples from 13 different canals fed from the five rivers of the Indus Basin (West Pakistan) over June, 1963 to April, 1964. Both sets of data show that for bed-material samples of sand-bed channels, lognormal distribution of size in the bulk of distribution is amply justified.

In order to correct the departure from lognormal distribution at the lower tail, a three parameter lognormal distribution was also tried for the river data. The lower limit in this case was maintained as 0.062 mm because this size generally forms the limit between the fine material and the bed-material load in sand-bed channels. The departure from lognormal distribution increased in this case.

The above analysis shows that in sand-bed rivers and canals, the particle size in bed material is lognormally distributed over about 10 to 90 percent cumulative frequency range. Thus for time steady flow, the size distribution can be described by two parameters : the median size and the geometric standard deviation. These parameters are defined in Appendix B and the relative merits of their methods of estimation are discussed. For application to the sand-mixtures, methods of graphics and quantiles are efficient and convenient. In the graphical method, the cumulative size distribution of a sample is plotted and three quantiles D_{16}, D_{50} and D_{84} are read to define the median and the average quantile standard deviation (σ). With a given D_{50} and

and σ, computation of other percentiles with the help of standard normal distribution tables is an easy matter. Thus, $D_{65} = D_{50}\,\sigma^{0.385}$ and $D_{35} = \sigma^{-0.385}$. Lognormal distribution of sand mixtures in flume, river and canal data were used in this study, in the computation of different percentile sizes, mean sizes of bed material fractions, etc. Use of this approximation to the actual distribution is adequate for most engineering computations relating to steady phenomenon in sand-bed channels.

CHAPTER VI

ANALYSIS FOR von KARMAN'S κ IN FLUME RUNS

Velocity profiles in flow over sand beds are typified by three regions. The region close to the bed is directly influenced by the location of the vertical with respect to the bed form. In ripple and dune runs, the flow separates from the boundary at the crest of the bed form to reattach on the upstream slope of the next form. A vertical located over one of the eddy zones experiences reverse flow in this zone and with the usual observations of velocity, it becomes difficult to define an origin for the depth in the profile. In plane and standing wave runs, there is no eddy zone, but the effects of contact load and the uncertainty about the location of origin for depth, introduce a curvature in the velocity profile. In a region close to the surface, there is a "cut-back" in the velocity profile caused by the secondary current. In the middle zone between the surface and the lower zones, the velocity profile is less effected by an error in the location of origin for y (because of larger absolute values of y) or by secondary currents. However, in this region if the bed forms are large compared to the depth of flow, the profile reflects the accelerations and decelerations of flow that occur with varying depths as the flow travorses the bed forms.

In addition to the variation in velocity gradient observed in the lower and middle regions along the length of a bed form, the distribution of velocities in a flume is affected by the three dimensionality of the bed forms. To gauge this variation in flume runs, the average velocity in individual profiles was checked against the average velocity of the runs obtained by dividing the total discharge over the mean flow depth

and width of the flume. It was found that, in general, the average velocity observed in the verticals varied from 0.8 to 1.2 times the mean velocity in the section.

The above description indicates that no individual velocity profile in sand-bed flumes can be considered representative of the average flow. In natural channels, the variation of depth in a cross section related to the channel curvature in plan is generally of a greater magnitude than the variation in depth along the bed form and the above effect is not generally noticed.

Ignoring the acceleration effects, the velocity profile in the middle region corresponds to the outer layer of the rigid boundary flow where the velocity defect law (Equation 3-3) applies. For matching the wall-law and defect-law in the overlapping region, constant A corresponds to the reciprocal of von Karman's κ. The function $B[\frac{U_{*o}}{U_{max}}]$ of Equation (3-3), is not known in rigid boundary flow except that its dependence on $\frac{U_{*o}}{U_{max}}$ is weak and generally B is taken as a constant. Equation (3-3) would plot as a straight line on semilog paper and the slope of the velocity profile would give the value of Kappa as

$$\kappa = 2.303\ U_{*o}/(u_2 - u_1) \qquad (6\text{-}1)$$

where

U_{*o} is the shear velocity $\sqrt{\tau_o/\rho}$ and

$(u_2 - u_1)$ is the difference in velocity over one log cycle.

In the presence of local acceleration of flow, the observed value of κ increases because the accelerated flow tends to be more uniformly distributed in the vertical. For decelerations, the effect may be the opposite. Downstream of the bed forms, where wake effect of roughness

elements is present, values of κ may increase or decrease depending on the relative effects of deceleration and the wakes. If one can accept the concept of an average velocity profile in a sand-bed flume based on spatial average of velocities observed in a plane along the mean direction of flow at specific heights above the mean bed, the slope of this profile in the middle region would correspond to the value of κ defined in Equation (6-1). In the absence of such an observation, if the verticals are assumed to be randomly located with respect to the bed forms, it can be argued that with a large sample, the dependonce of κ on alluvial flow parameters may still be studied. It is understood that the accuracy of such a derived correlation between κ and the flow parameters, would fall with an increasing noise (change in κ due to local acceleration effect) to signal (change in κ due to alluvial flow parameters) ratio.

Analysis of κ for Flume Data

In the flume data, velocity profiles have been observed for 252 runs out of the total 339 runs. Seventeen of these runs have no sediment discharge because $\tau_o < \tau_c$. For the 8 foot flume, the section in which the velocity profiles were observed, was located from 95-115 feet from the head box. In general, velocity profiles on three verticals at 1/4, 1/2, 3/4 width from the wall were observed. In some runs only one vertical at the middle of the section was used.

In this study, all the velocity profiles were plotted as log of the distance from bed versus the local velocity. This distance is measured from the local bed and depending on the location of vertical with respect to the bed form, the total depth in the vertical may be more or less than the mean depth of flow. Some typical profiles for

different bed forms are shown in Figures 6-1 through 6-14. From a study of some 650 profiles it was noticed that the lower region extended on the average to about ten percent of the local depth and the upper region constituted about twenty percent of the local depth. These two regions were excluded from the analysis for κ. In certain velocity profiles the average height of the bed form above the mean bed elevation was more than one-tenth of the local flow depth. In such cases the portion of flow close to the boundary and excluded from the analysis of velocity profile was increased to one and a half times the average height of the bed form above the mean bed elevation. Velocity profile in the central region thus defined corresponded to the outer-layer discussed in Chapters III and IV for the turbulent boundary layer flows on rigid and moving sand boundaries, respectively.

To determine the value of κ from Equation (6-1), the slope of the logarithmic velocity profile in the central region and the shear velocity are needed. The slope was determined by fitting a straight line through the logarithm of distances y from the bed and the corresponding point velocities u_y. This line was obtained by a least square regression of log y versus u_y (Draper and Smith, 1966). For eliminating the verticals in which a logarithmic velocity profile could not be defined, the goodness of fit of the regression line was checked by computing Student's T parameter and testing the null hypothesis H_o at an α level of 0.95. The velocity profiles for which H_o was true at this α level or which had fewer then three velocity points were eliminated from the analysis.

The average shear velocity, U_{*o} in the flow section was computed as $\sqrt{gdS}$ and the values of κ were computed from Equation (6-1) for

each observed vertical in the flow section. The value of κ for a flow section was assumed as the average of κ values obtained from the individual verticals. This value is labelled κ_1.

Shear velocity in the vertical may also be defined as the local shear velocity $U_{*o\ell}$ based on the local depth, d_ℓ. Average values of κ in the flow sections were also computed with $U_{*o\ell}$ and labelled κ_2.

An attempt was also made to generate a composite velocity profile in the central portion of flow depth. This was done by normalizing the individual velocity profiles in a section over local depths and average velocities in the verticals and treating the combined normalized profiles as one profile. The κ value from the composite normalized velocity profile was computed on the basis of U_{*o}. This value is labelled κ_n.

Various parameters have been suggested in the literature for possible correlation with κ in sand-bed channels. Some of these have already been introduced in Chapter IV in the discussion of the effect of suspensions. In general, the region of flow over which these parameters are supposed to predict the value of κ are not detailed. As seen from the discussion of velocity profiles on sand-bed channels, one logarithmic velocity distribution cannot be applied to the whole depth of flow. Nevertheless, all the parameters reportedly correlated with κ were computed for each flume run and their correlation with κ_1, and κ_2 and κ_n values were studied. These parameters are described in the following paragraphs.

Parameters Studied

(i) Einstein-Chien parameter - The Einstein-Chien parameter, as defined by them (1954) is the ratio of the power consumed in supporting the suspended load to the total power expended by the flow. This is written as

$$\sum_{i=1}^{n} \frac{C_t w}{V \cdot S} \cdot \frac{\rho_s - \rho_f}{\rho_s} \qquad (6\text{-}2)$$

where

C_t is the concentration by weight of sediment in the vertical of a size fraction;

w is the fall velocity of the size fraction,

V is the mean velocity of flow,

S is the energy gradient and

ρ_s, ρ_f are the mass densities of the sediment and the fluid, respectively. The summation is over the number of size fractions in which the suspended load is divided.

Einstein's definition of suspended bed-material load (1950) extends up to a bed layer of thickness equal to twice the mean grain diameter of each size fraction. With bed forms other than plane, the concept of bed layer becomes artificial, and so does the definition of suspended load of a stream. This becomes more important in the case of coarser sediments or lower regime runs, where the concentration of suspended load rapidly falls away from the bed. In natural channels, a zone of flow close to the bed, cannot be sampled due to the sampler shape, design and the use of weights when sampling in large streams. Only if the channel depth is large and the bed-material is of medium size, the

error introduced by the unsampled zone will be small. The concentration C_t in Equation (6-2) thus remains a somewhat ambigious quantity.

The sampled concentration for suspended bed-material load is reported for the flume runs in USGS Professional Paper 462-I along with the concentration of fine sediment (bentonite clay) when it was used. The median size of the suspended bed-material load for individual runs is also given for runs in Tables 2 through 9.

Suspended load sampling in shallow flume runs is particularly subject to errors due to direct suction of the material from the bed or due to sampling of an eddy with sediment concentration different from the average. The large standard deviations of repeated samples of suspended bed-material load reported for the flume runs are indicative of the error involved in suspended load sampling in shallow sand-bed channels. In transition and upper regime runs, especially with medium sands, the suspended load forms a major proportion of the total load. In such cases, errors in the sampling of the suspended load may exceed the bed load itself. Some runs in the data, show larger measured suspended load than the total load on this account. In view of this uncertainty in the measurement of suspended load, the Einstein-Chien parameter was calculated on the basis of the total load concentration. The median diameter of the suspended load in sand-bed channels is always smaller than that of the bed-material. For the flume runs, the average of the median diameters of the sampled bed-material suspended load for individual runs was computed for the whole series of runs for each sand. This average median diameter corresponded to about 9th to 26th percentile of the bed-material of each series. For six sands (Tables 2, 4, 5, 6, 7 and 8 of the flume data), the average suspended

bed material load size was related to 12th - 18th percentile of the respective bed-material. As an average, the median bed-material suspended load size was assumed as 16th percentile of the bed-material, D_{16}.

The fall velocity of a sediment particle in a fluid is affected by the specific gravity, shape and roundness of the particle as well as by the mass density and the viscosity of the fluid. The terminal fall velocity w, is given by

$$w = \sqrt{C_D \frac{4}{3} \left(\frac{\rho_s - \rho_f}{\rho_f}\right) g D_n}$$

where

D_n is the nominal diameter of the particle (i.e., the diameter of a sphere that has the same volume as the particle),

C_D is the drag coefficient for the terminal fall velocity and all other terms have been defined earlier.

The drag coefficient C_D in the case of naturally worn sediments is related to the fall velocity Reynolds number $\left(\frac{wD_n}{\nu}\right)$ and Corey's shape factor $(c/\sqrt{ab})$. Graphical relations for C_D are available in the Inter-Agency Committee on Water Resources' Report No. 12 (1958).

Rubey (1933) had provided an equation to determine the fall velocity of sands as

$$w = \frac{\sqrt{\frac{2}{3} g(S_s - 1)D^3 + 36\nu^2} - 6\nu}{D} \qquad (6\text{-}3)$$

where

S_s is the specific gravity of sand,

ν is the kinematic viscosity and

D is the particle diameter.

Although, Equation (6-3) does not account for the shape and other geometrical properties of the particles it was used to determine the fall velocity in this study because of the facility of its use on the computer. The fall velocities were based on the actual kinematic viscosity ν reported for each run.

The expression for the Einstein-Chien parameter was derived as follows:

$$\frac{1.65}{2.65} \cdot \frac{C_t w_{16}}{V \cdot S} \quad . \tag{6-4}$$

where

w_{16} is the fall velocity for D_{16} and all other terms have been defined earlier.

As an alternative to the use of suspended bed-material load size of D_{16}, the Einstein-Chien parameter based on D_{35} was also computed as

$$\frac{1.65}{2.65} \frac{C_t w_{35}}{V\ S} \tag{6-5}$$

where

w_{35} is the fall velocity of the 35th percentile size of the bed-material.

(ii) Shimoura's prediction equation for Kappa - An approximation of Hino's prediction equation for κ for small concentrations is given by Shimoura's Equation (4-2). A value of β in Equation (4-2) was given by Shimoura as 4.8. It will be subsequently shown that in the flow with sediment movement on the boundary the roughness is independent of viscosity and that the equivalent grain roughness is given by D_{84}. Shimoura's prediction equation was thus written as

$$\frac{1}{\kappa} = \frac{1}{\kappa_o} + 4.8 \frac{(\rho_s - \rho_f)}{\rho_f} g \frac{w(d - D_{84})\, c_v}{U_{*o}^3 \left(\ln \frac{d}{D_{84}} - 1\right)} \tag{6-6}$$

where

κ_o is 0.40,

w is the fall velocity of the representative size,

d is the depth of flow,

D_{84} is the 84th percentile size of the bed-material and

C_v is the volumetric concentration of the total transport, given by $C_t/(2.65 - 2.65\, C_t)$, C_t being the concentration of total transport by weight (PPM x 10^{-6}).

As for the Einstein-Chien parameter, two values of κ were computed from Equation (6-6); one based on w_{16} and the other on w_{35}.

(iii) Fall velocity-bed diameter Reynolds Number - Abdel-Aal (1969) had reasoned that since the upward velocity of an eddy close to the bed can be assumed to be a function of the kinematic viscosity of the fluid near the bed divided by the size of the grain roughness (ν/D), a ratio of the fall velocity of the particle w and the parametric velocity ν/D, would give a measure for the change in the value of κ. He used w_{35} for the fall velocity and D_{65} for the grain roughness. For some flume and river data, Abdel-Aal found that he could define a graphical relation between this parameter and the the value of κ.

The parameter $D_{65} w_{35}/\nu$, which has the form of a Reynolds number was also computed using two combinations of fall velocity and roughness size as follows:

$$\frac{D_{65}\, w_{35}}{\nu} \tag{6-7}$$

and

$$\frac{D_{84}\ w_{16}}{\nu} \tag{6-8}$$

Since these parameters are only dependent on sediment and the fluid properties and they do not involve the flow parameters, it does not seem correct to use these as predictors of κ. However, these two parameters were studied along with others.

(iv) Elata-Ippen's linear concentration - In the analysis of a sheared grain dispersion Bagnold (1956) introduced the linear concentration λ as the ratio of grain diameter and the mean radial separation distance between grains. This is related to the volumetric concentration of particles as

$$\lambda = \frac{1}{\left(\frac{C_o}{C_v}\right)^{\frac{1}{3}} - 1} \tag{6-9}$$

where

C_v is the volumetric concentration of the solid particles and

C_o is the maximum possible value of C_v.

Elata and Ippen (1961), also found that the κ value obtained from velocity profiles of flow with neutrally buoyant particles was related to λ as

$$\kappa = \kappa_o\ (1 - .15\ \lambda) \tag{6-10}$$

The ratio between volumetric concentration C_v and λ was experimentally determined in their study for the particles used.

Hino (1963) had also considered the reduction in effective space for the liquid to dissipate energy by turbulent viscosity as proportional to $(1 - \alpha^3 C_v)$, where α is the ratio between the effective diameter

and the diameter of the solid particle, and C_v is the volumetric concentration of sediment in suspension. For sediment mixtures in the sand range, average values of the maximum possible concentration of particles C_o can be obtained from soil mechanics texts. Terzaghi and Peck (1948) give values of porosity of sands as follows:

Uniform sands, dense	$n_o = 0.34$
Mixed grain sand, dense	$n_o = 0.30$
Uniform sand, loose	$n_o = 0.46$
Mixed grain sand, loose	$n_o = 0.40$.

The maximum volume concentration C_o is given by (1 - min. porosity). For flume sands, a value of C_o was adopted as 0.70, corresponding to dense mixed grain sands. Both λ and $(1 - .15\lambda)$ were studied for possible correlation with κ.

(v) Two-phase flow parameter - In Chapter IV, a relation between the κ value for clear water flow and flow with suspended sediment, was derived (Equation 4-5) on the basis of the shear stress obtained in the flow with the sediment suspensions taken as a two-phase flow.

In Equation (4-5), f_1 accounts for the replacement of the integration over the outer layer of the term containing the velocity u_y, the suspended load concentration c_v and the median size of the suspended load by their average values in the flow section. The analysis of data showed that a constant numerical value of 30 for f_1 with D_{16} as the representative size of the suspended load yielded better correlation with the κ values than other combinations of values of f_1 and representative suspended load sizes. Therefore, a parameter T_f, representing the effect of sediment suspension on κ on the basis of the two-phase flow was defined as

$$T_f = \left(1 + \frac{30(\rho_s - \rho_f)}{\rho_f} \cdot \frac{V\, w_{16}\, C_v}{U_{*o}^2}\right) \tag{6-11}$$

where

V is the average velocity of flow,

C_v is the volumetric concentration of total transported load (including the fine material load)

w_{16} is the fall velocity of the bed material D_{16} at the given viscosity,

U_{*o} is the shear velocity and

ρ_s, ρ_f are the mass density of the sediment and water, respectively.

In addition to the above parameters the Froude number of the flow and the (dimensionless) Chezy's resistance coefficient $C/\sqrt{g}$ were also computed for all the flume runs. Chezy's $C/\sqrt{g}$ is the ratio of mean velocity to the bed shear velocity. This parameter represents the overall resistance to flow and hence the effect of bed forms and other resistance characteristics of the flow. Froude number is important because of its effect on the bed forms and other characteristics of open channel flow.

The values of some of the parameters defined above and of the κ values κ_1, κ_2 and κ_n for all the flume runs are tabulated in Appendix C for reference.

Prediction of κ

As discussed earlier in this chapter the values of κ obtained from the individual velocity profiles are not representative of the "average" vertical velocity distribution in the flow section. Individual velocity profiles are influenced by their location with

respect to the bed forms. An unknown disturbance is, therefore, present in the computed values of κ_1, κ_2 and κ_n. Assuming that the velocity profiles are randomly located over the bed forms, the deviations from the "true" values of κ can be considered as a random component. A statistical analysis of κ can then be made to bring out the parameters most closely related with it. A gross assumption of the randomness of the location of velocity profiles with respect to the bed forms was made in this study.

Of the three kappas computed for each run κ_2 (the value based on local shear-velocity) and κ_n (the value obtained from normalized composite velocity profile) suffered from greater random variation and hence showed poorer correlation with the parameters considered. Therefore, after considerable analysis κ_2 and κ_n were dropped.

Out of 252 runs for which κ values were computed, 17 were dropped because they were without transport and 22 runs were dropped because the least square fit on the logarithmic velocity profile was not significant at an α level of 0.95. The velocity profiles for the remaining 213 runs were further classified, subjectively, as "good" and "poor". Sixty-five of these runs, which included many dune bed runs, were considered "poor", because the effect of bed form on the velocity distribution extended beyond the mean height of the form above the mean bed. This could have been caused by the presence of a bed form larger than the mean height of the forms. The statistical analysis was made for the 148 runs considered acceptable while the prediction parameters were tested for both the "good" and the "poor" runs.

The values of κ_1 are plotted against Einstein-Chien parameters in Figures (6-15) and (6-16). Points corresponding to various runs are

represented by a letter symbol related to the bed form. Letters R, D, T, P, S, A and C stand for ripple, dune, transition, plane, standing wave, antidune and chute-pool, respectively. Also plotted on these figures is the curve given by Einstein and Chien. Out of 148 points plotted in these figures, only about a score fall on or about their curve. All other points plot much higher. According to the description of velocity profiles presented earlier, a correlation between either of the parameters and κ_1 would have yielded an even spread about the prediction curve. If such a correlation was derived from this data, the prediction curve would be much higher. As shown subsequently, some other parameters provide a better correlation with the observed kappa values.

Figures (6-17) and (6-18), show the observed κ_1 values versus the values computed from Shimoura's Equation (6-6) for w_{16} and w_{35}, respectively. Lines of perfect agreement are also drawn on these figures. An attempt was made to improve the correlation between the observed values of κ and those predicted from Equation (6-6) by using values of β different from its value (4.8) given by Shimoura. However, no definite improvement could be made by such a change.

Plots of volumetric concentration C_v and linear concentration λ versus computed κ, are shown in Figures (6-19) and (6-20). For C_v, a minimum envelope for κ can be drawn. Figure (6-21) shows $(\kappa_o/\kappa_1)^2$ plotted against $1.65\ C_v w_{16} V/U_{*o}^2$ (Equation 6-11). Particle size-fall velocity parameters $w_{35}\ D_{65}/\nu$ and $w_{16} D_{84}/\nu$ are plotted in Figures (6-22) and (6-23). As expected, no correlation between these parameters and the observed kappa values is apparent.

Statistical Analysis

As shown by Figures (6-15) through (6-23), the parametric relations so far suggested are not adequate for predicting the values of κ obtained from the flume runs. Considering the presence of a random disturbance in the computed values of κ_1, a statistical analysis was made to bring out the parameters most closely related with κ_1. This was done by a stepwise regression (Draper and Smith, 1966) of the logarithm of κ_1 versus the logarithms of all the parameters studied in the above.

Statistical relations in contrast with functional relations do not have the implication of causality. However, functional relation may have to be derived from statistical analysis, when the independent and dependent variables suffer from random errors. The problem of determining the relation between κ_1 and the flow and sediment parameters is akin to the investigation of a functional relationship, between the dependent variable κ_1 in which random fluctuation are present and the independent variables in which measurement errors possibly exist. Another problem, inherent to the field of sedimentation is that of mutual interdependence of the independent variables. In the general problem of flow of water in a self formed sand-bed channel, none of the variables can be strictly considered independent. It is only in regard to the time scale of a phenomenon in this field, that one of the variables may be taken as dependent and others as independent. This complexity of mutual interaction has been discussed in the earlier chapters of this study. In the present context, it can be briefly restated that the mass diffusion of the fluid is influenced by the form of the boundary and the sediment in suspension and at the same

time the boundary and the suspended sediment are strongly influenced by the flow established in the section. Statistical analysis, in such cases can be used to bring out the relative importance of various interdependent variables and a causal relation can only be adduced from the consideration of the physical phenomenon.

Stepwise regression, in general, proceeds from a correlation matrix of the dependent and all the independent (though mutually dependent) variables. The variable selected for regression is the one most highly correlated with the dependent variable. After removing the effect of this variable the method is repeated with the remaining variables. This is done until either the desired level of correlation is obtained or the remaining variables are not significantly related.

In the stepwise regression, the correlation matrix indicated that the parameter most highly correlated with κ_1, is the Froude number F of the flow. After removing the effect of F, the next highest correlation was found with the gradation σ of the bed material. In the next two steps, parameters T_f (Equation 6-11) and Chezy's $C/\sqrt{g}$ were the ones most highly correlated with κ_1. The following regression equations were obtained in the 4 successive steps.

$$\kappa_1 = \frac{0.528}{F^{0.21}} \tag{6-12}$$

$$\kappa_1 = 0.282\,\frac{\sigma^{0.34}}{F^{0.22}} \tag{6-13}$$

$$\kappa_1 = 0.298\,\frac{\sigma^{0.34}}{F^{0.19}\,T_f^{\,0.10}} \tag{6-14}$$

$$\kappa_1 = 0.446\,\frac{\sigma^{0.34}}{F^{0.15}\left(\frac{C}{\sqrt{g}}\right)^{0.15}\,T_f^{\,0.11}} \tag{6-15}$$

The computed κ values are plotted versus these parameters in Figures (6-24) through (6-27). The best correlation is given by the Equation (6-15). A discussion of the variables in the dimensionless parameter involved in Equation (6-15) can now be made.

Daranandana (1962) worked with two sands of median diameter 0.33mm but different geometric standard deviations (1.25 and 2.07) to study the effect of bed material gradation on flow in alluvial channels. He noted, "...The resistance to flow covered by form roughness of the graded sand is lower than for the uniform bed material with the ripples, dunes, transitions and antidunes as bed roughness". He explained the higher form roughness experienced with the uniform sand in terms of the relative shapes and sizes of the bed forms experienced with the two sands. In general, Daranandana found that the ripples formed with the uniform sand were more angular and larger in both length and amplitude than those formed with the graded sand. With dunes, he found that the dunes with ripples superposed on their back were formed in the case of uniform sand but not with the graded sand. In the antidune range both the amplitude and amplitude-length ratio of the antidunes formed with the uniform sand were greater than those experienced with the graded sands.

It appears that the more angular bed forms of the uniform sand increase the turbulence generation in the inner layer and the diffusion of small scale turbulence to the outer layer is consequently increased. This changes the equilibrium condition in the outer layer and increases the mean velocity gradient in it. Value of κ in the outer layer would then be smaller in the case of uniform sands as reflected by Equation (6-15).

The relationship between the κ value in a two phase flow containing sediment in suspension was derived in Chapter IV (Equation 4-5) as inversely proportional to the square root of T_f. In Equation (6-15), the index of T_f is found as 0.11 against 0.5 predicted in Equation (4-5). Parameter T_f involves the average velocity V, the shear velocity U_{*o}, the total volumetric concentration C_v and the fall velocity w_{16}. Therefore, it is related to the Froude number F and resistance coefficient $C/\sqrt{g}$. The reduction of the exponent of T_f from 0.5 predicted on the basis of two phase flow analysis to a value of 0.11 in Equation (6-15) is caused by its interdependence on other parameters in the equation and therefore, is understandable.

The Froude number F, determines the relative phase of the bed and the water surface. The interaction between the two is therefore, related to F. In subcritical flow, the increment in average velocity of flow over a positive step would increase with increasing Froude number of the approaching flow. In supercritical flow, the water surface is in phase with the bed and the decrease in average velocity over a similar step, would be more with higher F values of the approaching flow. Thus, the effect of increasing the Froude number in both subcritical and supercritical flow is to increase the successive acceleration and deceleration as the flow traverses the bed forms. This should result in a more uniform velocity distribution in the outer layer with an increased κ value. Relation between κ_1 and F in Equation (6-15) is, however, opposite to this.

Kappa values were observed by Sayre and Albertson (1963) in subcritical flow over cleat roughness elements in an open channel flow. These values were obtained by fitting a straight line to that portion of the velocity profile, which followed the log-velocity relation.

The Froude numbers for different runs computed from the data given by Sayre and Albertson (1963, Table 1) are plotted against κ in Figure (6-28). It is seen that (for higher roughness concentrations) κ increases with an increasing Froude number as argued above. The contradiction between the rigid boundary and alluvial channel flow cannot be explained at present and must be connected with the behavior of the bed forms with the Froude number of flow.

Chezy's dimensionless resistance coefficient $C/\sqrt{g}$ is the ratio of mean velocity to shear velocity. In the review of rigid boundary turbulent flow, it was stated that in the outer layer velocity defect law (Equation 3-3), B has a dependence on U_{*o}/U_{max}. This does not imply a dependence of Kappa on this factor. In log-velocity equations for rigid boundary flow, a higher value of κ is associated with a lower value of the resistance coefficient of flow and vice versa. The relation between κ_1 and $C/\sqrt{g}$ in Equation (6-15) indicates a similar trend.

The above discussion of the parameters contained in equation (6-15) indicates that in sand-bed channels, Kappa in the outer layer is related to the total suspended load as well as to the parameters representing the shape, concentration and angularity of the bed forms. This conclusion is significant because so far studies of Kappa value have been generally restricted to the effect of the suspended load.

In rigid boundary turbulent flow, von Karman's Kappa is taken as a universal constant, in spite of the variation observed in Nikuradse's data by Vanoni (1953). In sand-bed channels, it is not only difficult to define a typical velocity profile, but these profiles are also characterized by two breaks. Therefore, an average slope of the profile

over the whole depth has no significance. The prediction Equation (6-15) has been determined from shallow flume flows and these data show greater variation in the profile slopes due to the effect of bed forms. It is not discernable with the data in hand, as to how this equation works for field channels. However, the advantages of deriving this equation from flume data, have been the use of a larger range in the values of bed material standard deviation, Froude number and Chezy's $C/\sqrt{g}$, than are available in the data for natural channels. This prediction equation is empirical and restricted to the data from which it has been derived.

In rigid boundary hydraulics κ is taken as a constant. However, Kappa enters the resistance equation. If a resistance equation for sand-bed channels of the same type as the logarithmic velocity equations has to be derived, can Kappa be incorporated in that? Equation (6-15), is unsuitable for this purpose because it contains the mean velocity and average concentration of total sediment load which cannot be determined unless both the resistance and transport functions have been solved. Hence, this study of Kappa perhaps cannot be used in the transport and resistance functions, but is useful in as much as it gives a clue to the behaviour of the mixing process in the flow over sand bed channels and its related variables.

CHAPTER VII

RESISTANCE FUNCTION FOR PLANE SAND-BED FLOWS

The characteristics of turbulent flow in rough and smooth channels has been discussed in Chapter III. For engineering purposes, a resistance function is required which relates the overall resistance to flow with fluid properties, geometry of channel section and roughness characteristics. A useful measure of resistance is provided by the Darcy-Weisbach friction factor f, which is dimensionless and is defined as

$$f = 8 \left(\frac{U_{*o}}{V}\right)^2 \tag{7-1}$$

where

V is the average velocity of flow and

U_{*o} is the shear velocity $\sqrt{\tau_o/p}$.

The logarithmic velocity distribution (Equation 3-1) can also be written as

$$\frac{u_y}{U_{*o}} = A \ln \frac{y}{y_o} \tag{7-2}$$

where

y_o is the distance from the boundary at which the velocity is zero. Equation (7-2) may not represent the actual velocity distribution close to the boundary (e.g., viscous sublayer), but is convenient for analyzing the resistance to flow in terms of some universal parameters.

The value of A is given by the mixing length theories as the reciprocal of von Karman's κ. Numerical values of κ and y_o have

been obtained from Nikuradse experiments on artificially roughened pipes as $\kappa = 0.40$, $y_o \doteq 0.1\ \nu/U_{*o}$ for smooth-turbulent flow and $y_o \doteq k/33$ for rough-turbulent flow. The resistance functions for the turbulent flow in pipes are (Schlichting, 1968)

$$\frac{1}{\sqrt{f}} = 2.0 \log (4.51 \frac{RU_{*o}}{\nu}) \tag{7-3}$$

for the smooth boundary and

$$\frac{1}{\sqrt{f}} = 2.0 \log (14.8 \frac{R}{ks}) \tag{7-4}$$

for the rough boundary[1],

where

R is the hydraulic radius of the pipe,

ks is Nikuradse's roughness height and

ν is the kinematic viscosity.

Equations (7-3) and (7-4) can be written in terms of y_o as

$$\frac{1}{\sqrt{f}} = 2.0 \log (.451 \frac{R}{y_o}) \tag{7-5}$$

In order to obtain one resistance function for the whole range of smooth-turbulent to rough-turbulent flow, Colebrook and White (1939), combined values of y_o for the two regimes as

$$\frac{1}{\sqrt{f}} = -2.0 \log (\frac{ks}{14.8R} + \frac{2.51}{R\sqrt{f}}) \tag{7-6}$$

---

[1]Value of the coefficient on the right hand side was found by Prandtl as 2.0 from Nikuradse's data. For a value of $\kappa = 0.40$, the value of the coefficient would be 2.03 instead of 2.0.

For open channel flow, Keulegan (1938) applied the log velocity law to Bazin's data to obtain equations which can be written as

$$\frac{1}{\sqrt{f}} = 2.03 \log \left(3.67 \frac{RU_{*o}}{\nu}\right) \tag{7-7}$$

for the smooth channels, and

$$\frac{1}{\sqrt{f}} = 2.03 \log \left(12.27 \frac{R}{ks}\right) \tag{7-8}$$

for the rough channels, where ks is the equivalent roughness in terms of Nikuradse's sand.

For subcritical flow in smooth rectangular channels, Tracy and Lester (1961) developed the resistance function

$$\frac{1}{\sqrt{f}} = 2.03 \log \left(2.59 \frac{RU_{*o}}{\nu}\right) \tag{7-9}$$

A resistance function covering the smooth to rough-turbulent range for open channel flow was given by Thijsse (Silberman, 1963, p. 106) as

$$\frac{1}{\sqrt{f}} = 2.03 \log \left(\frac{12.2\ R}{0.282\ \delta_v + ks}\right) \tag{7-10}$$

Where δ_v is the viscous layer thickness ($11.6\ \nu/U_{*o}$) and ks is the equivalent roughness size. Einstein (1950), also gave a function for effective roughness in the transition zone which is similar to the transition function obtained from Nikuradse's data (Schlichting, 1968 Fig. 20-21).

The sand roughness used by Nikuradse consisted of uniform size sand grains, tightly packed and glued to the wall. This roughness is accepted as almost a standard roughness and other roughnesses (k) are

expressed in terms of it as equivalent sand roughness (ks). Some values of ks/k quoted by Colebrook and White (1937) are given below:

Surface	ks/k
Uniform sand 0.35 mm diameter	1.36
Hamburg sand 1.35 mm diameter	1.64
Cup-head rivets touching 2.6 mm radius	1.40
Polished spheres touching 4.1 mm radius	0.63
Cup-head rivets, 5 diameters apart, 2.6 mm radius	0.12

For studying the effect of sand mixtures, Colebrook and White (1937) used a basic roughness of 0.35 mm diameter sand grains with different patterns of 3.5 mm diameter grains. They found that the large grains, even in small proportions, increased the roughness substantially. For example, with large grains covering 2.5 percent of the area, the resistance factor increased by about 15 percent.

In flow on sand-beds consisting of sand mixtures, a question arises about the equivalent roughness size. Different measures have been suggested for this in the literature. Einstein (1950) adopted D_{65} as the equivalent roughness ks. Meyer-Peter and Muller (1948) defined D_{90} as the roughness size. Goncharov (1964) recommended that D_{95} be taken as the roughness size, while Engelund (1966) stated that $2\ D_{65}$ is the equivalent roughness size. Richardson (1965) found in the analysis of plane bed runs that the representative roughness size is given by D_{85}. An effort will be made in this study to resolve this question of representative roughness.

Another problem in the analysis of laboratory studies of sand-bed channels is that of difference in the roughness between the smooth flume walls and the rough sand bed. If hydraulic mean radius is used as the

measure of flow depth and geometry, a scale effect is introduced due to varying proportions of wall and bed in different width-depth ratios. Some correction to hydraulic mean radius is thus considered necessary. This has been conventionally done by applying a wall correction after Einstein (1942) and Johnson (1942).

Correction for Side-Wall Friction

The concept of separating the wall friction from bed friction was given by Einstein (1942) as:

"The first assumption is that the entire cross section can be divided into units that will correspond to similar units of the wetted perimeter so that the potential energy of the area unit is transferred into eddy energy along the corresponding surface unit, and these eddies are accelerated and destroyed again in the former area unit." He stated that if the average velocity is assumed to be the same for all units of a simple cross section, a friction formula applicable to the entire section will also be applicable to each unit. Assuming that Manning's friction formula was applicable to both the bed and the side wall with different values of n, Einstein illustrated the division of hydraulic radius in a sand-bed flume between the walls and the bed.

Einstein's concept has been applied by Johnson (1942) to sand bed flumes, except that for the smooth walls Johnson used the resistance function for smooth pipes (first obtained by Prandtl), Equation (7-3). In Einstein's application of Manning's friction formula, the value of n for the wall is to be known, whereas in Johnson's method, a trial and error solution is needed. Vanoni and Brooks (1957) improved Johnson's procedure by showing that if the same average velocity is applicable to both bed and walls, then

$$\frac{R_w}{f_w} = \frac{R}{f} \tag{7-11}$$

where

R_w is the wall Reynolds number, $\frac{4R_wV}{\nu}$,

R_w is the hydraulic radius associated with the walls and

f_w is the wall friction factor.

Vanoni and Brooks also based the wall friction on the smooth-pipe formulae (Equation 7-3) and their method of analysis obviated a tria and error solution.

As far as Einstein's first assumption is concerned, it is valid if the flow along the mean direction is not oscillating (as it generally does in the presence of bed forms). However, a more logical division of the flow section can be made along lines orthogonal to the isovels. Since there is no shear transfer across these lines, the segments of flow formed by them can be treated as entities. If one divided the wall and bed regions on the basis of isovels, one would find that the mean velocity in the segment pertaining to the wall would be smaller than the mean velocity in the section and still smaller than the mean velocity in the bed segment. The effect of different mean velocities in the bed and wall segments is studied in the following paragraphs.

Effect of Unequal Velocities in Wall and Bed Regions on Wall Correction

If the mean velocity in the wall region V_w is α_1 times the mean velocity V in the section, using symbols of Equation (7-11),

$$R_w = R\left(\alpha_1 \cdot \frac{R_w}{R}\right)$$

Also using the definition of f, Equation (7-1),

$$R_w = \alpha_1^2 \frac{f_w}{f} \cdot R$$

and

$$\frac{R_w}{f_w} = \alpha_1^2 \frac{R}{f} \quad . \tag{7-12}$$

Since the total area of flow is equal to the sum of wall and bed segments

$$A_b = W \cdot d - 2\alpha_1^2 \frac{f_w}{f} \left(\frac{Wd^2}{W + 2d}\right)$$

where

W is the width of the flume,

d is the depth of the flow,

A_b is the area of the bed segment,

A_w is the area of the wall segment and

all other symbols are as defined earlier.

The discharge in the wall and the bed segments are

$$Q_w = 2d \cdot V \cdot \alpha_1^3 \frac{f_w}{f} R$$

$$Q_b = Q - Q_w$$

$$= W V d - 2 d \cdot V \cdot \alpha_1^3 \frac{f_w}{f} R$$

and the mean velocity in the bed sedment is,

$$V_b = V \frac{W - 2\alpha_1^3 \left(\frac{W \cdot d}{W + 2d}\right) \frac{f_w}{f}}{W - 2\alpha_1^2 \left(\frac{W \cdot d}{W + 2d}\right) \frac{f_w}{f}} \tag{7-13}$$

From Equation (7-13) and using definition Equation (7-1),

$$\frac{f_b}{f} = (1 + 2s_1) \frac{\left\{1 - 2\,\alpha_1^2 \left(\frac{s_1}{1 + 2s_1}\right) \frac{f_w}{f}\right\}^3}{\left\{1 - 2\,\alpha_1^3 \left(\frac{s_1}{1 + 2s_1}\right) \frac{f_w}{f}\right\}^2} \tag{7-14}$$

where s_1 (the inverse of aspect ratio) is given by d/W.

Similarly, the expression for the hydraulic radius of the bed segment can be written as

$$R_b = d\,\{1 - 2\,\alpha_1^2 \frac{f_w}{f} \left(\frac{s_1}{1 + 2s_1}\right)\}. \tag{7-15}$$

For values of $\alpha_1 = 1$, Equations (7-14) and (7-15) reduce to

$$\frac{f_b}{f} = (1 + 2s_1) \quad \{1 - \left(\frac{2s_1}{1 + 2s_1}\right) \frac{f_w}{f}\} \tag{7-16}$$

and

$$R_b = d\,\{1 - \frac{2f_w}{f} \left(\frac{s_1}{1 + 2s_1}\right)\}. \tag{7-17}$$

If the values of f_b and R_b are denoted by a subscript o for values derived from (7-14) and (7-15) and subscript 1 for values derived on the basis of $\alpha_1 = 1$, the ratios of these quantities can be written as

$$\frac{f_{b1}}{f_{bo}} = \frac{\{1 - \left(\frac{s_1}{1 + 2s_1}\right) \left(\frac{f_w}{f}\right)_1\} \quad \{1 - 2\,\alpha_1^3 \left(\frac{s_1}{1 + 2s_1}\right) \left(\frac{f_w}{f}\right)_o\}^2}{\{1 - 2\,\alpha_1^2 \left(\frac{s_1}{1 + 2s_1}\right) \left(\frac{f_w}{f}\right)_o\}^3} \tag{7-18}$$

and

$$\frac{R_{b1}}{R_{bo}} = \frac{1 - 2\left(\frac{s_1}{1 + 2s_1}\right) \left(\frac{f_w}{f}\right)_1}{1 - 2\,\alpha_1^2 \left(\frac{s_1}{1 + 2s_1}\right) \left(\frac{f_w}{f}\right)_o} \tag{7-19}$$

The order of magnitude of error introduced by assuming velocities in wall and bed segments equal to the mean velocity can now be worked out from Equations (7-18) and (7-19).

For $s_1 = 0.5$, $(\frac{f_w}{f})_1 = 0.2$ and $\alpha_1 = 0.7$,

$$\frac{f_{b1}}{f_{bo}} = 1.06$$

and

$$\frac{R_{b1}}{R_{bo}} = 0.96.$$

For s_1 equal to 2.0, these values are obtained as 1.10 and 0.93, respectively. For a value of $\alpha_1 < 1$, and ignoring the inequality of average velocity in the wall and bed segments, a positive error is introduced in the bed friction factor and a negative error in the bed hydraulic radius. However, the above analysis shows that the magnitude of these errors is small, as compared to other uncertainties involved.

Resistance Function for Smooth Flumes

For determining the friction factor f, Johnson (1942) used the resistance equation for smooth pipes, Equation (7-3). Vanoni and Brooks adopted the same function in deriving the f versus R/f curve. Equation (7-9) was obtained by Tracy and Lester (1961) from a highly accurate set of 50 measurements in a 3 1/2 feet wide, 80 feet long flume, covering a Reynolds number range of 3.6×10^4 to 5.3×10^5. Their resistance function, which gives higher values of f is more pertinent to flumes than the Equation (7-3) obtained from pipe flow.

Since the smooth-pipe equation continues to be used (Abdel-Aal, 1969), it was considered feasible to check some smooth flume data against both the Equations (7-3) and (7-9). Abdel-Aal had given the smooth flume experimental f and R/f values from his experiments. These values fall on Tracy and Lester's curve rather than on the pipe curve. Therefore, for applying smooth wall correction, Equation (7-9) was adopted in this study and a curve of f versus R/f values was constructed after Vanoni and Brooks. This is given in Figure (7-1), and its numerical values are tabulated in Table (7-1).

Analysis of Plane Sand-Bed Runs

As discussed in Chapter IV, plane bed condition in sand-bed channels can be experienced in lower regime with no movement or with significant movement with bed-material size greater than 0.6 mm. This condition can also be achieved in the transition region, with higher transport rates. Plane bed runs, in general, are devoid of irregularities associated with bed forms, except in small regions in the corners of the flow sections. Such runs therefore provide a good opportunity to study the questions about smooth-rough transition, equivalent roughness, wall correction etc., which have been raised earlier.

Resistance functions like Equation (7-6) and (7-10), which apply throughout the range of smooth to rough-turbulent flows, can be written as

$$\frac{1}{\sqrt{f}} = 2.03 \log \left(\xi \cdot \frac{R}{ks}\right) \tag{7-20}$$

where the coefficient 2.03 has been retained to correspond to $\kappa = 0.40$. For Colebrook-White Equation (7-6), ξ is

$$\xi = \frac{14.8}{1 + \frac{3.28}{R_{ks}}} \tag{7-21}$$

For the values of R_{ks} from 5 to 60, the value of ξ varies from 9.0 to 14.0. Factor ξ is used in this study to investigate the phenomenon of smooth to rough turbulent transition, the validity of wall correction and the representative roughness in plane-bed flows.

There are 51 plane bed runs in the flume data; 28 with movement of bed-material and 13 with no movement. Since the object is to study the roughness characteristics with moving bed, the 13 runs were dropped. Run 5-26 has some basically different characteristics from other plane-bed runs and was excluded from analysis. Out of the 27 runs, 20 are in the 8 feet wide and 7 are in the 2 feet wide flume. Eleven plane bed runs from Barton and Lin data were also included. These runs were studied in a 4 feet wide flume. In all, these 38 runs included 10 different sands and covered the following range of variables:

VARIABLE	RANGE
Median diameter, D_{50}	0.18 mm - 0.93 mm
Geometric standard deviation, σ	1.25 - 2.07
Flume width, W	2 feet - 8 feet
Mean of depth of flow, d	.30 feet- 1.03 feet
Aspect ratio (W/d)	2.81 - 26.7
Roughness Reynolds number $(U_{*o}D_{50}/\nu)$	2.55 - 52.1
Flow Reynolds number $(4dV/\nu$	5×10^5 - 1.04×10^6

All the runs were analyzed for ks equal to D_{33}, D_{35}, D_{50}, D_{65}, D_{67}, D_{84}, and D_{90}. These values of ks were computed for each sand

using lognormal distribution with the median size and standard deviation, as given in Table (7-2). For certain runs individual values of median size have been reported (column 13, U.S.G.S., pp. 462-I). Mean bed-material gradation curves for each sand were used in preference to the size gradation values reported for individual runs because individual samples can suffer from random errors which are eliminated in the average of many samples. The analysis was made both with and without wall corrections. When wall corrections were made, Equations (7-16) and (7-17) were used to determine the bed friction factor and the bed hydraulic radius. For determining f_w, Tracy and Lester's resistance equation for smooth walled flumes (Equation 7-9, Table 7-1, Figure 7-1) was used. For the case of no-wall-correction, the hydraulic radius was replaced by the mean depth. For all the above combinations the friction factor f was computed and values of ξ were determined from Equation (7-20). Values of the aspect ratio, flow Reynolds number R and roughness Reynolds number R_{ks} were also computed in each case.

The values of ξ, for each combination of conditions were statistically analyzed for variance and for possible correlation with the aspect ratio (W/d), R and R_{ks}. A two tail test for null hypothesis an an α level of 0.95 (Draper and Smith, 1966) was then made, for each combination of these variables.

The results of the statistical analysis of ξ values and its correlation with roughness Reynolds number R_{ks} are shown in Table (7-3) for each percentile tested. Similar results for ξ's correlation with the aspect ratio are shown in Table (7-4). Table (7-5) gives a summary of the observed data of runs used in this analysis along with the values of ξ, R, R_{ks} and the aspect ratio for both the conditions of analysis, i.e.,

with wall-correction and without wall-correction. The results shown in Table (7-5) are based on an equivalent roughness proportional to D_{84}. The conclusions about the equivalent roughness size, wall correction and the smooth to rough transitions are discussed below.

Equivalent Roughness Size

For each percentile bed-material size and for the analyses with and without wall-correction, the mean, standard deviation and coefficient of variance of ξ values are given in Table (7-3). This table shows that the coefficient of variance (which is a dimensionless measure of the spread of a distribution) in both the conditions of wall-correction decreases as the effective roughness size is increased from D_{33} to D_{90}. The minimum value in each case is achieved for D_{90}.

In the analysis of the gradations of natural mixtures of sands, it was shown that they exhibit lognormal distribution for sizes from the 10th to 90th percentiles of the cumulative size distribution. At the upper limit D_{90}, however, individual samples do show some departure from the lognormal distribution. Also in small samples, the error in the estimation of D_{90} is likely to be large. For these reasons and for reasons of convenience in the definition of effective roughness size, it is concluded that the effective roughness size in sand mixtures should be related to the 84th percentile, which for lognormal distributions is given by

$$D_{84} = D_{50} \cdot \sigma \qquad (7\text{-}22)$$

It will be subsequently shown that the friction factor f in plane bed runs is given by

$$\frac{1}{\sqrt{f}} = 2.03 \log (2.4 \frac{d}{D_{84}}) \qquad (7\text{-}23)$$

Comparing this equation with Keulegan's (Equation 7-8), it is seen that the equivalent roughness size for plane bed runs in terms of Nikuradse's sand and Keulegan's resistance equation is given by

$$ks = 5.1\ D_{84} \qquad (7\text{-}24)$$

It needs to be stated here that this does not represent the minimum roughness that can be experienced with sand bed channels.

Validity of the Wall Correction

The object of applying wall corrections to flow over sand-bed channels in smooth walled flumes has already been discussed. It would appear that once an appropriate correction for wall condition has been made, the flow phenomena would be independent of the aspect ratio (W/d) of the flow section. Figure (7-2) shows a plot of ξ versus the aspect ratio for the analysis without the wall correction. A similar plot for the analysis with the wall-correction is shown in Figure (7-3). A comparison of the two figures shows that whereas in the analysis with no-wall-correction there is no apparent dependence of ξ on the aspect ratio (W/d), the application of the wall correction introduces a strong dependence of ξ on the aspect ratio (W/R_b) of the flow section. Correlation coefficients of ξ with the aspect ratio (Table 7-4) show that for the representative roughness size D_{84}, the correlation on applying the wall correction increases from 0.255 to - 0.546 and the null hypothesis changes from true to false. Since a higher ξ value is associated with a smaller friction factor, it appears that the wall

correction over-corrects to the extent, that dependence on the aspect ratio of flow becomes worse than it would otherwise be.[1] It is difficult to suggest a definite reason for this phenomenon without further experimental investigation.

However, it can be concluded that with moving sand beds with aspect ratios of flow exceeding about 3, a realistic analysis of resistance can be made on the basis of the average depth of flow, without making any wall-correction.

Smooth to Rough Flow Transition

The relationship between ξ and R_{ks} for the Colebrook-White transition function has been given in Equation (7-21). Correlation between ξ and R_{ks} for both the analyses of plane bed runs (with and without wall-corrections) are given in Table (7-3). The ξ values are plotted against corresponding R_{ks} values in Figures (7-4) and (7-5). Figure (7-5) also shows the relationship of Equation (7-21). Both the figures and correlation coefficients (.069 and -.103) show that ξ has no dependence on the roughness Raynolds number.

It has been discussed in Chapter IV, that the effect of movement of bed particles, as well as of the porosity of the bed, is to disrupt the viscous sublayer. It has also been argued that the rigid boundary smooth-rough transition is not applicable to moving sand beds. Analysis of plane bed runs, amply justifies this argument and it can be concluded

1. Tracy-Lester equation used in making the wall correction gives higher friction factor for smooth walled flumes than the Prandtl's Equation (7-3) does for smooth pipes. If the wall corrections were based on Equation (7-3), the resulting values of ξ would have decreased by about four percent, but not enough to change the results of Figure (7-3).

that in sand bed channels with movement of the bed material, the boundary is always hydrodynamically rough.

Resistance Function for Plane Sand-Beds

As shown above, the application of a wall-correction to plane sand-bed flume runs makes their resistance factor dependent on the aspect ratio of the flow section. Also it has been shown that with the movement of the bed-material, the boundary behaves as hydrodynamically rough. A question can now be raised whether, the flow resistance in these runs is related to the κ values obtained from their velocity profiles or to their total sediment loads.

For a variable κ, Equation (7-20) can be written as

$$\frac{1}{\sqrt{f}} = \frac{.812}{\kappa} \log \left(\xi \frac{d}{D_{84}}\right) \tag{7-24}$$

where the hydraulic radius R has been replaced by the average depth d (for no-wall-correction), D_{84} is the equivalent roughness size for the sand-bed and factor ξ is defined in Equation (7-20).

For the plane-bed runs in which the velocity profiles had been observed, values of κ were computed for each profile on the basis of U_{*o}. The average of these κ values for the number of velocity profiles observed for each run κ_1, was then calculated.[1] Using κ_1, the value of ξ for individual runs was computed from Equation (7-24). These values of ξ were widely scattered and it was not possible to relate these with the flow parameters. Similarly, the value of ξ obtained from Equation (7-20), were analysed for a possible dependence

1. Refer Chapter VI, "Analysis of κ For Flume Data," for various definitions of κ in flume studies

on the total sediment load. No such dependence was found either. From the analysis of flume data it is concluded that the resistance factor f for plane sand-bed runs is not related with the values of κ obtained from velocity profiles or with the total sediment load of the flow.

To evaluate the resistance function for plane sand-bed runs for an unknown but constant value of κ, Equation (7-24) is written as

$$\frac{1}{\sqrt{f}} = a + b \log \left(\frac{d}{D_{84}}\right) \tag{7-25}$$

where $b = \frac{0.812}{\kappa}$ and

$$a = b \log \xi .$$

The values of a and b for the 2-feet and the 8-feet flume data as obtained by least square regression of $\frac{1}{\sqrt{f}}$ versus $\log \left(\frac{d}{ks}\right)$ are

$a = 2.21$ and $b = 2.21$.

Equation (7-24) for these values is

$$\frac{1}{\sqrt{f}} = 2.21 \log \left(\frac{10\ d}{D_{84}}\right) , \tag{7-26}$$

and the value of κ is 0.368.

For a value of $\kappa = 0.40$, Equation (7-24) is

$$\frac{1}{\sqrt{f}} = 2.03 \log \left(2.4 \frac{d}{D_{84}}\right) . \tag{7-23}$$

In the analysis of κ in flume runs (Chapter VI), it has already been shown that <u>a priori</u> prediction of κ in flow over sand-beds is not possible. Neither it is known as to how the average value of κ obtained in plane sand-bed flows is changed for the flow over other bed forms. Equation (7-23) has therefore, been adopted as the resistance

equation for plane sand-bed channels in this study. The values of observed friction factors f_o and those predicted from Equation (7-23) f_p are given in Table 7-6. Also given in this table are the values of total load concentration in PPM. In about two-thirds of the cases, the difference between the observed and the predicted values of friction factor f is less than or equal to 0.003.

CHAPTER VIII

RESISTANCE FUNCTION IN SAND-BED CHANNELS

Analysis of plane bed runs (Chapter VII) has shown that the equivalent roughness size of a plane sand-bed, in terms of Keulegan's resistance equation is given by about 5.1 D_{84}. This value was seen to be fairly constant with a coefficient of variation of 0.67. With bed configuration other than plane, the total roughness can be computed by writing Keulegan's resistance equation for flow on rough boundaries, as

$$\frac{1}{\sqrt{f}} = 2.03 \log \left(\frac{d}{k_a}\right)$$

where k_a is termed the absolute roughness, and f is the Darcy-Weisbach friction factor for the flow. This equation gives,

$$k_a = d\ 10^{\frac{-1}{2.03\sqrt{f}}}$$

On the analogy of plane bed runs if the equivalent roughness for sand-beds is related to D_{84}, they can be made equal for simplification as

$$k_s = D_{84}$$

Then the ratio of absolute roughness to Nikuradse's sand grain roughness is

$$\frac{k_a}{k_s} = \frac{k_a}{D_{84}} = \frac{d}{D_{84}}\ 10^{\frac{-1}{2.03\sqrt{f}}}$$

For Keulegan's resistance equation, $k_a/D_{84} = 0.08$ and for plane beds, $k_a/D_{84} = 0.42$. Values of the ratio of absolute roughness, k_a to D_{84}, for the flume runs are shown in Figure 8-1. These values range from 0.093 to 30.0 (excluding run 5-33 with a value of .038). Thus, in sand-bed channels, the overall roughness to flow in terms of k_a has a 300 fold range with the minimum value somewhat higher than Keulegan's.

Evaluation of the resistance to flow in sand-bed channels has always been a difficult problem. Except in regime methods, which use an integral approach to alluvial flows, most of the resistance functions so far developed, divide the total boundary shear stress τ_o in two parts; one relating to the grain roughness of rigid boundary flows and the other to the bed form roughness. The division of the shear stress τ_o is differently made in various methods. Einstein (1950) for one, based this division on the hydraulic radius of the flow section while Meyer-Peter and Muller (1948) based it on the energy gradient. The component relating to bed forms in such methods is related to some form of Shield's shear parameter. However, these methods do not make a distinction between different regimes of flow and consequently their results are either valid for one of the regimes or being an average for the lower to upper regime conditions are susceptible to large errors.

Simons and Richardson (1966) initiated the recognition of different resistance functions for different regimes. They considered the alluvial channels resistance as an adjustment in slope or depth, in the resistance due to hydraulically smooth boundaries (Equation 7-9) and provided curves relating this adjustment with depth and energy gradient for different regimes.

In addition to the overall resistance to flow, sometimes the vertical velocity distribution is required for the flow on sand-beds, as in the computation of suspended load transport and in other engineering problems. This distribution is not explicitly dealt with by any of the above methods.

Velocity Profiles in Sand-Bed Channels

In the discussion of turbulent flow in rigid boundary channels (Chapter III), it was concluded that the uncertainties about the location of the origin for the velocity profile, the value of von Karman's κ and other factors can be combined to yield a velocity distribution in the inner layer in terms of an effective shear velocity U_{*oe}, see Equation (3-14). There the ratio U_{*oe}/U_{*o} was given as a function of the roughness characteristics of the boundary and of other parameters which affect the value of κ. The effective shear velocity in sand-bed channels cannot be predicted directly because neither the roughness characteristics nor κ are known before hand. In Chapter VI, the value of κ was analyzed in the outer layer of the flume runs from the observed velocity profiles and it was found that κ is related to parameters which are not known a priori in problems where the resistance function or the velocity distribution is to be used. However, the concept of effective shear velocity in the inner-outer layer model of rough-turbulent flows can be used to define the velocity distribution and the resistance to flow in sand-bed channels.

In the discussion of velocity profiles over sand-bed channels (Chapter VI), it has been explained that the concept of a typical velocity profile in such channels can only be accepted on the average. Individual profiles in sand-bed channels are likely to show large variations from the average

depending on their location with respect to the bed forms. In the following paragraphs a velocity distribution is presented for such an average profile.

Consider the flow in a sand bed channel with average depth d and average velocity V.

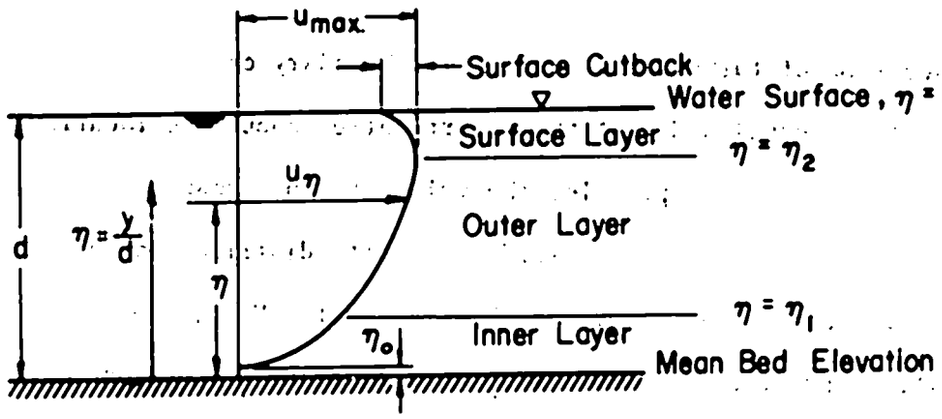

On the basis of the observation of velocity distribution in the flumes, this flow can be divided into three main regions as shown above: an inner layer, which is equal to or greater than the height of bed forms above the mean bed elevation, a surface layer, which contains the effect of cutback in velocity profile due to the secondary currents and the region between these two layers, labelled as the outer layer (because it is analogous to the outer layer of the turbulent boundary layer flows). In terms of the dimensionless ordinate $\eta = \frac{y}{d}$ (y being the distance from the mean bed elevation) the limits of these layers are shown as η_1 and η_2. Ordinate η_0 is the distance from the mean bed elevation at which the velocity is equal to 0.

Using the analogy of turbulent flow over hydraulically rough boundaries, the velocity distribution in these layers is,

Inner layer:

$$\eta_o \leq \eta \leq \eta_1 ,$$

$$\frac{u_\eta}{U_{*oe}} = \frac{1}{\kappa_o} \ln \left(\frac{\eta}{\eta_o}\right) , \tag{8-1}$$

$$u_{\eta_o} = 0.$$

Outer layer:

$$\eta_1 \leq \eta \leq \eta_2$$

$$\frac{u_{max} - u_\eta}{U_{*o}} = \frac{-1}{\kappa} \ln(\eta) , \tag{8-2}$$

$$\kappa = \kappa_o g_1 \left[C_v, F, \frac{C}{\sqrt{g}}, \frac{W_{50}}{U_{*o}}\right]$$

Surface layer:

$$\eta_2 \leq \eta \leq 1,$$

$$\frac{u_{max} - u_\eta}{U_{*o}} = \frac{-1}{\kappa} \ln(\eta) + f_1[\eta]. \tag{8-3}$$

Equations (8-1) through (8-3) are explained below.

In the inner layer, the origin for measuring the distance from a rough boundary for a logarithmic velocity distribution is below the mean bed elevation by a distance e (see Equation 3-10). The value of κ in the logarithmic velocity profile (for the inner layer) thus obtained is different from its "universal" value κ_o firstly because of the shift e in the origin and secondly due to the influence of the suspended load, the contact load and of the bed forms on the momentum

diffusion in the flow close to the boundary. All of these effects are accounted for, in Equation (8-1), by using the effective shear velocity U_{*oe} derived in Equation (3-14). With the introduction of U_{*oe}, the origin for the measurement of the distance η from the boundary becomes coincident with the mean bed elevation and the "universal" value of von Karman's kappa (κ_o) is used.

In the outer layer, the inclusion of the shift e in the origin for defining a logarithmic velocity profile becomes unimportant because of the larger absolute values of η. Also if the velocity profile is based on the actual value of κ, there is no need to introduce a change in the shear velocity in this region. Thus, the velocity defect law, Equation (8-2), is based on U_{*o} and the actual value of κ for the flow in this region. As shown in Chapter VI, κ in the outer layer is related to κ_o by a function g_1 of the parameters given in Equation (6-15). For a given sand-bed and flow, g_1 is a constant.

For the surface layer, the velocity profile is considered as an extension of that in the outer layer with the difference that there is a cut-back in the velocity near the water surface. In Equation (8-3), a correction term $f_1[\eta]$ is incorporated to account for this cut-back.

For a given sand-bed and flow, f_1 is dependent on η only. In the velocity profiles observed in the flumes, $f_1[\eta]$ can be expressed as the parabola

$$f_1[\eta] = a_1[1 - \frac{\eta}{0.8}]^2 \quad \text{for} \quad 0.8 < \eta \leq 1. \tag{8-4}$$

The coefficient a_1 in Equation (8-4) is a function of the secondary currents and hence a_1 depends on the geometry of the flow section, the distribution of roughness pattern across the section, etc. No attempt

was made to relate a_1 to other parameters in the flume runs and an average value of $a_1 = 35.0$ was found. In natural channels with non-rectangular sections, the value of a_1 would probably be smaller.

Using the form of $f_1[\eta]$ given above the velocity distribution in outer and surface layers can be combined as

$$\frac{u_{max} - u_\eta}{(U_{*o}^{a})} = \frac{-1}{\kappa} \ln(\eta) + I(\eta)\, a_1 \left[1 - \frac{\eta}{0.8}\right]^2$$

$$\text{for} \quad \eta_1 \leq \eta \leq 1 \tag{8-5}$$

where $I(\eta)$ is the indicator function such that

$I(\eta) = 0$ when $\eta \leq 0.8$

and

$I(\eta) = 1$, when $0.8 < \eta \leq 1$.

Further assuming that both Equation (8-1) and (8-5) apply in an overlapping region aroung $\eta = \eta_1$, the velocity profile in the depth of flow can be written as

$$u_\eta = \frac{U_{*oe}}{\kappa_o} \ln\left(\frac{\eta}{\eta_o}\right) \quad \text{for} \quad \eta_o \leq \eta \leq \eta_1 \quad \text{and} \tag{8-6}$$

$$u_\eta = \frac{U_{*oe}}{\kappa_o} \ln\left(\frac{\eta_1}{\eta_o}\right) + \frac{U_{*o}}{\kappa_o g_1} \ln\left(\frac{\eta}{\eta_1}\right) - I(\eta)\, U_{*o} a_1 \left(1 - \frac{\eta}{0.8}\right)^2 \quad \text{for } \eta_1 < \eta \leq 1 \tag{8-7}$$

In an open channel flow over a hydrodynamically rough and plane rigid boundary consisting of sand grains, the shift e in the origin (Equation 3-10) is negligible compared with the distances from the boundary even in the inner layer. Also other conditions like the presence of suspended load, rolling contact load and bed forms which effect the

momentum diffusion in the flow over mobile boundaries are absent. Therefore, the vertical velocity distribution for such flow can be expressed in terms of U_{*o} and κ_o as

$$u_{\eta p} = \frac{U_{*o}}{\kappa_o} \ln\left(\frac{\eta}{\eta_o}\right) - I(\eta)\, U_{*o}\, a_1 \left(1 - \frac{\eta}{0.8}\right)^2$$

$$\text{for} \quad \eta_o \leq \eta \leq 1.0 \quad . \tag{8-8}$$

In Equation (8-8) the subscript p refers to the rigid boundary flow and for want of more accurate information regarding the difference between the surface cut-back in the rigid boundary and the mobile boundary flows, the form of $f_1[\eta]$ as given by Equation (8-4) is assumed. For similar sands in the rigid and mobile boundaries, the value of η_o in Equation (8-8) is equal to its value in Equations (8-1) through (8-7).

Equations (8-6) and (8-7) can be integrated for the flow over the sand-bed and Equation (8-8) can be integrated for the rigid boundary flow (with similar grain roughness) from $\eta_o = 0$ to 1 to yield

$$\frac{U_{*oe}}{U_{*o}} = \frac{g_1(V_f + \rho_1) + B_2}{(V_p + \rho_1) + B_2} \tag{8-9}$$

where

$$V_f = 1/U_{*o} \int_0^1 u_\eta \cdot d\eta \quad \text{for the mobile sand-bed,}$$

$$V_p = 1/U_{*o} \int_0^1 u_{\eta p} \cdot d\eta \quad \text{for the rigid sand roughness,}$$

$$\rho_1 = \int_0^1 I(\eta)\, a_1 (1 - \eta/0.8)^2\, d\eta$$

and

$$B_2 = \kappa_o (1 + \ln \eta_1 - \eta_1)$$

Equation (8-9) provides a basis for deriving the resistance function for flow over sand-beds in terms of the velocity distribution. This equation can be somewhat simplified by assuming that the unknown value of g_1 is approximately equal to 1. Also, the value of ρ_1 is small (0.14 for the flume runs) and since it appears as an additive term to both V_f and V_p (which are of a much larger magnitude) in the numerator and the denominator, it can be ignored. Equation (8-9) then becomes

$$\frac{U_{*oe}}{U_{*o}} = \frac{V_f + B_2}{V_p + B_2} \quad . \tag{8-10}$$

For the inner layer with $\eta_1 = .15$ this equation can be written as

$$\frac{U_{*oe}}{U_{*o}} = \frac{V_f - 2.62}{V_p - 2.62} \tag{8-11}$$

Using Keulegan's resistance Equation (7-8), V_p is

$$V_p = 2.5 \ln\left(\frac{12.27}{\eta_{ks}}\right) \tag{8-12}$$

where

$$\eta_{ks} = \frac{D_{84}}{d}$$

With a known value of V_f, D_{84}, d and S, the vertical velocity distribution in the average velocity profile over a sand-bed can be computed from the above equation. To verify the above velocity profile, a comparison is made with the natural river observations given by Toffaleti (1963) for Atchaflaya River at Simmesport. For a $D_{84} = 0.0049$ ft,

$\eta_{ks} = 10^{-4}$ and $U_{*o}/U_{*oe} = 1.8$, the values of u_η/V for various relative depths computed from Equations (8-6) and (8-7) are given below, along with the average values from some 500 field observations reported by Toffaleti.

η	u_η/V Computed from Eq. (8-6) and (8-7)	u_η/V Reported by Toffaleti (1963)
05	.755	--
10	.814	.811
.15	.851	--
.20	.893	.893
.30	.959	.959
.40	1.009	1.009
.50	1.038	1.042
.60	1.067	1.066
.70	1.091	1.085
.80	1.112	1.097
.90	1.100	1.104

A plot of the two profiles is shown in Figure 8-2. The agreement between these profiles is good and may be further improved near the water surface by applying the cut-back correction from a value of η somewhat less than 0.80.

Prediction of the Regimes of Flow

The recognition of the regimes of flow in sand-bed channels and the difference in their resistance and transport characteristics has been

one of the most important contributions in the field of fluvial hydraulics. Experience with the application of various resistance functions to the flume and the canal data in this investigation has shown that different functions have to be defined in at least the two regimes and the transition zone. A method for predicting the form of bed roughness has been provided by Simons and Richardson (1966). This method, which has already been referred to in Chapter IV, distinguishes between different forms on the basis of median fall diameter of the sand-bed and the prevailing stream power $P(=\tau_o V)$, see Figure 4-1. If different resistance functions have to be used for different regimes, it is necessary to have some guide for predicting the final regime of flow before a resistance function is applied. This is especially true for the problem under investigation, in which the resistance and transport functions for flow over a sand-bed have to be solved for a given bed-material, depth and energy gradient.

Evaluation of the ratio of the absolute roughness k_a to D_{84} of the bed-material size (Figure 8-1) has shown that this ratio for sand-bed channels has a minimum value somewhat larger than the Keulegan's value. Considering the maximum velocity that can occur in flow over sand-beds, as that given by the Keulegan's equation for a fully rough boundary with similar sand roughness, the maximum stream power P_{max}, that can possibly occur on a sand-bed is given by $\rho V_p U_{*o}^3$, where V_p is defined by Equation (8-12). The value of P_{max} for a given sand-bed is uniquely determined by the bed-material D_{84}, depth d and the energy gradient S.

A study of the maximum stream power P_{max} and the regime of flow for the flume data showed that it is possible to predict the regime

of flow from the value of P_{max} and the median fall diameter of the bed-material. It was found that for a given bed-material in the flume runs, all values of P_{max} below a limiting value resulted in the lower regime bed forms (plane bed, ripples, dunes) and all values of P_{max} greater than another limiting value resulted in the upper regime bed forms (transition, plane, standing wave, antidunes, chutes and pools). For values of P_{max} between these two limiting values, the bed forms in the flumes were either of the lower or of the upper regime. The limits of P_{max} for various sands, corresponding to above conditions are given in Table 8-1 and are plotted against median fall diameter D_{50} in Figure 8-3. Envelopes for these values have been drawn as straight lines in Figure 8-3. It is likely that if depth-slope combinations other than those used in flume data were attempted, the limit envelopes would be approached for sands whose limits fall within the given envelope. It is also possible that for sand size range beyond the one used in the flumes (.19 mm - .93 mm), the envelopes may depart from the straight lines indicated. This seems more likely for median fall diameters greater than 1 mm.

In this investigation, many other parametric combinations were also tried, but all of these resulted in more complicated limit curves without giving a better prediction than the P_{max} - D_{50} combination. The limit curves shown in Figure 8-3 were therefore adopted for predicting the final regime of flow and for selecting the resistance function to be used.

The implication of Figure 8-3 is that a depth-slope combination for a given sand falling below the lower envelope would always result in a lower regime bed form, while that falling above the upper envelope would always result in an upper regime bed form. For values in between

these two limits, the bed form may be either in the lower or the upper regime. It is believed that it is in a part of this intermediate range that a multiplicity of flow solutions (Chapter I) can occur. On the basis of the existing knowledge (1971) of the mechanism by which bed forms are generated and changed, it is not possible to explain this multiplicity.

Resistance Functions

The integration of the empirical velocity profile for sand-bed channels has been shown to yield Equation (8-11), which relates average velocity in the flow section to the effective shear velocity U_{*oe} in the inner layer. Parameters V_f and V_p in this equation can also be interpreted as dimensionless Chezy coefficients $(C/\sqrt{g})$ for the observed velocity and the maximum possible velocity on a rigid hydrodynamically rough boundary. To solve the resistance equation and to determine the velocity distribution in the vertical, ratio U_{*oe}/U_{*o} must be determined. This ratio is always less than unity. Therefore, U_{*oe} can be expressed as

$$U_{*o}^2 = U_{*oe}^2 + \Delta U_{*o}^2 \qquad (8\text{-}13)$$

U_{*oe} as derived in this study, seems similar to the grain-associated shear velocity (U_{*g}) defined by Einstein (1950). There is a difference in the derivation and interpretation of U_{*g} used by Einstein and U_{*oe} used here. Shear velocity U_{*g} is the result of a division of the bed hydraulic radius into the resistance associated with grains and the resistance associated with bed forms, analogous to the losses in pipe fittings and bends which are add to the energy losses in uniform flow. On the other hand, U_{*oe} is a corrected shear velocity

in the inner layer (of a thickness of about one-sixth of the flow depth near the boundary) which accounts for the following distinct factors; effect of suspended load, rolling contact load, porous boundary and change in the origin for logarithmic velocity profile due to these factors and due to the bed forms.

Since ΔU_{*o}^2 is caused by the mobility of sand-bed, it correlates with the Shields' parameter

$$S = \frac{\rho U_{*oe}^2}{(\gamma_s - \gamma_f) D_{50}}$$

where

γ_s and γ_f refer to the unit weights of the sediment and the fluid, respectively.

The values of $V/\Delta U_{*o}$ and $1/S$ are plotted in Figure 8-4 for the flume and the canal data for a value of $\eta_1 = 0.15$. The points in the lower, upper and intermediate $P_{max} - D_{50}$ range are separately shown in Figures 8-5 through 8-7. It is apparent from these figures that each range has to be defined by a separate function.

In order to use the relation between $V/\Delta U_{*o}$ and S for the prediction of velocity, a solution curve is to be provided so that for a given bed-material, depth and energy gradient, the value of U_{*oe} for which both $V/\Delta U_{*o}$ and S are coincident with the curve, gives the correct solution. The value of U_{*oe} can be determined from such a curve either by a trial and error solution or graphically by the intersection of $V/\Delta U_{*o} - S$ curve for the given data with the solution curve. As U_{*oe} and ΔU_{*o} are related to each other by Equation (8-13), a correlation between $V/\Delta U_{*o}$ and S exists besides the functional

correlation being sought. A word of caution is necessary in such cases, because a grouping of data points around a mean curve does not necessarily imply that predictions from the mean curves will be equally good. To illustrate this point, Figure 8-8 shows the mean curve obtainable from the intermediate range runs (Fig. 8-7) and the loci of $V/\Delta U_{*o}$ - $1/S$ points for five different runs. It may be seen that although the solution points are located close to the mean curve, the intersections of the loci and the mean curve are at a small angle, so that a minor relocation of the mean curve or of a locus can cause a large change in the solution. On this account, the solution curves do not necessarily correspond to the mean curves obtainable for different ranges.

For the lower and upper P_{max} - D_{50} ranges, the solution curves are given in Figure 8-9. The drooping portion of the upper curve around $S = 1.0$ corresponds to the higher energy loss in breaking antidune and chute and pool runs. Similarly, the depression in the lower curve corresponds to the increase in resistance as ripples grow into dunes.

For the intermediate range, though it is not apparent from Figure 8-7, two solution curves are needed; one for the upper regime bed forms and the other for the lower regime. These curves are shown in Figure 8-10. Curves on Figures 8-9 and 8-10 have been approximated by straight segments (on log-log scale) and their coordinates are given in Table 8-2. The segmented curves are useful in the analysis by digital computers and were accordingly used in this study.

For all the flume runs and for 43 West Pakistan canals (Chapter II), the mean velocities were predicted on the basis of these resistance curves. For each run the value of P_{max} was computed to determine the range to which the run belonged. If this range was upper or lower, values

of $1/S$ and $V/\Delta U_{*o}$ were computed for different U_{*oe} values, starting from the largest possible value and the point of intersection with the corresponding resistance curve in Figure 8-9 was taken as the solution. When a run belonged to the intermediate range, solution points were obtained on the upper curve of Figure 8-9 for the canals. For the flume data the solutions for the intermediate P_{max} - D_{50} range were obtained on the upper curve of Figure 8-10 for the upper regime bed forms and on the lower curve of Figure 8-10 for the lower regime bed forms. An exception to this was made for the transition bed form runs of 0.93 mm sand, which fell on the lower-intermediate curve.

For the runs falling in the intermediate range, solutions were also obtained on the alternate curve in Figure 8-10 to test if both the solutions gave consistent prediction of the bed form in terms of Simons-Richardson criterion, Figure 4-1. Most of the runs did yield stream power P for the velocities predicted by upper-intermediate and lower-intermediate curves which corresponded to the actual bed form. In such cases, in practice, the resistance curve to be used is uniquely determined if the analysis is made in conjunction with Simons-Richardson criterion. However, in some runs the solution from lower-intermediate curve indicated a lower regime bed form, while that from upper-intermediate curve indicated an upper regime bed form.

Twenty-Five runs from Barton and Lin data (1955) have also been analyzed on the above basis. For the prediction velocities in all the 383 cases (comprising 315 runs of the flume data, 25 runs of Barton-Lin data and 43 West Pakistan canals) the error, percentage error and other parameters including the aspect ratio (W/d) and roughness Reynolds number R_{ks} were computed. Values of predicted versus observed

velocity are plotted in Figure 8-11 on an arithmetical scale. The figure also shows the ±15% deviation lines. Considering the range of condition represented in this analysis (Chapter II), the solution curves seem adequate for flume runs and for West Pakistan canals, both of which are characterized by a nearly uniform depth across the sections and an equilibrium bed condition due to a constant discharge. These curves have not been tested for non-rectangular river sections. It is possible that their modification may become necessary for such sections.

Since the above analysis is based on average depth instead of hydraulic radius and no correction for the wall friction effect or the smooth-rough turbulent transition was made, the percentage error in the predicted velocity is plotted in Figures 8-12 and 8-13 against the aspect ratio (W/d) and R_{ks}. No apparent correlation exists between these parameters and the percentage error.

Summary

In this chapter, an empirical model of the velocity distribution in sand-bed channels has been formed. Integration of this distribution yields a relation between the effective shear velocity in the inner layer and the average velocity of flow. This relation can be used to determine the velocity profile if the average velocity is known.

Since the resistance to flow in sand-bed channels is related to the regime of the flow, a criterion has been developed to predict this regime from known bed-material, depth and energy gradient. Graphical relations between $V/\Delta U_{*o}$ and Shield's parameter S developed for the flume and the canal data are found to be different for the different flow regimes. These relations can be used to predict the average velocity

if the bed-material, depth and slope are known. Three hundred eighty-three sections including 43 canals from West Pakistan have been analyzed on the basis of these curves and show velocity predictions within 15 percent of the observed values in most of the cases. Example problems are solved in Chapter X to illustrate the use of these resistance curves.

CHAPTER IX

TRANSPORT FUNCTION FOR SAND-BED CHANNELS

After the threshold conditions for the movement of sand-bed have been exceeded in a flow, there is a net transport of sediment past any section. This transport consists of particles which may be moving by rolling along the bed and others which are carried by suspension in the fluid medium. The movements of an individual particle in the bed ar however, random. At any instant, the particle may be in a state of rest in the bed or it may be moving. In a time homogeneous case it is possible to define the average number of particles undergoing different modes of transport at any section. This involves the concept of a continuous exchange between the bed and the transported material, i.e., every particle that settles in the bed is, on the average, replaced by another.

The total quantity of sediment moving past a section is called the total load. For graded sands, the size distribution of the total load differs from that of the bed, as a result of the differential transport of sizes in a mixture (partly discussed in Chapter V). A concept of transport capacity of the flow is also associated with graded sand beds. Given a sand mixture in the bed, a flow can transport a certain quantity of each size fraction of the mixture which is larger for the smaller sizes. If the availability of the size fraction in the bed is less than the transport capacity of the flow, the bed would be ultimately denuded of this fraction. In sand mixtures because of a continuous size variation, the difference between the availability and capacity of transport is noticeable at the lower end of the

cumulative size distribution curve. The portion of the total load consisting of sizes not available in sufficient quantities in the shifting portions of the bed is called the fine material load. In sand-bed channels, this load is taken as consisting of sizes less than D_{10} of the bed-material by some investigators (Einstein, 1950 and others). Alternatively some investigators like Colby (1964) and Nordin and Beverage (1965) have used the portion of the total load finer than .062 mm size as the fine material load for their situations. Since for this part of the total load, capacity of transport by the flow is greater than its availability in the bed, its rate of transport is not dependent on the bed-material or on the flow and it cannot be determined from local transport phenomena. The transport of fine material past any section is only dependent on the quantity arriving from upstream and it is the indeterminate component of the total load. The rest of the total load is called the bed-material load.

Based on the mode of transport, the bed-material load can be divided into suspended and contact (or bed) load fractions. This division, though somewhat hazy close to the bed, is necessary because the transport mechanism of the two modes is different. Contact load is that part of the bed-material load which during its movement is continuously supported by the bed, while suspended load is the part whose weight is supported by the transporting fluid.

If the bed form of a sand-bed channel is other than plane, the rate of bed-material transport over a typical bed form length, varies from section to section. This variation is the cause of bed form movement and can be expressed after Simons et al., (1965a) as

$$\frac{\partial}{\partial x}\left(\frac{g_{bt}}{(1-n_o)\gamma_s}\right) = -\frac{\partial y_b}{\partial t} \qquad (9\text{-}1)$$

where

g_{bt} is the rate of transport of the contact load in weight per unit width per unit time,

n_o is the porosity of the surface of the bed,

γ_s is the unit weight of the bed-material,

y_b is the elevation of the bed and

t is the time.

Averaging y_b over lengths of time greater than that required for the passage of a bed form past any section, yields the concept of equilibrium of the bed. If on such averaging, $\overline{\partial y_b/\partial t} = 0$, the bed at that section is said to be in equilibrium. And if this is true for all sections in a reach of a sand-bed channel, the reach is said to be in equilibrium. In such cases, if the flow discharge is steady, the long time average of total bed-material transport phenomenon would have time and space homogeneity. The time required for the achievement of this homogeneity from the inception of the phenomenon, depends on the rate of transport and the associated change in the bed form. Evidently, such a homogeneity can only be created under controlled laboratory conditions by continuous running of flow over a sand-bed at constant discharge and slope. In natural channels, the discharge is continuously varying in general and the state of homogeneity at any instant depends on the rate of change of discharge and the related rate of adjustment by the bed.

As a last part of this study of flow in sand-bed channels, the transport function for a time and space homogeneous conditions will be derived. The objective is to formulate a transport function, which predicts the

bed-material load as well as its gradation. The fine material load is indeterminate and will only be considered in as much as it effects the apparent viscosity of the fluid and hence the fall diameter of the particles.

General Form of Transport Function

In view of the difference in the sediment transport mechanism close to the boundary from that in the region of flow away from it, Einstein (1950) introduced the concept of a bed layer. The bed layer is a layer of thickness equal to twice the diameter of each size fraction of the bed-material under consideration. The division between the suspended and the bed load was also made by Einstein on the basis of this layer. The bed load is the load being transported in the bed layer with a constant concentration. The concept of the bed layer was also used by Einstein to relate the bed-material suspended load with the moving sand boundary, by using the concentration in the bed layer as the reference concentration in the computation of the suspended load.

With the bed forms other than plane, the bed elevation, as well as the portion of transport moving as the bed load varies along the bed form. The concept of the bed layer, as originally defined by Einstein, therefore breaks down in such cases. However, the assumption of a "bed layer" is necessary for two reasons. One is to account for the difference in the mechanism of transport and the other is to relate the suspended load to the bed-material. As an average, the existence of such a layer close to the boundary will be assumed here.

In the case of sand mixtures, the transport rate of different particles is a function of their size. In non-uniform sand-beds, it is

convenient to divide the bed-material into a number of size fractions and to consider the transport phenomenon for each size fraction as determined by its geometric mean size.

The unit bed-material transport rate g_i (in units of weight per unit time per unit width of the flow section) of size fraction i of the bed-material can be written as

$$g_i = g_{bi} + g_{si}$$

in which g_{bi} and g_{si} are the bed load and the suspended load transport of size fraction i, respectively. Similarly the total bed-material transport rate g_t can be written as

$$g_t = \sum_{i=1}^{n} g_i = \sum_{i=1}^{n} g_{bi} + \sum_{i=1}^{n} g_{si} = g_{tb} + g_{ts} \tag{9-3}$$

where n is the number of size fractions into which the bed-material is divided.

The suspended load, g_{si} of the size fraction i in terms of the concentration of suspended sediment and the local velocity is

$$g_{si} = d \int_{\eta_{ai}}^{1} C_{\eta i} \, u_\eta \, d\eta \tag{9-4}$$

where,

η_{ai} is the dimensionless thickness of the bed layer,

$C_{\eta i}$ is the concentration of suspended sediment in units of weight per unit volume of the mixture at η,

u_η is the velocity along the mean direction of flow at η,

η is the dimensionless elevation above the mean bed level, and the subscript i refers to the size fraction.

Gradation of the total bed-material load in terms of the portion of the transported material in the size fraction i of the bed-material, f_{gi} is

$$f_{gi} = \frac{g_i}{g_t} \qquad (9\text{-}5),$$

where

$$\sum_{i=1}^{n} f_{gi} = 1 \quad .$$

To evaluate Equation (9-3) through (9-5) hypotheses about the movement of material in the bed layer and the variation of concentration in the vertical above the bed layer are required.

Variation of Concentration in the Vertical

The source of all bed-material in suspension for channels with rigid walls is the channel bed. Sediment particles are lifted from the bed by turbulent eddies and once caught in the eddy, the height to which they are raised in the flow, depends on the characteristics of the eddy. Simultaneously, the particles are settling with respect to the transporting eddy under the influence of gravity. Because of this slippage between the eddy and the sediment and the mass exchange of the eddy with layers of smaller concentration, the bed-material concentration in the vertical reduces with distance from the bed. Instantaneous concentrations of bed-material at any point in a vertical experience great variations. However, a time average concentration at each level can be determined to define an average concentration profile in the depth of flow.

The equation for the variation of concentration in the vertical has been derived on the basis of momentum exchange in the sediment-liquid

mixture (ASCE Task Committee, 1963). For uniform flow conditions, the derivation of the differential equation for the concentration profile is presented in Appendix A, see Equation A-38. In general, not enough is known about the behavior of the diffusivity coefficient ε_s for the sediment but it is related to the turbulent diffusivity for water as $\varepsilon_s = \beta\, \varepsilon_f$ where $\beta = 1$. For this condition Equation (A-38) reduces to

$$\beta\varepsilon_f \frac{d\, C_y}{dy} + C_y w = 0 \tag{9-6}$$

in which C_y is the concentration of sediment in weight per unit volume of the mixture at distance y above the mean bed elevation. In Equation (9-6) the value of β is generally assumed as 1 for want of better information. To solve this equation, the functional relationship of ε_f with y is required. For turbulent flow with $\varepsilon_f >> \nu$,

$$\varepsilon_f = \frac{\tau}{\rho \cdot \frac{du}{dy}} \tag{9-7}$$

For a logarithmic velocity distribution and a linear variation of the shear τ along the depth ε_f is parabolically distributed as

$$\varepsilon_f = \kappa_o U_{*o} \left(y - \frac{y^2}{d}\right) \tag{9-8}$$

Integration of the differential Equation (9-6), then yields,

$$\frac{C_\eta}{C_{\eta_a}} = \left[\frac{1-\eta}{1-\eta_a} \quad \frac{\eta_a}{\eta}\right]^z \tag{9-9}$$

where

$z = \frac{w}{\beta\kappa_o U_{*o}}$ is the Rouse number and (9-9a)

η_a is the dimensionless reference level at which the concentration is C_{η_a}.

For a logarithmic velocity distribution and a constant shear stress equal to the boundary shear stress τ_o, Equation (9-7) yields, a linearly increasing value of ε_f, as

$$\varepsilon_f = \kappa_o U_{*o}\, y \quad . \tag{9-10}$$

The relative concentration equation in this case becomes

$$\frac{C_\eta}{C_{\eta_a}} = \left(\frac{\eta_a}{\eta}\right)^z \tag{9-11}$$

If a constant value of ε_f is assumed, the relative concentration is given by

$$\frac{C_\eta}{C_{\eta_a}} = e^{\frac{-w \cdot d}{\beta \varepsilon_f}(\eta - \eta_a)} \tag{9-12}$$

Equations (9-9), (9-11), and (9-12) provide values of the relative concentration in the vertical for various distributions of ε_f. Of these, Equation (9-9) is the one most widely used and it has been verified for both the laboratory flumes and the natural channels. However, the values of z obtained from laboratory and field data show a departure from that given by Equation (9-9a) for a value of $\beta = 1$. Anderson's study for example, showed that the values of z measured from concentration profiles of Enoree River were smaller than those computed from Equation (9-9a). Similar results were obtained by Colby and Hembree (1955) in their study of Niobrara River. A lower z value in any of the three equations means higher relative concentrations throughout the depth.

Use of Equation (9-9a), therefore, results in an underestimation of total suspended load.

Although, Equations (9-9), (9-11) and (9-12) are based on grossly different distributions of ϵ_s, they yield nearly similar distributions of concentration. Equations (9-9) and (9-11) both plot as straight lines on log-log paper, with the ordinate $(\frac{1-\eta}{\eta})$ for Equation (9-9) and η for Equation (9-11). Equation (9-9) has no particular advantage over the latter, expecially when the uncertainty about the value of z in sand-bed channels is of far greater import than the minor difference between the distributions resulting from the two equations. As far as the underlying hypotheses are concerned, Equation (9-11) corresponds to the conditions stipulated for the inner layer and Equation (9-9) for the conditions of the outer layer. Values of relative concentrations C_η/C_{η_a} for different z values (0.3 - 5.0) are shown in Table 9-1. In this table the values of relative concentration in column 1, have been computed by Equation (9-9) and those in column 2, have been based on Equation (9-11) in the inner layer ($\eta \leq 0.15$) and on Equation (9-9) in the outer layer ($\eta > 0.15$). The values in column 2, correspond to the shear distribution assumed in the inner and outer layer model of the turbulent flow. There is almost no difference in the values of the relative concentrations obtained for the conditions of the two-layer model of flow and those obtained from the conventionally used Equation (9-9).

For sand mixtures, the above derivations of relative concentration apply to individual size fractions of the mixture. There is an affect of the concentration of sediment on the fall velocity of individual particles, but this again is smaller than the uncertainities in z.

Evaluation of the Suspended Load

To evaluate the total suspended load in flow over a sand-bed, the model of an inner layer up to 0.15 d from the mean bed elevation and an outer layer from 0.15 d to d, developed in Chapter VIII will be used Near the water surface the cut-back in the surface layer will be ignored, as in the developing of the resistance function. In the context of the suspended load, the 'cut-back' in the surface layer is of even lesser importance, because the concentration of bed material in this layer is generally small.

The vertical distribution of sediment for size fraction i and local mean velocity in the two layers are given below.

Inner layer

$$\eta_{ai} \leq \eta \leq .15$$

$$u_\eta = \frac{U_{*o}}{Ae.\kappa_o} \ln\left(33.35 \frac{\eta}{\eta_{ks}}\right) \tag{9-13}$$

$$C_{\eta i} = C_{\eta_{ai}} \left(\frac{\eta_{ai}}{\eta}\right)^{Aez_i} \tag{9-14}$$

Outer layer

$$.15 \leq \eta \leq 1.0$$

$$u_\eta = \frac{U_{*o}}{\kappa_o} \left[\frac{1}{Ae} \ln\left(33.35 \times \frac{0.15}{\eta_{ks}}\right) + \ln\left(\frac{\eta}{.15}\right)\right] \tag{9-15}$$

$$C_{\eta i} = C_{\eta_{ai}} \left\{\left(\frac{\eta_{ai}}{0.15}\right)^{Aez_i} \left(\frac{0.15}{0.85}\right)^{z_i}\right\} \left(\frac{1-\eta}{\eta}\right)^{z_i} \tag{9-16}$$

In Equations (9-13) to (9-16) which pertain to the fraction i of the bed material, Ae is the ratio of total shear velocity U_{*o} to the effective

shear velocity U_{*oe} and $Ae \geq 1$ as discussed in Chapter VIII. For the inner layer, the concentration distribution is based on Equation (9-11) in conformity with its shear distribution. Equation (9-16) for the outer layer is based on Equation (9-9) for a similar reason. The dimensionless grain roughness η_{ks} is given by $ks/d = D_{84}/d$ and η_{ai} is the dimensionless distance from the mean elevation of the boundary at which the reference concentration is $C_{\eta_{ai}}$. As discussed subsequently, $\eta_{ai} = \frac{2D_i}{d}$, where D_i is the geometric mean diameter of the fraction i. In Equations (9-13) and (9-15), constant 33.35 conforms with the expression for the average velocity used in developing the resistance function.

In the flume data information about the variation of bed-material concentration with the depth is not available. Therefore, it was not possible to directly verify the applicability of the exponent Aez_i in Equation (9-14). However, analysis of the flume data for the total bed-material transport showed that a greater consistency in the transport function was obtained if exponent Aez_i is replaced by z_i. With this change Equations (9-14) and (9-16) become

$$C_{\eta i} = C_{\eta_{ai}} \left(\frac{\eta_{ai}}{\eta}\right)^{z_i} \quad \text{for} \quad \eta_{ai} \leq \eta \leq 0.15 \tag{9-17}$$

and

$$C_{\eta i} = C_{\eta_{ai}} \left(\frac{\eta_{ai}}{0.85}\right)^{z_i} \left(\frac{1-\eta}{\eta}\right)^{z_i} \quad \text{for} \quad 0.15 < \eta \leq 1.0 \tag{9-18}$$

The total suspended load for size fraction i, evaluated for the velocity and concentration distributions given in Equations (9-13), (9-15), (9-17) and (9-18) is

$$g_{si} = 2.5\, U_{*o}\, d\left(\frac{\tau_o - \tau_{ci}}{\tau_o}\right) C_{\eta_{ai}} \left[\frac{1}{Ae}(A_i + B_i) + C_i\, I_i + D_i\, J_i\right] \quad (9\text{-}19)$$

where

$\left(\frac{\tau_o - \tau_{ci}}{\tau_o}\right)$ is a dimensionless weighting function for the reference concentration of size fraction i,

τ_{ci} is the critical shear for size fraction i,

τ_o is the boundary shear stress, γdS

$$A_i = \frac{\eta_{ai} \ln\left(\frac{33.35}{\eta_{ks}}\right)}{(1 - z_i)} \left\{\left(\frac{0.15}{\eta_{ai}}\right)^{1-z_i} - 1\right\}, \quad \text{for } z \neq 1 \quad (9\text{-}20)$$

$$B_i = \eta_{ai} \left\{\frac{\left(\frac{0.15}{\eta_{ai}}\right)^{1-z_i} \ln(.15) - \ln(\eta_{ai})}{(1 - z_i)} - \frac{\left(\frac{.15}{\eta_{ai}}\right)^{1-z_i} - 1}{(1 - z_i)^2}\right\}, \quad (9\text{-}21)$$

for $z \neq 1$

$$C_i = D_i \cdot \ln\left[\frac{1}{0.15} \cdot \left(\frac{5.0}{\eta_{ks}}\right)\right]^{\frac{1}{Ae}}, \quad (9\text{-}22)$$

$$D_i = \left(\frac{\eta_{ai}}{0.85}\right)^{z_i}, \quad (9\text{-}23)$$

$$I_i = \int_{.15}^{1} \left(\frac{1-\eta}{\eta}\right)^{z_i} \cdot d\eta \quad (9\text{-}24)$$

and

$$J_i = \int_{.15}^{1} \left(\frac{1-\eta}{\eta}\right)^{z_i} \ln \eta \cdot d\eta \quad (9\text{-}25)$$

when $z = 1$, values of A_i and B_i are,

$$A_i = \eta_{ai} \ln\left(\frac{33.35}{\eta_{ks}}\right) \cdot \ln\left(\frac{0.15}{\eta_{ai}}\right) \text{ and} \quad (9\text{-}26)$$

$$B_i = \frac{1}{2}\eta_{ai}\{\ln(0.15\eta_{ai})\ \ln(\frac{0.15}{\eta_{ai}})\} \tag{9-27}$$

In Equation (9-19) through (9-27), all other symbols have the same meanings as previously given. $C_{\eta_{ai}}$, in Equation (9-17) is as yet unknown. It has the units of weight of sediment per unit volume of the mixture. The shear velocity U_{*o} has units of length per unit time and depth d is a length. All other terms in Equation (9-17) are dimensionless except g_{si}. For any consistent system of units used for $C_{\eta_{ai}}$, U_{*o} and d, resulting units of g_{si} are in similar units of weight per unit time per unit width of the channel.

Evaluation of the Bed Load

In the above evaluation of the suspended load, the reference concentration has been taken at a dimensionless distance η_{ai} from the bed for the size fraction i. The distance $\eta = 0$ to $\eta = \eta_{ai}$ is defined as the bed layer. As explained earlier, the concept of bed layer is artificial in general but it is expedient. The bed load is contained in this layer and is assumed to be moving with the flow velocity at the top of the layer with a uniform concentration in its thickness. In graded sand beds, the thickness of the bed layer can be either assumed similar for all size fractions or as a variable related to the mean size of each size fraction. In this study it was found that for the flume data a variable thickness of the bed layer gives a better prediction of the gradation of the transported bed-material than some other assumptions. Therefore, the bed layer for different size fractions is assumed to have a thickness equal to twice the geometric mean diameter (D_i) of each size fraction. For this condition the bed load g_{bi} in terms of concentration $C_{\eta_{ai}}$ is,

$$g_{bi} = 2.5\, U_{*o}\, \eta_{ai} \left(\frac{\tau_o - \tau_{ci}}{\tau_o}\right) \cdot C_{\eta_{ai}} \ln\left(\frac{33.35\, \eta_{ai}}{\eta_{ks}}\right) \cdot \frac{d}{Ae} \tag{9-28}$$

where $\eta_{ai} = \frac{2D_i}{d}$ and all the other terms are as defined earlier.

Evaluation of the Reference Concentration

The total load g_t for all the fractions of the bed material can now be obtained by using Equation (9-3) in conjunction with Equation (9-19) and (9-28). The reference concentration $C_{\eta_{ai}}$ for the ith fraction pertains to the bed layer. In this layer the relative concentration of each fraction is the frequency of its availability in the bed material itself. If n fractions represent equal proportions of the bed-material

$$C_{\eta_{ai}} = \frac{1}{n}\, C_b \;,\; i = 1, 2, \ldots, n \;,$$

and the total bed-material transport is

$$g_t = C_b \cdot F_1 \tag{9-30}$$

where

C_b = concentration in the bed layers in weight of sediment per unit volume of the water sediment mixture and,

$$F_1 = \frac{2.5\, U_{*o}}{n} \left[\sum_{i=1}^{n} \left(\frac{\tau_o - \tau_{ci}}{\tau_o}\right) \frac{d}{Ae} \cdot \eta_{ai} \ln\left(\frac{33.35\eta_{ai}}{\eta_{ks}}\right) + \right.$$

$$\left. + d \sum_{i=1}^{n} \left(\frac{\tau_o - \tau_{ci}}{\tau_o}\right) \left\{\frac{1}{Ae} (A_i + B_i) + C_i I_i + D_i J_i\right\}\right] \tag{9-31}$$

The size range of each fraction of the bed-material can be obtained from the lognormal distribution parameters D_{50} and σ (Appendix B), and its geometric mean size determined. Alternatively, the cumulative

(percent finer) gradation curve can be used with the percentiles of mean fraction sizes determined from lognormal distribution. For $n = 5$, the geometric mean sizes of the fractions correspond to D_{90}, D_{71}, D_{50}, D_{29} and D_{10}. Critical shear τ_{ci} for these sizes can be determined from Shields' diagram. All the terms in Equation (9-30) are either known or can be computed from known bed-material (median size and geometric standard deviation), effective shear velocity U_{*oe}, depth and energy gradient. Therefore, the quantity F_1 is fully known and it has units of discharge intensity (velocity times depth).

Analysis of flume data showed that the mean reference concentration is related as

$$C_b \sim \gamma_s S^{0.75} \left(\frac{W_{50}}{U_{*oe}}\right) \tag{9-32}$$

where

S is Shields' parameter, $\rho U_{*oe}^2/(\gamma_s - \gamma_f)D_{50}$

W_{50} is the fall velocity of the median size D_{50} in the fluid medium,

U_{*oe} is the effective shear velocity defined in Chapter VIII

and,

γ_s is the specific weight of the sediment.

Both the Shields' parameter and the fall velocity ratio are dimensionless.

Transport Function

Introducing the functional relationship of C_b in Equation (9-30) gives the transport parameter

$$G = \gamma_s S^{0.75} \left(\frac{W_{50}}{U_{*oe}}\right) F_1 \tag{9-33}$$

G is in units of weight per unit time per unit width.

The relation between g_t and G has been obtained for the flume data by analyzing all the runs with bed movement. This analysis was carried out as follows:

For a given average bed-material gradation curves, geometric mean sizes of five fractions of equal frequency (0.20) were selected for each run. For these sizes and the given depth and energy gradient, the factor F_1 was computed. The effective shear velocity ratio Ae to be used in F_1 could have been obtained by solving the resistance function in Chapter VIII. However, since the average velocity of flow was known, Ae was computed from Equation (8-11). The fall velocity for each fraction size was computed by Equation (6-3) for the kinematic viscosity ν corrected for the temperature and the fine material load (column 23, USGS P.P. 462-I, 1966, Tables 2-11). The value of the transport parameter G was computed for each run from Equation (9-33). The gradation of the bed-material transport was also computed with the help of Equation (9-5). Values of measured g_t were plotted against computed values of G to determine the transport function.

The relation between the total bed-material transport per unit width g_t and the transport parameter G for all the flume runs is shown in Figure 9-1. To indicate the difference in this relation between the two regimes of flow, Figure 9-2 shows the data relating to the upper and intermediate $(P_{max} - D_{50})$ range (Chapter VIII) and Figure 9-3 shows the same for the runs in the lower $(P_{max} - D_{50})$ range. These figures show that the transport function is different in the two ranges. Figure 9-4 shows all the flume runs and the Rio Grande data (Chapter II) analyzed in the same way as flume runs. The river data comprise 112 points, most of which fall with the flume data;

and show the applicability of the analysis to both the river and the flume data. The derived relation between g_t and G is shown in Figure 9-5. The accuracy of this relation in predicting the total bed-material discharge is the same as indicated by the scatter in Figures (9-1) through (9-4). The use of the transport function in the computation of the total bed-material load will be illustrated in Chapter X.

The size gradation of the total bed-material transport as predicted by the transport parameter developed in this chapter and as observed in the flume runs was also studied in this analysis. In general, five size fractions are not enough to completely define the size gradation of the transported material. However, the cumulative size distribution curves defined by these fractions provide an adequate check on the accuracy of the prediction of size gradation. In Figure 9-6 through 9-10, the observed and the computed cumulative size distribution curves of the bed-material transport in flumes are shown for five different sands. For each sand, the comparison is made for four different transport rates from the lowest to the highest. These figures cover median bed-material diameters of 0.19 - 0.93 mm, bed-material transport rates of 0.00024 - 8.06 lbs per sec per ft and the bed forms from ripples to chutes and pools. In each case, the prediction of the size gradation of the transported bed-material is good. It may be stated that the Einstein's method (1950) in general predicts a much greater median size of the bed-material transport in the lower regime runs of the flume data than is actually observed.

For the use of the transport function to predict the bed-material transport in sand-bed channels, graphs have been developed in Chapter X. The use of these graphs is also illustrated there by solving an example.

CHAPTER X

APPLICATIONS OF THE RESISTANCE AND TRANSPORT FUNCTIONS

The resistance and transport functions developed in Chapters VIII and IX can be used for solving engineering problems related to uniform flow and equilibrium (bed) conditions in sand-bed channels. The resistance function can be used to predict average velocity and bed form, for a given energy gradient, average depth of flow, median bed-material size D_{50} and bed-material gradation σ. The transport function can be used to predict the total bed-material transport, its gradation and the vertical distribution of bed-material concentration in the flow. For the transport computations the average velocity of flow is needed in addition to the data required for the application of the resistance function. If the average velocity is not known, the resistance function can be used to determine it before using the transport function. In this chapter, the applications of these two functions will be illustrated and graphs will be developed and presented as an aid in solving the resistance and bed-material transport problems.

Resistance Function

Except in the range of slope-depth combinations, where non-unique solutions may exist, the flow resistance problem reduces to the determination of average velocity for a given slope, depth and bed-material. To determine the average velocity of flow, the resistance curve appropriate to the regime of flow is selected first. This selection is made from the P_{max} - D_{50} range (Figure 8-3) of the data. If the range is upper or lower, the corresponding resistance curve of Figure (8-9) is used. On the other hand, if the data fall in the intermediate

range, the solutions are obtained from both the upper-intermediate and lower-intermediate curves of Figure 8-10 and checked for the predicted bed form from Simons-Richardson criterion (Fig. 4-1). If the bed forms for the velocity predicted by both resistance curves of Figure 8-10 belong to either the upper or the lower regime, the solution obtained for the corresponding intermediate resistance curve is used. Should the predicted bed forms from the two curves fall in different regimes, the data are probably such that both solutions are possible. The average velocity in such cases cannot be predicted. The above method is illustrated in the following with the data of flume runs 2-31 and 2-07.

Given data:

Depth $d = 1.02$ ft

Slope $S = 0.00043$

$D_{50} = 0.19$ mm

$\sigma = 1.30$

to find average velocity of flow and bed form,

(i) Selection of resistance curve

$$U_{*o} = \sqrt{g\,d\,S}$$

$$= \sqrt{32.2 \times 1.02 \times 0.00043}$$

$$= 0.119 \text{ ft per sec}$$

$$D_{84} = D_{50} \times \sigma$$

$$= 0.19 \times 1.30$$

$$= 0.247 \text{ mm} = 0.810 \times 10^{-3} \text{ ft}$$

$$V_p = 2.5 \ln(12.27 \frac{d}{D_{84}})$$

$$= 2.5 \ln(\frac{12.27 \times 1.02}{0.810 \times 10^{-3}})$$

$$= 24.11$$

$$P_{max} = \rho U_{*o}^3 V_p$$

$$= 1.94 \times (0.027)^3 \times 21.65$$

$$= 0.078 \text{ ft-lb per sec per ft}^2.$$

From Figure 8-3 for $D_{50} = 0.19$ mm the upper limit of P_{max} for the lower regime bed form curve is 0.164 ft-lb per sec per ft^2. Hence, use the lower range resistance curve.

(ii) Computation of effective shear velocity U_{*oe}

From Equation (8-11) and (8-13):

$$\frac{V}{\Delta U_{*o}} = \frac{V_f}{\sqrt{1 - (\frac{U_{*oe}}{U_{*o}})^2}} \tag{10-1}$$

and

$$V_f = \frac{U_{*oe}}{U_{*o}} (V_p - 2.62) + 2.62 \tag{10-2}$$

Also, from Equation (8-14) for $g = 32.2$ ft^2 per sec, $\rho = 1.94$ slugs per ft^3 and $S_s = 2.65$, the relation between U_{*oe} and Shields' shear parameter S is

$$U_{*oe} = \sqrt{53.13\, D_{50} S} \tag{10-3}$$

From Equations (10-1), (10-2) and (10-3)

$$\frac{V}{\Delta U_{*o}} = \frac{\sqrt{53.13\, D_{50} S} \cdot (\frac{V_p - 2.62}{U_{*o}}) + 2.62}{\sqrt{1 - \frac{53.13\, D_{50} S}{U_{*o}^2}}} \tag{10-4}$$

Introducing values of U_{*o}, V_p and D_{50}, Equation (10-4) reduces to

$$\frac{V}{\Delta U_{*o}} = \frac{32.91 \quad \sqrt{S} + 2.62}{\sqrt{1 - 2.34S}}$$

Values of $V/\Delta U_{*o}$ are now calculated for different values of shear parameter S as given below:

$1/S$	S	$\frac{V}{\Delta U_{*o}}$
3.0	0.333	46.2
5.0	0.200	23.8
10.0	0.100	14.9
20.0	0.050	10.6
50.0	0.020	7.4

The curve defined by these values intersects the lower range resistance curve (Figure 8-9) at $1/S = 18.3$. For this value from Equation (10-3),

$$U_{*oe} = \sqrt{\frac{53.13 \times 0.623 \times 10^{-3}}{18.3}}$$

$$= 0.042 \text{ ft per sec.}$$

This is the value of effective shear velocity for the inner layer. The velocity profile of the flow can be computed from this using Equations (9-13) and (9-15).

(iii) Determination of average velocity

From Equation (10-2)

$$V = V_f \, U_{*o}$$

$$= (V_p - 2.62) \, U_{*oe} + 2.62 \, U_{*o}$$

$= (21.49)\ 0.042 + 2.62 \times 0.119$

$= 1.21$ ft per sec.

The actual average velocity obtained in the flume was 1.30 ft/sec.

(iv) Prediction of bed form,

Simons-Richardson criterion for bed form prediction can be used with the computed velocity to determine the bed form.

Stream power $P = \rho U_{*o}^2 V$

$= 1.94 \times (0.119)^2 \times 1.21$

$= 0.033$ ft-lb per sec per ft^2.

From Figure 4-1 for $D_{50} = 0.19$ mm and $P = 0.033$ ft-lb per sec per ft^2, the indicated bed form is ripples, as actually observed in the flume.

(v) Treatment for intermediate range cases

The problem solved above belonged to the lower $(P_{max} - D_{50})$ range. For cases belonging to the upper range, a similar solution would apply, except that the upper range curve of Figure (8-9) would be used. To indicate the use of the resistance function in the intermediate range, flume run 2-07 is now analyzed, with the given data.

Depth $d = 0.68$ ft

Slope $S = 0.0014$

$D_{50} = 0.19$ mm

$\sigma = 1.30$.

(a) Selection of resistance curve.

$U_{*o} = 0.175$ fps

$D_{84} = 8.1 \times 10^{-4}$ ft

$V_p = 23.10$

$P_{max} = 0.240$ ft-lb per sec per ft.

From Figure 8-3 the regime of flow could be either upper or lower. This indicates the use of resistance curves for the intermediate range in Figure 8-10.

(b) Effective shear velocity.

Equation (10-4) for the variables of this problem reduces to

$$\frac{V}{\Delta U_{*o}} = \frac{21.29\sqrt{S} + 2.62}{\sqrt{1 - 1.08\,S}}$$

and values of $V/\Delta U_{*o}$ for different S values are obtained as

$1/S$	$V/\Delta U_{*o}$
1.5	37.8
2.0	26.1
4.0	15.5
5.0	13.7
8.0	10.9
9.0	10.4
10.0	9.9

The solutions obtained on the upper and lower intermediate curves are as follows:

Upper-intermediate curve

$I/S = 1.6$

$U_{*oe} = 0.144$ ft per sec

$V = 3.4$ ft per sec

$P' = 0.20$ ft-lb per sec per ft.

Lower-intermediate curve

$$1/S = 9.5$$

$$U_{*oe} = 0.059 \text{ ft per sec}$$

$$V = 1.7 \text{ ft per sec}$$

$$p = 0.100 \text{ ft-lb per sec per ft.}$$

From Figure 4-1 the bed form prediction for both the solutions is dunes. Hence the solution obtained on the lower-intermediate curve, viz., $V = 1.7$ ft per sec is correct. (Actual velocity observed in the run is 1.78 ft per sec with a dune bed form).

If the bed forms predicted from both the curves were upper regime bed forms, the solution obtained from the upper-intermediate curve would have been adopted. If, however, the bed form regime corresponding to upper-intermediate curve was found as upper and that for the solution from lower-intermediate curve was lower, there is no way of indicating the correct solution by this method.

Transport Function

Engineering problems relating to the transport of sediment by flow over sand-bed channels involve prediction of bed-material load, size-distribution of this load, vertical distribution of sediment concentration and of the sediment transport. Equations (9-19) through (9-27) and Figure 9-5 can be used to determine these aspects. Computations needed for this purpose are easily performed with a digital computer, but may become cumbersome when ordinary desk calculations or slide rules are used. It is possible to simplify these computations by developing graphs for different components of the transport parameter G.

(i) Development of graphs

In general, the bed-load transport computations would involve evaluation of seven parameters A, B, C, D, I, J and g_b for each size fraction, which are dependent on two or more of the following variables.

η_{ai}, the relative thickness of the hypothetical boundary layer, $2\ D_i/d$

η_{ks}, the relative representative grain roughness D_{84}/d

Ae, the ratio of total and effective shear velocities in the boundary layer, U_{*o}/U_{*oe} and

z_i, the Rouse number, w_i/k_oU_{*o}.

Graphical representation of parameters A_i, C_i and the bed layer transport g_{bi} can be simplified by introducing

$$A1 = \ln\left(\frac{33.35}{ks}\right) \tag{10-5}$$

$$A2_i = \frac{\eta_{ai}}{(1-z_i)}\left\{\left(\frac{.15}{\eta_{ai}}\right)^{1-z_i} - 1\right\},\ z_i \neq 1 \tag{10-6}$$

$$C_1 = \ln\left[\frac{\left(\frac{5.0}{\eta_{ks}}\right)^{\frac{1}{Ae}}}{.15}\right] \tag{10-7}$$

and

$$b_{1i} = \eta_{ai}\ \ln\left(\frac{33.35\ \eta_{ai}}{\eta_{ks}}\right) \tag{10-8}$$

The transport parameter G for n equal fractions (Equation 9-33), then becomes

$$G = \frac{2.5U_{*o}}{n} \gamma_s S^{0.75} \left(\frac{w_{50}}{U_{*oe}}\right) \left[\sum_{i=1}^{n} \left(\frac{\tau_o - \tau_{ci}}{\tau_o}\right) b_{1i} \cdot \frac{d}{Ae} \right.$$

$$\left. + d \sum_{i=1}^{n} \left(\frac{\tau_o - \tau_{ci}}{\tau_o}\right) \left\{\frac{1}{Ae}(A1 \cdot A_{2i} + B_i) + C_1 \mathcal{D}_i I_i + \mathcal{D}_i J_i\right\}\right] \quad (10\text{-}9)$$

and fraction f_{gi} of the bed-material load in size fraction i (Equation 9-5) becomes

$$f_{gi} = \frac{\left(\frac{\tau_o - \tau_{ci}}{\tau_o}\right)\left\{b_{1i} \cdot \frac{d}{Ae} + \frac{d}{Ae}(A1 \cdot A2_i + B_i) + d(C_1 \mathcal{D}_i I_i + \mathcal{D}_i J_i)\right\}}{\sum_{i=1}^{n} \frac{\tau_o - \tau_{ci}}{\tau_o} \cdot \frac{d}{Ae} b_{1i} + d \sum_{i=1}^{n} \left(\frac{\tau_o - \tau_{ci}}{\tau_o}\right) \left\{\frac{1}{Ae}(A1 \cdot A2_i + \ _i) + C_1 \mathcal{D}_i I_i \right.}$$

$$\left. + \mathcal{D}_i J_i\right\} . \quad (10\text{-}10)$$

Values of A1, A2, B, C_1, $\mathcal{D}$, I, J and b_1 are shown in Tables 10-1 through 10-7 at convenient intervals of the independent variables. These are graphically presented in Figures (10-1) through (10-7). The range of variables covered by these tables and figures is

$$10^{-6} \leq \eta_a \leq 5 \times 10^{-2}$$

$$10^{-6} \leq \eta_{ks} \leq 5 \times 10^{-2}$$

$$0.1 \leq z \leq 6$$

$$1 \leq Ae \leq 7.$$

(ii) Evaluation of critical shear

For evaluating G or f_{gi}, the value of critical shear for the geometric mean size of each fraction is also needed. This can be obtained from Shields' diagram by trial and error. For constant kinematic viscosity ν and specific weight of fluid γ_f it is possible to express the critical shear τ_c in terms of grain diameter alone, by approximating the Shields' curve by straight line segments. Shulits and Hill (1968)

used such an approximation by adopting straight line segments between values of $U_{*o}D/\nu$ of 1, 4, 10, 600 and 1000 with the following resulting equations:

$$\tau_c = 0.0215\ D^{0.25} \qquad 3.0 \times 10^{-4} < D < 9.0 \times 10^{-4}\ \text{ft} \qquad (10\text{-}11)$$

$$\tau_c = 0.315\ D^{0.633} \qquad 9.0 \times 10^{-4} < D < 1.8 \times 10^{-3}\ \text{ft} \qquad (10\text{-}12)$$

$$\tau_c = 16.8\ D^{1.262} \qquad 1.8 \times 10^{-3} < D < 2.2 \times 10^{-2}\ \text{ft} \qquad (10\text{-}13)$$

$$\tau_c = 6.18\ D \qquad D > 2.2 \times 10^{-2}\ \text{ft.} \qquad (10\text{-}14)$$

These equations are valid for a value of $\nu = 10^{-5}$ ft^2 per sec, $\gamma_w = 62.5$ and $S_s = 2.65$. In view of the uncertainity about the critical shear indicated by Shields' original diagram in the form of a scatter band, these values can be adopted for other values of ν, without the need for recomputation.

(iii) Computation of total bed-material load.

Application of the transport function G in computing the total bed-material transport will now be illustrated by using the data for the following Rio Grande Section (Nordin and Beverage, 1965). These computations are made with the help of Figure 10-1 through 10-7.

Section: Rio Grande at Albuquerque, N. M. observed on March 26, 1954.

Given data:

Discharge, $Q = 670$ cfs

Width, $W = 333$ ft

Mean Depth, $d = 1.10$ ft

Mean Velocity, $V = 1.83$ ft/sec

Energy Gradient, $S = 0.0011$

Water Temperature, $T = 47^{o}$F

Bed-Material Gradation:

Size in mm:	0.125	0.250	0.500	1.000	2.000	4.000	8.000
Percent finer than	2.2	37.5	88.5	96.9	98.5	99.0	99.8

To determine total bed material load transport.

(a) Determination of fraction sizes.

The gradation of bed material is plotted on log-probability paper in Figure 10-8. From this plot, D_{84} = 0.456 mm., D_{50} = .289 mm., and D_{16} = .189 mm.

Thus,

$$\sigma = \frac{1}{2}\left(\frac{D_{84}}{D_{50}} + \frac{D_{50}}{D_{16}}\right) = \frac{1}{2}(1.58 + 1.53) = 1.55.$$

For 5 equal fractions of lognormally distributed bed-material their geometric mean sizes of the fractions are given by D_{90}, D_{71}, D_{50}, D_{29}, and D_{10}, and for the two extreme fractions, the limit sizes are taken as D_{95} and D_5. These sizes can either be interpolated from Figure 10-8 or calculated from the lognormal distribution as below.

Percentile	Interpolated Size mm	Interpolated Size ft x 10^3	Lognormal Size mm
D_{90}	.543	1.780	$D_{50}\sigma^{1.28}$ = .506
D_{71}	.372	1.220	$D_{50}\sigma^{.55}$ = .368
D_{50}	.289	0.948	$D_{50}\sigma^{0.0}$ = .289
D_{21}	.227	0.744	$D_{50}\sigma^{.55}$ = .227
D_{10}	.169	0.544	$D_{50}\sigma^{-1.28}$ = .165

For illustration, the interpolated sizes are adopted here.

(b) Computation of the transport parameter G.

$$U_{*o} = \sqrt{32.2 \times 1.10 \times 0.0011}$$

$$= 0.197 \text{ ft per sec}$$

$$V_f = \frac{V}{U_{*o}} = \frac{1.83}{0.197} = 9.27$$

$$V_p = 2.5 \ln\left(\frac{12.27d}{D_{84}}\right)$$

$$= 2.5 \ln(12.27 \times 1.10/1.47 \times 10^{-3})$$

$$= 22.8.$$

From Equation (8-11)

$$U_{*oe} = U_{*o} \cdot \frac{V_f - 2.62}{V_p - 2.62}$$

$$= 0.197 \times \frac{6.65}{20.18}$$

$$= 0.065 \text{ ft per sec}$$

$$Ae = \frac{U_{*o}}{U_{*oe}} = \frac{0.197}{.0065} = 3.03 \quad .$$

$$\tau_o = \gamma dS = 62.4 \times 1.10 \times 0.0011 = 0.0755 \text{ lb per ft}^2$$

$$S = \frac{U_{*oe}}{53.13\, D_{50}} = \frac{(0.065)^2}{53.13 \times 0.948 \times 10^{-3}} = 0.084.$$

$$\eta_{ks} = D_{84}/d = 1.47 \times 10^{-3}/1.10 = 1.336 \times 10^{-3}$$

Using the above parameters, the computation of transport function is illustrated in Table 10-8. Entries in this table are explained below.

Line 1. Geometric mean size of different size fractions of the bed-material as computed above.

Line 2. Fall velocity of each size in line 1 as computed for $\nu = 1.488 \times 10^{-5}$ (corresponding to water temperature of $47^{o}F$)

Line 3. Value of z_i, computed as $w_i/\kappa_o U_{*o}$ with $\kappa_o = 0.40$.

Line 4. Critical shear τ_{ci} for each fraction computed from Equations (10-11) through (10-14).

Line 6. Dimensionless depth $\eta_{ai} = 2D_i/d$ computed for each bed-material size fraction. η_{ai} is the thickness of hypothetical bed layer for each fraction.

Line 7. $A2_i$ for each fraction, obtained from Figure 10-2 for corresponding values of z_i and η_{ai}.

Line 8. Value of Ai for each size fraction computed as $Ai = A1 \times A2_i$. For $\eta_{ks} = 1.336 \times 10^{-3}$, value of $A1$ from Figure 10-1 is 10.10.

Line 9. Value of B_i for each size fraction obtained from Figure 10-3, for corresponding z_i and η_{ai} values. Note that values of B_i are always negative.

Line 10. Value of $\frac{1}{Ae}[A_i + B_i]$ computed for each size fraction, for $Ae = 3.03$.

Line 11, 12. Values of integrals I_i and J_i as read from Fig[illegible]-7. Note that values of J_i are always negative.

Line 13. Value of $\mathcal{D}_i$ read from Figure 10-5 for each size fraction.

Line 14. Value of C_i computed as $C_i = C_1 \mathcal{D}_i$. For $\eta_{ks} = 1.336 \times 10^{-3}$ and $Ae = 3.03$, $C_1 = 4.6$ from Figure 10-4.

Line 15, 16. Expressions computed for each size fraction from values of A_i, B_i, C_i, D_i, I_i, J_i and Ae.

Line 17. Obtained by multiplying line 16 with depth $d = 1.10$ and $(\frac{\tau_o - \tau_{ci}}{\tau_o})$ for each size fraction. Note that g_{si} is the total suspended load of size fraction i in lbs per sec per ft width.

Line 18. Value of b_{li} read from Figure 10-6 for values of η_{ai} and η_{ks} and multiplied with factor d/Ae .

Line 19. Obtained by multiplying line 18 with $(\frac{\tau_o - \tau_{ci}}{\tau_o})$ for each size fraction. Note that g_{bi} is the total bed load of size fraction i in lbs per sec per ft width.

Line 20. Obtained as sum of the values in lines 17 and 19 for each size fraction.

Line 21. Fraction of the total bed-material load in size fraction i computed as $f_{gi} = g_{ti} / \sum_{i=1}^{n} g_{ti}$.

Line 22. Value of the transport parameter G computed from Equation (10-9).

(c) Computation of total bed-material load.

For $G = 0.486$ lbs per sec per ft, Figure 9-5 gives $g_t = 0.10$ lbs per sec per ft. The concentration of bed-material load computed by the modified Einstein procedure for this section is reported by Nordin and Beverage (1966, p. F27) as 1060 ppm which corresponds to $g_t = 0.13$ lbs per sec per ft width.

(d) Size distribution of bed-material load.

Values of f_{gi} for each fraction have been calculated in Table 10-8. The size distribution of the bed-material load is then computed as follows:

Fraction No	Geometric Mean Size mm	Percentage of Bed-Material load in size fraction	Percentage Finer than size fraction in Bed-Material Load
1	.543	6.4	100.0
2	.372	6.5	93.6
3	.289	7.6	87.1
4	.227	16.1	79.5
5	.169	63.4	63.4

The cumulative frequency curve for the bed-material load is plotted in Figure 10-8. The median diameter of bed material load is found as 0.135 mm, with $\sigma = 1.78$.

The number of fractions required for defining the gradation of bed-material load generally should be greater than 5. However, for computing the total bed-material transport, five fractions are adequate.

CHAPTER XI

SUMMARY AND CONCLUSIONS

The object of this study was to develop resistance and transport functions for flow in sand-bed channels for two dimensional, time-homogeneous cases. This has been done for laboratory and field data. The functions obtained can be used to solve engineering problems. The main conclusions and results of this study are summarized below.

1. A two layer model of turbulent flow of incompressible fluids on rigid boundaries, proposed by Townsend, is presently (1971) considered adequate for describing the vertical velocity distribution in such flows. Townsend's model of the turbulence structure of flow in the vicinity of the wall and in the region away from the wall is also adequate. However, in the presence of large roughness elements on the boundary and other conditions which alter the momentum diffusion in the flow, emperical modifications of his model are necessary. A velocity distribution equation, in the inner layer, has been proposed for such conditions. This distribution is based on an effective shear velocity U_{*oe}. Using the mean bed elevation as the origin for vertical velocity distribution, and a value of von Karman's $\kappa = 0.40$, U_{*oe} is that shear velocity which gives the same logarithmic velocity distribution in the inner layer, as is actually observed.

2. A review of the differences between flow on rigid and mobile sand boundaries has been made to qualitatively bring out the changes in flow that occur due to the sand-beds. It is concluded that the bed forms constitute the most important difference between the two flows. Also, the suspended load near the boundary, the contact load and the porosity of the bed change the turbulence structure of the flow

in the inner layer and tend to increase the effective roughness of the boundary. Further it is concluded that in the case of sand-beds the viscous sublayer being subjected to a greater disturbance by the contact load and an increase in the turbulence intensity close to the porous bed is less stable than in the case of rigid boundary flows.

3. The properties of bed-material in the sand-size range have been reviewed. It has been concluded that out of all the properties of a particle in bed-material sand-mixtures, the particle size shows the greatest variation. An analysis of the size distribution in the bed-material samples from the Rio Grande and the West Pakistan Canals has been made. This analysis has shown that in the range of interest in the time-homogeneous flow problems in sand-bed channel (i.e., 10th to 90th percentile size) these samples exhibit lognormal size distribution. This distribution function is convenient to apply in the bed-material size analysis and in the interpolation of various percentile sizes. A summary of the lognormal distribution and of the methods for estimation of its parameters has been presented. It has been concluded that the methods of quantiles using the cumulative size distribution curves is an efficient and a convenient method for estimating the two parameters of the lognormal distributions.

4. A gross measure of momentum diffusion in turbulent flows is provided by the von Karman's κ. A study of the boundary conditions peculiar to the sand-bed channels has been made to show that because of the local non-uniformity of the flow, a typical velocity profile and hence a typical value of κ for the flow over a sand-bed cannot be determined from one vertical. The velocity profiles observed in the flumes have been analyzed to compute κ values in the region

corresponding to the outer layer of the turbulent boundary layer flow. Analysis of these values shows that κ is related to parameters which represent both the total sediment load and the bed forms.

5. Plane sand-bed condition offers a good opportunity to study the turbulent flow over mobile sand-beds without the complications created by other configurations. It has been shown from the analysis of such runs that the representative grain roughness size is related to D_{84} of the bed-material. It is also seen that the application of wall correction to flow in smooth walled sand-bed flumes over-corrects for width depth ratios greater than 3 so that the two dimensional conditions are better approximated by not making this correction and by using the mean depth of flow instead of the hydraulic radius. On the hydrodynamic roughness of the boundary, this analysis has shown that for the condition of general grain movement, the boundary always behaves as hydrodynamically rough.

6. In developing the resistance function for flow in a sand-bed channel, it has been found that different functions are needed for different regimes of flow. A criterion for predicting the regime for a given depth, slope and bed-material has been developed. A resistence factor in terms of the effective shear velocity is derived and resistance functions for different regimes have been developed. For the laboratory flumes and the West Pakistan canals, the method predicts average velocity of flow within 15 percent of the observed mean velocity for most of the data used.

7. A transport function has been developed using the inner-outer layer model of flow in sand-bed channels same as used in deriving the mean vertical velocity distribution and the resistance functions. The

transport function has been presented as a graphical relation between the bed-material discharge per unit width and a transport parameter G. This parameter (G) is the sum of the suspended load from the water surface down to a hypothetical bed layer and the transport in the bed layer, all in terms of a reference concentration at the bed. The reference concentration is a function of the Shields' grain shear parameter S and the ratio of fall velocity to the effective shear velocity, w_{50}/U_{*oe}. For non-uniform sand-beds, the bed-material has been divided into size fractions of equal frequency and in this case the transport function also predicts the size distribution of the bed-material load. The transport function has been found to be the same for the Rio Grande data and the flume data. The size gradation of the bed-material load as obtained from the transport function is identical to that obtained in the flume data in the whole range of bed forms and transport.

8. Example problems have been solved to illustrate the use of the resistance and transport functions. To facilitate the use of the transport function with ordinary slide rules, graphs and tables have been developed to evaluate its components.

Recommendations for Future Study

There is no theory of turbulent flow over mobile sand-beds comparable to the theories available for rigid boundary flows. Therefore, recourse has to be made to the rigid boundary turbulent flow theories when dealing with sand-beds. A qualitative survey of the differences between the two flows has been made in Chapter III. This survey brings out the areas where additional research is needed to produce quantitative results. Future studies in the field of flow in sand-bed channels

should concentrate on these areas as well as on the easy and meaningful measurement of turbulence quantities in sand-bed channels. It is believed that the final solution to the problem of flow in sand-bed channels will emerge out of a parallel effort in these two related areas in the form of a theory of turbelent flow which quantitatively accounts for the effects of bed forms, bed porosity, contact load, suspended load, etc.

Study of turbulence characteristics in fluids and especially solid-fluid mixtures have been hampered by lack of suitable measuring technique. Work done by Raichlen (1967) and McQuivey and Richardson (1969) has opened a fruitful avenue which needs to be pursued. The answer to some of the more vexing problems like the changes in the flow structure with the regimes of flow, can be provided by such studies through the exploration of basic turbulent mechanisms associated with these regimes.

The phenomenon of the evolution of bed forms in sand-bed channels remains somewhat of a mystery. Considering the importance of these forms in delineating regions of flow identified with different behaviors of resistance and transport, basic research into their mechanism is urgently needed. The need is for a phenomenological model which explains the generation of the bed forms and their growth; especially, the change from the lower to the upper regime bed forms. Such a model should also yield parameters which can more accurately predict the bed form from known bed-material, depth and slope.

The analysis of plane sand-bed flows in smooth walled flumes, made in this study, has shown that two dimensional flow conditions with mean depth as the length parameter are adequate for the resistance analysis with width depth ratios of the flow varying from about 3 to 60. Probably a minimum aspect ratio of about 5 should be maintained in smooth

walled flume studies to remove the effects of varying width depth ratios. To evaluate the wall correction needed with smaller width depth ratios, some basic research is needed. This can be done by observing the mean velocity distributions in the flow for similar bed forms and average velocities and by dividing the flow in regions corresponding to the wall and the bed.

In this study it has been argued that the viscous sublayer in the flow of water on moving sand-beds is unstable because of the movement of the particles at the boundary and the porosity of the bed. The instability of the sublayer has also been indirectly inferred from the analysis of plane sand-bed runs. A direct experimental verification of this conclusion is a difficult task because of the small length scales involved in the study of the viscous sublayer. However, similar conditions can be simulated by using more viscous fluids and larger (artificial) roughness elements. Such a study should also be undertaken to clarify the hydrodynamic roughness behavior of plane sand-bed channels.

REFERENCES

REFERENCES

Abdel-Aal, Farouk M., "Extension of Bed-Load Formulas to High Sediment Rates," Tech. Report No. HEL22-1, Hydraulic Engineering Laboratory, College of Engineering, University of California, Berkeley, September 1969.

Aitchison, J., and Brown, J.A.C., "The Lognormal Distribution with Special Reference to its Use in Economics," Cambridge University Press, 1957.

Anderson, A. G., "The Characteristics of Sediment Waves Formed by Flow in Open Channels," Proceedings Third Mid-western Conference on Fluid Mechanics, Univ. of Minnesota, Minneapolis, pp. 379-395, 1953.

Anderson, G. E., "Experiments on the Rate of Wear of Sand Grains," Journal of Geology, Vol. 34, pp. 144-158, 1926.

ASCE Task Committee on Preparation of Sedimentation Manual, Committee on Sedimentation, "Sediment Transport Mechanics: Introduction and Properties of Sediment," Journal of Hyd. Div., ASCE, Vol. 88, No. HY4, pp. 77-107, July, 1962.

ASCE Task Committee on Preparation of Sedimentation Manual, Committee on Sedimentation, "Sediment Transport Mechanics: Suspension of Sediment," Journal of Hyd. Div., ASCE, Vol. 89, No. HY5, pp. 45-76, September 1963.

Bagnold, R. A., "The Flow of Cohesionless Grains in Fluids," Royal Society (London) Philosophical Transactions, Vol. 249, p. 235-297, December, 1956.

Barton, J. R. and Lin, P. N., "A Study of Sediment Transport in Alluvial Channels," Report No. 55, JRB2, Civil Engineering Department, Colorado A and M College, Fort Collins, Colorado, 1955.

Blench, T., "Normal Size Distribution Found in Samples of River-Bed Sand," Civil Engineering, p. 49, February 1952.

Brush, Lucien M. Jr., "Sediment Sorting in Alluvial Channels," Primary Sedimentary Structures and Their Hydrodynamic Interpretation Society of Economic Paleontologists and Mineralogists Special Publication No. 12, pp. 25-33, August 1965.

Chabert, J. and Chauvin, J. L., "Formation des dunes et des rides dans les modeles fluviaux Bull. Centre Rech. Essais de Chatou, Vol. 4, pp. 31-51, 1963.

Chu, Hsien and Streeter, V. L., "Fluid Flow and Heat Transfer in Artificially Roughened Pipes," Final Report, Project 4918, Illinois Institute of Technology, 62 p., 1949.

REFERENCES - Continued

Clauser, F. H., "The Turbulent Boundary Layer Advances in Applied Mechanics," Vol. 4, New York, pp. 1-51, 1956.

Colby, B. R., "Discharge of Sands and Mean-Velocity Relationships in Sand-Bed Streams," U. S. Geol. Survey Prof. Paper, 462-A, 1964.

Colby, B. R. and Hembree, C. H., "Computations of Total Sediment Discharge Niobrara River Near Cody, Nebraska," U.S.G.S. Water Supply Paper 1357, 1955.

Colebrook, C. F., "Turbulent Flow in Pipes with Particular Reference to the Transition Region between the Smooth and Rough Pipe Laws," Journal of the Institute of Engineers, Vol. II, pp. 133-155, February 1939.

Colebrook, C. F., and White, C. M., "Experiments with Fluid Friction in Roughened Pipes," Proceedings Royal Society of London, Series A, Vol. 161, pp. 367-381, 1937.

Daranandana, Niwat, "A Preliminary Study of the Effect of Gradation of Bed Material on Flow Phenomena in Alluvial Channels," Ph.D. Dissertation, Colorado State University, 1962.

Draper, N. R., and Smith, H., "Applied Regression Analysis," John Wiley and Sons, Inc., New York, 1966.

Einstein, H. A., "Formulas for the Transportation of Bed Load," Trans. ASCE, Vol. 107, pp. 575-577, 1942.

Einstein, H. A., "The Bed-Load Function for Sediment Transportation in Open Channel Flows," Technical Bulletin, No. 1026, U. S. Department of Agriculture, Soil Conservation Service, 1950.

Einstein, H. A. and Chien, Ning, "Second Approximation to the Solution of the Suspended-Load Theory," Sediment Series No. 3, Corps of Engineers, Missouri River Division, U. S. Department of the Army, Omaha, Nebraska, 1954.

Einstein, H. A. and Chien, Ning, "Effects of Heavy Sediment Concentration near the Bed on Velocity and Sediment Distribution," U. S. Army Engineer Division, Missouri River, Corps of Engineers, Omaha, Nebraska, MRD, Series No. 8, August 1955.

Elata, C. and Ippen, A. T., "The Dynamics of Open Channel Flow with Suspensions of Neutrally Buoyant Particles," Technical Report No. 45, Hydrodynamic Lab., Massachussetts Institute of Technology, Cambridge, Massachusetts, January 1961.

Engelund, Frank, "Hydraulic Resistance of Alluvial Streams," Proceedings ASCE, Journal of Hydraulics Div., ASCE, Vol. 92, No. HY2, March 1966.

REFERENCES - Continued

Engelund, Frank, "Instability of Erodible Beds," Journal of Fluid Mechanics, Vol. 42, Pt. 2, pp. 225-244, 1970.

Epstein, Benjamin, "The Mathematical Description of Certain Breakage Mechanisms Leading to the Logarithmico-Normal Distribution," Journal of the Franklin Institute, Vol. 244, No. 6, Dec. 1947.

Friedman, Gerald M., "On Sorting, Sorting Coefficients and the Lognormality of the Grain-Size Distribution of Sandstones," Journal of Geology, V. 70, pp. 737-753, 1962.

Goma, R. J. M., and Gelhar, L. W., "Turbulent Pipe Flow with Rough and Porous Wall," Report No. 109, Hydrodynamics Laboratory, Massachusetts Institute of Technology, Cambridge, Massachusetts, April 1968.

Goncharov, V. N., "Dynamics of Channel Flow," Translated from Russian by Israel Program for Scientific Translations, Jerusalem 1964.

Gradowczyk, M. H., "Wave Propagation and Boundary Instability in Erodible-bed Channels," Journal of Fluid Mechanics, Vol. 33, pc. 1, pp. 93-112, 1968.

Guy, H. P., Simons, D. B., and Richardson, E. V.,"Summary of Alluvial Channel Data from Flume Experiments, 1956-61," U. S. Geol. Survey Prof. Paper, 462-I, 1966.

Halmos, Paul R., "Random Alms," The Annals of Mathematical Statistics, Vol. XV, No. 2, June 1944.

Hama, F. R.,"Boundary Layer Characteristics for Smooth and Rough Surfaces," Transactions Society of Naval Architects and Marine Engineers, Vol. 62, pp. 333-358, 1954.

Hatch, Theodore, "Determination of Average Particle Size from the Screen-Analysis of Non-Uniform Particulate Substances," Journal of the Franklin Institute, Vol. 215, Jan. 1933.

Hino, Mikio, "Turbulent Flow with Suspended Particle," Journal of Hydraulics Division, Proceedings ASCE, Vol. 89, No. HY4, July 1963.

Hinze, J. O., "Turbulence, an Introduction to its Mechanism and Theory," McGraw-Hill Book Company, Inc., New York, 1959.

Inter-Agency Committee on Water Resources, "Some Fundamentals of Particle Size Analysis," Subcommittee on Sedimentation Report No. 12., U.S. Government Printing Office, 1958.

Johnson, J. W., "The Importance of Considering Side-Wall Friction in Bed-Load Investigations," Civil Engineering, Vol. 12, No. 6, pp. 329-331, June 1942.

REFERENCES - Continued

Kendall, M. G. and Stuart, A., "The Advanced Theory of Statistics," Vol. 2, Second Edition, Hafner Publishing Company, New York, 1967.

Kennedy, J. F., "Stationary Waves and Antidunes in Alluvial Channels," Report No. KH-R-2, California Institute of Technology, Pasadena, California, January 1961.

Keulegan, G. H., "Laws of Turbulent Flow in Open Channels," U. S. National Bureau of Standards, Journal of Research, Vol. 21, pp. 708-741, 1938.

Kolmogoroff, von A. N., "Uber Das Logarithmisch Normale Verteilungsgesetz Der Dimensionen der Teilchen Bei Zerstuckelung," Akademiia Nauk SSSR, Comptes Rendus (Doklady), Vol. 31, pp. 99-101, 1941.

Kolosous, H. J., and Davidian, J., "Roughness Concentration Effects on Flow Over Hydrodynamically Rough Surfaces," U. S. Geol. Survey Water Supply Paper 1592-D, pp. D-1 to D-21, 1966.

Krumbein, W. C., "Size Frequency Distribution of Sediments," Journal of Sedimentary Petrology, Vol. 4, pp. 65-77, 1934.

Krumbein, W. C., "Sediments and Exponential Curves," Journal of Geology, Vol. 45, pp. 577-601, 1937.

Krumbein, W. C., "Size Frequency Distribution of Sediments and the Normal Phi Curve," Journal of Sedimentary Petrology, Vol. 18, pp. 84-90, 1938.

Krumbein, W. C., "The Effects of Abrasion on the Size, Shape and Roundness of Rock Fragments," Journal of Geology, Vol. 49, pp. 482-520, 1941.

Krumbein, W. C., "Applications of Statistical Methods to Sedimentary Rocks," Journal of the American Statistical Association, Vol. 49, pp. 51-66, March 1954.

Lane, E. W. and Carlson, E. J, "Some Observations on the Effect of Particle Shape on the Movement of Coarse Sediments," Transactions American Geophysical Union, Vol. 35, No. 3., pp. 453-462, June 1954.

Laursen, E. M., "The Total Load of Streams," Paper No. 1530, Journal of the Hydraulics Division, ASCE, Vol. 84, No. HY1, Feb. 1958.

McQuivey, Raul S. and Richardson, E. V., "Some Turbulence Measurements in Open-Channel Flow," Proceedings of ASCE, Journal of Hydraulics Division, Vol. 95, No. HY1, Jan. 1969.

Mercer, A. G., "Characteristics of Sand Ripples in Low Froude Number Flow," Ph.D. Dissertation, University of Minnesota, June 1964.

REFERENCES - Continued

Meyer-Peter and Muller, R., "Formulas for Bed-load Transport," International Association for Hydraulic Structures Research Proceeding 2nd Meeting, Stockholm, pp. 39-65, 1948.

Nordin, C. F. Jr., and Beverage, J. P., "Sediment Transport in the Rio Grande New Mexico," U. S. Geological Survey Professional Paper 462-F, 1965.

Nordin, C. F. Jr., and Culbertson, J. K., "Particle-Size Distribution of Stream Bed Material in the Middle Rio Grande Basin," Geological Survey Research, U. S. Geological Survey Professional Paper 424-C, pp. C323-C326, 1961.

O'Loughlin, E. M., "Resistance to Flow over Boundaries with Small Roughness Concentrations," Ph.D. Dissertation, University of Iowa, August 1965.

Perry, A. E. and Joubert, P. N., "Rough-Wall Boundary Layers in Adverse Pressure Gradients," Journal of Fluid Mechanics, Vol. 17, Pt. 2., pp. 193-211, 1963.

Perry, A. E., Schofield, W. H., and Joubert, P. N., "Rough Wall Turbulent Boundary Layers," Journal of Fluid Mechanics, Vol. 37, pt 2, pp. 383-413, 1969.

Pettijohn, F. J., "Sedimentary Rocks," Harper and Row, New York, Second Edition, 1957.

Plumley, W. J., "Black Hill Terrace Gravels: A Study in Sediment Transport," Journal of Geology, Vol. 56, pp. 526-577, 1948.

Rafay, Tariq, "Analysis of Change in Size of Bed Material along Alluvial Channels," M.S. Thesis, Colorado State University, Nov. 1964.

Raichlen, F., "Some Turbulence Measurements in Water," Journal, Engineering Mechanics Div., Proceedings ASCE, Vol. 93, No. EM2, April 1967.

Raudkivi, A. J., "Bed Forms in Alluvial Channels," Journal of Fluid Mechanics, Vol. 26, pt. 3, pp. 507-514, 1966.

Reynolds, A. J., "Waves on the Erodible Bed of Open Channel," Journal of Fluid Mechanics, Vol. 22, Part 1, pp. 113-133, 1965.

Richardson, E. V., "Resistance to Flow in Sand Channels," Ph.D. Dissertation, Colorado State University, CED65EVR20, 1965.

Rotta, J. C, "Turbulent Boundary Layers in Incompresible Flow," Progress in Aeronautical Sciences, Vol. 2, Boundary Layer Problems, Pergamon Press, New York, 1962.

REFERENCES - Continued

Rouse, H., "Critical Analysis of Open-Channel Resistance," Proceedings ASCE, Journal of Hydraulics Division, Vol. 91, No. HY4, pp. 1-25, July 1965.

Rouse, H., Koloseus, H. J., and Davidian, J., "The Role of Froude Number in Open-Channel Resistance," Journal of Hydraulic Research, IAHR, Vol. I-1, 1963.

Rubey, W. W., "Settling Velocities of Gravel, Sand, and Silt," American Journal of Science, Vol. 25, pp. 325-338, 1933.

Russell, R. D. and Taylor, R. E., "Roundness and Shape of Mississippi River Sands," Journal of Geology, Vol. 45, pp. 225-267, 1937.

Sayre, W. W., and Albertson, M. L., "Roughness Spacing in Rigid Open Channels," Am. Soc. Civil Engineers Trans., V. 128, 1963.

Schlichting, H., "Boundary Layer Theory," McGraw-Hill Book Company, New York, 6th Ed., 1968.

Shulits, Sam and Hill, Ralph D. Jr., "Bedload Formulas," The Pennsylvania State University, 1968.

Simons, D. B. and Richardson, E. V., "Forms of Bed Roughness in Alluvial Channels," Paper No. 3414, Transactions ASCE, Vol. 128, Pt. I, pp. 284-323, 1963.

Simons, D. B. and Richardson, E. V., "Resistance to Flow in Alluvial Channels," U.S. Geol. Survey Professional Paper 422-J, 1966.

Simons, D. B., Richardson, E. V., and Nordin, C. F. Jr., "Sedimentary Structures Generated by Flow in Alluvial Channels," Primary Sedimentary Structures and their Hydrodynamic Interpretation, Society of Economic Paleontologists and Mineralogists Special Publication No. 12, pp. 34-52, Aug. 1965.

Simons, D. B., Richardson, E. V., and Nordin, C. F. Jr., "Bedload Equation for Ripples and Dunes," U.S. Geol. Survey Prof. Paper 462-H, 1965(a).

Stringham, G. E., Simons, D. B., and Guy, H. P., "Behaviour of Large Particles Falling in Quiescent Liquids," U. S. Geol. Survey Professional Paper 562-C, pp. C1-36, 1969.

Subcommittee on Sediment Terminology, "Report of the Subcommittee on Sediment Terminology," Trans. Amer. Geophysical Union, Vol. 28, No. 6, pp. 936-938, Dec. 1947.

Terzaghi, Karl and Peck, Ralph B., "Soil Mechanics in Engineering Practice," John Wiley and Sons, New York, 1948.

REFERENCES - Continued

Thiel, G. A., "The Relative Resistance to Abrasion of Mineral Grains of Sand Size," Journal of Sedimentary Petrology, Vol. 10, pp. 102-124, 1940.

Toffaleti, F. B., "Deep River Velocity and Sediment Profiles and the Suspended Sand Load," Paper No. 28, Proceedings of the Federal Inter-Agency Sedimentation Conference, Misc. Publication No. 970, Agricultural Res. Service, U.S.D.A., p. 207-228, 1963.

Townsend, A. A., "The Structure of Turbulent Shear Flow," Cambridge University Press, New York, 1956.

Vanoni, V. A., "Some Effects of Suspended Sediment of Flow Characteristics," Proceedings Fifth Hyd. Conference, State University of Iowa, Studies in Engineering Bulletin 34, pp. 137-158, 1953.

Vanoni, Vito A. and Brooks, N. H., "Laboratory Studies of the Roughness and Suspended Load of Alluvial Streams," Report No. E-68, Sedimentation Laboratory, California Institute of Technology, Pasadena, California, Dec. 1957.

Vasiliev, Oleg, F., "Problems of Two-Phase Flow Theory," Vol. 5-3, Proceedings XIII Congress, International Association for Hydraulic Research, Kyoto, Japan, pp. 39-84, 1969.

Wadell, H., "Sphericity and Roundness of Rock Particles," Journal of Geology, Vol. XLI, No. 3, pp. 310-331, May 1933.

Wentworth, C. K., "A Laboratory and Field Study of Cobble Abrasion," Journal of Geology, Vol. 27, pp. 507-522., 1919

West Pakistan Water and Power Development Authority, "Canal and Headworks Data Observation Programme, Data Tabulation," Part II, Lahore, 1962-63.

Yano, Katsumasa and Daido, Atsuyuki, "The Effect of Bed-Load Movement on the Velocity Distribution of Flow," Proceedings XIIIth Congress of the International Association for Hydraulic Research, Vol. 2, pp. 325-332, 1969.

Yatsu, E., "On the Longitudinal Profile of the Graded River," American Geophysical Union Trans., Vol. 36, p. 655-663, 1955.

Zagustin, A. and Zagustin, K., "Mechanics of Turbulent Flow in Sediment-Laden Streams," Proceedings XIII Congress of the International Association for Hydraulic Research, Kyoto, Japan, Vol. 2, pp. B33-1 to B33-8, 1969.

APPENDICES

APPENDIX A

TWO-PHASE FLOW

APPENDIX A.

TWO-PHASE FLOW

Considering the sediment water complex as a combination of two independent phases, the equations of motion for a two-dimensional, steady turbulent flow in an open channel are derived in the following.

Let X and Y be the coordinate axes along and normal to the bed of the channel and let c_v be the volumetric concentration of the sediment at a distance y above the bed. For a volume $\forall$ of the mixture, the fraction occupied by the sediment is $\forall c_v$ and that by the water is $\forall(1-c_v)$. If ρ_s and ρ_f are the mass density of the sediment and the water, respectively, then the mass density ρ and mass density fluxes ρu and ρv of the mixture along the X and the Y directions are given by

$$\rho = \rho_f(1-c_v) + \rho_s c_v \tag{A-1}$$

$$\rho.u = u_f\rho_f(1-c_v) + u_s\rho_s c_v \tag{A-2}$$

$$\rho.v = v_f\rho_f(1-c_v) + v_s\rho_s c_v \tag{A-3}$$

where

u is the velocity along x-direction,

v is the velocity along y-direction,

the unscripted values refer to the mixture and

the scripts f and s refer to the water and the sediment phase, respectively.

The continuity equations for the two phases are

water:

$$\frac{\partial}{\partial x}\,[\rho_f(1-c_v)\,u_f] + \frac{\partial}{\partial y}\,[\rho_f(1-c_v)v_f] = 0 \quad , \tag{A-4}$$

sediment:

$$\frac{\partial}{\partial x}\,[\rho_s c_v u_s] + \frac{\partial}{\partial y}\,[\rho_s c_v v_s] = 0 \ . \tag{A-5}$$

Adding Equation (A-4) and (A-5) and substituting Equations (A-1) through (A-3),

$$\frac{\partial \rho u}{\partial x} + \frac{\partial \rho v}{\partial y} = 0. \tag{A-6}$$

Since both the sediment and the water are incompressible, Equations (A-4) and (A-5) can also be added to yield

$$\frac{\partial}{\partial x}\,[c_v\,u_s + (1-c_v)\,u_f] + \frac{\partial}{\partial y}\,[c_v\,v_s + (1-c_v)v_f] = 0 \ . \tag{A-7}$$

The momentum equations for the two phases along x and y directions are

water:

$$\frac{\partial}{\partial x}\,[\rho_f(1-c_v)\,u_f^2] + \frac{\partial}{\partial y}\,[\rho_f(1-c_v)\,u_f \cdot v_f] =$$

$$\rho_f(1-c_v)g_x - (1-c_v)\,\frac{\partial p}{\partial x} - (1-c_v)\,[\frac{\partial}{\partial x}\,\tau_{xx_f} + \frac{\partial}{\partial y}\,\tau_{xy_f}] - R_x \tag{A-8}$$

$$\frac{\partial}{\partial x}\,[\rho_f(1-c_v)\,u_f\,v_f] + \frac{\partial}{\partial y}\,[\rho_f(1-c_v)\,v_f^2] =$$

$$\rho_f(1-c_v)g_y - (1-c_v)\,\frac{\partial p}{\partial y} - (1-c_v)\,[\frac{\partial}{\partial x}\,\tau_{yx_f} + \frac{\partial}{\partial y}\,\tau_{yy_f}] - R_y \tag{A-9}$$

sediment:

$$\frac{\partial}{\partial x}[\rho_s c_v u_s^2] + \frac{\partial}{\partial y}[\rho_s c_v u_s v_s] =$$

$$\rho_s c_v g_x - c_v \frac{\partial p}{\partial x} - c_v [\frac{\partial}{\partial x} \tau_{xx_s} + \frac{\partial}{\partial y} \tau_{xy_s}] + R_x \qquad \text{(A-10)}$$

$$\frac{\partial}{\partial x}[\rho_s c_v u_s v_s] + \frac{\partial}{\partial y}[\rho_s c_v v_s^2] =$$

$$\rho_s c_v g_y - c_v \frac{\partial p}{\partial y} - c_v [\frac{\partial}{\partial x} \tau_{yx_s} + \frac{\partial}{\partial y} \tau_{yy_s}] + R_y \qquad \text{(A-11)}$$

where g_x and g_y are the components of gravity and R_x and R_y are the forces due to interaction of the two phases along X and Y direction, respectively. τ_{xx} and τ_{xy} are the shear terms subscripted f for the water and s for the sediment phase.

If w is the fall velocity of the sediment and the relative velocities of the sediment and the entraining fluid mass are given by

$$u_f = u_s \qquad \text{(A-12)}$$

$$v_f - w = v_s \qquad \text{(A-13)}$$

then from Equations (A-2) and (A-3)

$$u = \frac{1}{\rho} [u_f \rho_f (1-c_v) + u_f \rho_s c_v] \qquad \text{(A-14)}$$

and

$$v = \frac{1}{\rho} [v_f \rho_f (1-c_v) + (v_f - w)\rho_s c_v]$$

$$= v_W - \frac{\rho_s}{\rho} w c_v \qquad \text{(A-15)}$$

Using Equations (A-14) and (A-15), Equation (A-7) is

$$\frac{\partial}{\partial x}\,[c_v\, u_f + (1-c_v)\, u_f] + \frac{\partial}{\partial y}\,[c_v\, v_s + (1-c_v)\, v_f] = 0$$

or,

$$\frac{\partial u}{\partial x} + \frac{\partial}{\partial y}\,[c_v(v_f - w) + (1-c_v)\, v_f] = 0$$

or,

$$\frac{\partial u}{\partial x} + \frac{\partial u}{\partial y} = \frac{\partial}{\partial y}\,[c_v\, w - \frac{\rho_s}{\rho}\, w\, c_v] = -(\rho_s - \rho_f)\cdot\frac{\partial}{\partial y}\,[\frac{w\, c_v(1-c_v)}{\rho}]. \tag{A-16}$$

Also adding Equations (A-8), (A-10) and Equations (A-9), (A-11), and using Equations (A-12) and (A-13), one gets the momentum equations for the sediment-water mixture along X and Y directions as

$$\frac{\partial \rho u^2}{\partial x} + \frac{\partial \rho u v}{\rho y} = \rho g_x - \frac{\partial p}{\partial x} + \frac{\partial \tau_{xx}}{\partial x} + \frac{\partial \tau_{xy}}{\partial y} \tag{A-17}$$

$$\frac{\partial \rho u v}{\partial x} + \frac{\partial \rho v^2}{\partial y} = \rho g_y - \frac{\partial p}{\partial y} + \frac{\partial \tau_{yx}}{\partial x} + \frac{\partial \tau_{yy}}{\partial y} - \rho_f\, \rho_s\, \frac{\partial}{\partial y}\,[\frac{c_v(1-c_v)w^2}{\rho}] \tag{A-18}$$

where

$$\tau_{xy} = \tau_{xy_f} + \tau_{xy_s}\,,$$

$$\tau_{yy} = \tau_{yy_f} + \tau_{yy_s} \qquad \text{and}$$

$$\tau_{xx} = \tau_{xx_f} + \tau_{xx_s}\,.$$

Considerable simplification of above equations can be achieved for small concentrations.

If $c_v << 1$, then $c_v(1-c_v) \approx c_v$ and the volumetric continuity Equation (A-16) can be written as

$$\frac{\partial u}{\partial x} + \frac{\partial v}{\partial y} = - (\rho_s - \rho_f) \frac{\partial}{\partial y} \left[\frac{w\, c_v(1-c_v)}{\rho}\right] \approx - (S_s-1) \cdot w \frac{\partial c_v}{\partial y} \qquad \text{(A-19)}$$

where S_s is the specific gravity of the sediment.

The mass conservation equation for the solid phase (A-5), can be reduced with the help of Equations (A-12) and (A-13) as

$$u \frac{\partial c_v}{\partial x} + v \cdot \frac{\partial c_v}{\partial y} = \frac{w}{\rho} \cdot \frac{\partial c_v}{\partial y} \{\rho_f(2c_v^2 - c_v + 1) - 2c_v^2 \rho_s\} \approx w \cdot \frac{\partial c_v}{\partial y} . \qquad \text{(A-20)}$$

In Equation (A-18), the magnitude of last term $\partial/\partial y\ [c_v(1-c_v)/\rho]$ is smaller than other terms and can be dropped to yield momentum equation along Y-direction as

$$\frac{\partial(\rho uv)}{\partial x} + \frac{\partial \rho v^2}{\partial y} = \rho g_y - \frac{\partial p}{\partial y} + \frac{\partial \tau_{yx}}{\partial x} + \frac{\partial \tau_{yy}}{\partial y} . \qquad \text{(A-21)}$$

Following the method of time average and fluctuating components of all fluctuating quantities, equations for the two-phase turbulent flow can now be derived.

Let $u = \bar{u} + u'$

$v = \bar{v} + v'$

$p = \bar{p} + p'$

$c_v = \bar{c}_v + c_v'$

and

$\rho = \bar{\rho} + \rho'$.

Equation (A-1) yields

$$\bar{\rho} + \rho' = \rho_f(1-\bar{c}_v) - \rho_f c_v' + \rho_s \bar{c}_v + \rho_s c_v' .$$

Since

$$\bar{\rho} = \rho_f(1-\bar{c}_v) + \rho_s \bar{c}_v,$$

$$\rho' = (\rho_s - \rho_f)c_v' \tag{A-22}$$

Similarly Equation (A-19) yields

$$\frac{\partial u'}{\partial x} + \frac{\partial v'}{\partial y} - (S_s-1)\, w \frac{\partial c_v'}{\partial y} \tag{A-23}$$

Equation of mass conservation (A-6) gives

$$\frac{\partial \bar{\rho}\bar{u}}{\partial x} + \frac{\partial \bar{\rho}\bar{v}}{\partial y} + \frac{\partial \overline{\rho' u'}}{\partial x} + \frac{\partial \overline{\rho' v'}}{\partial y} = 0 .$$

For $\bar{\rho} = \rho_f(1-\bar{c}_v) + \rho_s \bar{c}_v$

and

$$\rho' = (\rho_s - \rho_f)\, c_v' ,$$

the equation of mass conservation can be reduced to

$$\bar{u} \cdot \frac{\partial \bar{c}_v}{\partial x} + \bar{v} \frac{\partial \bar{c}_v}{\partial y} + \frac{\partial \overline{u'c_v'}}{\partial x} + \frac{\partial \overline{v'c_v'}}{\partial y} = \frac{\rho(S_s-1)}{\rho_s - \rho_f} \cdot w \frac{\partial \bar{c}_v}{\partial y}$$

For a small c_v, $\rho \approx \rho_f$ and

$$\bar{u} \frac{\partial \bar{c}_v}{\partial x} + \bar{v} \frac{\partial \bar{c}_v}{\partial y} + \frac{\partial \overline{u'c_v'}}{\partial x} + \frac{\partial \overline{v'c_v'}}{\partial y} = w \cdot \frac{\partial \bar{c}_v}{\partial y} . \tag{A-24}$$

The momentum Equations (A-17) and (A-21) can be similarly treated to yield the Reynold's stresses in a two-phase flow. Equation (A-17) gives

$$\frac{\partial \bar{\rho}\bar{u}^2}{\partial x} + \frac{\partial}{\partial y}\ \bar{\rho}\bar{u}\bar{v} = \bar{\rho}\ g_x - \frac{\partial \bar{p}}{\partial x} + \frac{\partial}{\partial x}\ (\tau_{xx} - \bar{\rho}\bar{u}'^2 - 2\bar{u}\ \overline{\rho' u'}$$

$$-\overline{\rho' u'^2}) + \frac{\partial}{\partial y}\ (\tau_{xy} - \bar{v}\ \overline{\rho' u'} - \overline{\rho' u' v'} - \bar{\rho}\overline{u' v'} - \bar{u}\overline{\rho' v'}). \qquad \text{(A-25)}$$

And Equation (A-21) gives

$$\frac{\partial \bar{\rho}\bar{u}\bar{v}}{\partial x} + \frac{\partial \bar{\rho}\bar{v}^2}{\partial y} = \bar{\rho} g_y - \frac{\partial \bar{p}}{\partial y} + \frac{\partial}{\partial x}\ (\tau_{yx} - \bar{v}\overline{\rho' u'} - \overline{\rho' u' v'} - \bar{\rho}\overline{u' v'} - \bar{u}\overline{\rho' v'})$$

$$+ \frac{\partial}{\partial y}\ (\tau_{xx} - \bar{\rho}\overline{v'^2} - 2\bar{v}\ \overline{\rho' v'} - \overline{\rho' v'^2}). \qquad \text{(A-26)}$$

Comparing Equations (A-25) and (A-26) with Equation (A-17) and (A-18), the turbulent shear stress in a two-phase flow

$$\tau_{xy}(T) = -\bar{\rho}\ \overline{u' v'} - \bar{u}\ \overline{\rho' v'} - \overline{\rho' u' v'} - \bar{v}\ \overline{\rho' u'}$$

$$= -\bar{\rho}\overline{u' v'} - (\rho_s - \rho_f)\ [\bar{u}\ \overline{c_v' v'} + \bar{v}\ \overline{c_v' u'} + \overline{u' v' c_v'}]. \qquad \text{(A-27)}$$

For uniform flow conditions, when all the derivations with respect to x vanish, Equation (A-19) gives

$$\bar{v} = -\ (S_s - 1)\ \bar{w}\ \bar{c}_v \qquad \text{(A-28)}$$

and

$$v' = -(S_s - 1)\ \bar{w}\ c_v' \qquad \text{(A-29)}$$

From Equation (A-4)

$$\overline{v_w\ (1 - c_v)} = 0, \qquad \text{(A-30)}$$

from Equation (A-5)

$$\overline{v_s\ c_v} = 0, \qquad \text{(A-31)}$$

and from Equation (A-24)

$$\frac{\partial \overline{v'c_v'}}{\partial y} = w \frac{\partial \overline{c_v}}{\partial y} - \overline{v} \frac{\partial \overline{c_v}}{\partial y}$$

Integration of the last equation yields

$$\overline{v'c_v'} = w\,\overline{c_v} - \overline{v}\,\overline{c_v} = w\,c_v + (S_s - 1)\,w\,\overline{c_v^2} \qquad \text{(A-32)}$$

Again, for $c_v \ll 1$

$$\overline{v'c_v'} = w\,c_v\ . \qquad \text{(A-33)}$$

The turbulent shear stress, Equation (A-27), becomes

$$\tau_{xy}(T) = -\rho\overline{u'v'} - (\rho_s - \rho_f)\,[\overline{u}\,\overline{w}\,\overline{c_v} + \overline{v}\,\overline{c'_v u'} + \overline{u'v'c_v'}].$$

Here, since $|v'| < v$, $\overline{u'v'c_v'} < \overline{v}\,\overline{c_v' u'}$

and since $|\overline{v}| < w$, (for $c_v \ll 1$) the last two terms can be dropped so that

$$\tau_{xy}(T) \approx -\rho\overline{u'v'} - (\rho_s - \rho_f)\,\overline{u}\,\overline{w}\,\overline{c_v} \qquad \text{(A-32)}$$

This is the approximate equation for turbulent shear stress in sediment water mixture flows with small values of c_v.

The differential equation for the variation of the sediment concentration can be written for uniform flow conditions with the help of Equations (A-30), (A-31) and (A-13). Introducing the time average and fluctuating components of various quantities, (A-30) and (A-31) give

$$\overline{v_f}\ (\overline{1-c_v}) + \overline{v_f'(1-c_v')} = 0\ , \qquad \text{(A-35)}$$

$$\overline{v_s}\,\overline{c_v} + \overline{v_s'\,c_v'} = 0. \qquad \text{(A-36)}$$

Using Equation (A-13) with Equation (A-36)

$$(\overline{v_f} - w)\,\overline{c_v} + \overline{v_f' c_v'} = 0. \tag{A-37}$$

Defining turbulent diffusion coefficients for the liquid and solid phase as

$$\overline{c_v' v_f'} = -\,\varepsilon_s \frac{\overline{dc_v}}{dy}$$

and

$$\overline{(1-c_v')\,v_f'} = \varepsilon_f \frac{\overline{dc_v}}{dy},$$

and by eliminating $\overline{v}_f$ between Equation (A-35) and (A-37),

$$(\varepsilon_s + c_v\,(\varepsilon_f - \varepsilon_s))\,\frac{dc_v}{dy} + c_v(1-c_v)\,w = 0,$$

where the overscore of the time averaged volumetric concentration has been dropped.

For $c_v << 1$,

$$(\varepsilon_s + c_v\,(\varepsilon_f - \varepsilon_s))\,\frac{dc_v}{dy} + c_v\,w = 0. \tag{A-38}$$

This is the differential equation for the variation of the sediment concentration along the depth of the flow.

APPENDIX B

LOGNORMAL DISTRIBUTIONS AND ESTIMATION OF THEIR PARAMETERS

APPENDIX B

LOGNORMAL DISTRIBUTIONS AND ESTIMATION OF THEIR PARAMETERS

Two-Parameter Lognormal Distribution

If two variates X and Y are defined as $Y = \ln[X]$, $0 < X < \infty$ and if, Y has a gaussian distribution with mean μ_y and standard deviation σ_y

$$F_Y(y) = \int_{-\infty}^{y} \frac{1}{\sigma_y \sqrt{2\pi}} \cdot \exp[-\frac{1}{2} (\frac{y-u_y}{\sigma_y})^2] \cdot dy$$

then, variate X is said to have a lognormal distribution, and is distributed as

$$F_X(x) = \int_{o}^{x} \frac{1}{\sigma_y \cdot x\sqrt{2\pi}} \exp[-\frac{1}{2} (\frac{\ln x-u_y}{\sigma_y})^2] dx$$

If W is another variate defined by

$$W = a.X^n, \quad o < X < \infty$$

then distribution function of W is given by

$$F_W(w) = \int_{o}^{w} \frac{1}{\sigma_z w\sqrt{2\pi}} \exp[-\frac{1}{2} (\frac{\ln w-u_z}{\sigma_z})^2] \cdot dw$$

where

$$\sigma_z = n \cdot \sigma_y$$

$$\mu_z = n \cdot u_y + \ln a \qquad \text{and}$$

$$Z = \ln W.$$

A lognormal distribution is skewed and its mode, median and mean are given by a value of x equal to

$$e^{\mu_y - \sigma_y^2}, \quad e^{\mu_y} \quad \text{and} \quad e^{\mu_y + \frac{1}{2}\sigma_y^2}, \text{ respectively.}$$

The median size X_{50} of a lognormal variate X corresponds to the median size of Y_{50} of its transformation Y (= ln [X]) and to the median size W_{50} of any power transformation $W(=a\ X^n)$. This is also true of other quantiles.

The rth moment of variate X about the origin is,

$$\mu_r'(x) = \int_0^{\infty} x^r\ f_x(x) \cdot dx$$

$$= \int_{-\infty}^{-\infty} e^{ry}\ f_y(y) \cdot dy$$

$$\exp\left[\tfrac{1}{2} r^2\ \sigma_y^2 + r\ \mu_y\right] \qquad \text{(B-1)}$$

The two-parameter lognormal distributions are multiplicatively reproductive in the same sense as the normal distributions are additively reproductive. If two mutually independent variates Y_1 and Y_2 are normally distributed as $Y_1 \sim N(\mu_1, \sigma_1^2)$ and $Y_2 \sim N(\mu_2, \sigma_2^2)$ then their sum $Y = Y_1 + Y_2$ is also normally distributed as $Y \sim N(\mu_1 + \mu_2, \sigma_1^2 + \sigma_2^2)$. For the lognormal distributions, the reproductive properties are as follows.

If, $X_1 \sim LN(\mu_{y1}, \sigma_{y1}^2)$, $o < X_1$

$X_2 \sim LN(\mu_{y2}, \sigma_{y2}^2)$, $o < X_2$

are mutually independent random variables, then

$$X = X_1 \cdot X_2 \sim LN(\mu_{y1} + \mu_{y2}, \sigma_{y1}^2 + \sigma_{y2}^2) \ .$$

Three-Parameter Lognormal Distribution

The lower bound for the two-parameter lognormal distribution is 0. However, if the lower bound is different from 0, and there exists a lower bound τ, such that

$$X_1 = (X - \tau) \sim LN(\mu_y, \sigma_y^2)$$

then X has a three parameter lognormal distribution. The mean, mode and all quantiles of a three-parameter lognormal distribution are simply shifted by τ from their values in a two-parameter distribution. Also, the moments about the mean of a three parameter distribution are the same as for the two-parameter lognormal distribution. A four-parameter lognormal distribution can be created if there is also an upper bound for the variate. Thus if

$$X_2 = \left(\frac{X - \tau}{X - \theta}\right) \sim LN(\mu_y, \sigma_y^2)$$

then X_2 is distributed as a four-parameter lognormal distribution with lower and upper bounds as τ and θ, respectively.

Although, the three-and four-parameter distributions are more flexible and can be fitted to a variety of empirical distributions, the estimation procedures for the parameters become less reliable and cumbersome than for the two-parameter distribution.

Estimation of Parameters

If there is a sample of size n from a lognormal population $X \sim LN(\mu_y, \sigma_y^2)$, parameters μ_y and σ_y^2 can be estimated from the sample. The problem of estimation is basic to the theory of mathematical statistics and estimators are assigned various qualities like consistency,

unbiased, minimum variance, efficiency, sufficiency[1], etc., (Kendall and Stuart, 1967). For lognormal distributions, Aitchson and Brown (1957) have discussed five estimation methods, namely, (i) the method of maximum likelihood, (ii) the method of moments, (iii) the method of quantiles (iv) the graphical method, and (v) mixed methods. Relevants equations of these methods are given below with remarks on their efficiencies.

(1) Method of Maximum Likelihood

If m_1 and s_1^2 are the maximum likelihood estimators of μ_y and σ_y^2, then

$$m_1 = \frac{1}{n}\sum_{i=1}^{n} \ln [x_i]$$

$$s_1^2 = \frac{1}{n}\sum_{i=1}^{n} (\ln [x_i] - m_1)^2$$

Where n is the size of sample $x_1, x_2, \ldots, x_n$; m_1 and s_1 are minimum variance unbiased estimators and their variances are given by $\text{var}\{m_1\} = \frac{\sigma_y^2}{n}$ and $\text{var}\{s_1^2\} = \frac{2\sigma_y^4}{n}$.

---

1. Consistency. An estimator is consistent if the variance of the sampling distribution decreases with the increasing size of sample.

Unbiased. An estimator is unbiased if it is consistent and its expected value is value of parameter (in population) being estimated.

Minimum variance. An estimator of a function of a parameter which has smaller variance than any other estimator is called a minimum variance estimator. This is not bound to the size of sample.

Efficient. Among consistent, asymptotically normal estimators of some parametric function, that with the minimum variance in large samples is called an efficient parameter.

Efficiency of an estimator relative to an efficient estimator is defined as the reciprocal of the ratio of sample numbers required to give the estimators equal sampling variances.

Sufficient. A statistic is sufficient if it provides all the information about a parameter under estimation and given a sufficient statistic no other function of any other independent statistic provides any additional information.

(2) Method of Moments

In this method, the first two sample moments are equated to the expressions for μ_y and σ_y^2 from Equation (B-1). If m_2 and s_2 are the estimators from method of moments, then

$$\exp\{m_2 + \frac{1}{2} s_2^2\} = \frac{1}{n}\sum_{i=1}^{n} x_i$$

$$\exp\{2m_2 + 2 s_2\} = \frac{1}{n}\sum_{i=1}^{n} (x_i - \bar{x})^2$$

where $\bar{x} = \frac{1}{n}\sum_{i=1}^{n} x_i$.

This yields

$$m_2 = 2 \ln [\frac{1}{n}\sum_{i-1}^{n} x_i] - \frac{1}{2} \ln [\frac{1}{n}\sum_{i=1}^{n} (x_i - \bar{x})^2]$$

and $s_2^2 = \ln [\frac{1}{n}\sum_{i=1}^{n} (x_i - \bar{x})^2] - 2 \ln [\frac{1}{n}\sum_{i=1}^{n} x_i]$

m_2 and s_2^2 are consistent estimators, but their efficiencies fall off rapidly as σ_y^2 increases.

(3) Method of Quantiles

In this method, the sample quantiles are equated to the expressions in terms of estimators m_3 and s_3. Thus, if X_{q_1} and X_{q_2} are the quantiles of X, of order q_1 and $q_2 (q_1 < q_2)$ then,

$$m_3 = \frac{\nu_{q_2} \ln [X_{q_1}] - \nu_{q_1} \ln [X_{q_2}]}{\nu_{q_2} - \nu_{q_1}}$$

and $s_3 = \dfrac{\ln [X_{q_2}] - \ln [X_{q_1}]}{\nu_{q_2} - \nu_{q_1}}$

Where ν_{q_2} and ν_{q_1} are q_2th and q_1th order quantiles of standardized normal distribution and m_3 and s_3 are estimates of μ_y and σ_y. Maximum efficiency is achieved in this method when the quantiles are of order q_o and $1-q_o$ ($q_o < \frac{1}{2}$), then

$$\nu_{1-q_o} = -\nu_{q_o} = \nu_o$$

and

$$m_3 = \frac{1}{2}\left(\ln[X_{1-q_o}] + \ln[X_{q_o}]\right),$$

$$s_3 = \frac{1}{2\nu_o}\left(\ln[X_{1-q_o}] - \ln[X_{q_o}]\right)$$

Optimum values of q_o for the maximum large sample efficiencies are different for μ_y and σ_y. For μ_y, the values are 27 and 73% and for σ, these are 7 and 93%. At 16 and 84% quantiles these efficiencies for μ_y and σ_y are 70% and 53% respectively, compared to their respective maxima of 81% and 65%.

(4) Graphical Method

The graphical method consists of plotting the cumulative normalized frequencies on the logarithmic probability paper and determining m_4 and s_4 as follows:

$$m_4 = \ln[X_{50}]$$

$$s_4 = \ln\left[\frac{1}{2}\left\{\frac{X_{50}}{X_{16}} + \frac{X_{84}}{X_{50}}\right\}\right].$$

In an empirical test of these methods on 65 sets of lognormal data, Aitchson and Brown (1957) found that the order of these methods in terms of their efficiencies in estimating both μ_y and σ_y is:

Maximum Likelihood closely followed by Method of Quantiles Method of Moments, Graphical Method. They recommended that in view of the falling efficiency of method of moments for increasing σ_y^2 and the expense of computations for large samples, the methods of quantiles and graphics to be used.

In the size analysis of sand samples if a lognormal distribution is applicable, the two parameters required to define this distribution are μ_y and σ_y. In practice the median diameter D_{50} and gradation $\sigma[= \frac{1}{2}(\frac{D_{50}}{D_{16}} + \frac{D_{84}}{D_{50}})]$ of the sand-mixture are usually reported. For a two-parameter lognormal distribution, D_{50} and σ are related to μ_y and σ_y as

$$\mu_y = \ln [D_{50}]$$

and

$$\sigma_y = \ln [\sigma] \quad .$$

The qth percentile of the sand size distribution D_q (i.e., q percent of the mixture is finer than the size D_q) in this case is

$$D_q = D_{50}\, \sigma^{\nu_q}$$

where ν_q is the qth percentile of standard normal distribution [~N(0,1)]. Thus, for $q = 65\%$, $\nu_q = 0.385$ and

$$D_{65} = D_{50}\, \sigma^{0.385} \quad ,$$

similarly for $q = 35\%$, $\nu_q = -0.385$ and

$$D_{35} = D_{50}\, \sigma^{-0.385}$$

APPENDIX C

VALUES OF κ AND RELATED PARAMETERS FOR FLUME RUNS

APPENDIX C

VALUES OF ϵ AND RELATED PARAMETERS FOR FLUME RUNS

S.No.	Table No.	Run No.	Bed Form	Mean Velocity fps	Mean Depth ft	Geometric Standard Deviation σ of Bed Material	Froude Number $V/\sqrt{gd}$	ϵ_1 (1)	ϵ_2 (2)	ϵ_3 (3)	γ_f (4)	Linear Concentration of Total Load, λ	Einstein-Chien Parameter (5)
1	2	02	Ripple	.79	1.06	1.30	.135	.645	.637	.546	1.000	.478 E-02	.470 E-04
2	2	25	Ripple	.87	.93	1.30	.150	.375	.371	.421	1.000	.548 E-02	.630 E-04
3	2	30	Ripple	1.11	1.00	1.30	.196	.362	.360	.424	1.000	.127 E-01	.367 E-03
4	2	01	Ripple	.74	.58	1.30	.171	.300	.307	.416	1.000	.872 E-02	.137 E-03
5	2	31	Ripple	1.30	1.02	1.30	.227	.367	.366	.393	1.002	.256 E-01	.163 E-02
6	2	27	Ripple	.93	.55	1.30	.231	.400	.385	.405	1.000	.131 E-01	.237 E-03
7	2	05	Ripple	1.54	1.03	1.30	.267	.363	.366	.436	1.000	.418 E-01	.400 E-02
8	2	32	Dune	1.79	.95	1.30	.324	.411	.390	.472	1.034	.563 E-01	.753 E-02
9	2	06	Dune	1.99	.93	1.30	.364	.396	.380	.440	1.047	.700 E-01	.116 E-01
10	2	28	Ripple	1.04	.54	1.30	.240	.433	.413	.402	1.002	.271 E-01	.130 E-02
11	2	29	Ripple	1.13	.56	1.30	.264	.417	.396	.472	1.004	.325 E-01	.196 E-02
12	2	03	Ripple	1.18	.55	1.30	.280	.414	.406	.467	1.005	.370 E-01	.216 E-02
13	2	34	Dune	1.68	.52	1.30	.411	.516	.502	.540	1.037	.602 E-01	.723 E-02
14	2	12	Dune	2.60	1.02	1.30	.460	.416	.411	.530	1.075	.967 E-01	.118 E-01
15	2	06	Dune	1.67	.61	1.30	.377	.417	.403	.401	1.060	.630 E-01	.119 E-01
16	2	07	Dune	1.78	.68	1.30	.380	.507	.496	.400	1.068	.956 E-01	.157 E-01
17	2	08	Dune	2.10	.40	1.30	.520	.354	.325	.400	1.079	.950 E-01	.947 E-02
18	3	51	Ripple	1.24	.90	1.56	.230	.649	.644	.664	1.001	.190 E-01	.830 E-03
19	3	52	Ripple	1.63	.94	1.56	.296	.557	.573	.544	1.030	.300 E-01	.365 E-02
20	3	57	Ripple	1.33	.48	1.56	.350	.300	.306	.301	1.007	.363 E-01	.211 E-02
21	3	56	Dune	1.85	.75	1.56	.376	.457	.460	.272	1.030	.715 E-01	.921 E-02
22	4	00	Ripple	.96	1.01	1.67	.160	.425	.425	.307	1.000	.115 E-01	.417 E-03
23	4	10	Ripple	.80	.90	1.67	.302	.372	.370	.310	1.000	.821 E-02	.163 E-03
24	4	05	Ripple	1.34	1.00	1.67	.236	.323	.324	.270	1.001	.190 E-01	.753 E-03
25	4	13	Ripple	1.60	1.00	1.67	.306	.292	.294	.244	1.007	.353 E-01	.360 E-02
26	4	04	Ripple	1.46	.86	1.67	.306	.478	.475	.316	1.004	.311 E-01	.173 E-02
27	4	11	Ripple	1.04	.50	1.67	.230	.586	.570	.406	1.002	.226 E-01	.974 E-03
28	4	12	Ripple	1.58	.57	1.67	.360	.472	.425	.389	1.013	.452 E-01	.331 E-02
29	4	30	Dune	3.16	1.05	1.67	.371	.650	.647	.650	1.030	.604 E-01	.730 E-02
30	4	17	Dune	1.92	.65	1.67	.430	.528	.502	.430	1.037	.603 E-01	.711 E-02
31	5	16	Ripple	.79	.81	1.60	.155	.515	.563	.435	1.000	.872 E-02	.511 E-03
32	5	15	Ripple	.79	.80	1.60	.156	.534	.529	.542	1.000	.720 E-02	.360 E-03
33	5	03	Ripple	1.16	.85	1.60	.222	.502	.554	.502	1.002	.170 E-01	.155 E-02
34	5	09	Ripple	.88	.53	1.60	.300	.466	.470	.404	1.000	.919 E-02	.281 E-03
35	5	05	Ripple	1.32	.75	1.60	.300	.400	.407	.353	1.007	.250 E-01	.304 E-02
36	5	08	Ripple	.93	.51	1.60	.220	.519	.407	.500	1.001	.163 E-01	.963 E-03
37	5	06	Ripple	1.07	.46	1.60	.270	.372	.370	.412	1.007	.301 E-01	.306 E-02
38	5	13	Ripple	.85	.70	1.60	.270	.651	.301	.651	1.000	.821 E-02	.780 E-04
39	5	21	Dune	1.58	.96	1.60	.304	.462	.450	.312	1.030	.636 E-01	.156 E-01
40	5	20	Dune	1.68	.61	1.60	.379	.631	.676	.620	1.050	.605 E-01	.116 E-01
41	6	18	Dune	1.66	1.01	1.54	.301	.428	.423	.516	1.013	.230 E-01	.495 E-02
42	6	28	Dune	1.75	1.04	1.54	.362	.421	.431	.484	1.017	.253 E-01	.632 E-02
43	6	15	Dune	1.83	1.05	1.54	.332	.403	.402	.372	1.020	.326 E-01	.831 E-02
44	6	14	Dune	1.60	.58	1.54	.370	.362	.377	.430	1.033	.338 E-01	.801 E-02
45	6	34	Dune	1.64	.54	1.54	.303	.362	.377	.457	1.037	.352 E-01	.889 E-02
46	6	16	Dune	2.03	1.04	1.54	.351	.464	.454	.314	1.033	.441 E-01	.896 E-02
47	6	35	Dune	1.80	.53	1.54	.436	.354	.366	.320	1.070	.501 E-01	.124 E-01
48	6	17	Dune	2.10	1.00	1.54	.370	.452	.444	.406	1.044	.809 E-01	.107 E-01
49	6	05	Dune	2.21	.93	1.54	.404	.466	.401	.375	1.054	.582 E-01	.130 E-01
50	6	37	Dune	2.54	1.11	1.54	.425	.500	.548	.500	1.060	.738 E-01	.175 E-01

Numbers in parentheses refer to footnotes at end of table.

APPENDIX C

VALUES OF ϵ AND RELATED PARAMETERS FOR FLUME RUNS - Continued

S.No.	Table No.	Run No.	Bed Form	Mean Velocity fps	Mean Depth ft	Geometric Standard Deviation σ of Bed Material	Froude Number $V/\sqrt{gd}$	$\epsilon_1^{(1)}$	$\epsilon_2^{(2)}$	$\epsilon_3^{(3)}$	$\tau_0^{(4)}$	Linear Concentration of Total Load, λ	Einstein-Chien Parameter (5)
51	6	07	Dune	2.14	.59	1.54	.401	.367	.317	.054	1.114	.825 E-01	.164 E-01
52	6	30	Dune	2.79	1.03	1.54	.485	.365	.363	.363	1.112	.911 E-01	.190 E-01
53	6	00	Dune	2.46	.57	1.54	.574	.361	.354	.727	1.301	.303 E-00	.304 E-01
54	10	05	Ripple	1.13	.78	1.54	.325	.513	.511	.543	1.001	.150 E-01	.063 E-03
55	10	06	Ripple	1.14	.76	1.54	.330	.444	.453	.450	2.130	.150 E-00	.713 E-00
56	10	07	Ripple	1.16	.75	1.54	.336	.400	.502	.481	3.047	.190 E-00	.131 E-01
57	10	08	Ripple	1.20	.74	1.54	.346	.336	.331	.318	3.630	.225 E-00	.143 E-01
58	10	09	Ripple	1.45	.60	1.54	.330	.519	.516	.545	3.204	.185 E-00	.604 E-00
59	10	00	Ripple	1.47	.60	1.54	.334	.490	.464	.417	3.273	.305 E-00	.715 E-00
60	10	92	Dune	1.43	.63	1.54	.317	.277	.301	.348	2.133	.176 E-00	.373 E-00
61	10	91	Dune	1.53	.58	1.54	.384	.307	.312	.346	2.370	.300 E-00	.363 E-00
62	10	53	Dune	1.77	.57	1.54	.413	.331	.319	.301	2.034	.334 E-00	.190 E-00
63	10	77	Dune	1.68	.65	1.54	.347	.315	.300	.315	2.179	.230 E-00	.320 E-00
64	10	54	Dune	2.00	.92	1.54	.382	.354	.347	.300	1.181	.136 E-00	.414 E-01
65	10	52	Dune	2.04	.94	1.54	.371	.360	.330	.312	1.327	.160 E-00	.791 E-01
66	10	57	Dune	2.30	.87	1.54	.416	.372	.303	.196	1.376	.163 E-00	.722 E-01
67	10	95	Dune	2.33	.80	1.54	.471	.301	.358	.370	4.630	.341 E-00	.444 E-00
68	7	03	Ripple	1.34	.54	1.57	.297	.324	.313	.334	1.015	.310 E-01	.181 E-02
69	7	04	Ripple	1.34	.54	1.57	.297	.368	.300	.403	1.000	.331 E-01	.330 E-02
70	8	00	Ripple	1.02	.50	1.25	.254	.407	.301	.407	1.001	.155 E-01	.535 E-03
71	8	05	Ripple	1.17	.40	1.25	.295	.404	.430	.406	1.000	.303 E-01	.329 E-02
72	8	01	Plane	4.03	.51	1.25	.992	.388	.392	.386	1.566	.135 E-00	.191 E-01
73	9	05	Ripple	1.43	.53	2.07	.340	.427	.434	.360	1.013	.371 E-01	.367 E-02
74	9	01	Dune	1.90	.50	2.07	.406	.318	.319	.367	1.075	.604 E-01	.101 E-01
75	9	30	Dune	1.80	.48	2.07	.454	.440	.435	.440	1.053	.646 E-01	.845 E-02
76	9	00	Dune	2.42	.53	2.07	.901	.400	.500	.374	1.180	.103 E-00	.172 E-01
77	11	03	Ripple	1.08	.63	1.53	.234	.406	.405	.406	1.000	.601 E-02	.218 E-03
78	11	04	Ripple	1.27	.50	1.53	.314	.430	.436	.430	1.000	.314 E-01	.311 E-02
79	11	00	Dune	2.51	.70	1.53	.561	.403	.430	.403	1.096	.947 E-01	.131 E-01
80	11	00A	Dune	2.33	.64	1.53	.640	.581	.566	.581	1.407	.182 E-00	.804 E-01
81	2	13	Transition	3.00	.00	1.30	.577	.403	.401	.442	1.130	.954 E-01	.120 E-01
82	2	14	Transition	3.22	.86	1.30	.612	.331	.334	.330	1.100	.103 E-00	.141 E-01
83	2	15	Plane	3.46	.79	1.30	.686	.300	.306	.300	1.235	.114 E-00	.167 E-01
84	2	16	Transition	3.84	.72	1.30	.796	.251	.348	.273	1.200	.130 E-00	.146 E-01
85	2	30	Plane	3.06	.51	1.30	.706	.318	.309	.413	1.365	.174 E-00	.364 E-01
86	3	45	Transition	3.25	.64	1.56	.425	.360	.333	.361	1.135	.067 E-01	.115 E-01
87	3	46	Plane	3.66	.74	1.56	.754	.341	.324	.342	1.192	.107 E-00	.112 E-01
88	4	21	Transition	3.02	.91	1.67	.559	.453	.472	.327	1.306	.916 E-01	.114 E-01
89	4	20	Transition	3.06	.64	1.67	.674	.274	.278	.347	1.157	.994 E-01	.115 E-01
90	4	22	Plane	3.11	.60	1.67	.706	.347	.350	.330	1.172	.104 E-00	.115 E-01
91	4	25	Plane	3.79	.72	1.67	.757	.376	.386	.407	1.246	.128 E-00	.132 E-01
92	4	28	Plane	3.57	.56	1.67	.848	.395	.396	.417	1.271	.179 E-00	.175 E-01
93	4	29	Plane	3.77	.52	1.67	.931	.348	.343	.361	1.252	.195 E-00	.111 E-01
94	4	26	Antidune	3.00	.50	1.67	.967	.327	.322	.360	1.415	.165 E-00	.167 E-01
95	5	36	Plane	5.38	.34	1.60	1.636	.333	.396	.231	2.385	.156 E-00	.174 E-01
96	5	39	Standing Wave	4.71	.53	1.60	1.119	.321	.331	.369	1.663	.148 E-00	.176 E-01
97	5	28	Transition	5.53	.60	1.60	.961	.297	.297	.361	1.703	.152 E-00	.243 E-01
98	5	31	Standing Wave	4.34	.44	1.60	1.196	.419	.378	.384	1.746	.190 E-00	.794 E-01
99	5	36	Transition	2.04	.19	1.60	.625	.431	.434	.430	1.236	.994 E-01	.115 E-01
100	5	41	Standing Wave	5.05	.54	1.60	1.211	.333	.333	.325	1.616	.153 E-00	.100 E-01

APPENDIX C

VALUES OF ϵ AND RELATED PARAMETERS FOR PLANE BEDS - Continued

S.No.	Table No.	Run No.	Bed Form	Mean Velocity fps	Mean Depth ft	Geometric Standard Deviation σ of Bed Material	Froude Number $V/\sqrt{gd}$	ϵ_1 (1)	ϵ_2 (2)	ϵ_3 (3)	γ_f (4)	Linear Concentration of Total Load, λ	Einstein-Chien Parameter (5)
101	5	32	Transition	3.47	.27	1.60	.830	.301	.274	.341	1.461	.142 E-00	.219 E-01
102	5	35	Transition	3.99	.25	1.60	.907	.297	.189	.295	1.713	.157 E-00	.240 E-01
103	5	34	Standing Wave	3.73	.28	1.60	1.341	.302	.313	.386	1.972	.170 E-00	.300 E-01
104	5	33	Standing Wave	4.60	.27	1.60	1.560	.317	.340	.233	2.320	.183 E-00	.180 E-01
105	5	36	Standing Wave	5.30	.50	1.60	1.341	.420	.420	.411	1.771	.176 E-00	.143 E-01
106	5	37	Transition	5.54	.43	1.60	1.480	.372	.300	.345	1.822	.160 E-00	.123 E-01
107	5	33	Antidune	5.03	.37	1.60	1.457	.347	.336	.256	1.901	.176 E-00	.141 E-01
108	5	45	Antidune	2.60	.20	1.60	.833	.300	.317	.400	1.712	.210 E-00	.341 E-01
109	6	27	Plane	1.47	1.01	1.54	.256	.436	.435	.435	1.002	.114 E-01	.900 E-03
110	6	30	Plane	1.32	1.03	1.54	.230	.374	.362	.374	1.000	.663 E-02	.158 E-03
111	6	31	Plane	1.40	1.01	1.54	.361	.375	.373	.375	1.000	.663 E-02	.131 E-03
112	6	31	Plane	1.36	.50	1.54	.330	.402	.402	.471	1.003	.133 E-01	.824 E-03
113	6	32	Plane	1.50	.52	1.54	.367	.446	.440	.541	1.016	.247 E-01	.300 E-02
114	6	34	Plane	1.46	.49	1.54	.368	.374	.373	.374	1.000	.366 E-01	.230 E-02
115	6	13	Transition	3.37	.82	1.54	.446	.305	.368	.403	1.363	.120 E-00	.302 E-01
116	6	41	Transition	4.45	.44	1.54	1.182	.300	.300	.225	3.177	.230 E-00	.170 E-01
117	6	42	Standing Wave	5.01	.44	1.54	1.544	.253	.252	.300	3.141	.168 E-00	.150 E-01
118	6	40	Standing Wave	5.11	.38	1.54	1.441	.314	.301	.230	2.522	.215 E-00	.336 E-01
119	6	43	Standing Wave	5.86	.44	1.54	1.557	.303	.292	.301	2.010	.185 E-00	.130 E-01
120	6	39	Standing Wave	6.07	.43	1.54	1.631	.319	.223	.301	2.061	.195 E-00	.132 E-01
121	10	59	Transition	2.96	.65	1.54	.647	.402	.359	.544	1.792	.190 E-00	.636 E-01
122	10	60	Plane	4.28	.62	1.54	.950	.251	.340	.251	2.050	.184 E-00	.382 E-01
123	10	61	Plane	4.36	.61	1.54	.964	.375	.363	.362	2.456	.300 E-00	.400 E-01
124	10	71	Plane	3.31	.32	1.54	1.000	.348	.344	.185	2.270	.293 E-00	.422 E-01
125	10	72	Plane	3.36	.33	1.54	1.036	.366	.368	.307	2.730	.236 E-00	.557 E-01
126	10	70	Plane	3.41	.30	1.54	1.097	.425	.430	.460	2.360	.215 E-00	.378 E-01
127	10	65	Antidune	4.63	.42	1.54	1.710	.301	.302	.193	3.001	.347 E-00	.417 E-01
128	10	81	Standing Wave	4.85	.55	1.54	1.152	.327	.318	.360	1.446	.155 E-00	.112 E-01
129	10	63	Standing Wave	4.80	.54	1.54	1.173	.336	.333	.362	2.043	.307 E-00	.252 E-01
130	10	67	Standing Wave	4.91	.53	1.54	1.189	.300	.300	.281	2.630	.256 E-00	.370 E-01
131	10	79	Standing Wave	4.82	.55	1.54	1.145	.333	.332	.354	2.718	.273 E-00	.433 E-01
132	10	84	Antidune	4.67	.41	1.54	1.288	.160	.146	.281	1.817	.186 E-00	.165 E-01
133	10	68	Standing Wave	4.95	.53	1.54	1.196	.300	.356	.362	2.368	.348 E-00	.314 E-01
134	10	100	Plane	5.78	.51	1.54	1.303	.279	.276	.314	1.825	.300 E-00	.161 E-01
135	10	87	Antidune	4.07	.37	1.54	1.170	.462	.434	1.082	2.251	.258 E-00	.797 E-01
136	7	87	Transition	3.95	.60	1.57	.671	.296	.300	.344	1.360	.180 E-00	.118 E-01
137	7	30	Antidune	4.23	.55	1.57	1.005	.300	.308	.484	1.343	.160 E-00	.111 E-01
138	7	19	Plane	4.18	.56	1.57	.904	.177	.182	.177	1.434	.153 E-00	.144 E-01
139	7	10	Antidune	4.13	.50	1.57	.945	.731	.607	.773	1.303	.164 E-00	.753 E-02
140	7	09	Antidune	4.35	.56	1.57	1.034	.304	.294	.381	1.440	.168 E-00	.142 E-01
141	7	12	Plane	4.03	.67	1.57	.860	.814	.501	.612	1.311	.148 E-00	.913 E-02
142	7	11	Antidune	4.51	.60	1.57	1.036	.370	.363	.436	1.502	.165 E-00	.150 E-01
143	9	03	Transition	3.27	.53	2.07	.790	.422	.430	.422	1.205	.153 E-00	.100 E-01
144	11	29	Transition	3.36	.72	1.52	.606	.174	.172	.174	1.325	.136 E-00	.223 E-01
145	11	10	Plane	4.30	.64	1.52	.947	.362	[illegible]	.362	1.330	.138 E-00	.125 E-01
146	11	15	Standing Wave	4.75	.74	1.52	.973	.304	.308	.304	1.362	.136 E-00	.124 E-01
147	11	13	Standing Wave	4.52	.72	1.52	.930	.315	.322	.305	1.330	.130 E-00	.125 E-01
148	11	18	Standing Wave	5.44	.71	1.52	1.130	.350	.350	.350	1.445	.136 E-00	.115 E-01
149	3	16	Dune	3.06	1.00	1.56	.340	.334	.376	1.126	1.035	.754 E-01	.970 E-02
150	4	01	Dune	1.00	.06	1.67	.330	.630	.645	.564	1.030	.641 E-24	.036 E-02

APPENDIX C

VALUES OF ϕ AND RELATED PARAMETERS FOR FLUME RUNS - Continued

S.No.	Table No.	Run No.	Bed Form	Mean Velocity fps	Mean Depth ft	Geometric Standard Deviation σ of Bed Material	Froude Number $V/\sqrt{gd}$	$\sigma_1^{(1)}$	$\sigma_2^{(2)}$	$\sigma_3^{(3)}$	$\gamma_f^{(4)}$	Linear Concentration of Total Load, λ	Einstein-Chien Parameter (5)
151	4	14	Dune	1.74	.62	1.67	.300	.572	.550	.537	1.025	.575 E-01	.553 E-02
152	5	01	Ripple	1.23	.80	1.60	.342	.687	.619	.757	1.005	.237 E-01	.303 E-02
153	5	11	Ripple	.70	.35	1.60	.300	.686	.671	.863	1.001	.136 E-01	.962 E-03
154	5	22	Dune	1.70	1.00	1.60	.300	.479	.560	.644	1.062	.716 E-01	.194 E-01
155	6	33	Dune	1.83	.56	1.54	.431	.706	.661	.765	1.077	.543 E-01	.130 E-01
156	6	06	Dune	2.60	1.04	1.54	.463	.684	.660	.106	1.060	.700 E-01	.930 E-02
157	6	11	Dune	2.02	.92	1.54	.555	.757	.740	.837	1.123	.941 E-01	.144 E-01
158	7	05	Dune	1.72	.56	1.57	.406	.121	.136	.395	1.021	.522 E-01	.430 E-02
159	7	06	Dune	1.62	.50	1.57	.372	.167	.172	.413	1.021	.470 E-01	.504 E-03
160	9	08	Dune	2.11	.51	2.07	.521	.521	.360	.472	1.133	.896 E-01	.162 E-01
161	10	46	Dune	1.64	1.11	1.54	.276	.170	.156	.170	1.033	.463 E-01	.183 E-01
162	10	49	Dune	2.00	1.33	1.54	.308	.610	.593	.610	1.026	.720 E-01	.129 E-01
163	10	73	Dune	1.67	.61	1.54	.377	.121	.150	.231	1.581	.170 E-00	.136 E-00
164	10	74	Dune	1.50	.65	1.54	.345	.642	.602	.252	1.704	.300 E-00	.1[illegible] E-00
165	10	75	Dune	1.00	.64	1.54	.253	.143	.143	.216	1.002	.214 E-00	.236 E-00
166	10	56	Dune	2.14	.90	1.54	.300	.658	.590	.630	1.301	.140 E-00	.634 E-01
167	10	58	Dune	2.11	.90	1.54	.302	.660	.663	.921	1.654	.175 E-00	.903 E-01
168	7	21	Transition	2.74	.50	1.57	.634	.570	.554	.570	1.103	.855 E-01	.848 E-02
169	7	00	Transition	2.40	.72	1.57	.515	.200	.267	1.110	1.173	.110 E-00	.217 E-01
170	11	19	Transition	2.50	.76	1.52	.522	.510	.470	.510	1.001	.947 E-01	.111 E-01
171	11	11	Standing Wave	5.00	.66	1.52	1.250	.154	.155	.154	1.500	.170 E-00	.123 E-01
172	2	23	Ripple	.85	.44	1.30	.226	.620	.579	.753	1.003	.161 E-01	.119 E-03
173	2	33	Dune	1.96	1.06	1.30	.335	1.301	1.136	1.415	1.054	.631 E-01	.140 E-01
174	2	11	Dune	2.35	1.00	1.30	.307	.531	.567	1.264	1.005	.975 E-01	.[illegible]9 E-01
175	2	35	Dune	1.81	.52	1.30	.442	.726	.701	.679	1.070	.806 E-01	.130 E-01
176	3	500	Ripple	.84	.91	1.56	.155	.700	.781	1.102	1.000	.660 E-02	.130 E-03
177	3	54	Dune	1.83	.93	1.56	.334	.959	.929	.755	1.018	.900 E-01	.534 E-02
178	3	53	Dune	1.91	1.02	1.56	.333	.950	.041	.002	1.023	.613 E-01	.607 E-02
179	3	43	Dune	2.13	1.13	1.56	.363	1.290	1.423	.810	1.047	.863 E-01	.136 E-01
180	3	44	Dune	2.62	1.03	1.56	.455	.011	.700	1.341	1.043	.829 E-01	.779 E-02
181	4	33	Dune	1.86	1.06	1.67	.318	2.226	2.176	1.304	1.023	.304 E-01	.763 E-02
182	4	19	Dune	1.90	.65	1.67	.415	1.141	1.051	1.376	1.043	.721 E-01	.818 E-02
183	4	16	Dune	2.11	1.02	1.67	.360	1.447	1.330	1.734	1.029	.714 E-01	.736 E-02
184	4	03	Dune	2.17	.60	1.67	.400	.757	.747	.643	1.046	.702 E-01	.934 E-02
185	4	18	Dune	2.05	.61	1.67	.553	.636	.636	.180	1.302	.890 E-01	.111 E-01
186	4	34	Dune	1.56	.44	1.67	.414	.679	.643	.701	1.038	.681 E-01	.746 E-02
187	4	15	Dune	2.14	.75	1.67	.436	.732	.684	.744	1.047	.813 E-01	.830 E-02
188	4	34	Transition	3.35	.83	1.67	.652	.600	.602	.633	1.195	.131 E-00	.153 E-01
189	5	17	Ripple	.80	.96	1.60	.142	.686	.963	.880	1.000	.726 E-02	.309 E-03
190	5	18	Ripple	.75	.50	1.60	.180	.706	.856	.804	1.000	.663 E-02	.116 E-02
191	5	62	Ripple	1.30	.82	1.60	.234	1.002	1.077	1.002	1.002	.175 E-01	.152 E-02
192	5	04	Dune	1.64	.60	1.60	.306	.723	.704	.774	1.022	.301 E-01	.774 E-02
193	5	07	Dune	1.43	.70	1.60	.301	1.190	1.104	2.125	1.046	.354 E-01	.140 E-01
194	5	10	Ripple	.75	.33	1.60	.230	.600	.567	.791	1.003	.300 E-01	.160 E-02
195	5	23	Dune	2.57	.65	1.60	.562	1.835	2.370	4.664	1.095	.830 E-01	.990 E-02
196	5	34	Dune	1.70	.62	1.60	.304	.566	.645	2.630	1.063	.850 E-01	.135 E-01
197	5	40	Dune	3.32	.01	1.60	.650	.106	.134	.301	1.230	.133 E-00	.100 E-01
198	6	13	Dune	1.80	.66	1.54	.460	1.020	.070	1.332	1.170	.665 E-01	.181 E-01
199	10	67	Dune	1.60	.75	1.54	.336	.620	.600	.636	1.006	.337 E-01	.363 E-02
200	10	68	Dune	1.83	1.33	1.54	.346	.061	.060	.014	1.010	.327 E-01	.564 E-02

APPENDIX C

VALUES OF ϵ AND RELATED PARAMETERS FOR PLANE BEDS - Continued

S.No.	Table No.	Run No.	Bed Form	Mean Velocity fps	Mean Depth ft	Geometric Standard Deviation σ of Bed Material	Froude Number $V/\sqrt{gd}$	ϵ_1 (1)	ϵ_2 (2)	ϵ_3 (3)	Υ_f (4)	Linear Concentration of Total Load, λ	Einstein-Chien Parameter (5)
301	10	93	Dune	1.45	.62	1.54	.325	.753	.720	.762	1.034	.303 E-01	.764 E-02
302	10	82	Dune	1.60	.64	1.54	.352	.672	.700	1.026	1.045	.720 E-01	.121 E-01
303	10	52	Dune	1.81	.55	1.54	.430	1.840	1.776	3.030	1.242	.118 E+00	.434 E-01
304	10	76	Dune	1.60	.63	1.54	.375	1.147	1.165	.279	1.926	.311 E+00	.318 E+00
305	10	96	Dune	1.94	.53	1.54	.470	2.430	1.907	.281	3.918	.319 E+00	.433 E+00
306	9	16	Ripple	1.07	.50	2.07	.267	1.667	1.602	1.667	1.001	.125 E-01	.425 E-03
307	9	06	Ripple	1.06	.51	2.07	.262	1.720	1.642	1.720	1.002	.190 E-01	.936 E-03
308	9	07	Dune	2.23	.53	2.07	.560	1.046	1.130	1.046	1.115	.953 E-01	.132 E-01
309	9	02	Transition	2.57	.52	2.07	.630	.775	.782	.775	1.366	.120 E+00	.223 E-01
310	11	05	Dune	1.95	.81	1.52	.382	.930	.895	.930	1.043	.642 E-01	.100 E-01
311	11	06C	Dune	2.28	.86	1.52	.433	1.300	1.360	1.300	2.771	.317 E+00	.300 E+00
312	11	07	Dune	2.44	.72	1.52	.507	1.336	1.180	1.336	1.000	.961 E-01	.120 E-01
313	11	158	Standing Wave	4.73	.75	1.52	.963	.627	.629	.627	4.750	.416 E+00	.131 E+00

1. ϵ_1 is average of ϵ values computed from all velocity profiles observed in the section and is based on average shear velocity.

2. ϵ_2 is same as ϵ_1, but based on local shear velocity.

3. ϵ_3 is the value obtained from composite normalized velocity profile based on average shear velocity.

4. $\Upsilon_f = 1 - \frac{30(\rho_s - \rho_f)}{\rho_f} \frac{w_{s16} C_T}{g d_{50}}$ as defined in equation (6-11).

5. Einstein-Chien Parameter based on w_{s16}.

$$\left(\frac{\rho_s - \rho_f}{\rho_f}\right) \frac{C_T w_{s16}}{gd}$$

FIGURES

The Symbols Used in the Following Figures have the Following Meanings Unless Otherwise Indicated.

(i) Symbols Representing Bed Forms

R	Ripple
D	Dune
T	Transition
P	Plane
S	Standing Wave
A	Antidune
C	Chute and Pool

(ii) Symbols Identifying Data

B	Rio Grande at Bernalillo, N.M.
G	Rio Grande at Albuquerque, N.M.
W	West Pakistan Canals

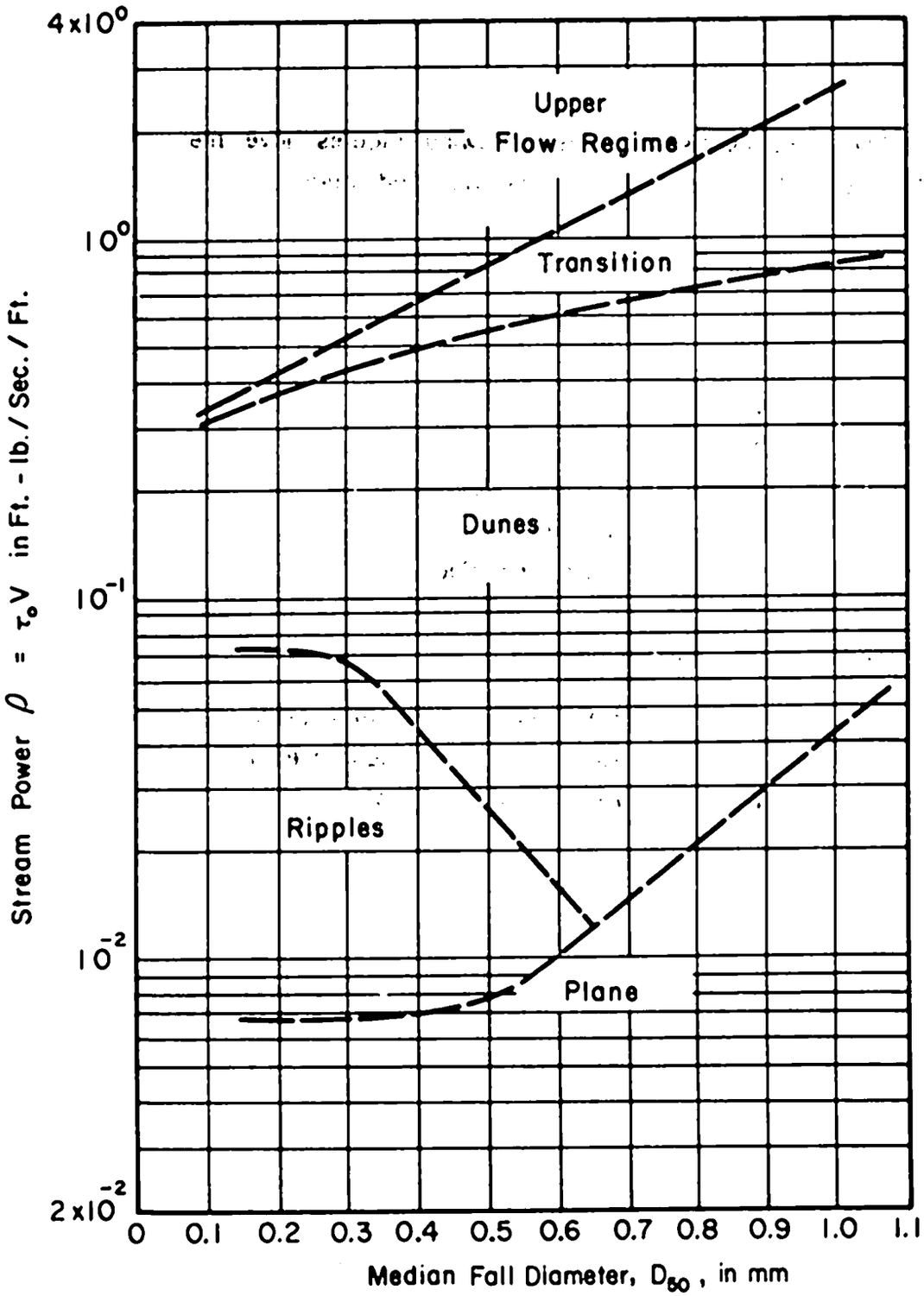

FIG. 4 - 1 PREDICTION OF BED FORM IN SAND-BED CHANNELS
(AFTER SIMONS AND RICHARDSON, 1966)

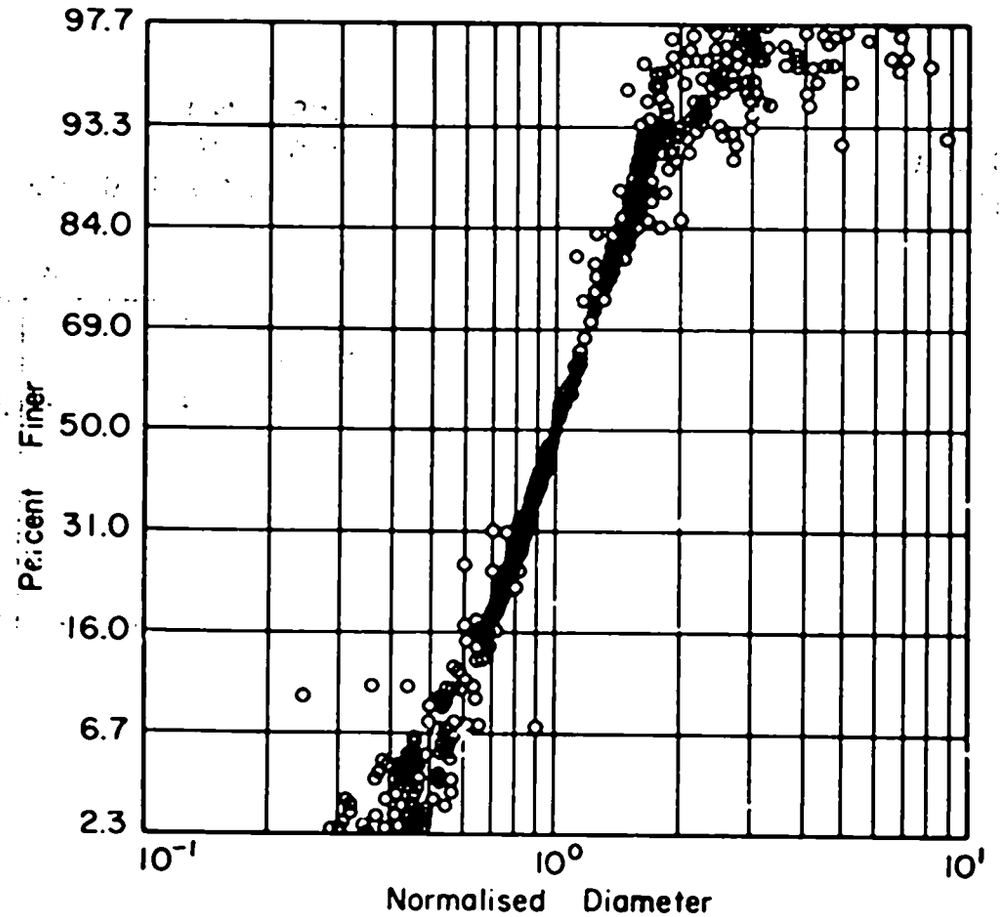

FIG. 5-1 NORMALIZED LOGNORMAL PLOT OF BED-MATERIAL SIZE DISTRIBUTION IN RIO GRANDE AT ALBUQUERQUE AND BERNALILLO, N.M. (112 SAMPLES)

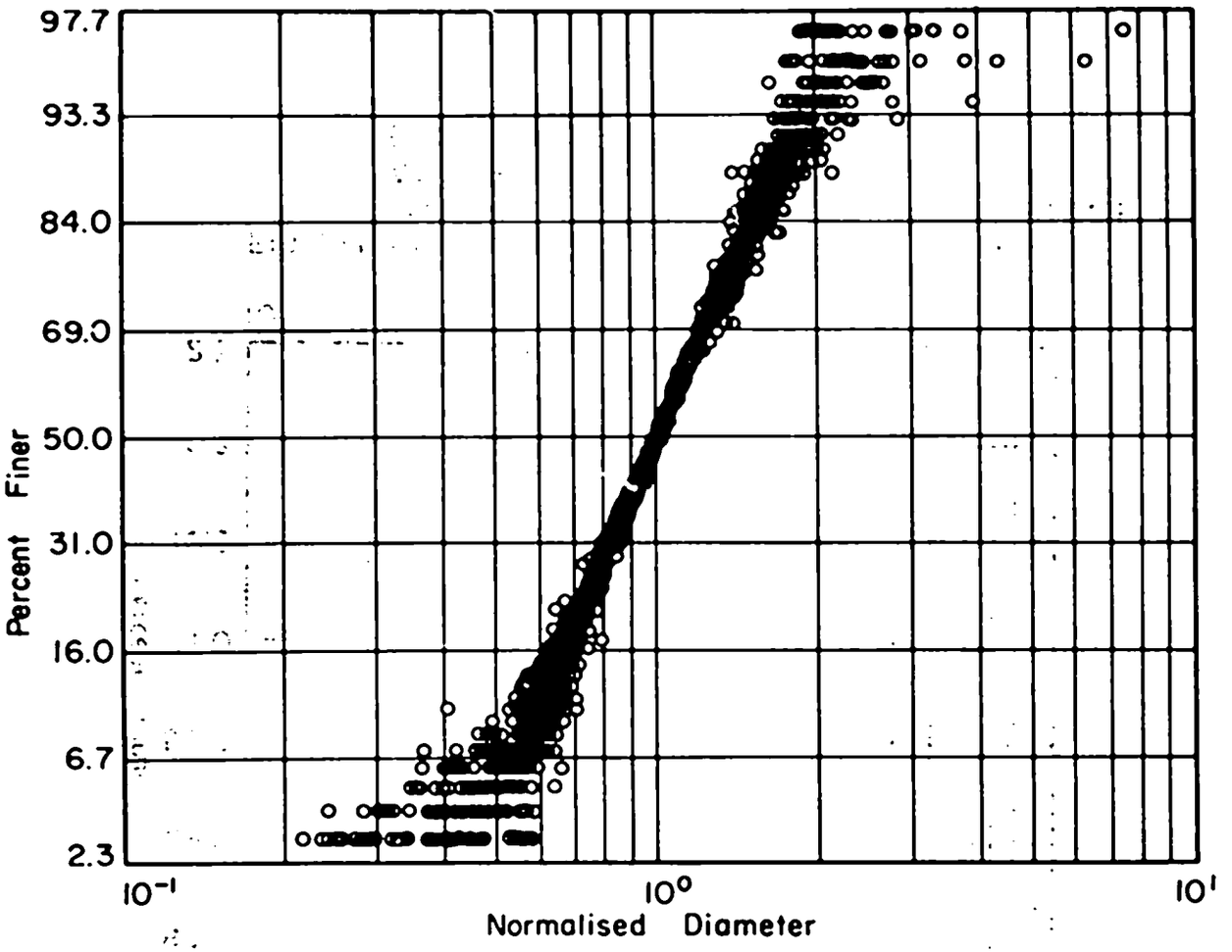

FIG. 5-2 NORMALIZED LOGNORMAL PLOT OF BED-MATERIAL SIZE DISTRIBUTION IN WEST PAKISTAN CANALS. (327 SAMPLES)

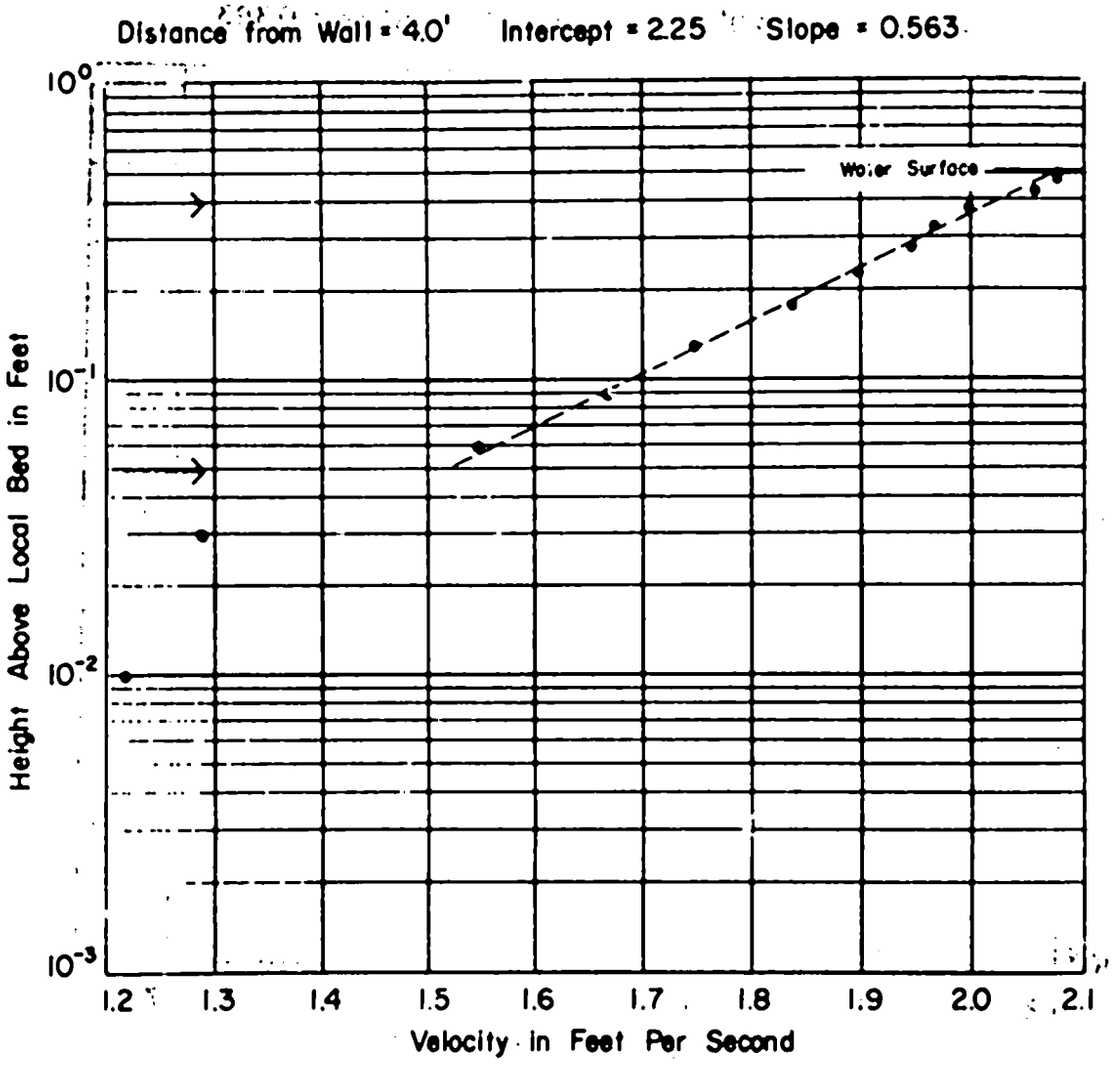

FIG. 63.1 VELOCITY PROFILE IN RUN 6-32.
PLANE BED

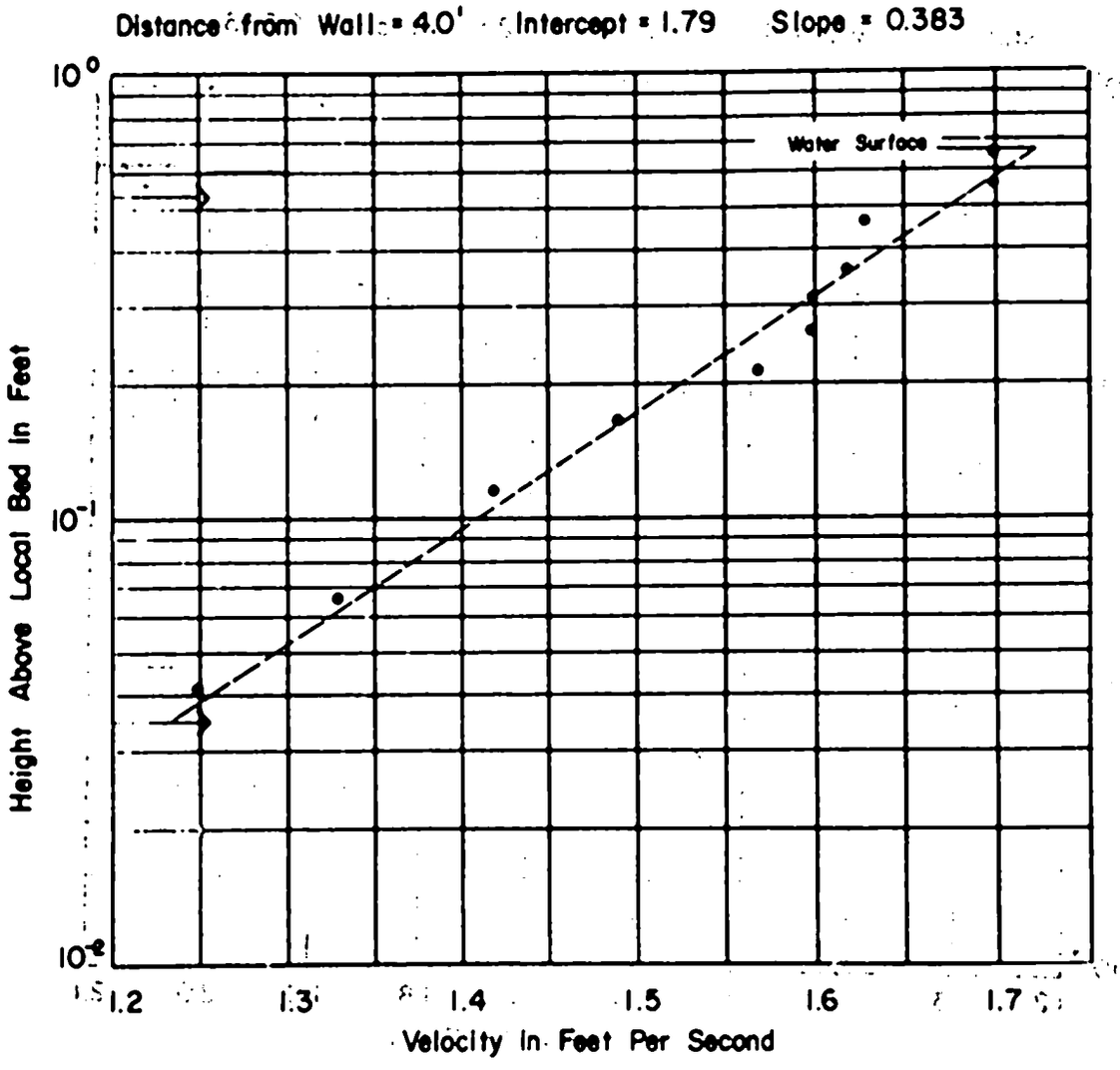

FIG. 6-2 VELOCITY PROFILE IN RUN 5-05
RIPPLE BED

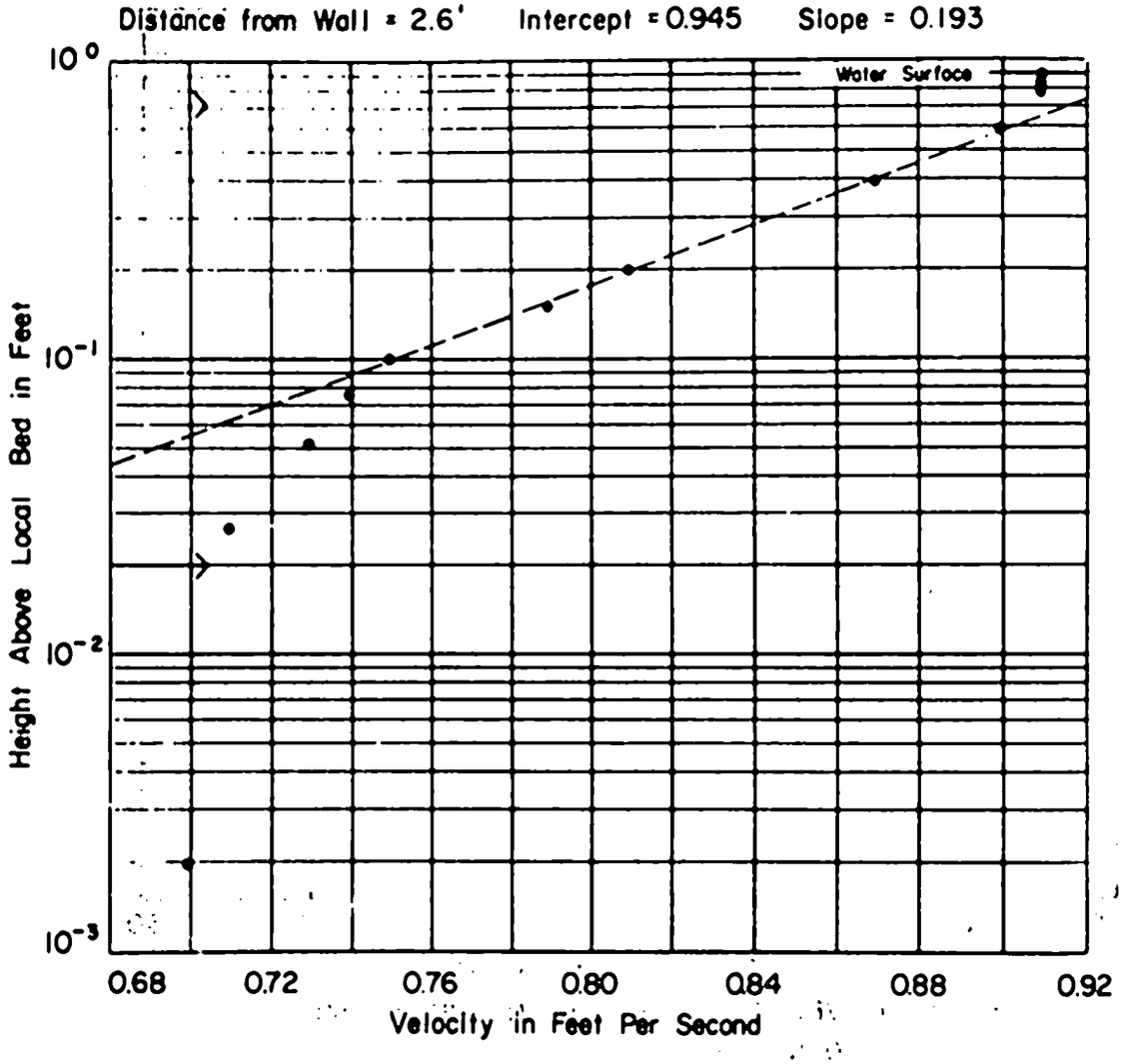

FIG. 6-3 VELOCITY PROFILE IN RUN 5-17
RIPPLE BED

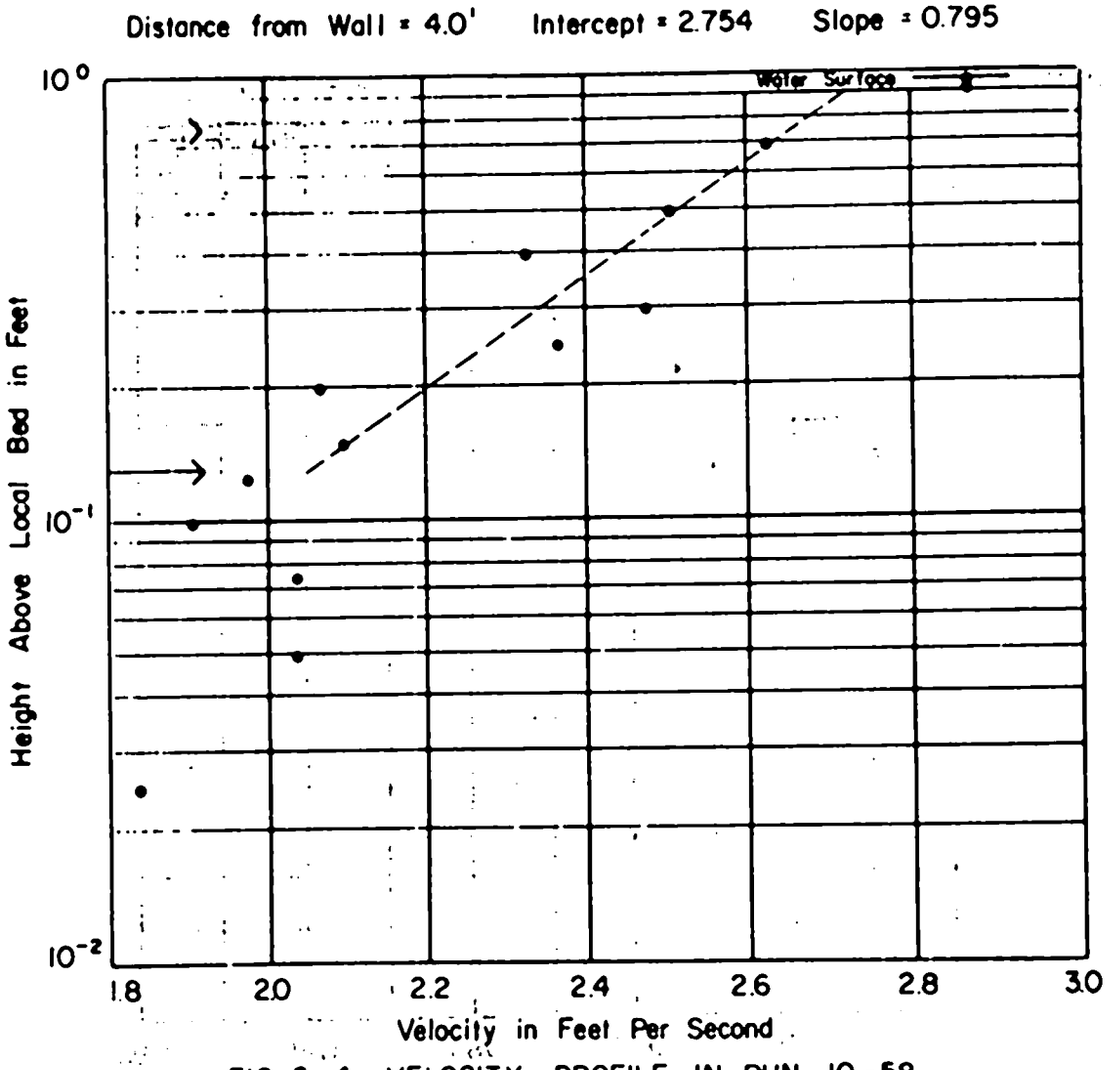

FIG. 6-4 VELOCITY PROFILE IN RUN 10-58
DUNE BED

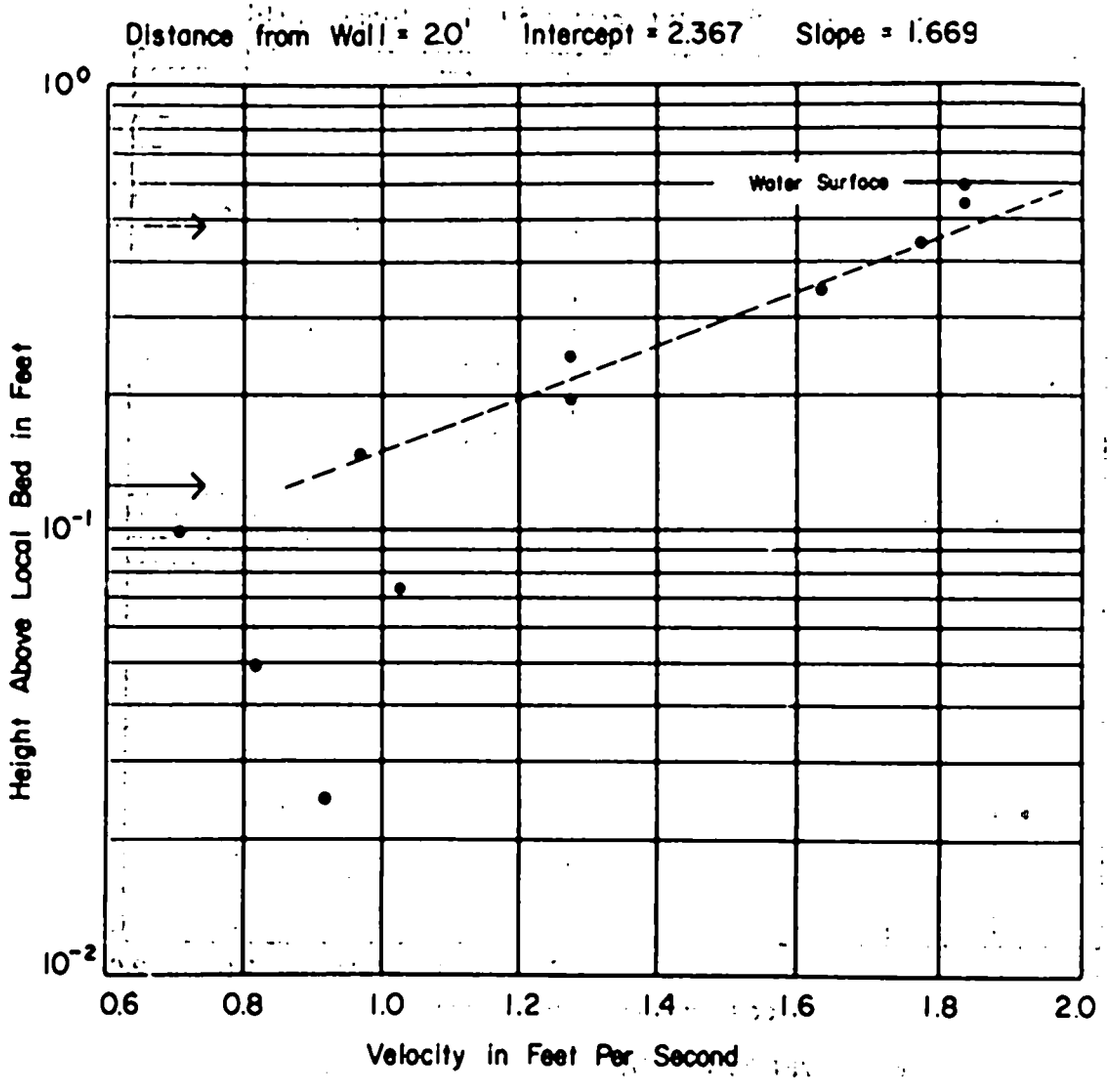

FIG. 6 ·5 VELOCITY PROFILE IN RUN 10-91
DUNE BED

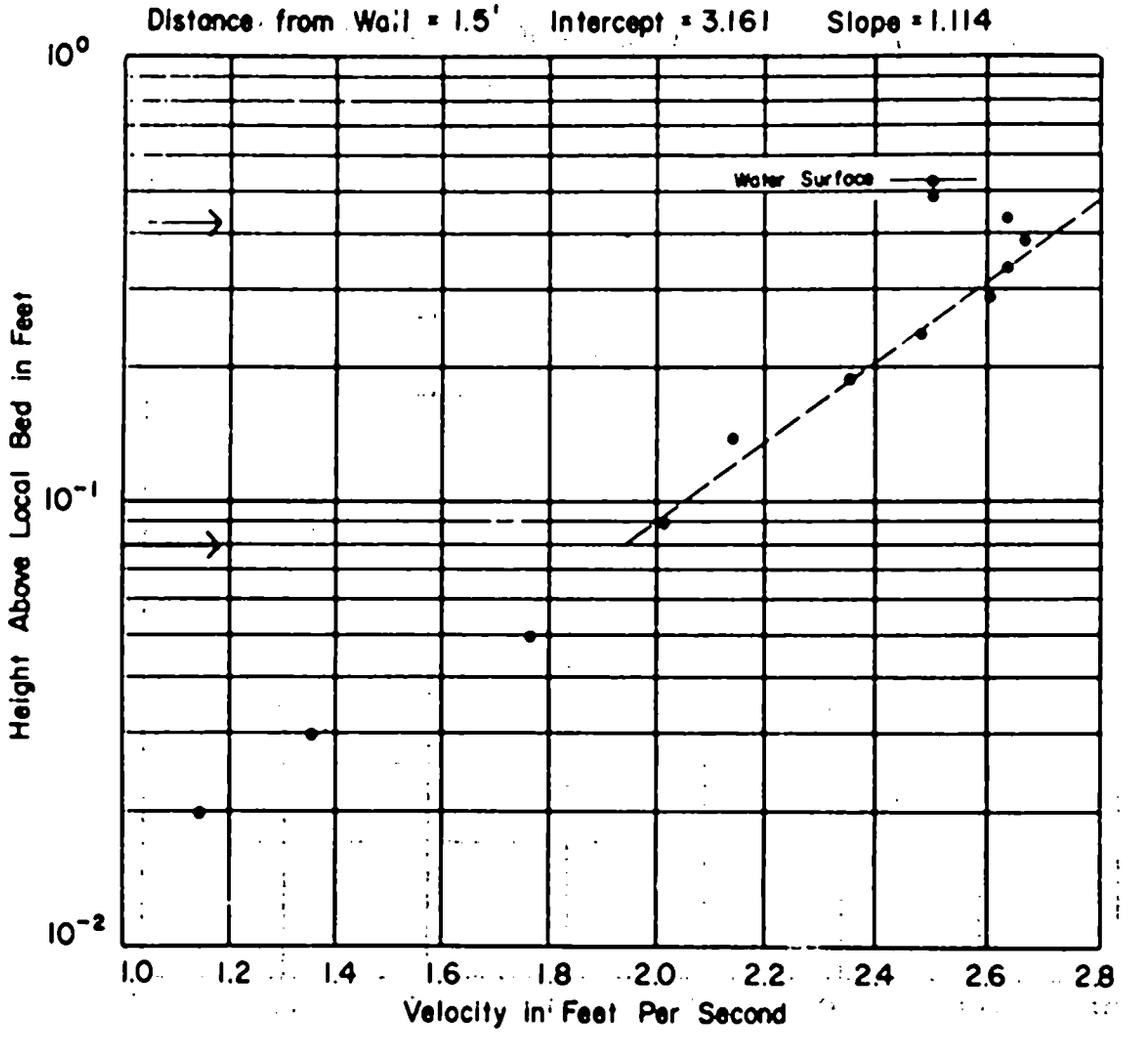

FIG. 6-6 VELOCITY PROFILE IN RUN 9-01
DUNE BED

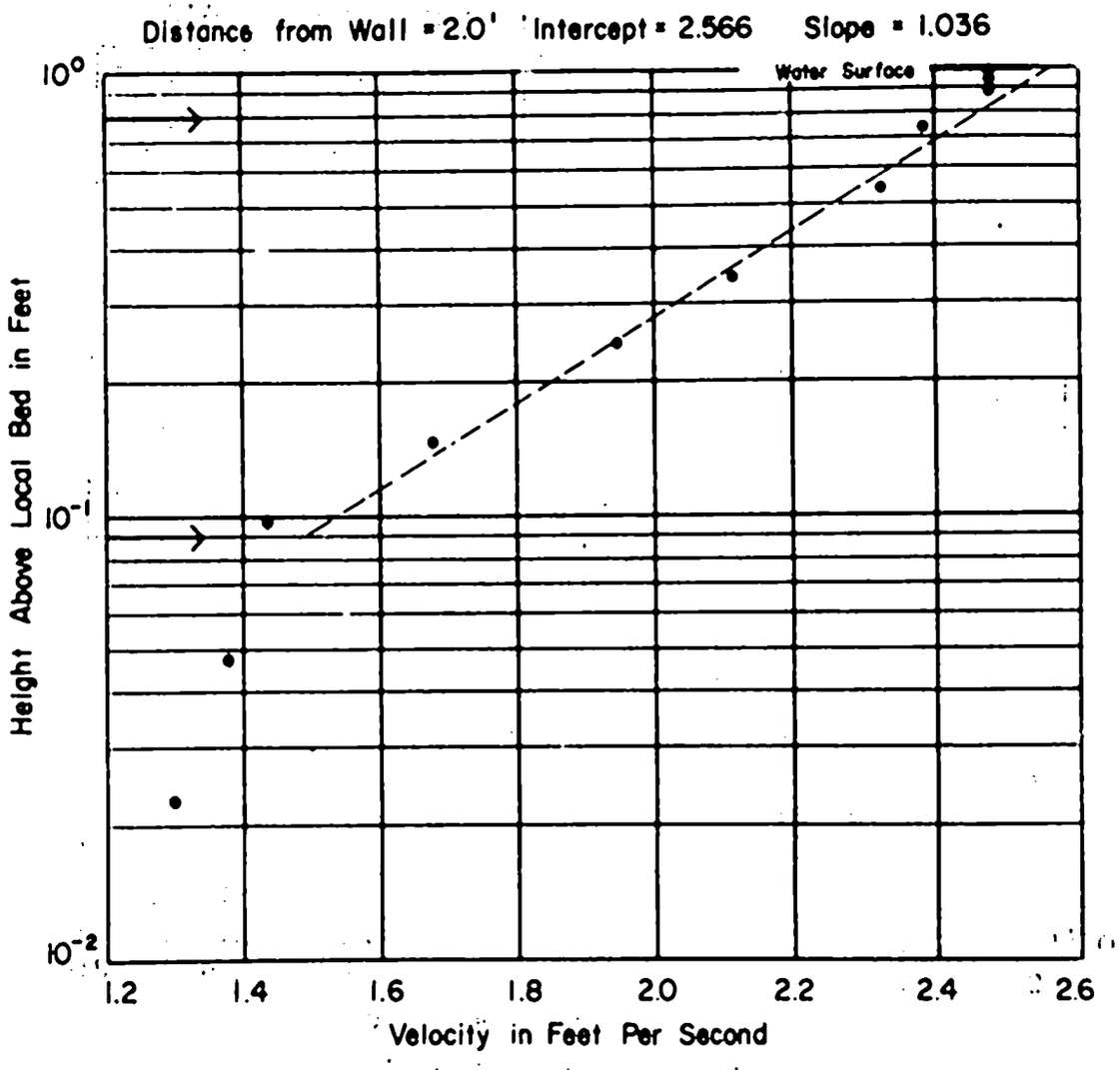

FIG. 6-7 VELOCITY PROFILE IN RUN 2-08
DUNE BED

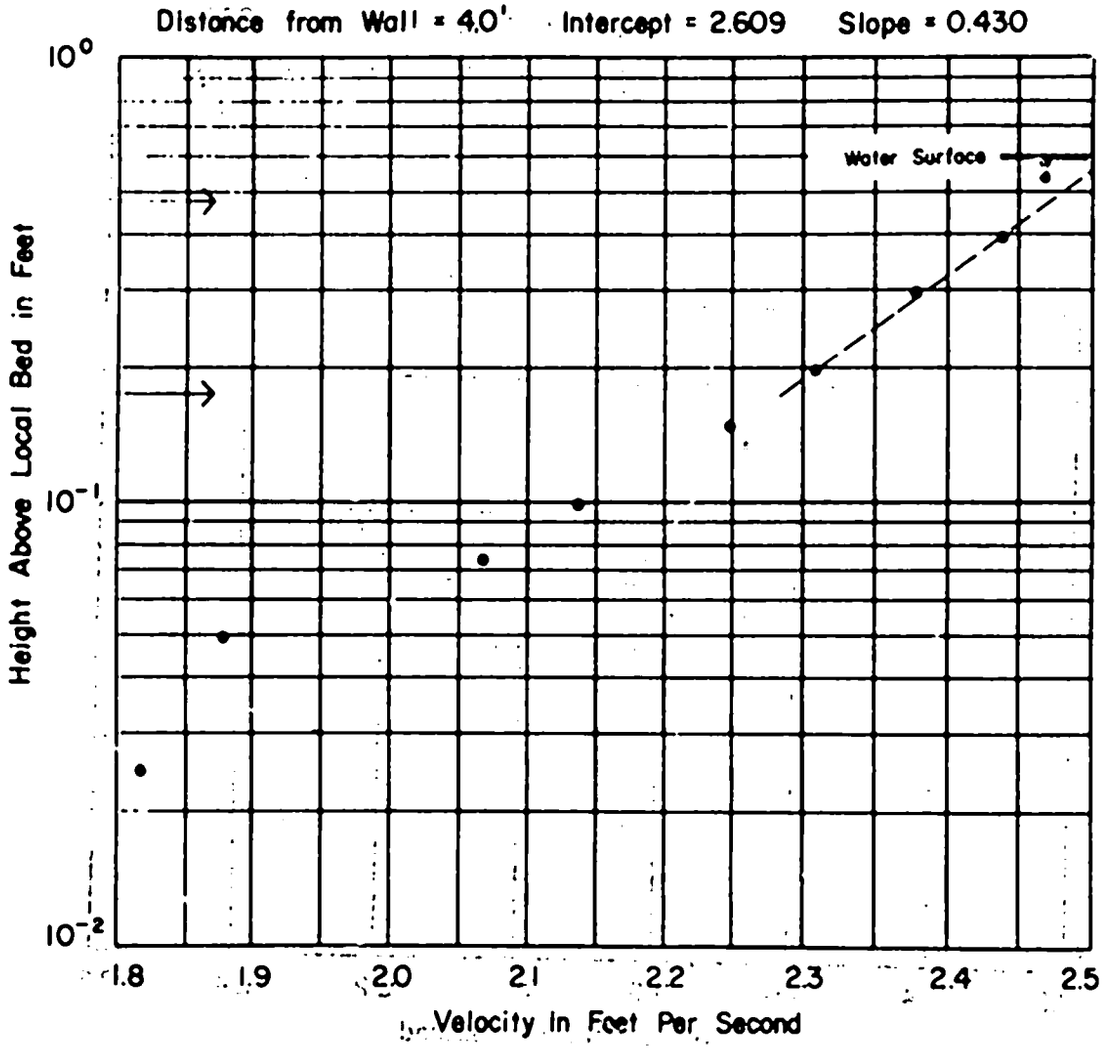

FIG. 6-8 VELOCITY PROFILE IN RUN 4-15
DUNE BED

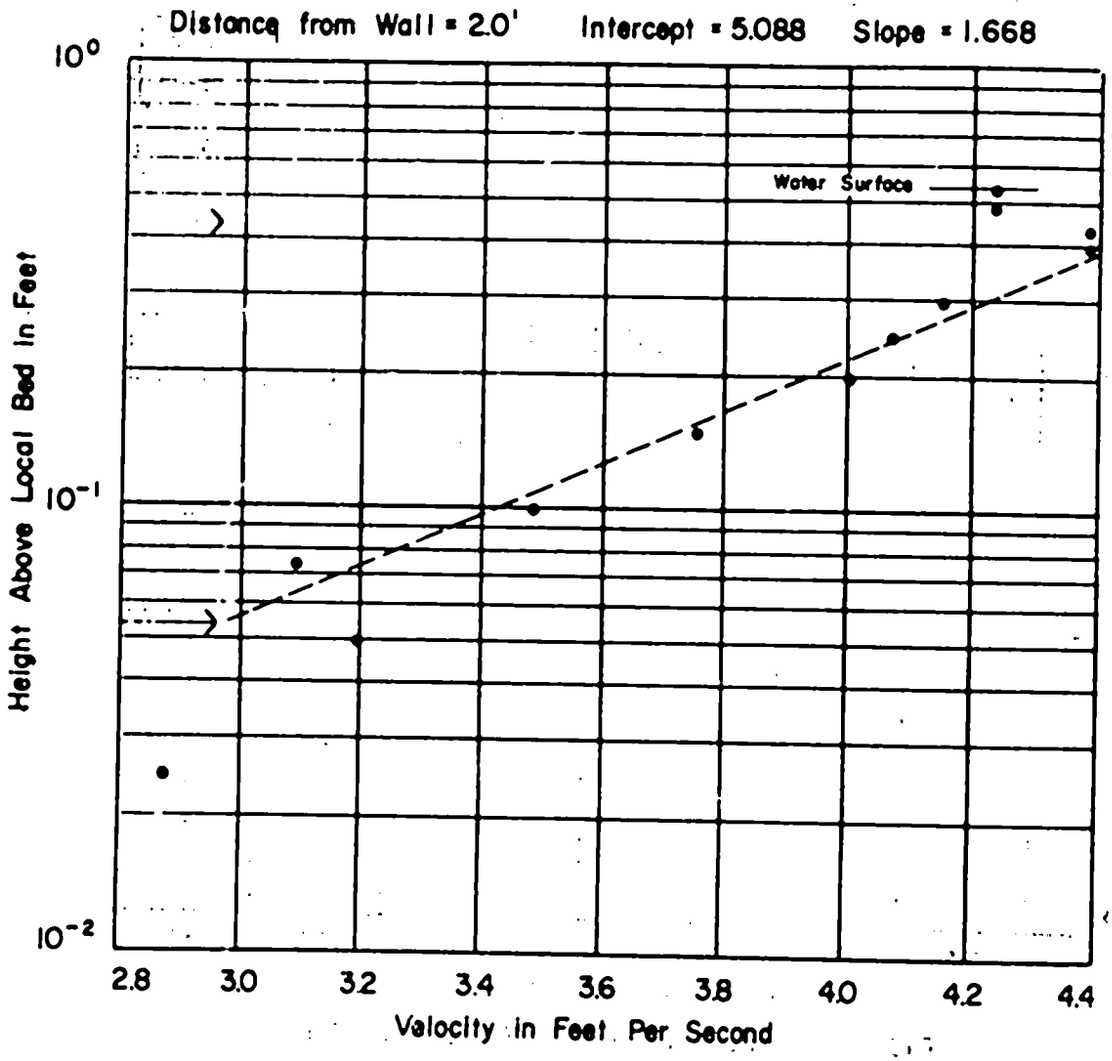

FIG. 6-9 VELOCITY PROFILE IN RUN 4-29
PLANE BED

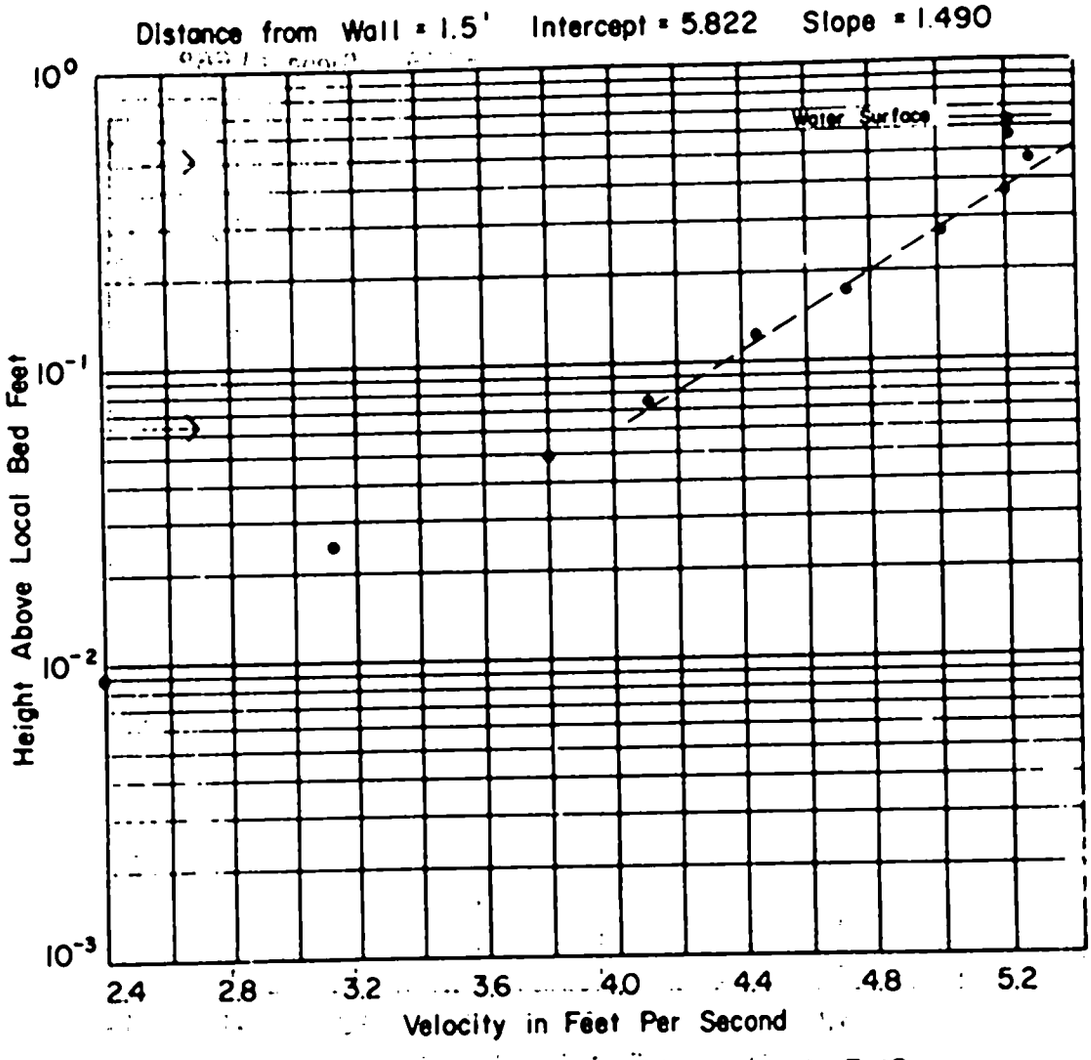

FIG. 6-10 VELOCITY PROFILE IN RUN 7-12
PLANE BED

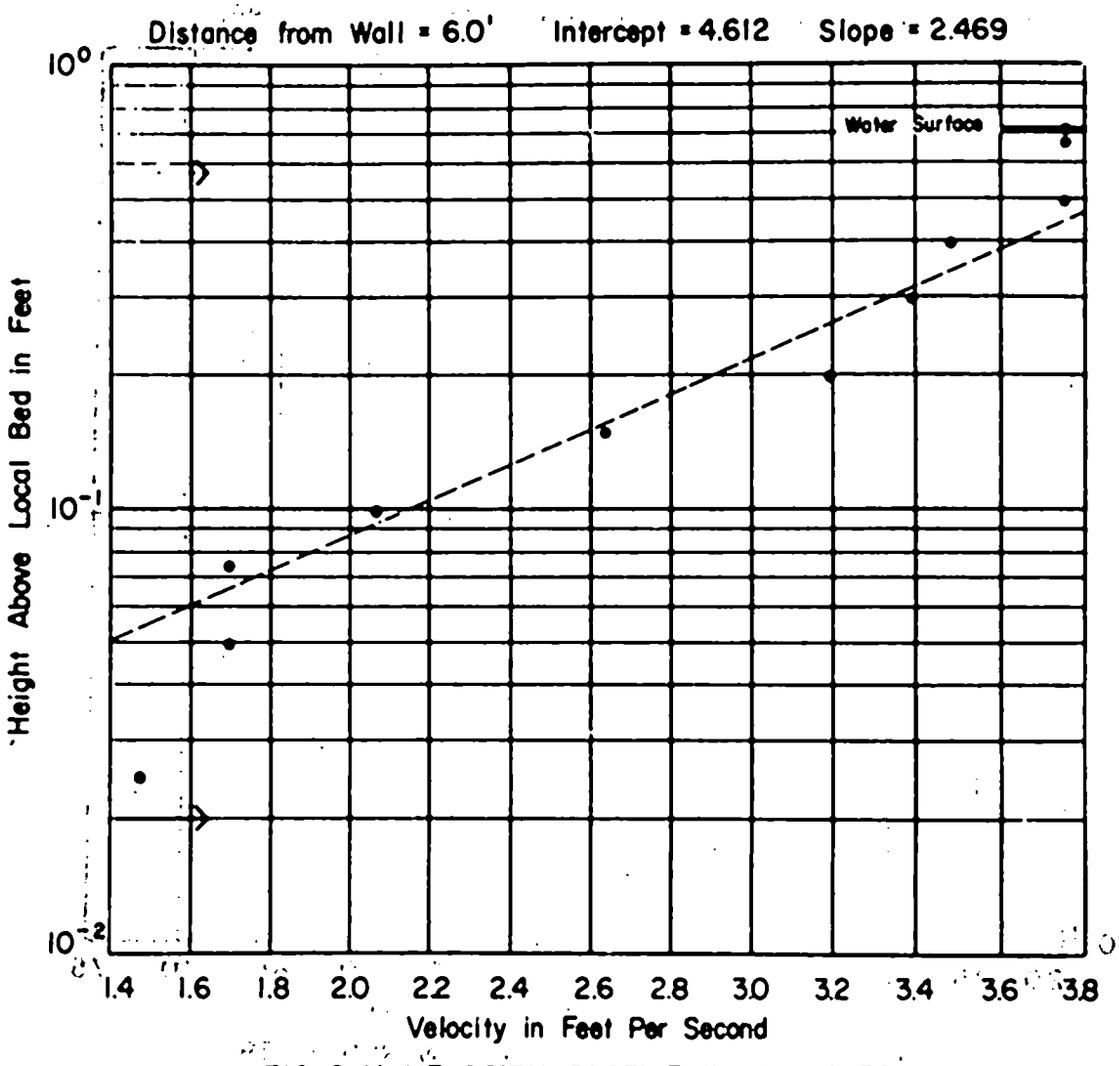

FIG. 6-11 VELOCITY PROFILE IN RUN 4-30
TRANSITION BED

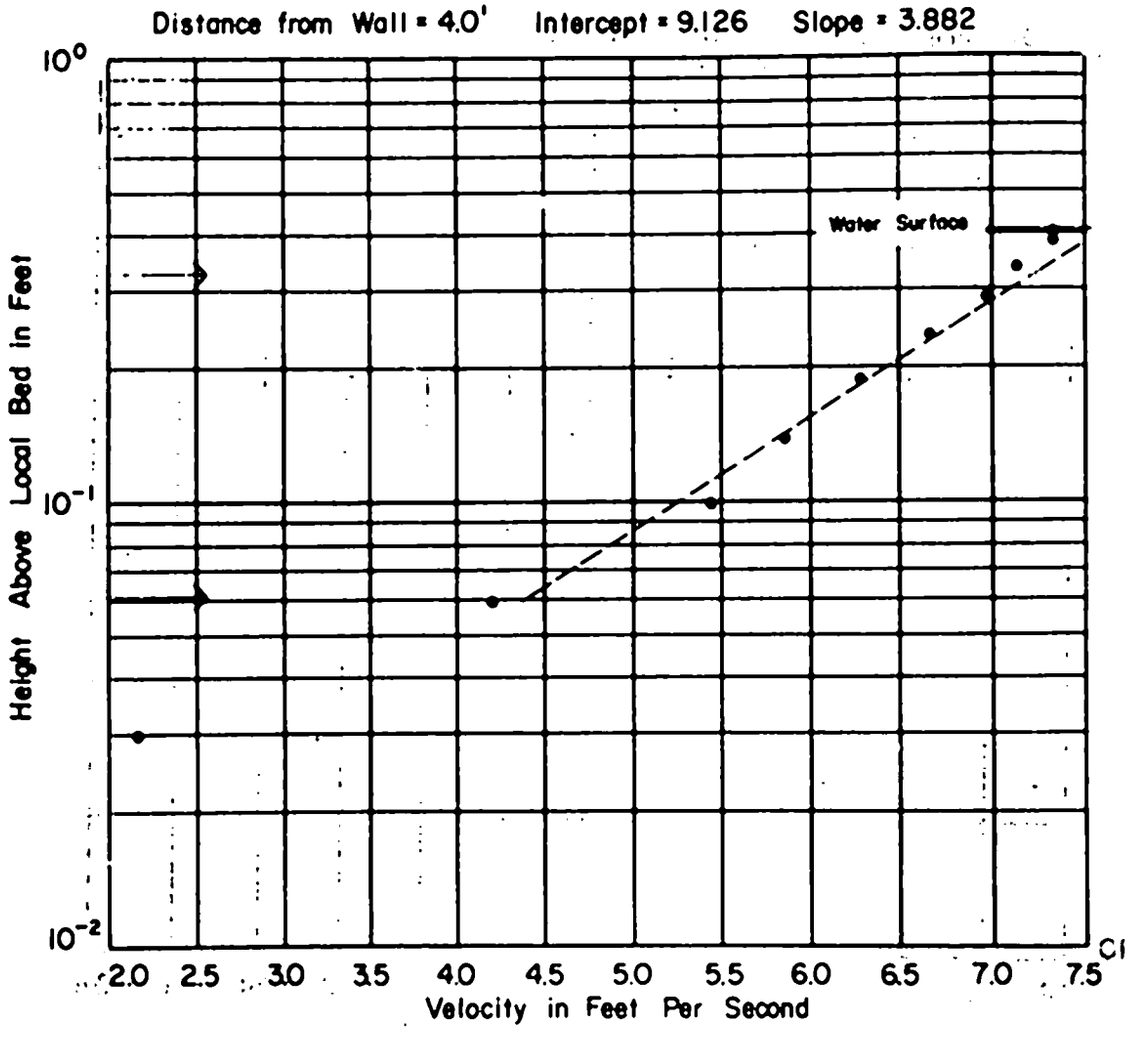

FIG. 6-12 VELOCITY PROFILE IN RUN 6-39
STANDING WAVE

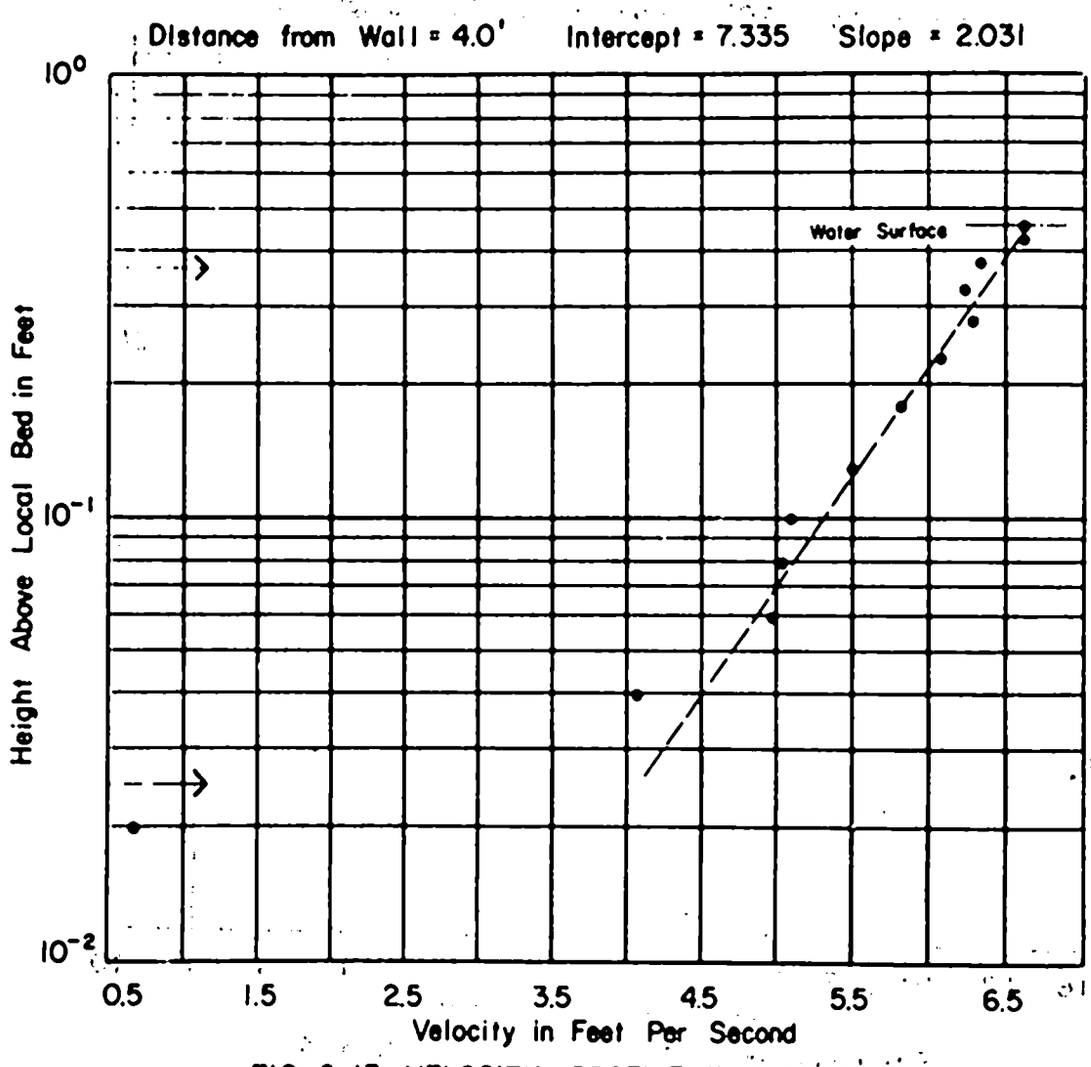

FIG. 6-13 VELOCITY PROFILE IN RUN 10-68
STANDING WAVE

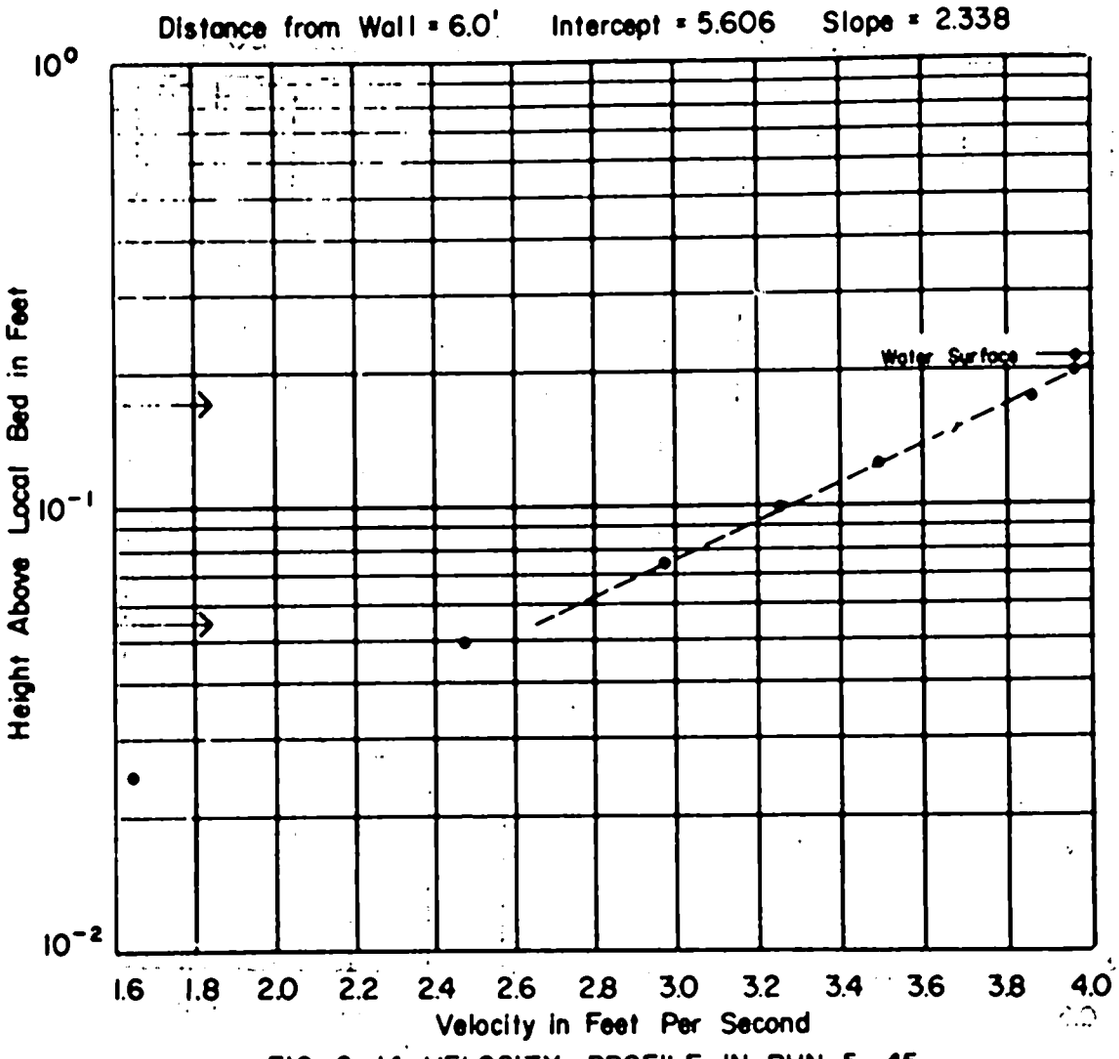

FIG. 6-14 VELOCITY PROFILE IN RUN 5-45
ANTIDUNE

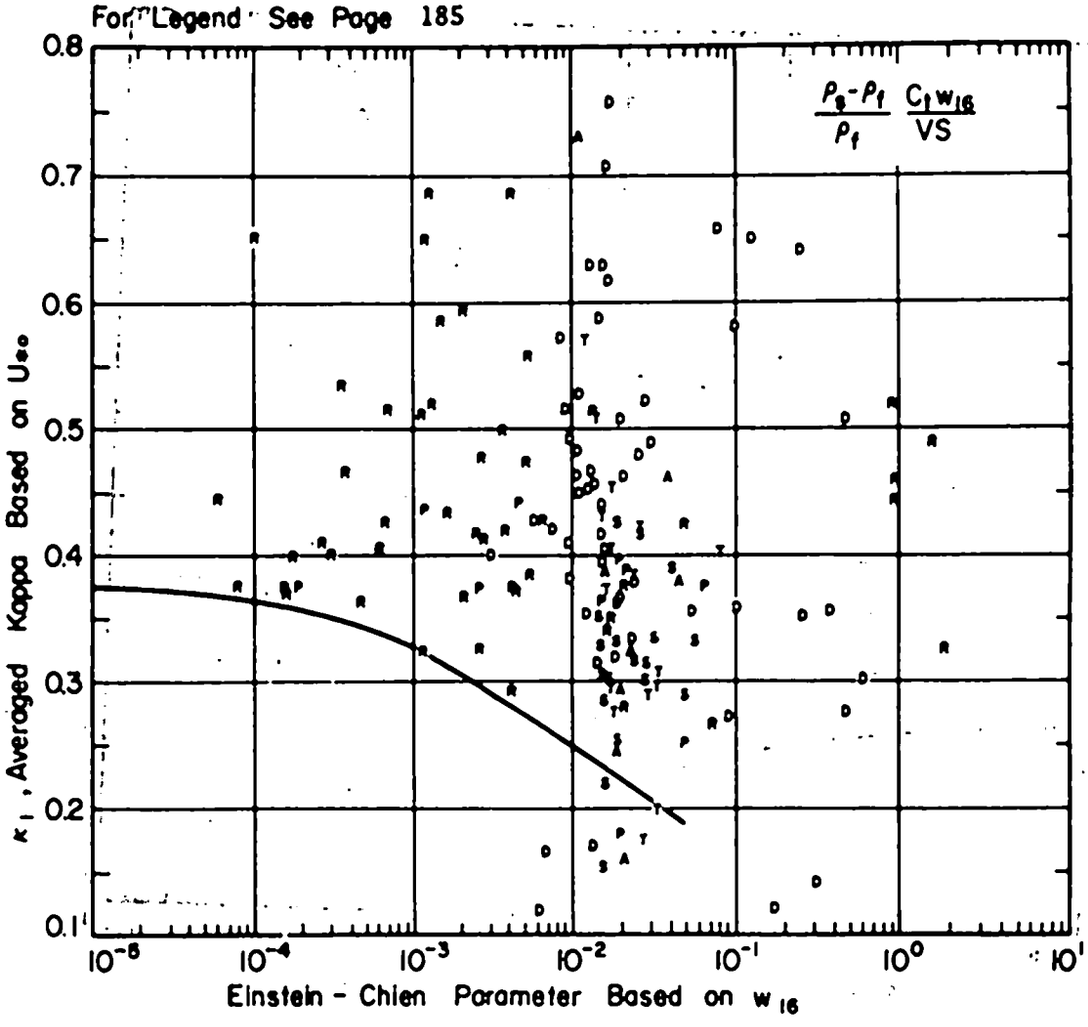

FIG. 6-15, VARIATION OF KARMAN'S KAPPA (213 RUNS)

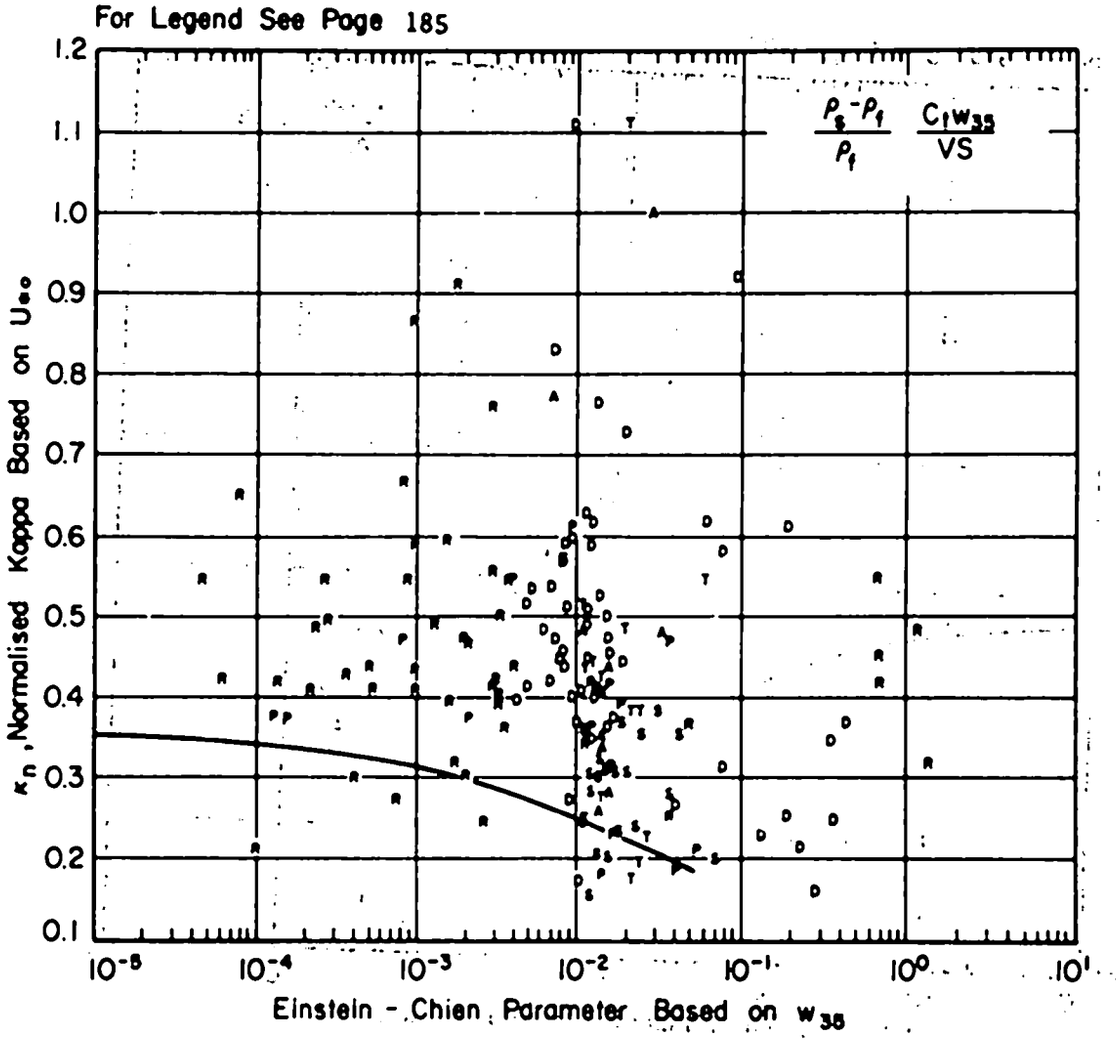

FIG. 6-16 VARIATION OF KARMAN'S KAPPA (213 RUNS)

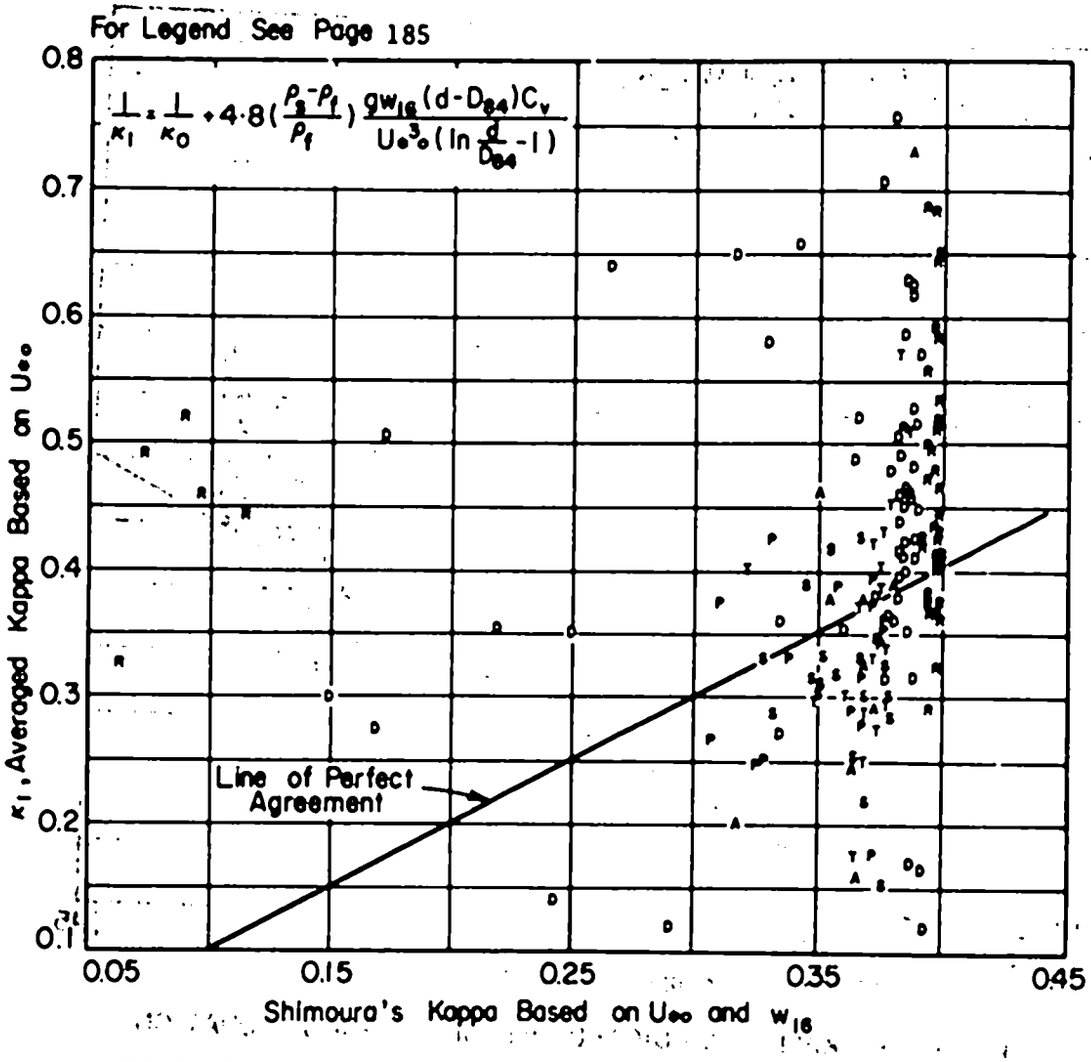

FIG. 6-17, KAPPA PREDICTED BY SHIMOURA'S EQUATION (213 RUNS)

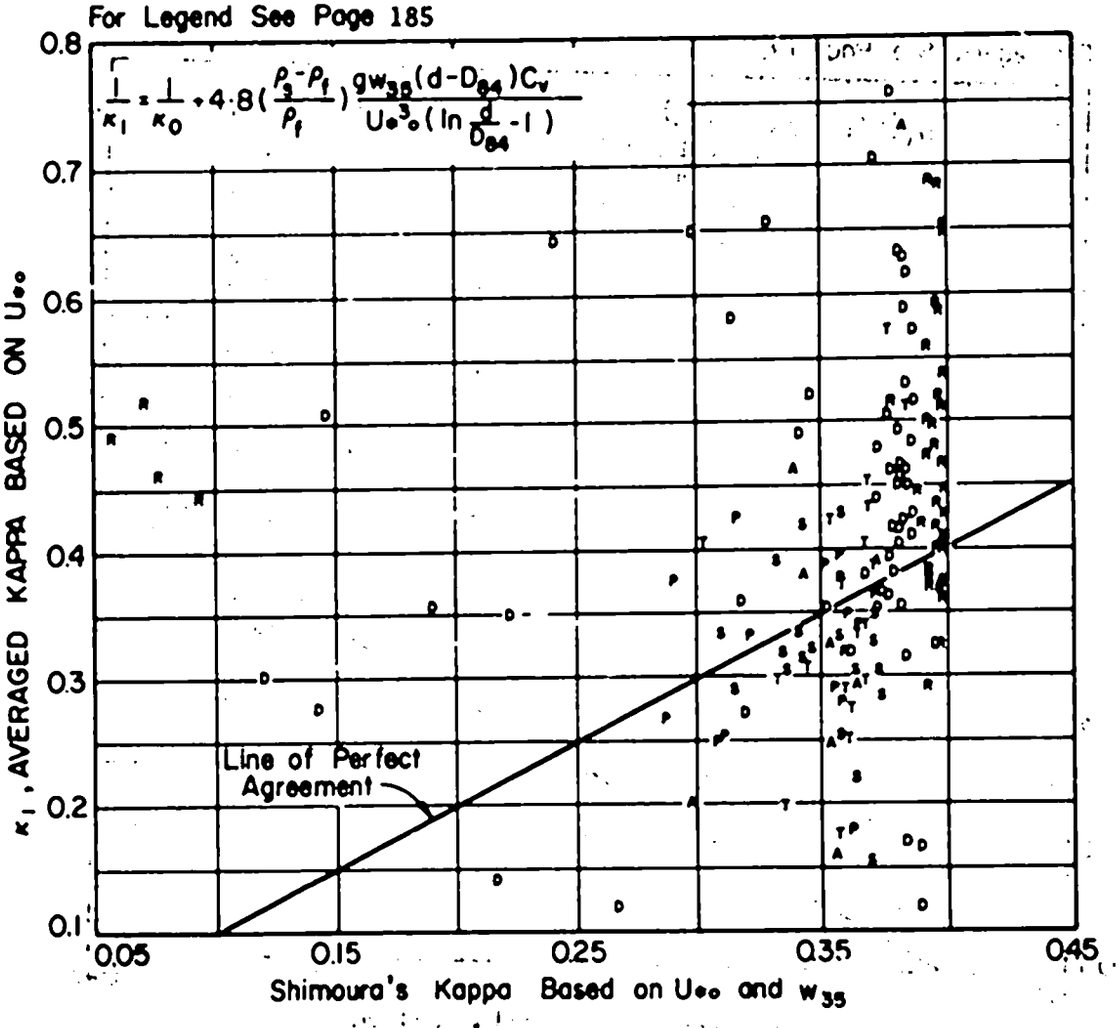

FIG. 6-18, KAPPA PREDICTED BY SHIMOURA'S EQUATION (213 RUNS)

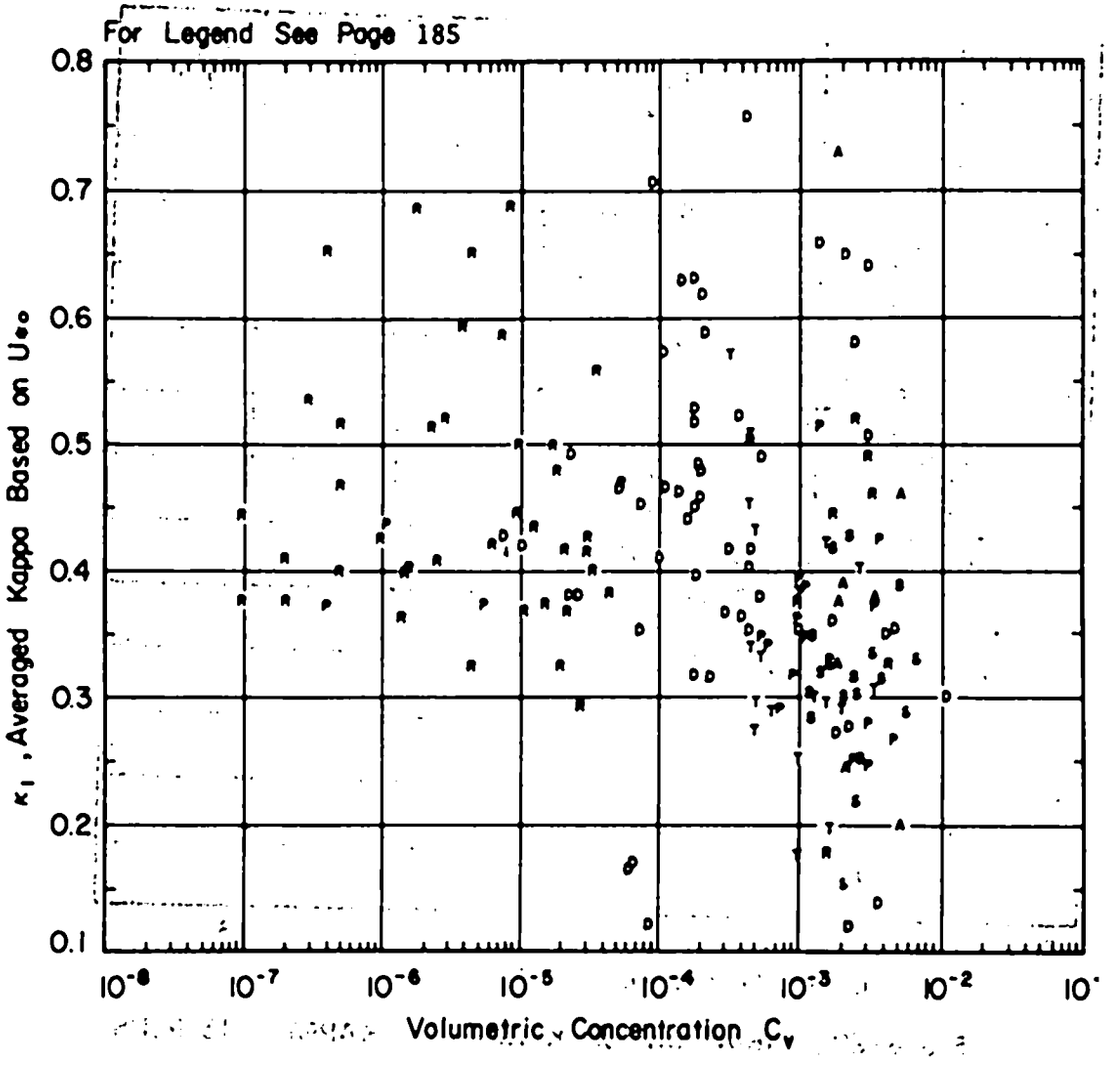

FIG. 6-19, VARIATION OF KARMAN'S KAPPA (213 RUNS)

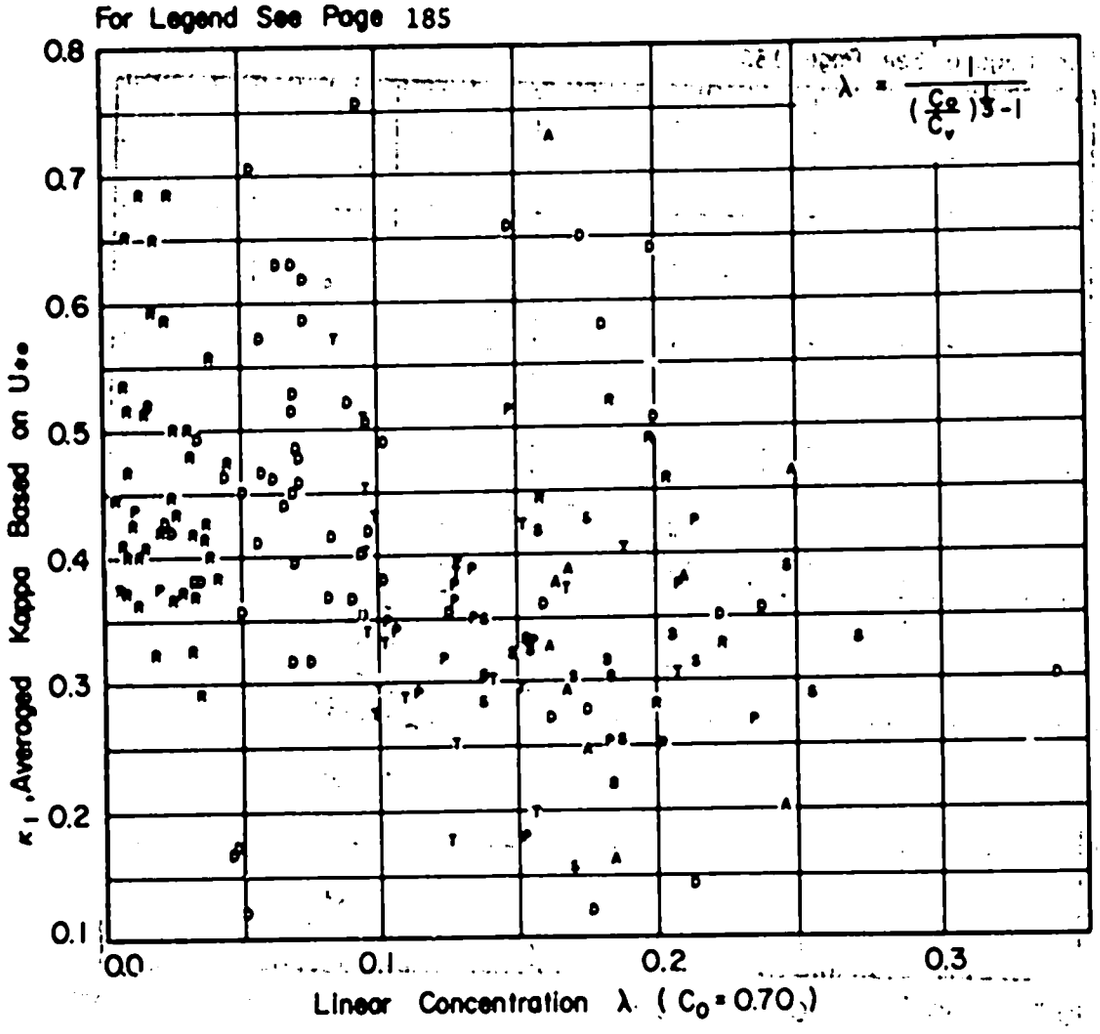

FIG. 6-20, VARIATION OF KARMAN'S KAPPA (213 RUNS)

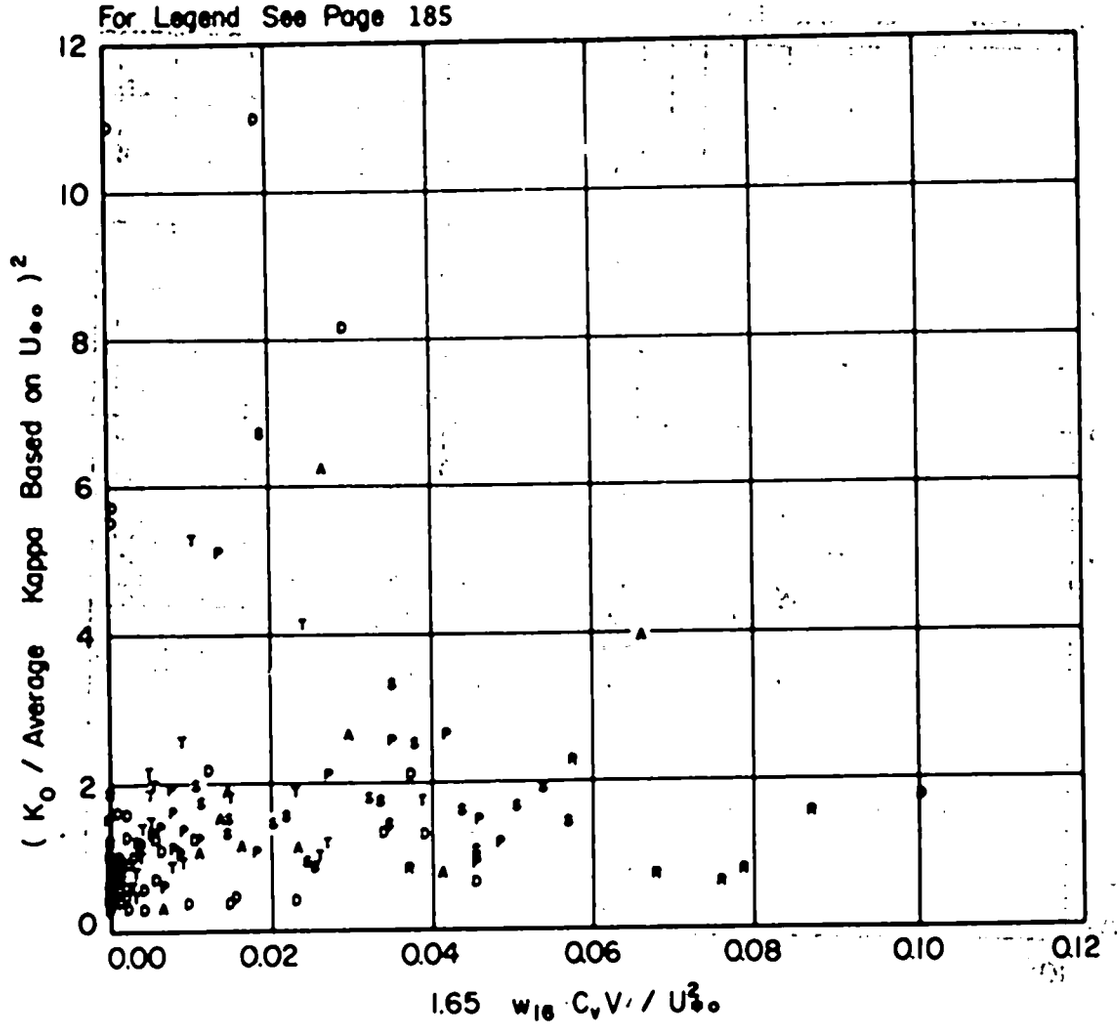

FIG. 6-21, VARIATION OF KARMAN'S KAPPA (213 RUNS)

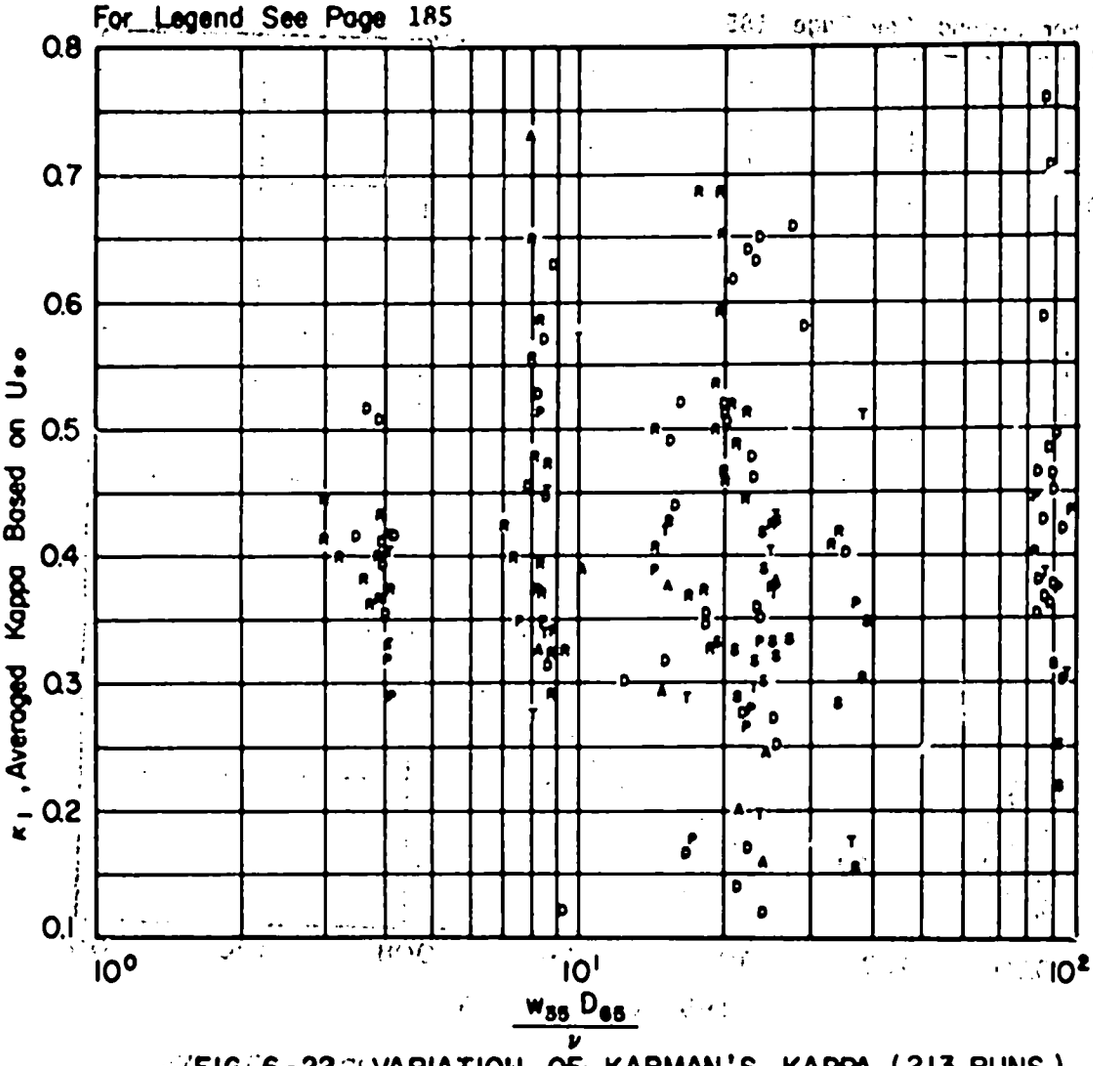

FIG. 6-22 VARIATION OF KARMAN'S KAPPA (213 RUNS)

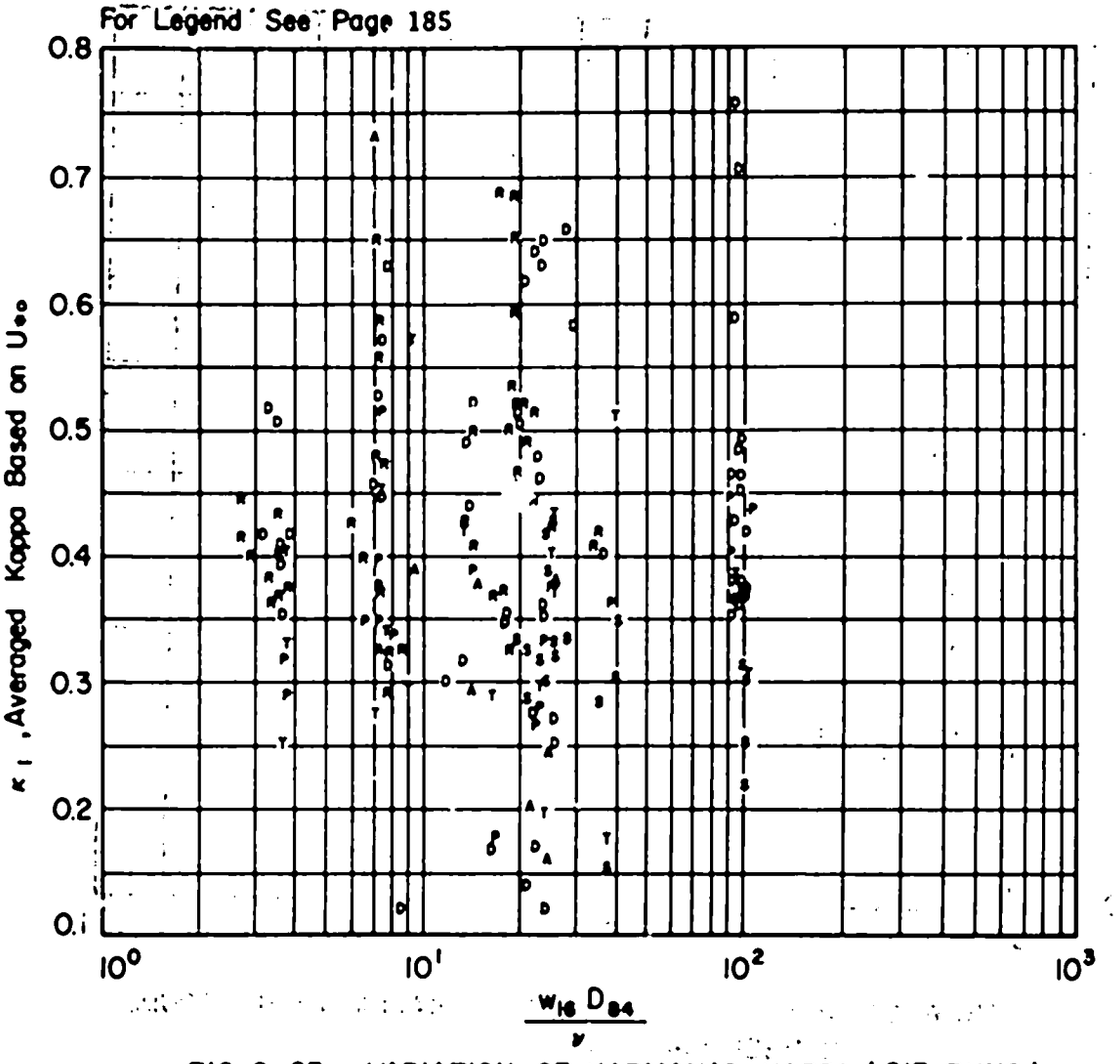

FIG. 6-23 , VARIATION OF KARMAN'S KAPPA (213 RUNS)

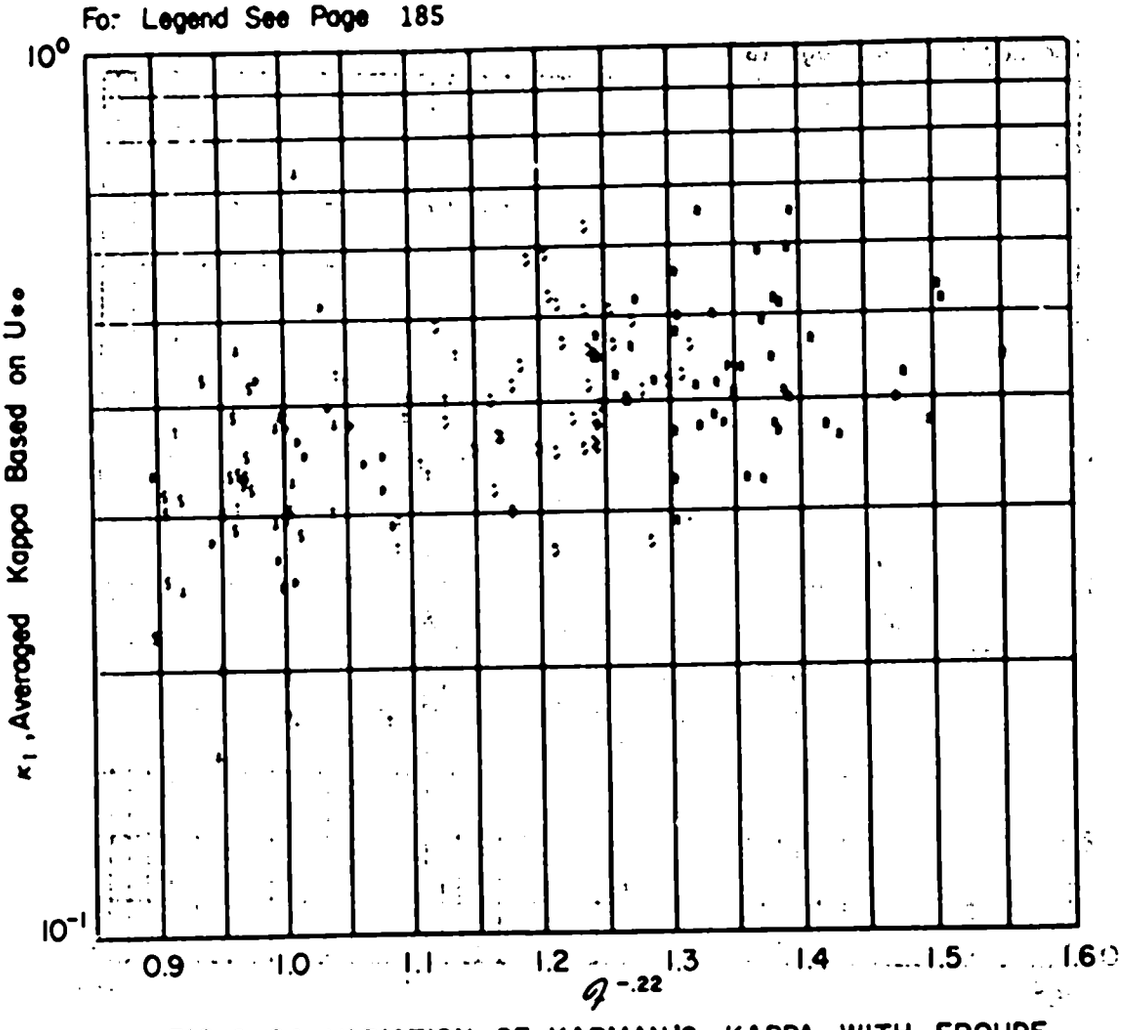

FIG. 6-24 VARIATION OF KARMAN'S KAPPA WITH FROUDE NUMBER (148 RUNS)

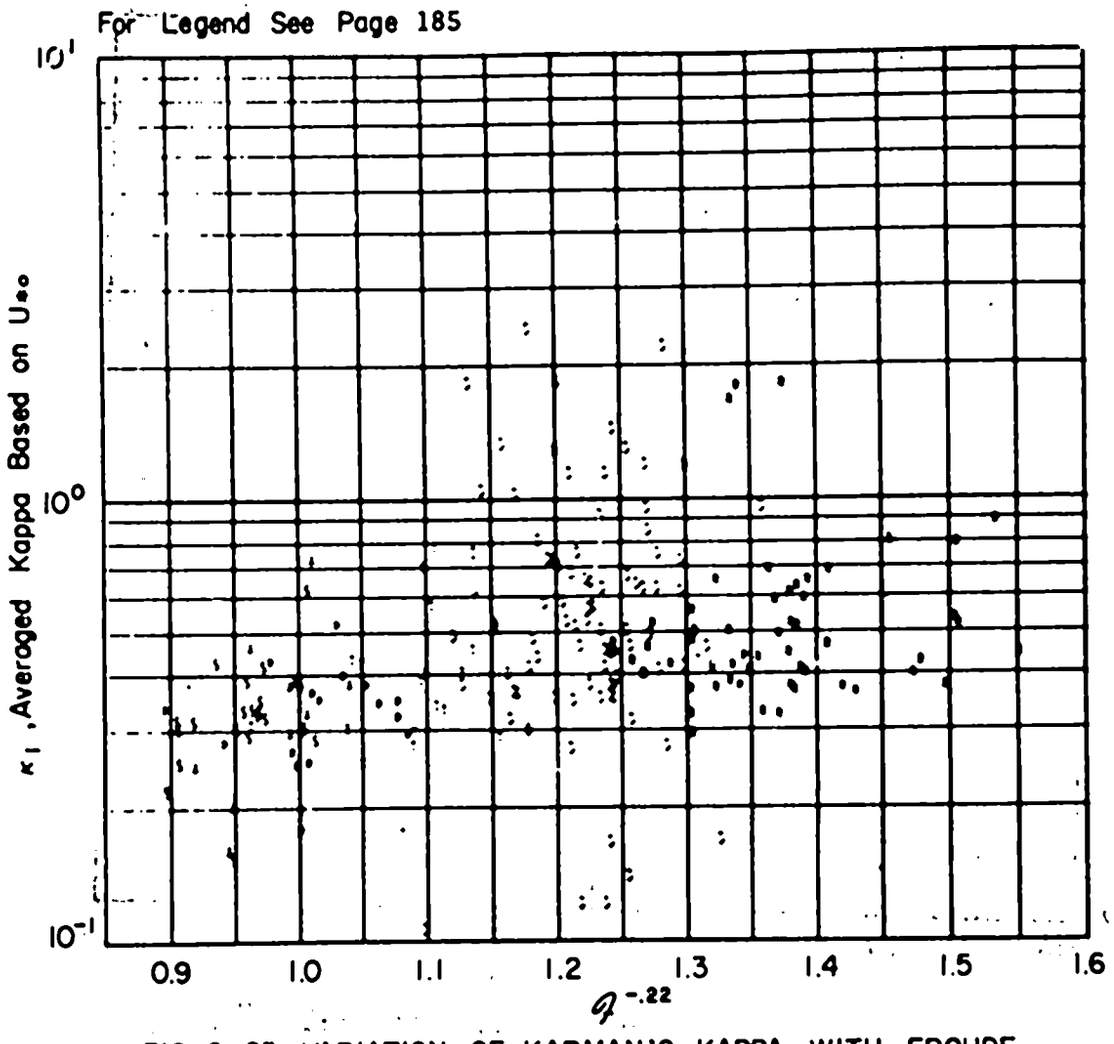

FIG. 6-25 VARIATION OF KARMAN'S KAPPA WITH FROUDE NUMBER (213 RUNS)

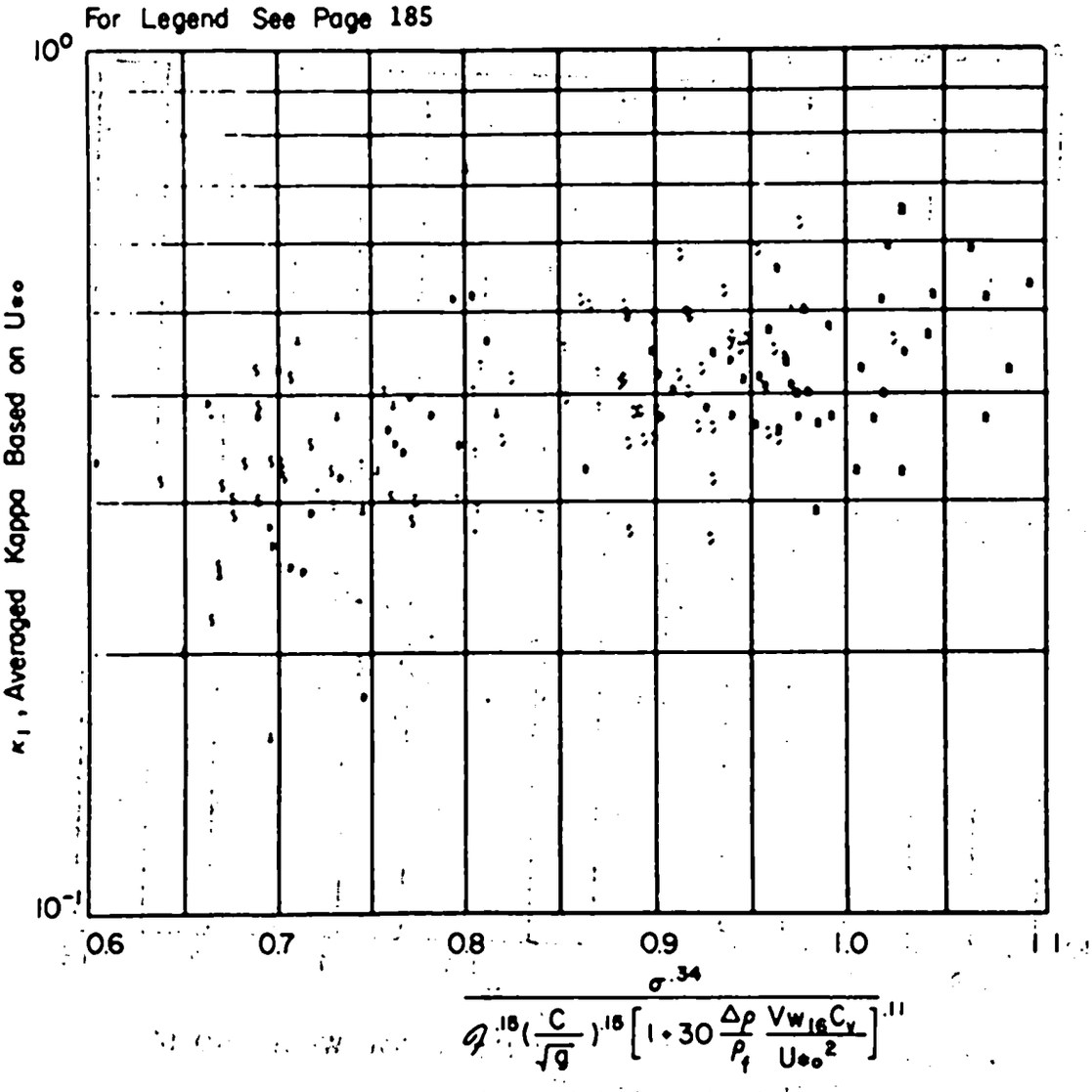

FIG. 6-26 VARIATION OF KARMAN'S KAPPA WITH PREDICTION PARAMETER (148 RUNS)

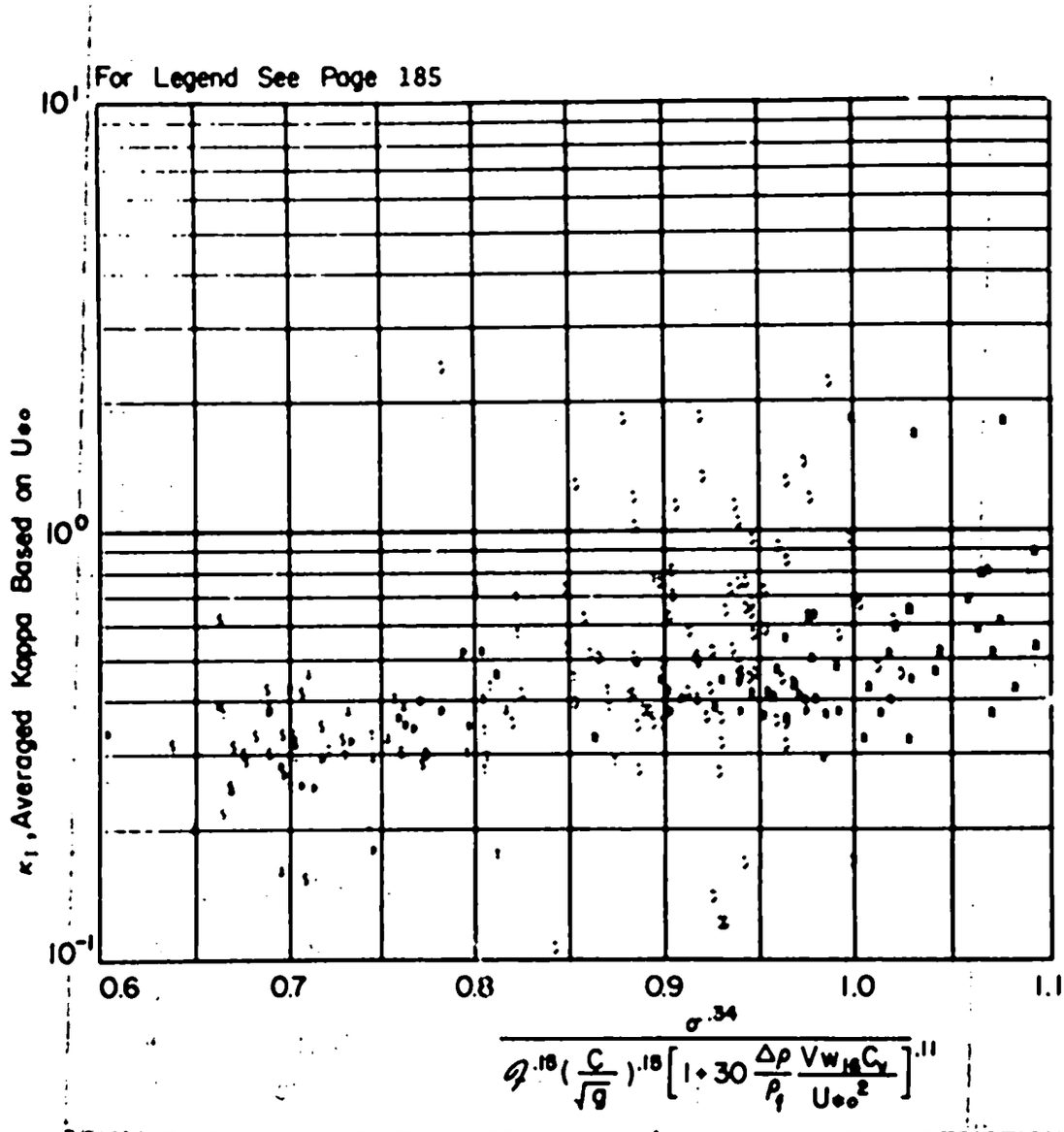

FIG. 6-27 VARIATION OF KARMAN'S KAPPA- WITH-PREDICTION PARAMETER (213 RUNS)

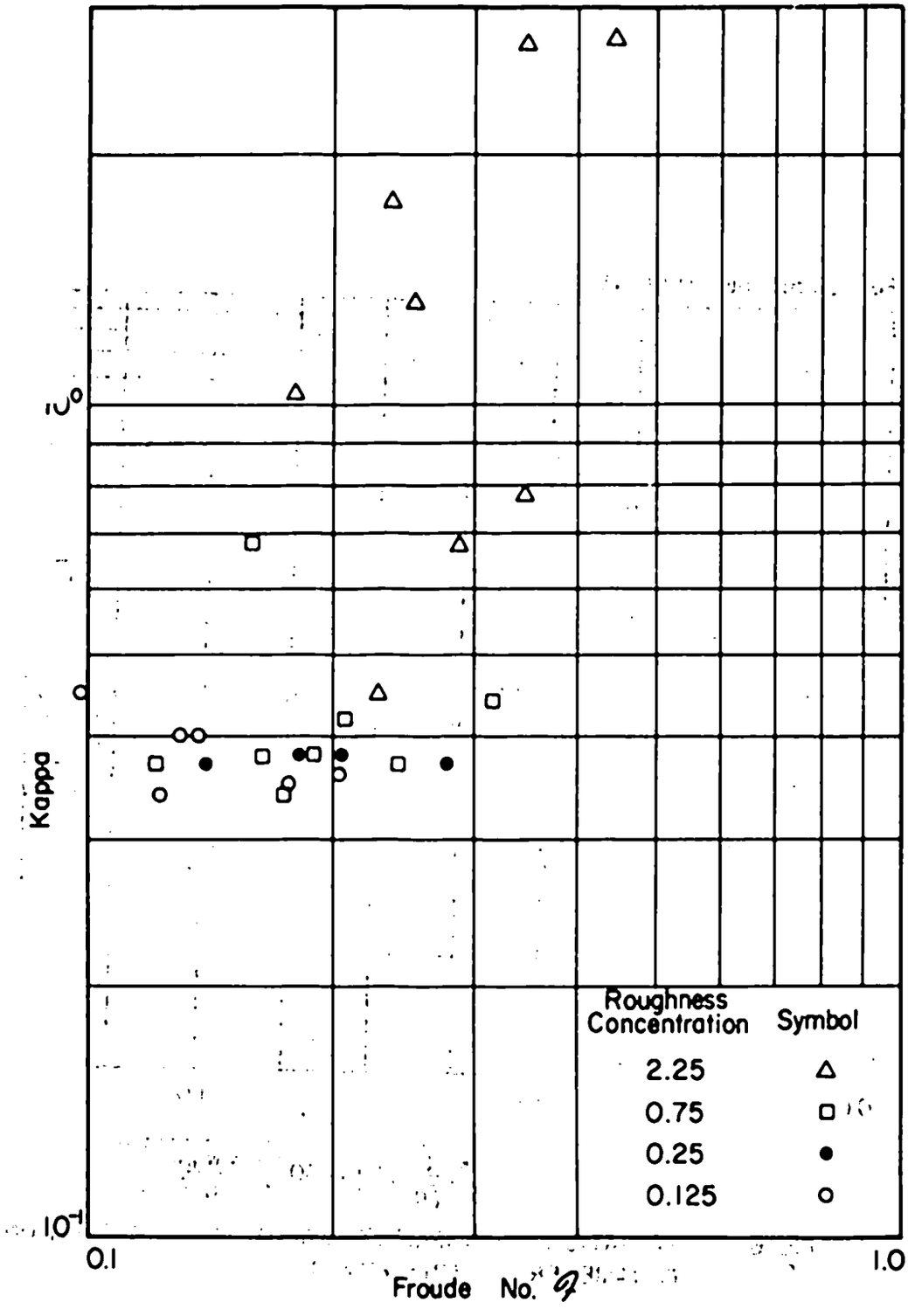

FIG. 6-28, VARIATION OF von KARMAN'S KAPPA WITH FROUDE NO. (SAYRE-ALBERTSON DATA - 1963)

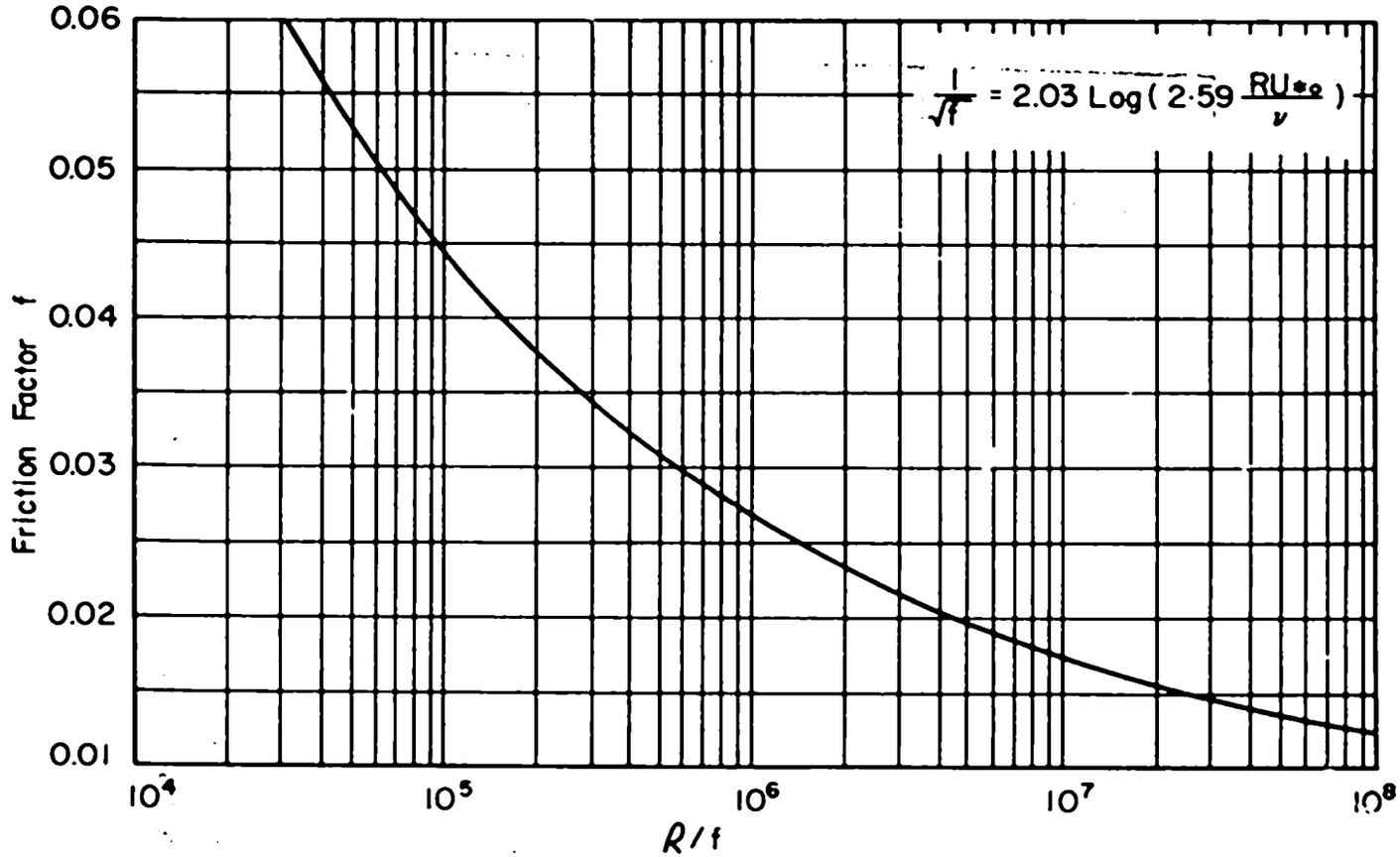

FIG. 7-1 f VERSUS R/f FOR SMOOTH FLUMES BASED ON TRACY - LESTER'S EQUATION (1961)

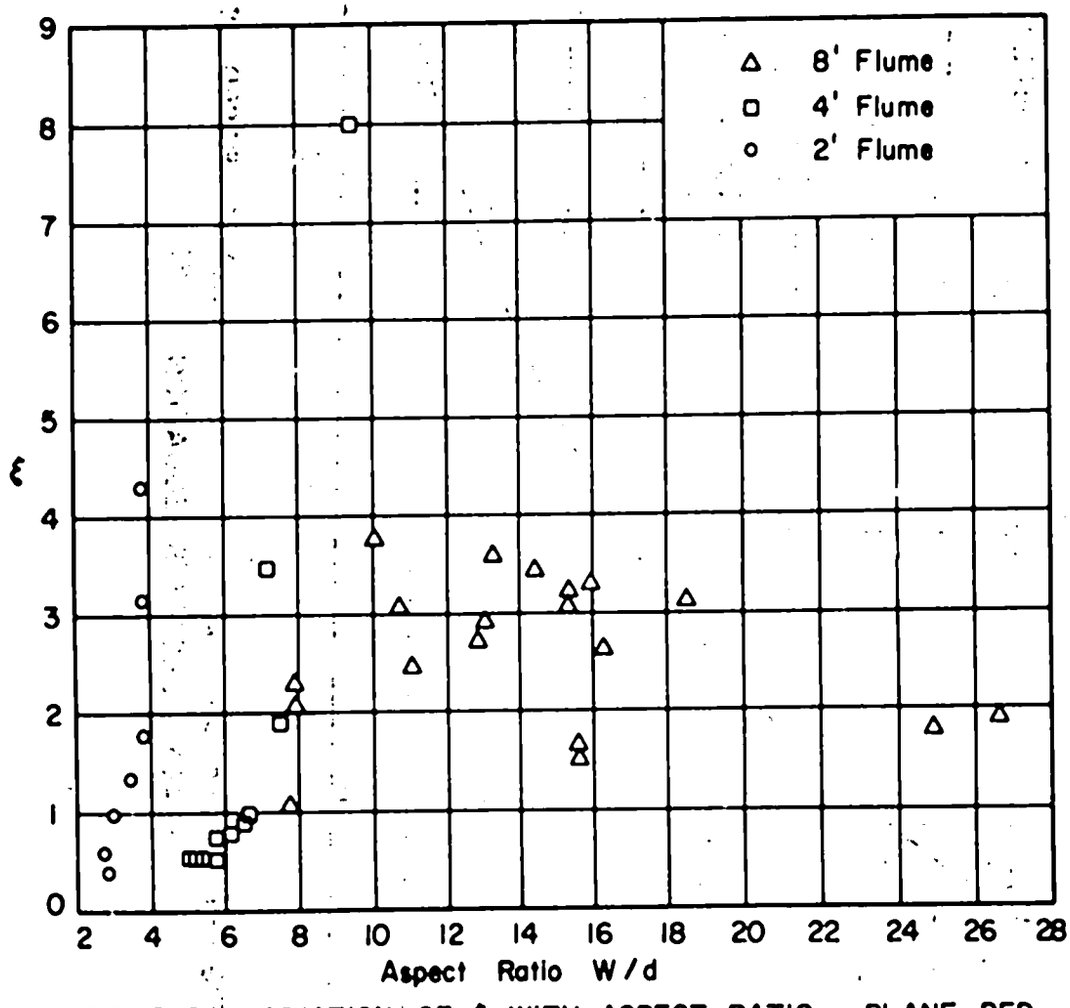

FIG. 7-2, VARIATION OF ξ WITH ASPECT RATIO — PLANE BED RUNS, WITHOUT WALL CORRECTION ($k_s = D_{84}$)

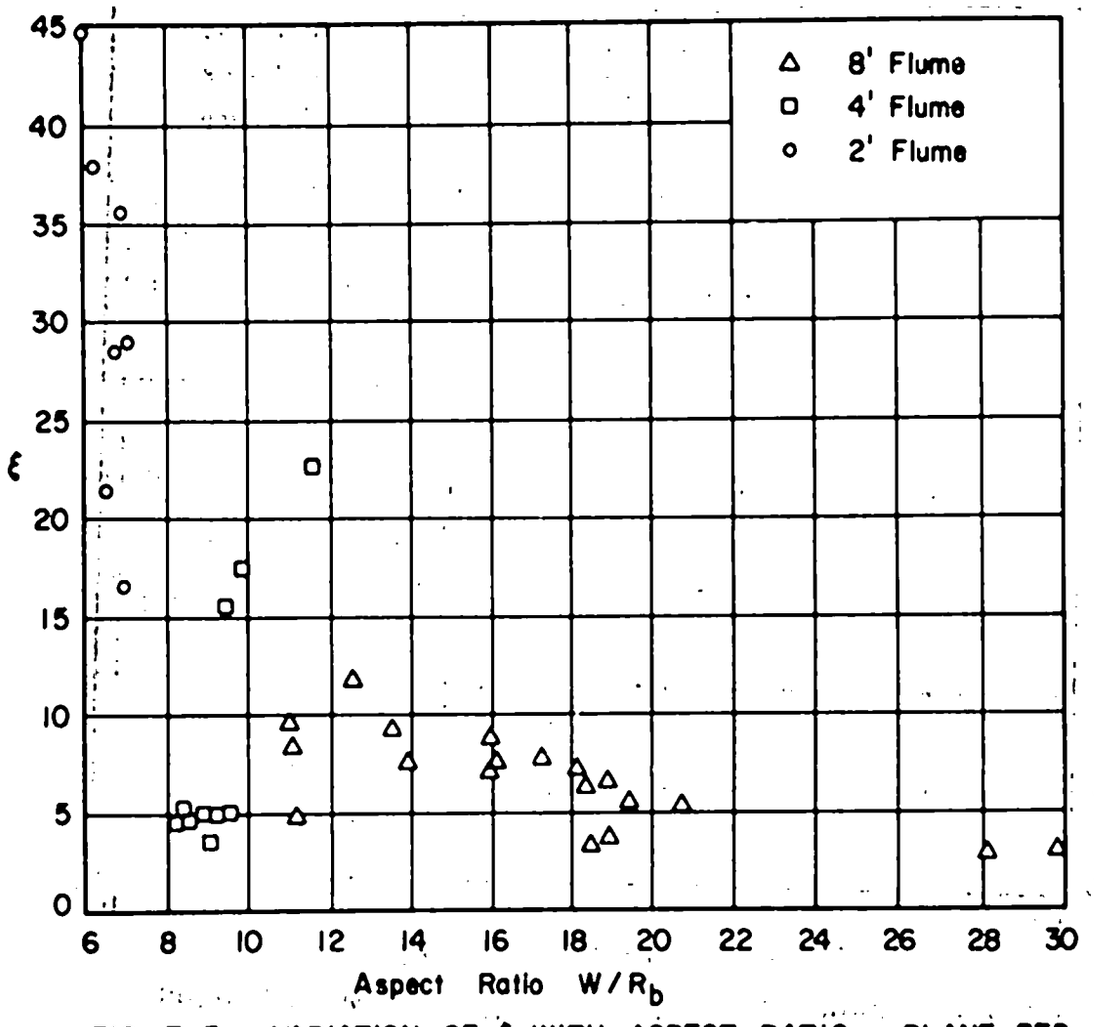

FIG. 7-3, VARIATION OF ξ WITH ASPECT RATIO — PLANE BED RUNS WITH WALL CORRECTION (BASED ON TRACY-LESTER SMOOTH FLUME EQUATION) [$ks = D_{84}$]

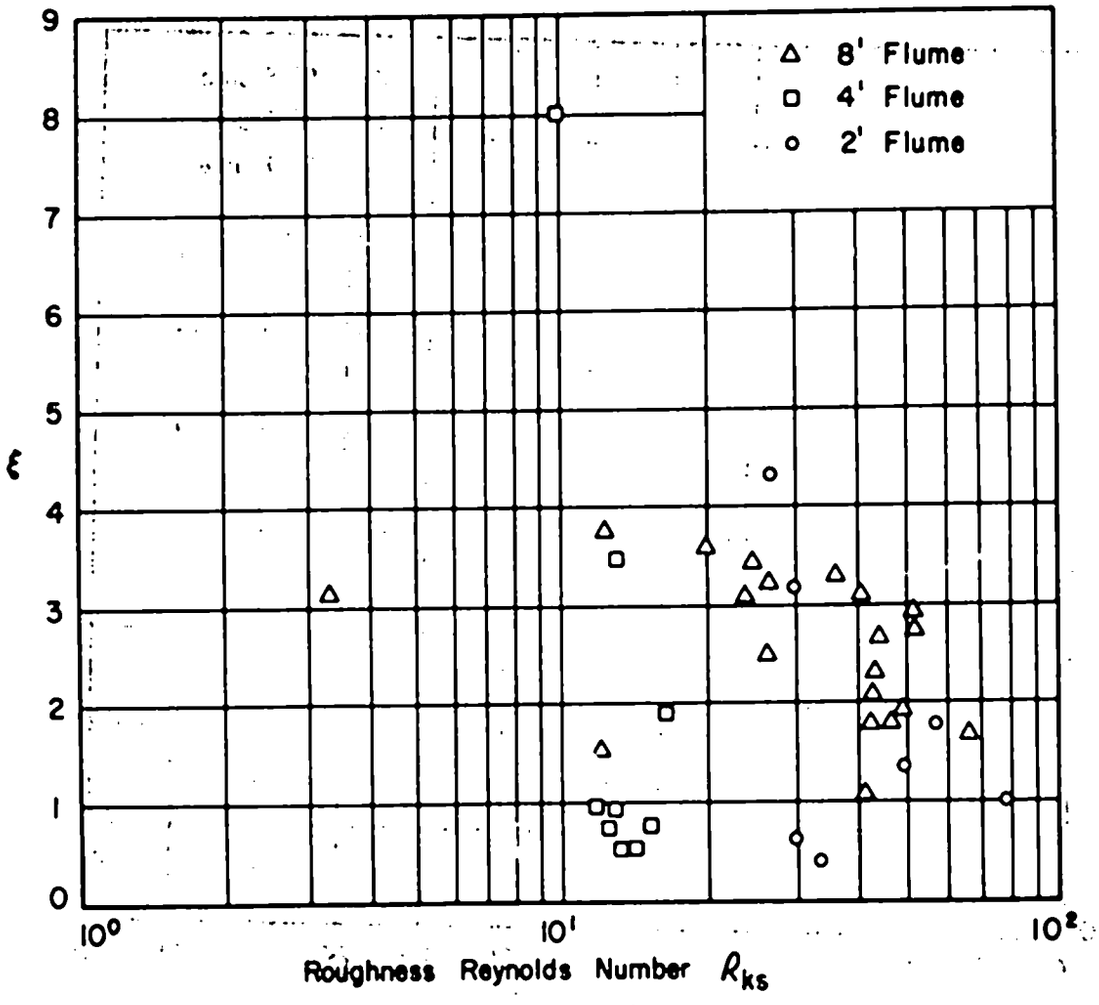

FIG. 7-4, VARIATION OF ξ WITH R_{ks} — PLANE BED RUNS WITHOUT WALL CORRECTION ($ks = D_{84}$)

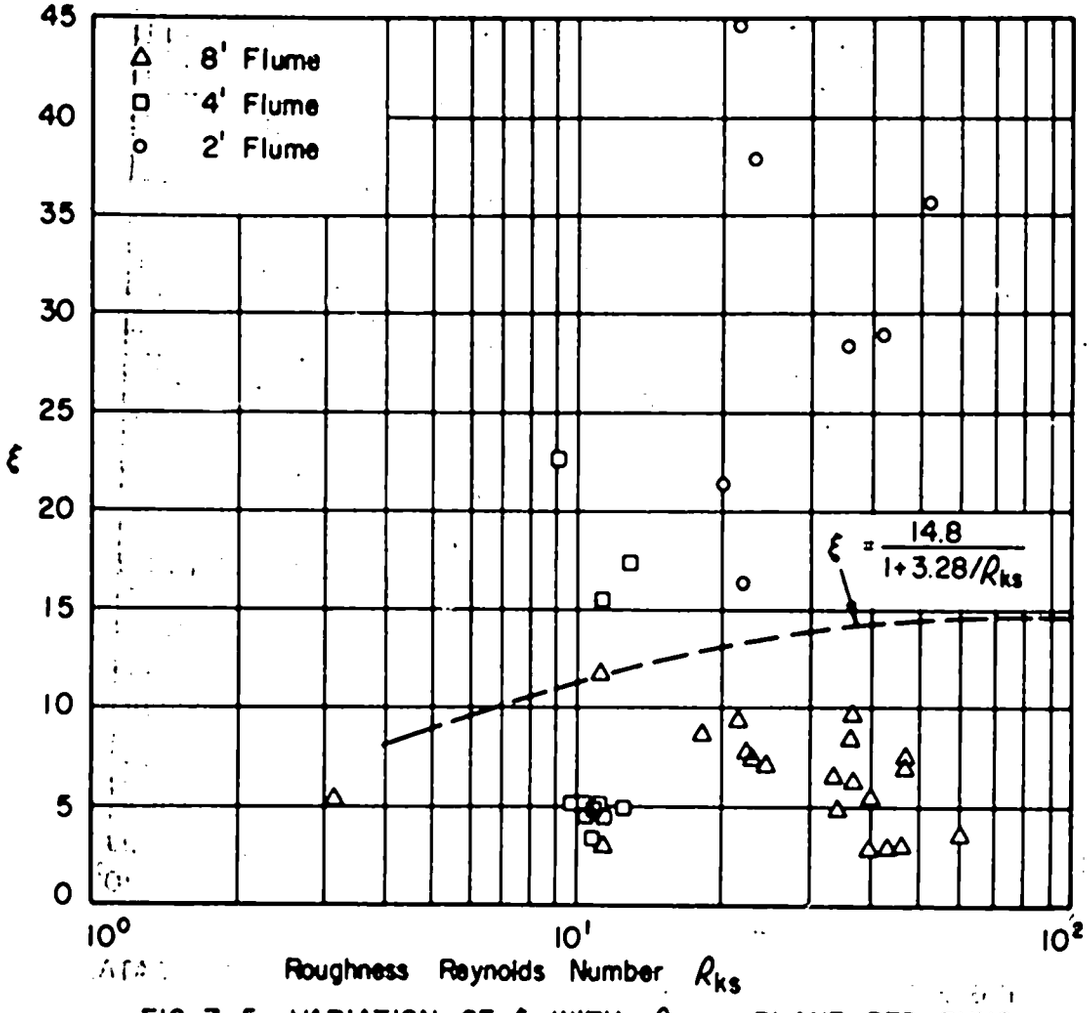

FIG. 7-5, VARIATION OF ξ WITH R_{ks} – PLANE BED RUNS WITH WALL CORRECTION (BASED ON TRACY-LESTER SMOOTH FLUME EQUATION) [$k_s = D_{84}$]

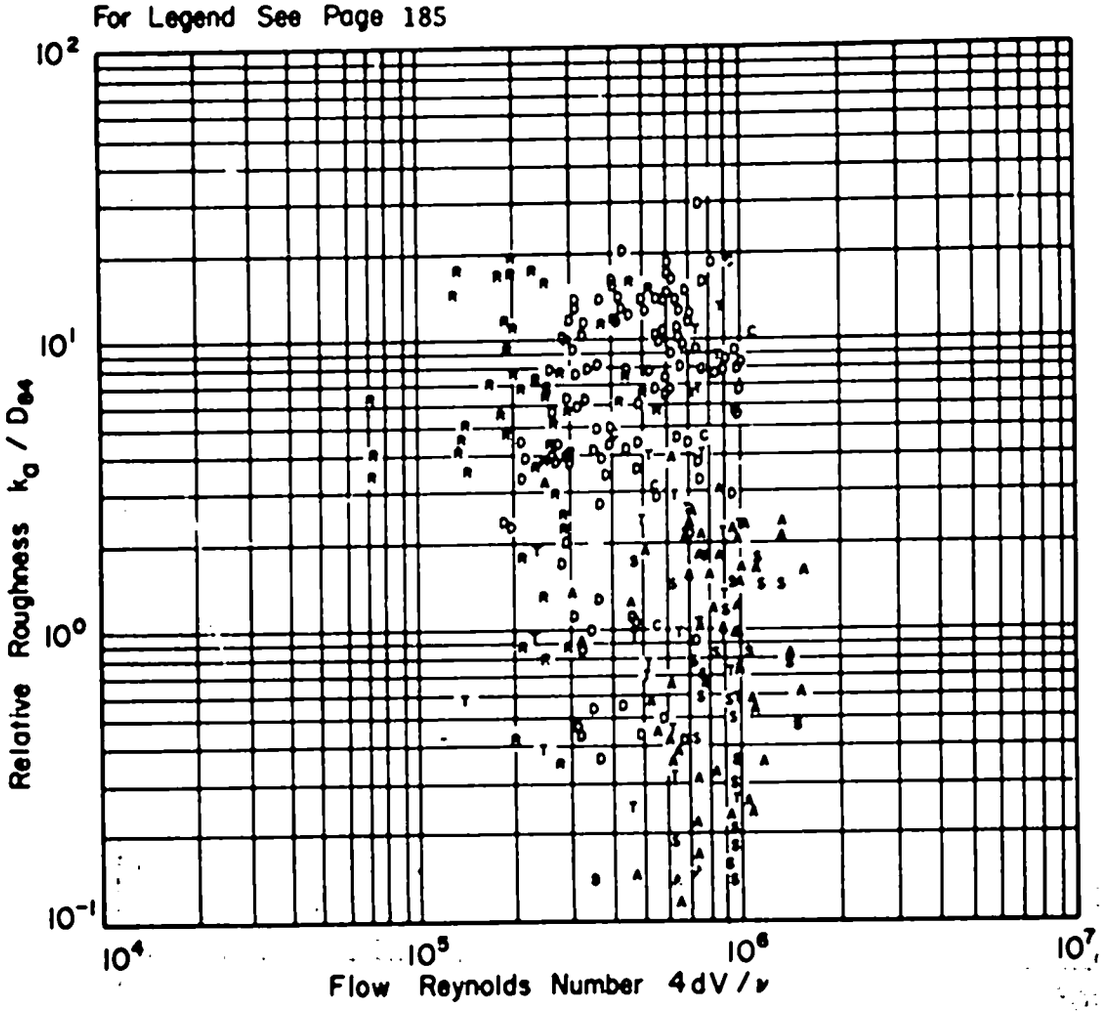

FIG. 8-1 VARIATION OF TOTAL ROUGHNESS IN FLUME DATA.

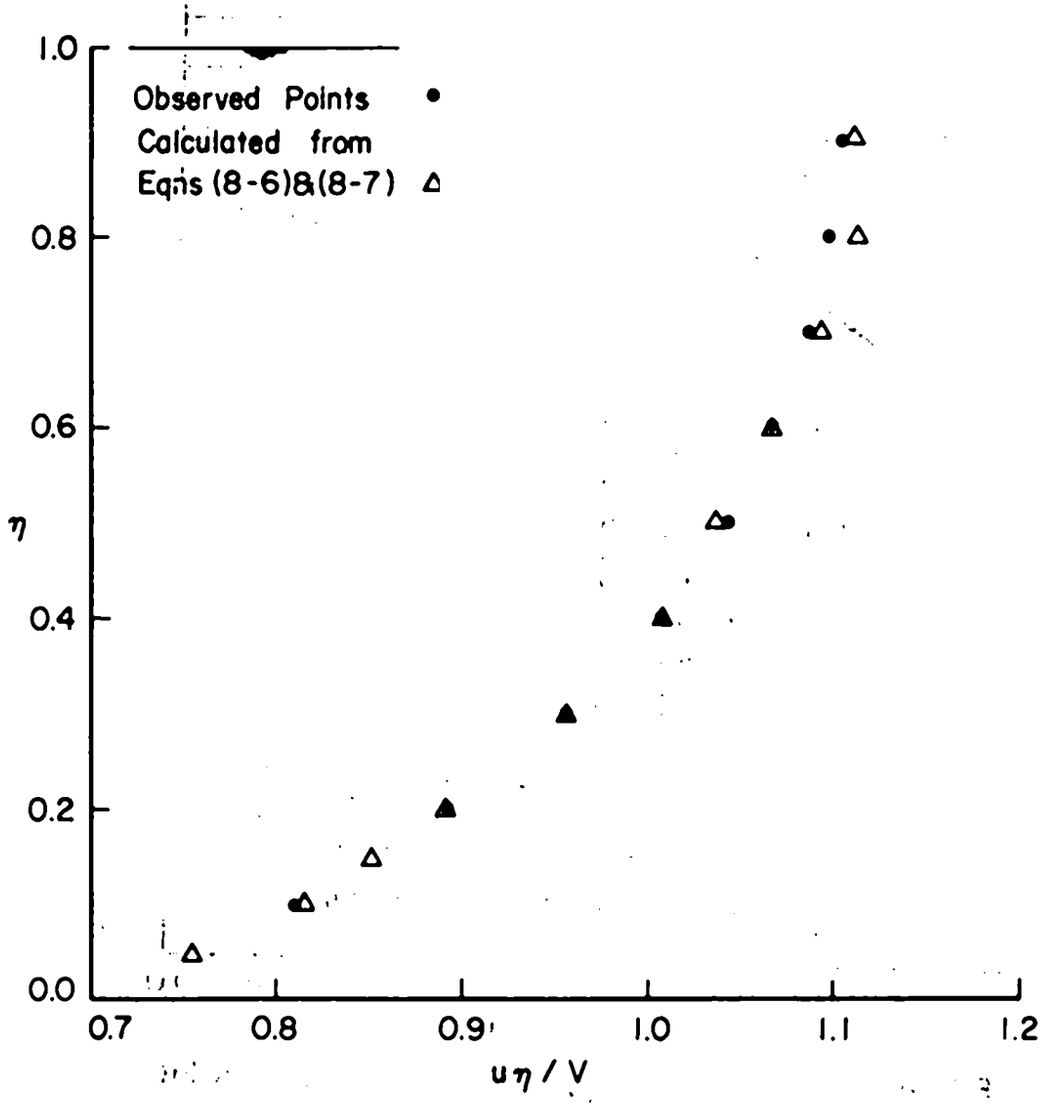

FIG. 8-2 COMPARISON OF AVERAGE VELOCITY PROFILE FOR ATCHAFLAYA RIVER AT SIMMESPORT FROM 500 OBSERVATIONS (TOFFALETI, 1963) AND FROM EQNS. (8-6) & (8-7).

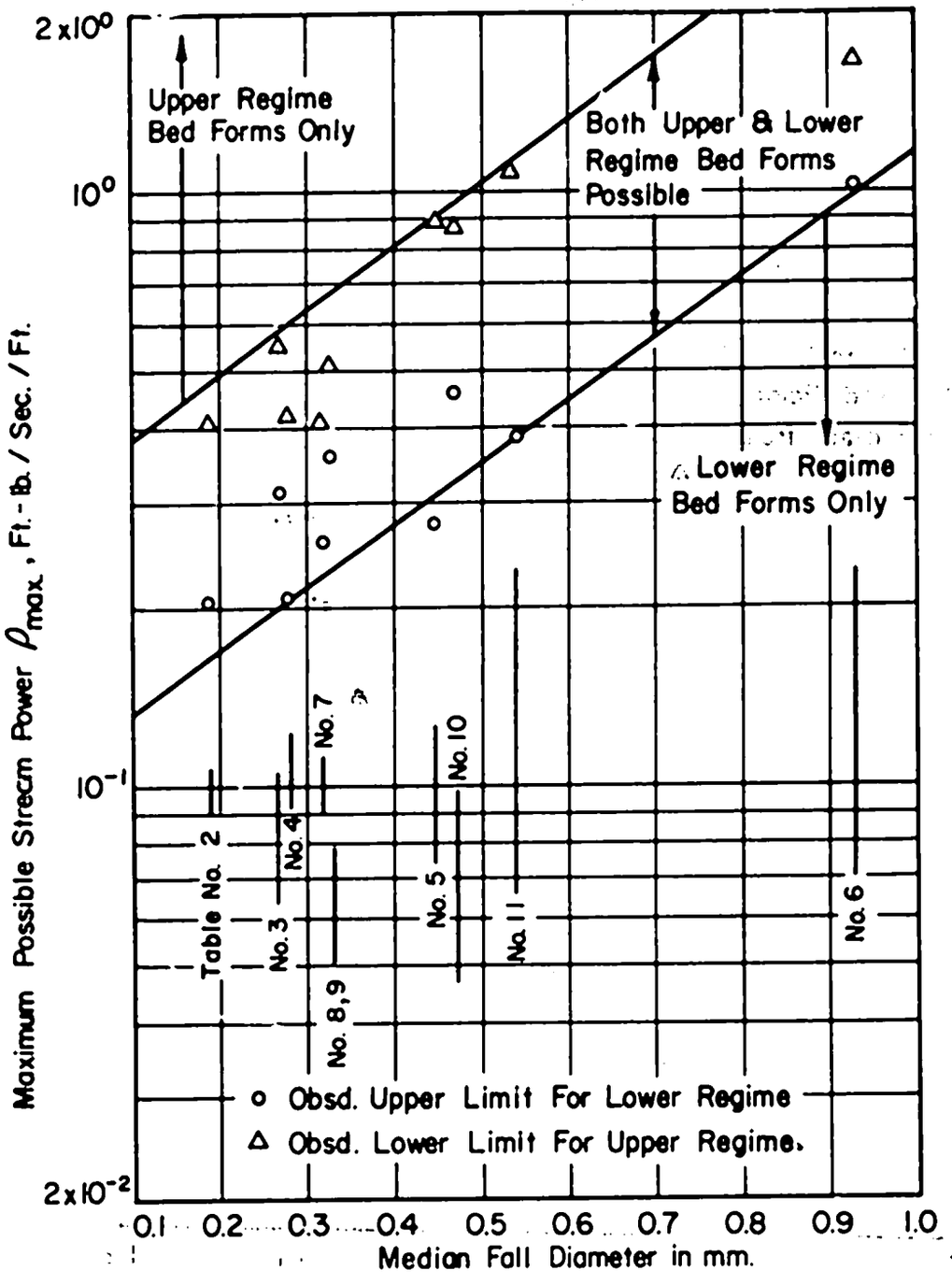

FIG. 8-3 LIMITS OF $\rho_{max.}$ FOR UPPER AND LOWER REGIME BED FORMS (FLUME DATA)

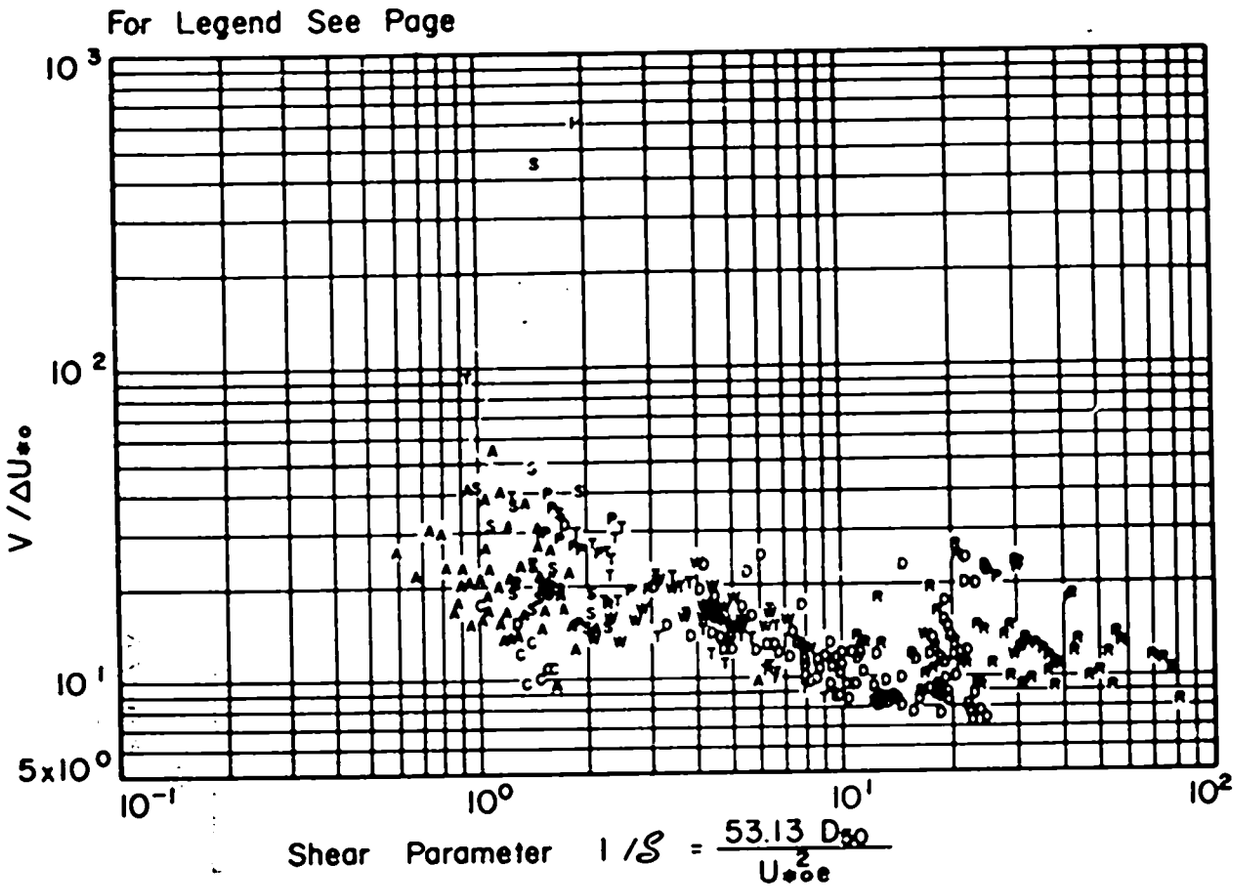

FIG. 8-4 $V/\Delta U_{*o}$ VERSUS SHEAR PARAMETER $1/S$ FOR THE FLUME AND WEST PAKISTAN CANALS DATA.

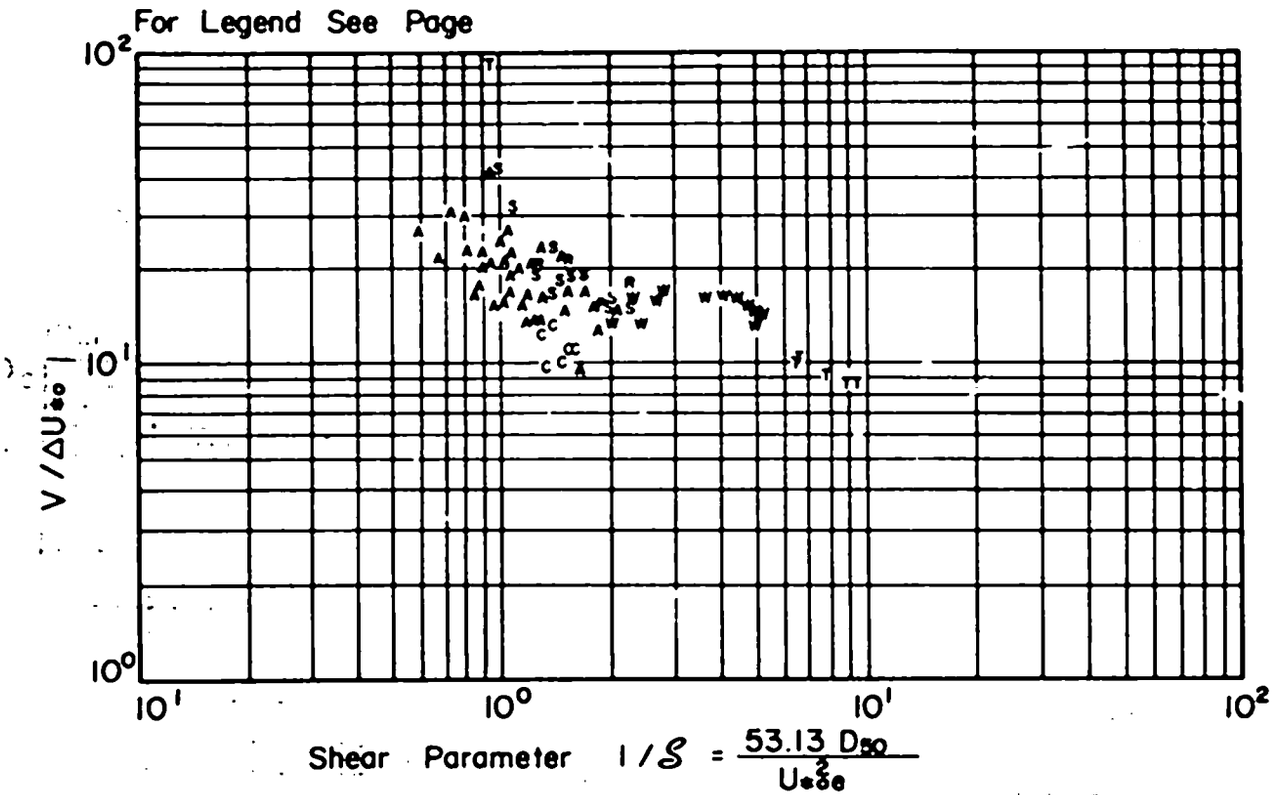

FIG. 8-5 SEPARATION OF FLOW REGIME – UPPER RANGE POINTS.

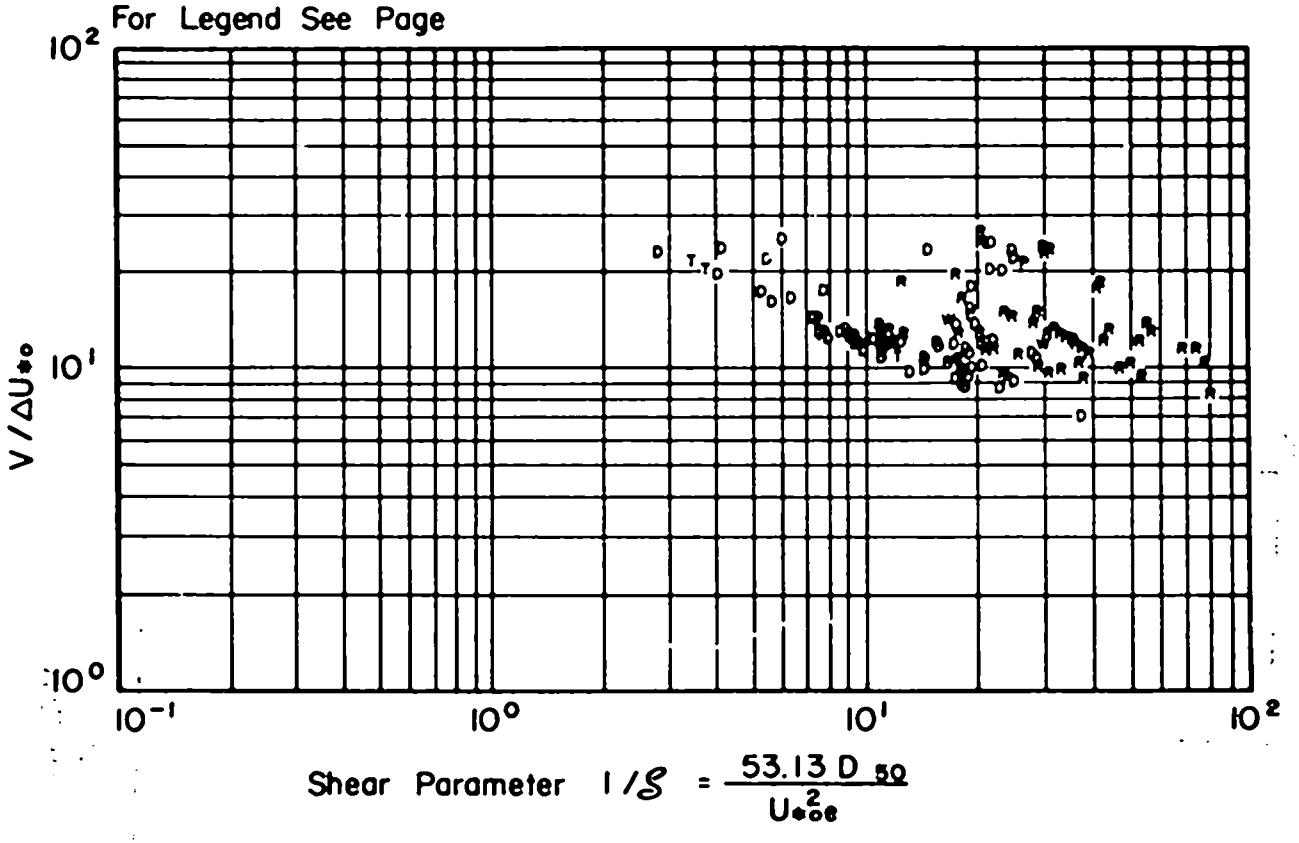

FIG. 8-6 SEPARATION OF FLOW REGIME – LOWER RANGE POINTS.

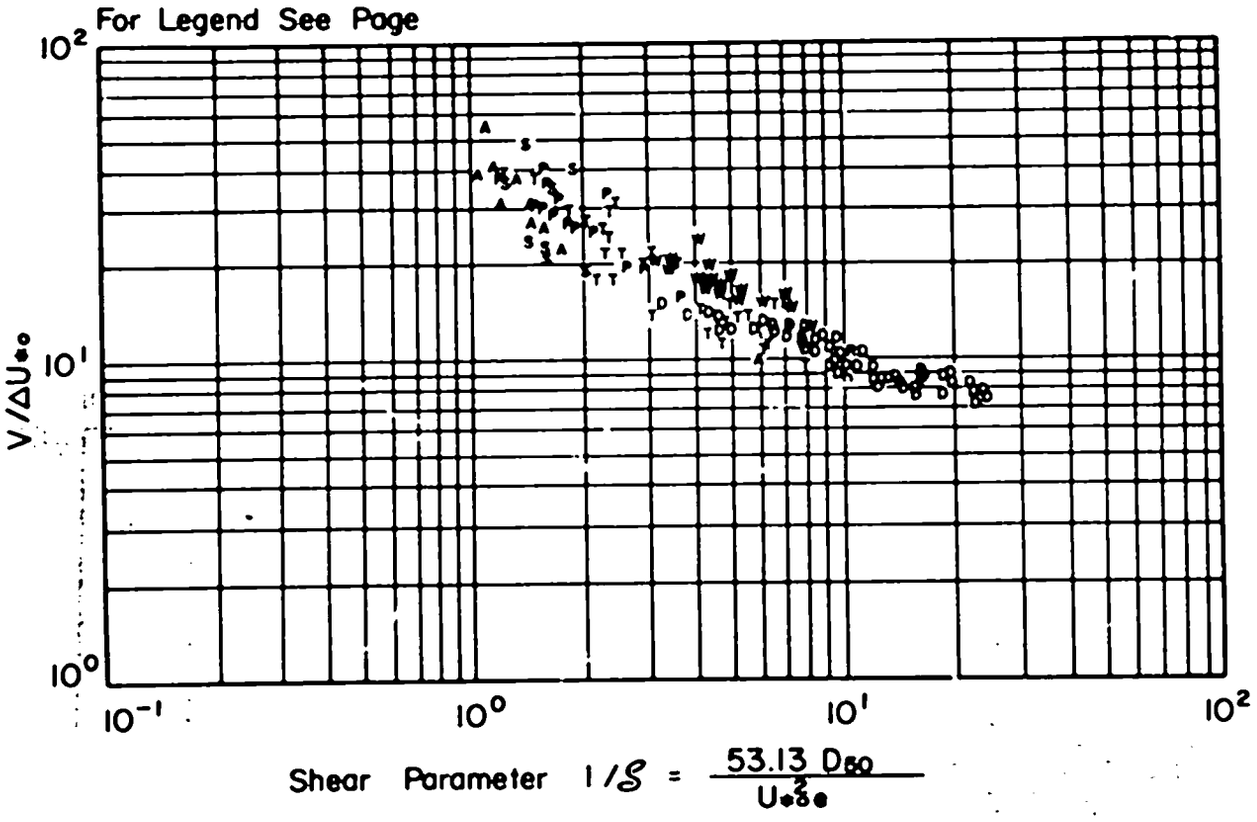

FIG. 8-7 SEPARATION OF FLOW REGIME – INTERMEDIATE RANGE POINTS.

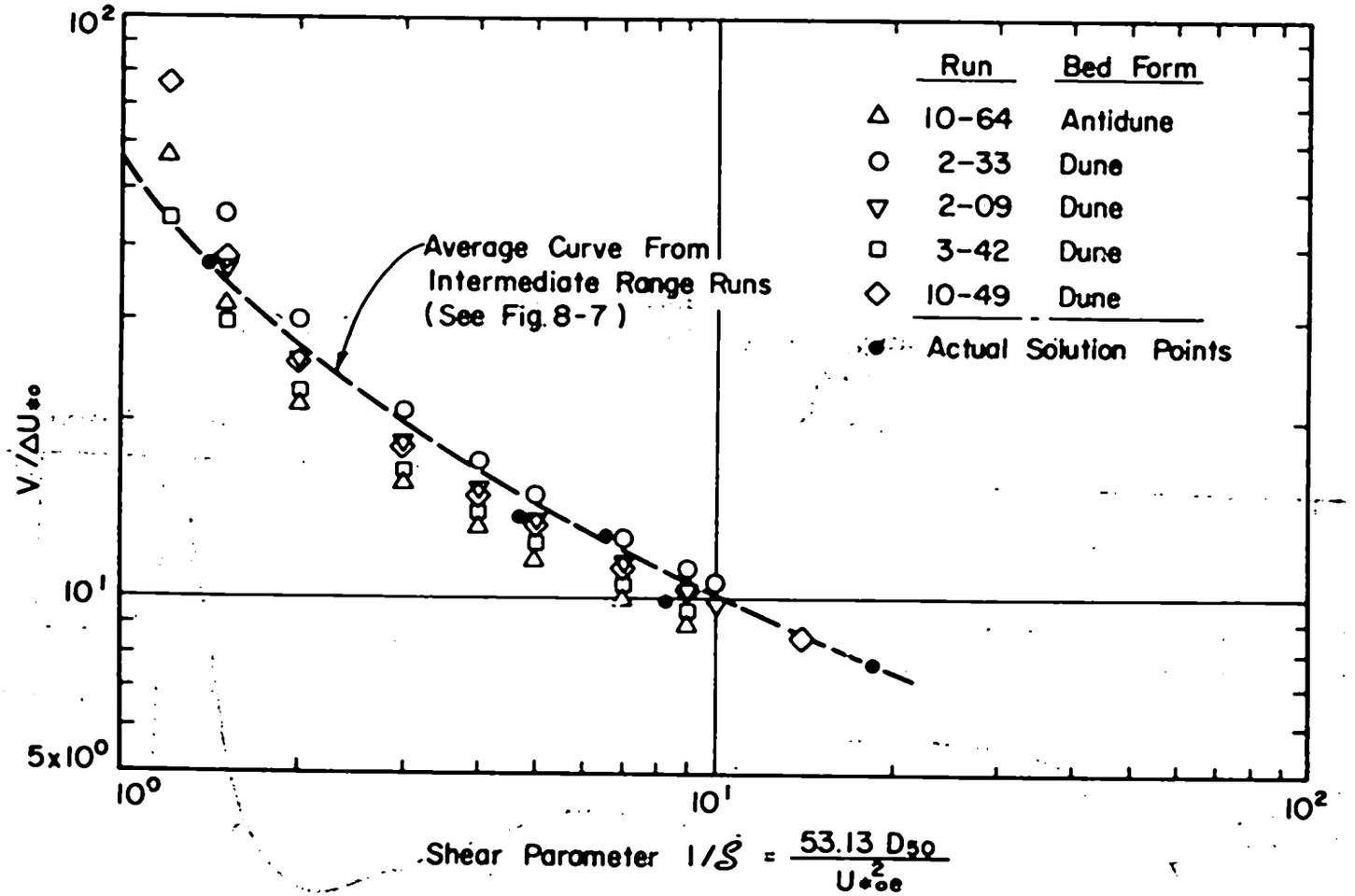

FIG. 8-8 LOCI OF SOLUTION POINTS IN INTERMEDIATE RANGE.

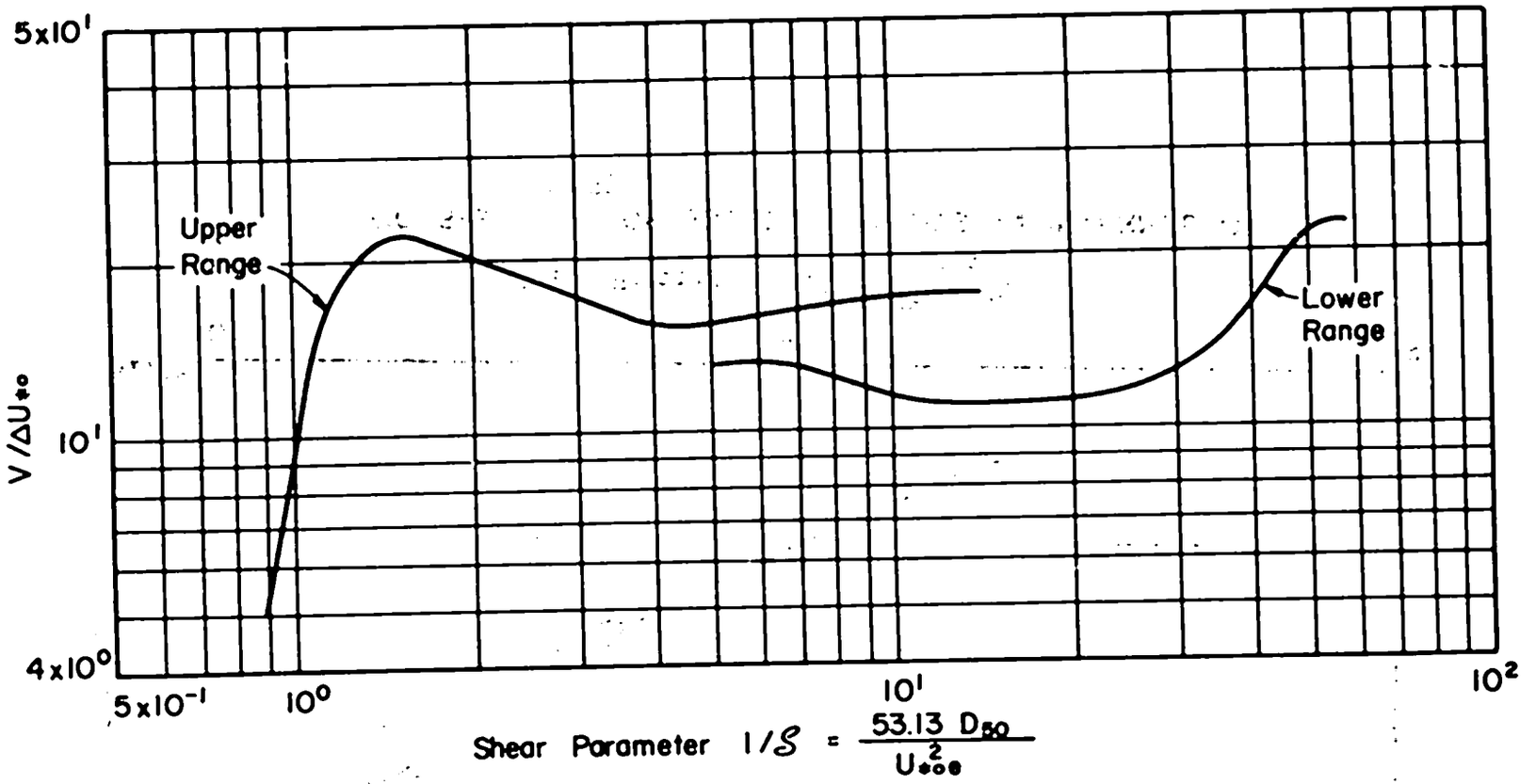

FIG. 8-9 RESISTANCE CURVES FOR UPPER AND LOWER $\rho_{max.}$ — D_{50} RANGE

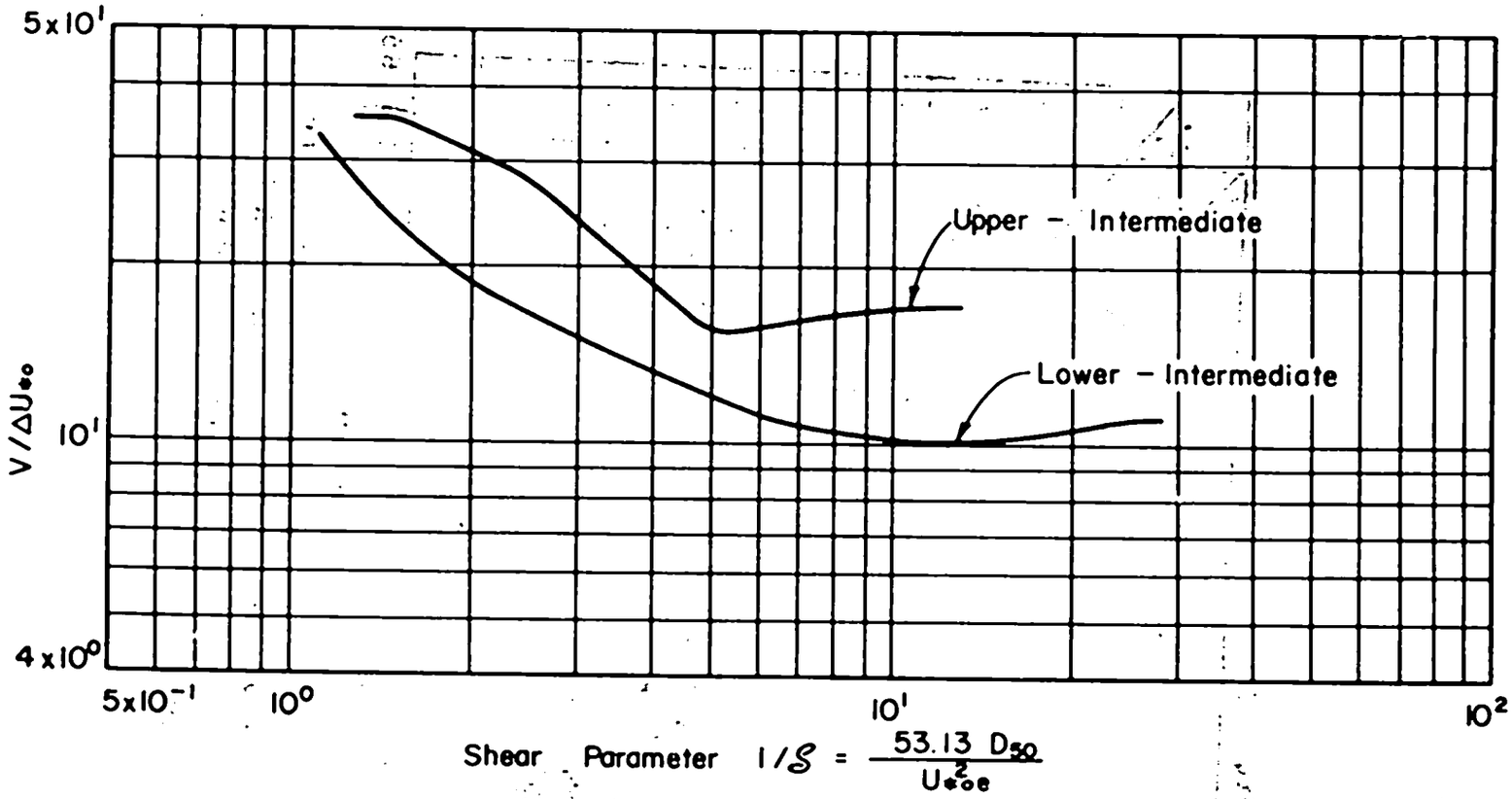

FIG. 8-10 RESISTANCE CURVES FOR INTERMEDIATE $\rho_{max.}$ - D_{50} RANGE.

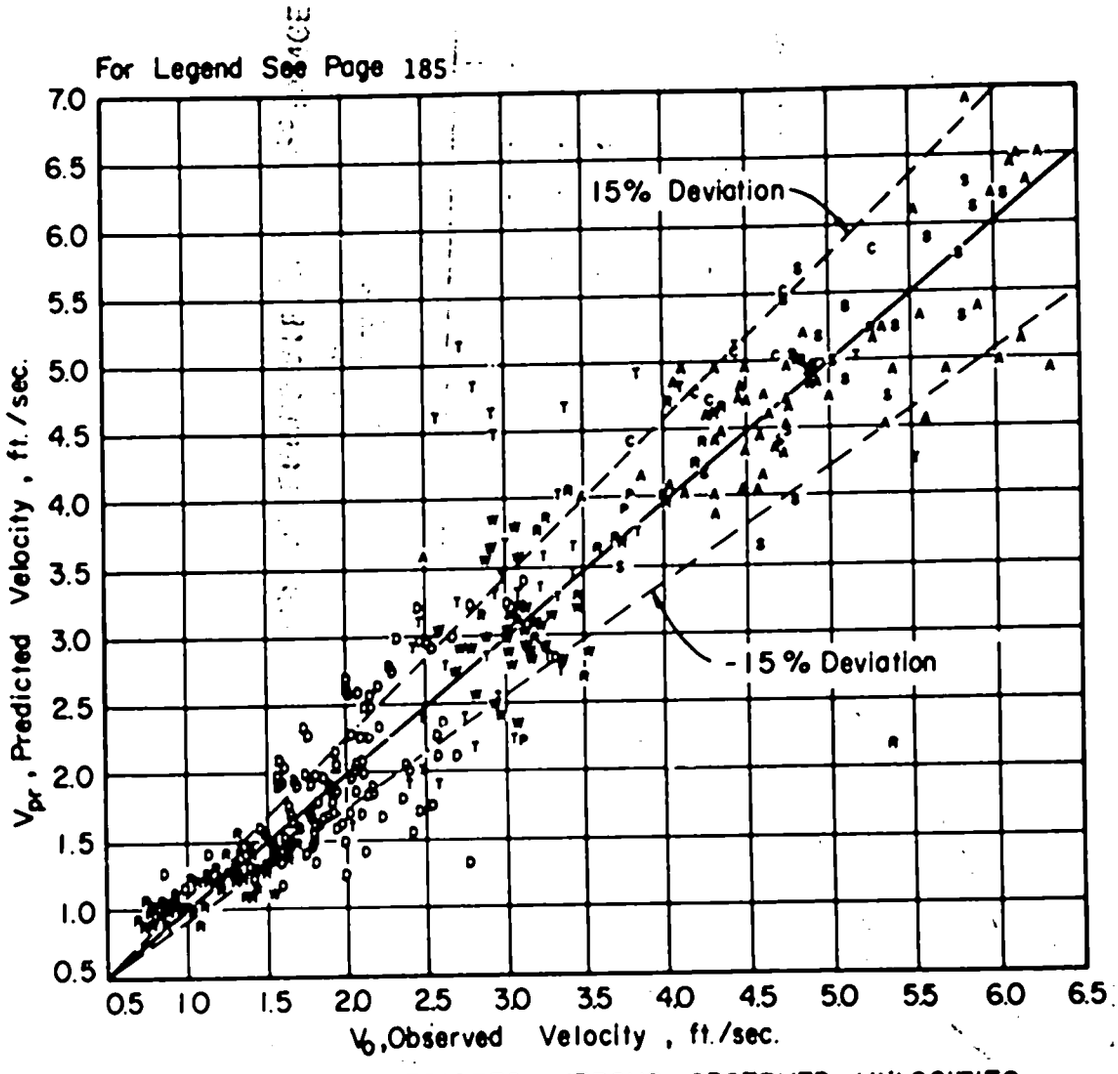

FIG. 8-11 PREDICTED VERSUS OBSERVED VELOCITIES FOR ANALYSIS BASED ON RESISTANCE CURVES (FLUME, BARTON-LIN AND WEST PAKISTAN CANALS DATA).

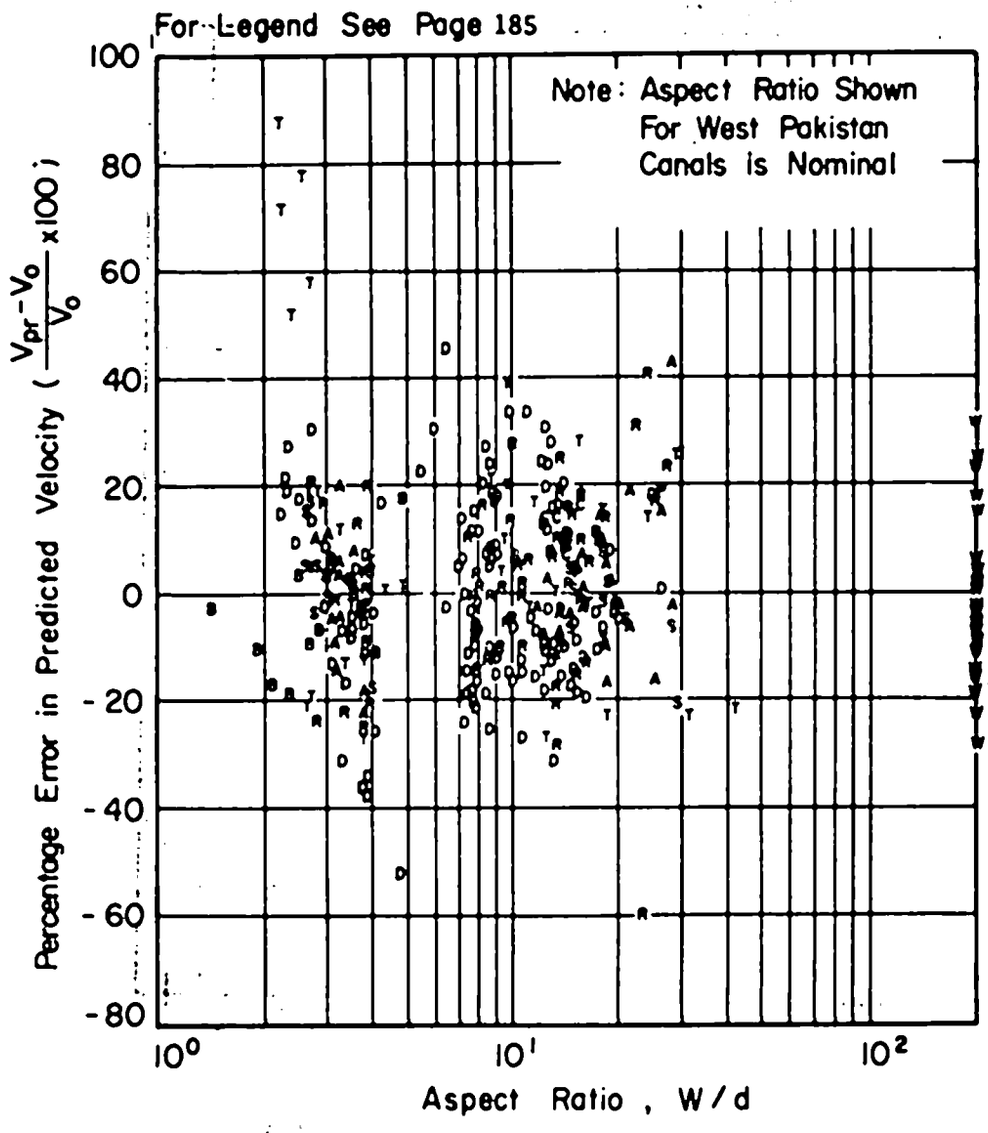

FIG. 8-12 PERCENTAGE ERROR IN PREDICTED VELOCITY VERSUS ASPECT RATIO OF SECTION (FLUME, BARTON-LIN AND WEST PAKISTAN CANALS DATA).

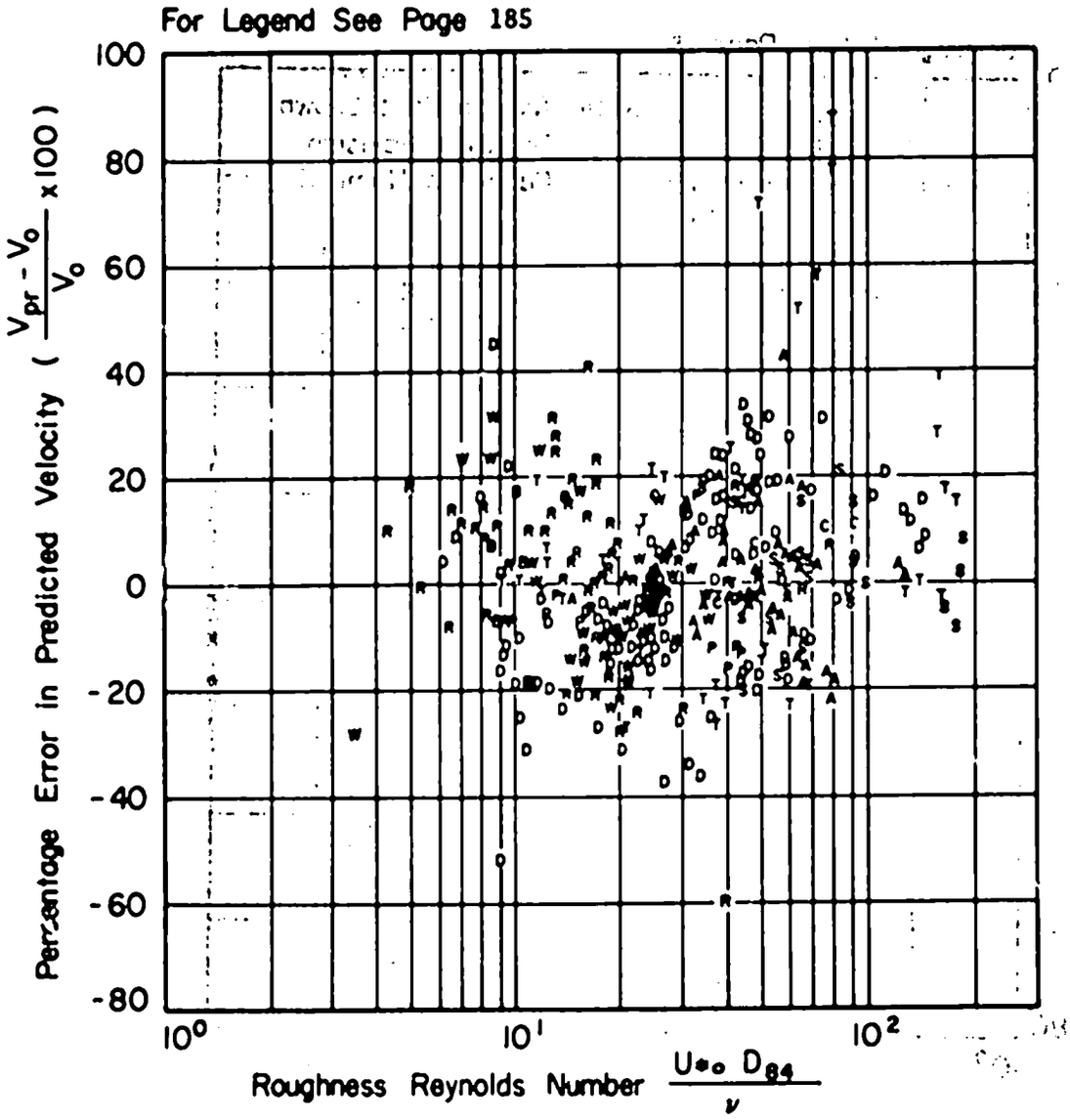

FIG. 8-13 PERCENTAGE ERROR IN PREDICTED VELOCITY VERSUS ROUGHNESS REYNOLDS NUMBER (FLUME, BARTON-LIN AND WEST PAKISTAN CANALS DATA).

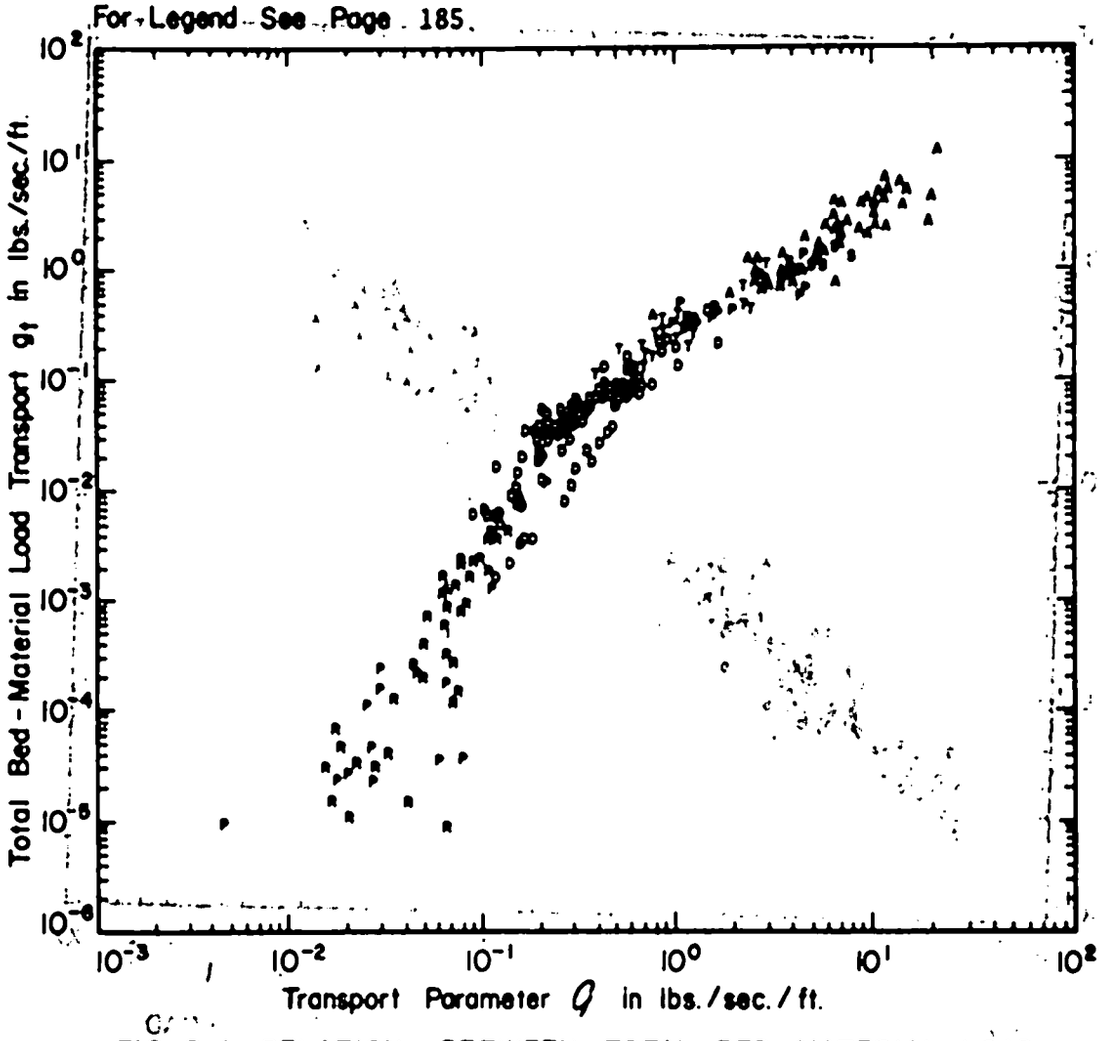

FIG. 9-1. RELATION BETWEEN TOTAL BED-MATERIAL LOAD TRANSPORT AND TRANSPORT PARAMETER Q FOR FLUME RUNS. (315 RUNS)

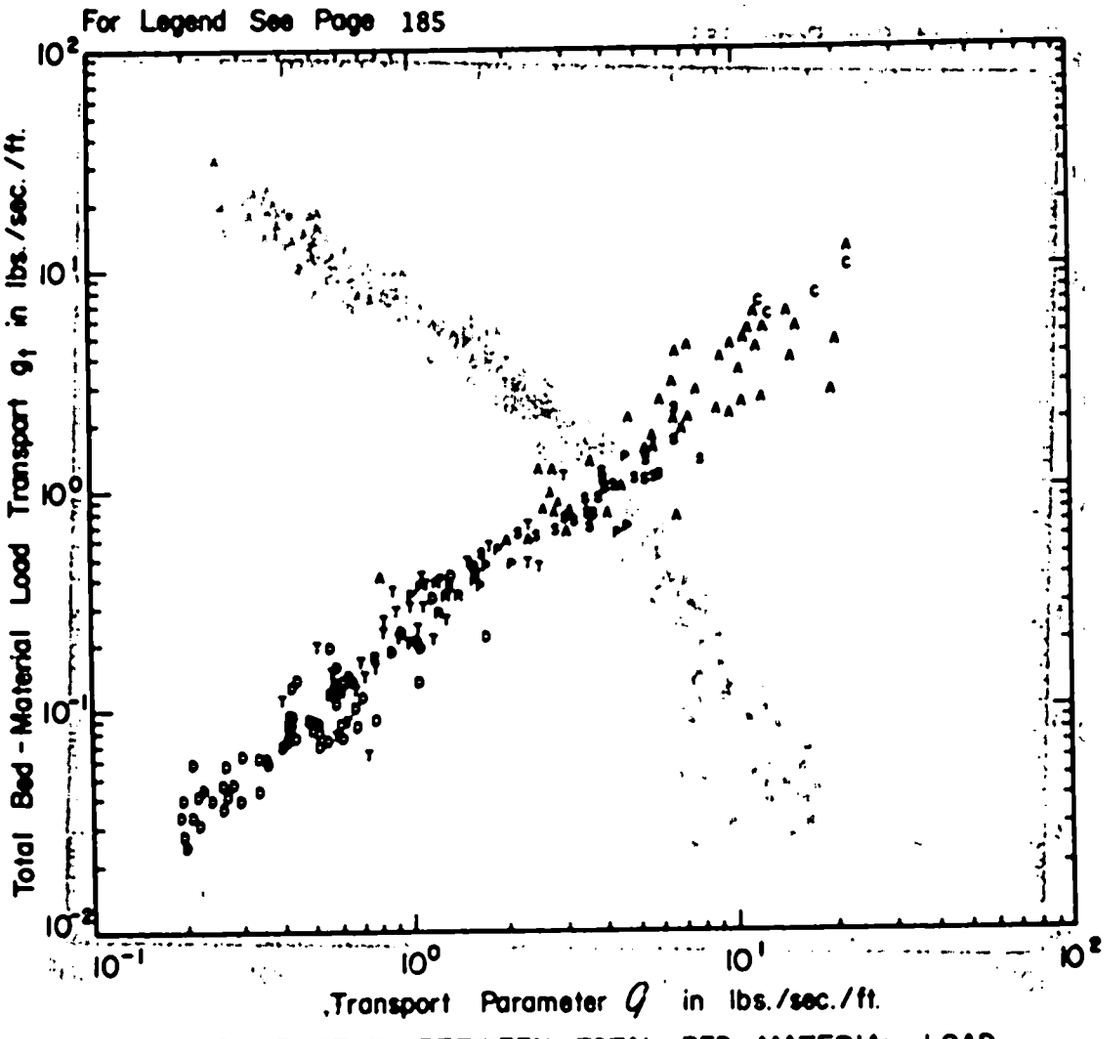

FIG. 9-2. RELATION BETWEEN TOTAL BED-MATERIAL LOAD TRANSPORT AND TRANSPORT PARAMETER Q FOR UPPER AND MIDDLE RANGE FLUME RUNS. (203 RUNS)

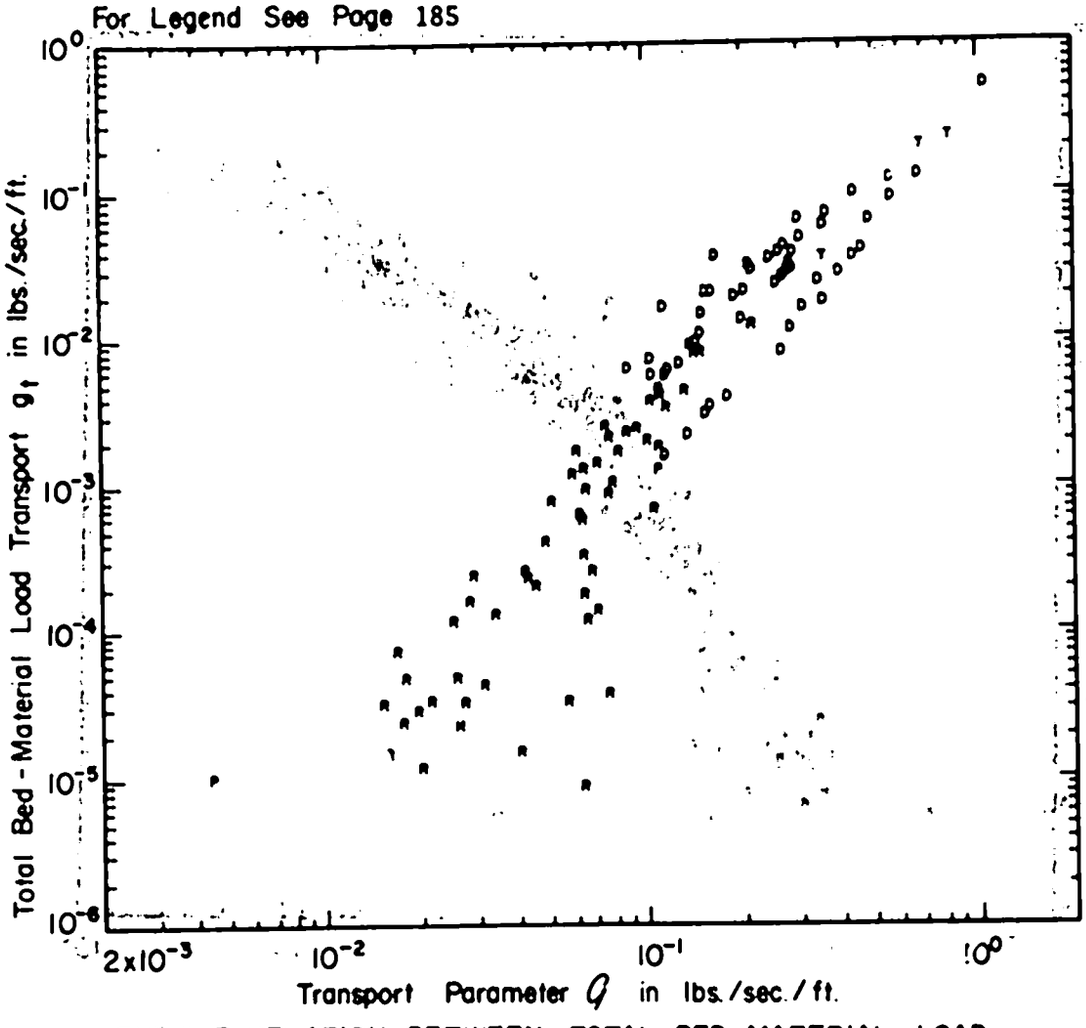

FIG. 9-3 RELATION BETWEEN TOTAL BED-MATERIAL LOAD TRANSPORT AND TRANSPORT PARAMETER Q FOR LOWER RANGE FLUME RUNS. (112 RUNS)

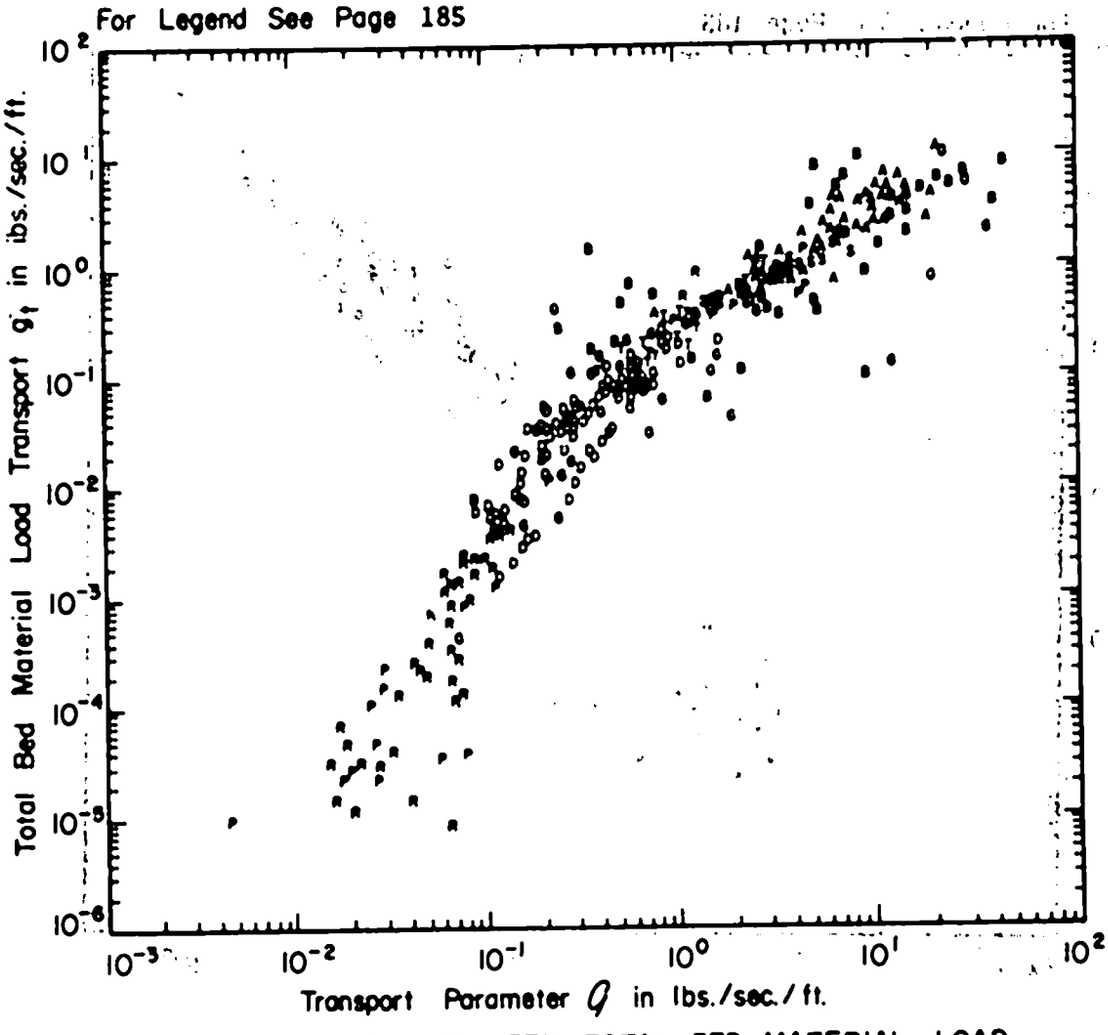

FIG. 9-4 RELATION BETWEEN TOTAL BED-MATERIAL LOAD TRANSPORT AND TRANSPORT PARAMETER Q FOR FLUME RUNS (315 RUNS) AND RIO GRANDE DATA 112 SECTIONS.

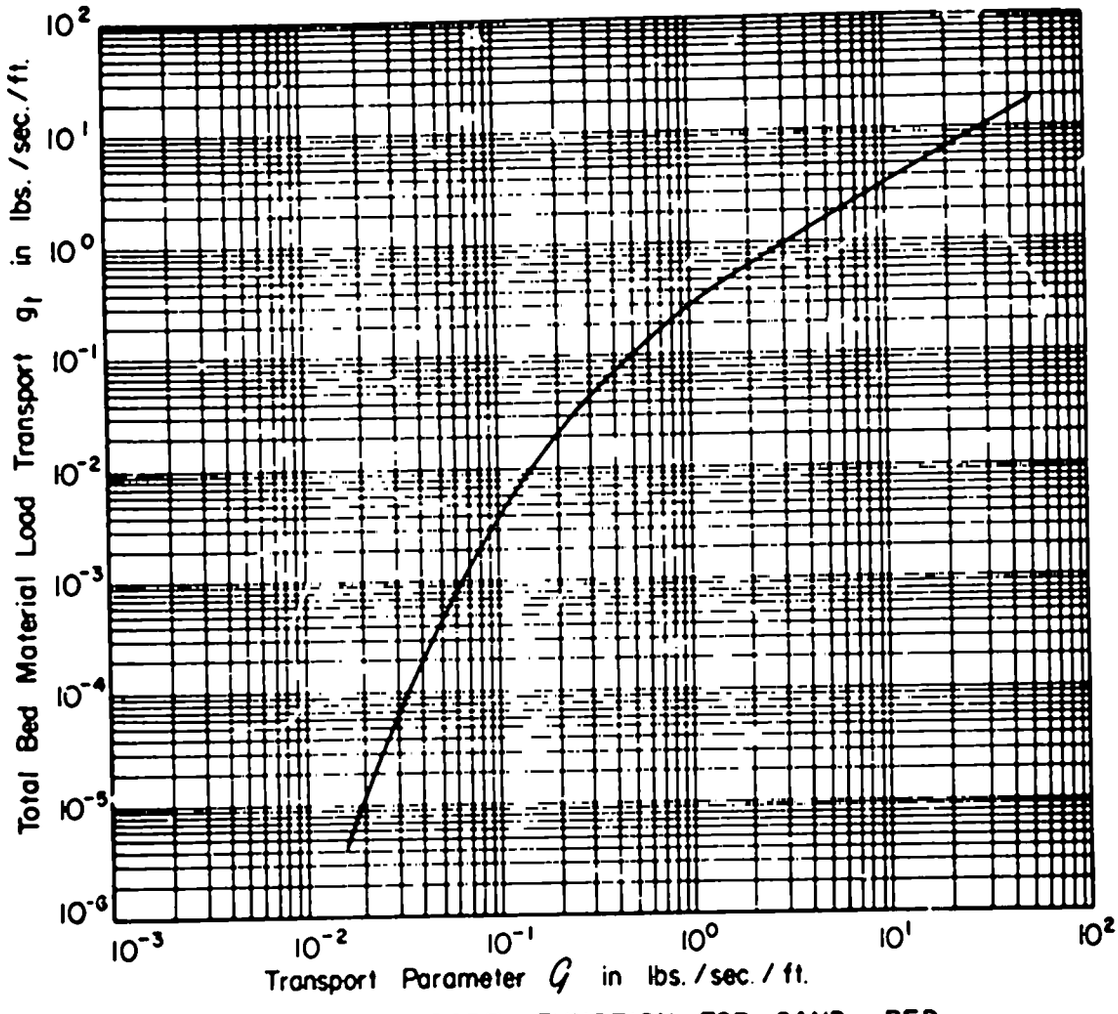

FIG. 9-5 TRANSPORT FUNCTION FOR SAND - BED CHANNELS.

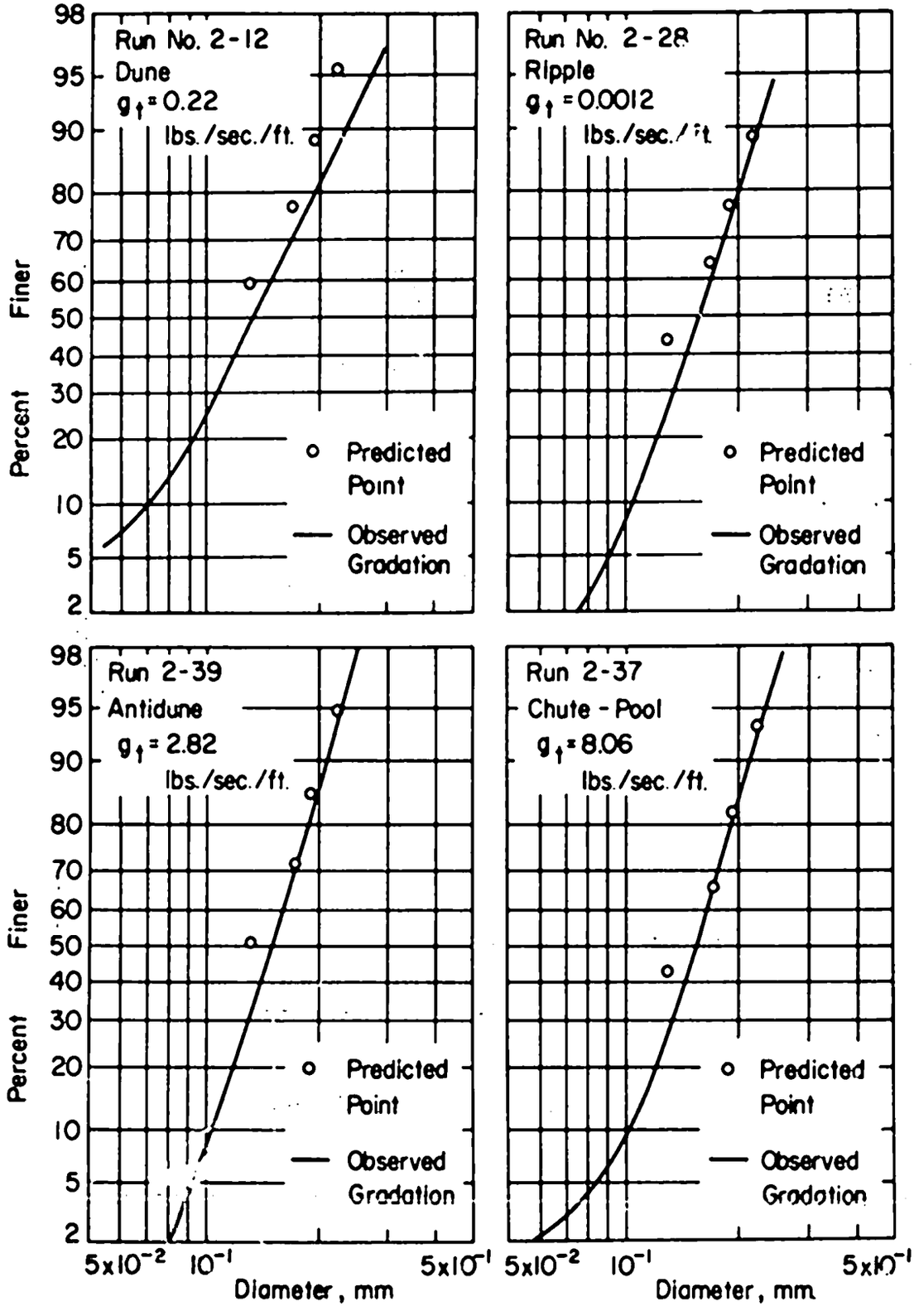

FIG. 9-6 COMPARISON OF OBSERVED AND PREDICTED GRADATION OF TOTAL BED-MATERIAL LOAD
(Bed Material D_{50}=0.19 mm., σ = 1.30)

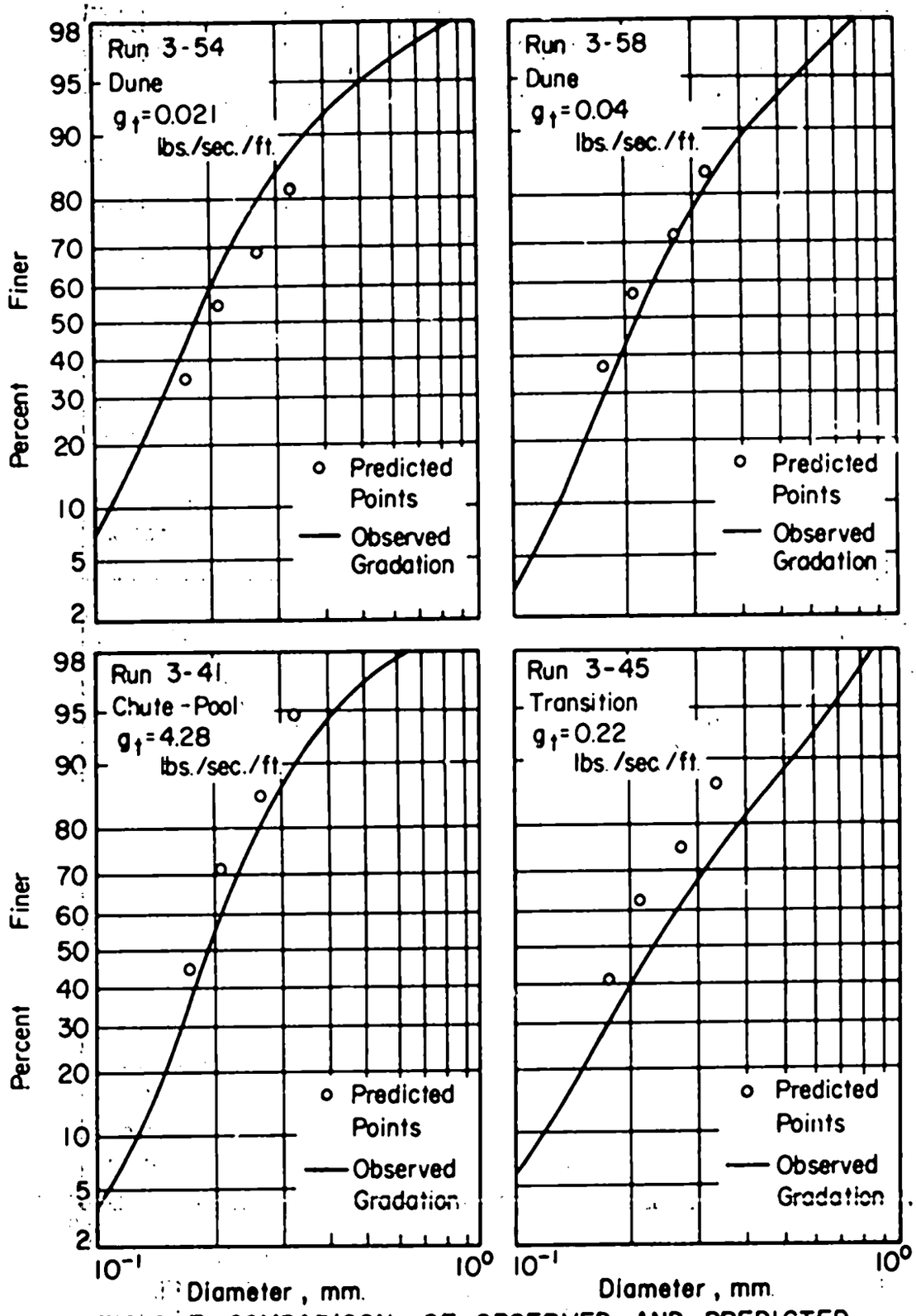

FIG. 9-7 COMPARISON OF OBSERVED AND PREDICTED GRADATION OF TOTAL BED-MATERIAL LOAD
(Bed Material D_{50}=0.27 mm., σ = 1.56)

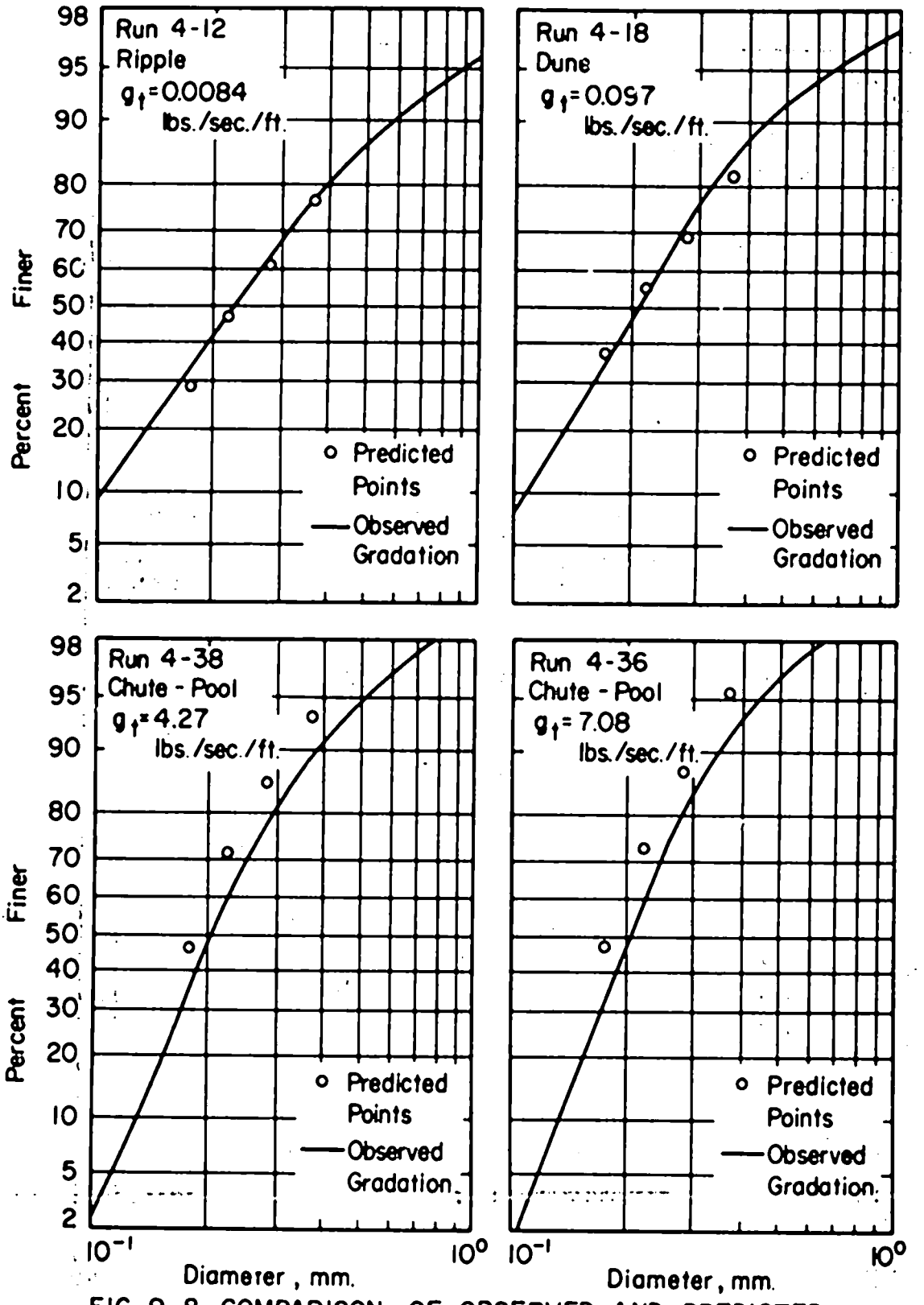

FIG. 9-8 COMPARISON OF OBSERVED AND PREDICTED GRADATION OF TOTAL BED-MATERIAL LOAD
(Bed Material D_{50} = 0.28 mm., σ = 1.67)

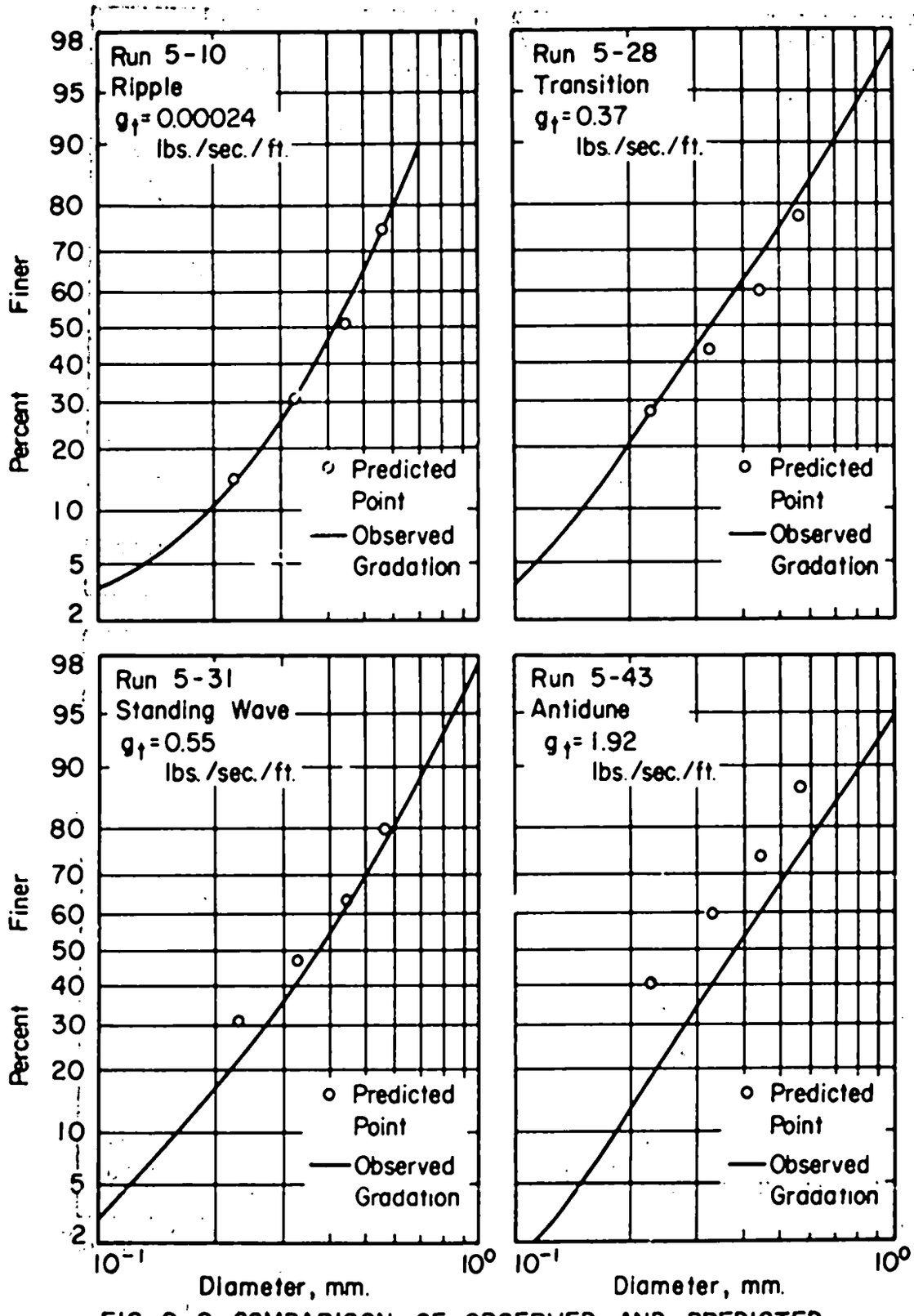

FIG. 9-9 COMPARISON OF OBSERVED AND PREDICTED GRADATION OF TOTAL BED-MATERIAL LOAD
(Bed Material D_{50} = 0.45 mm. , σ = 1.60)

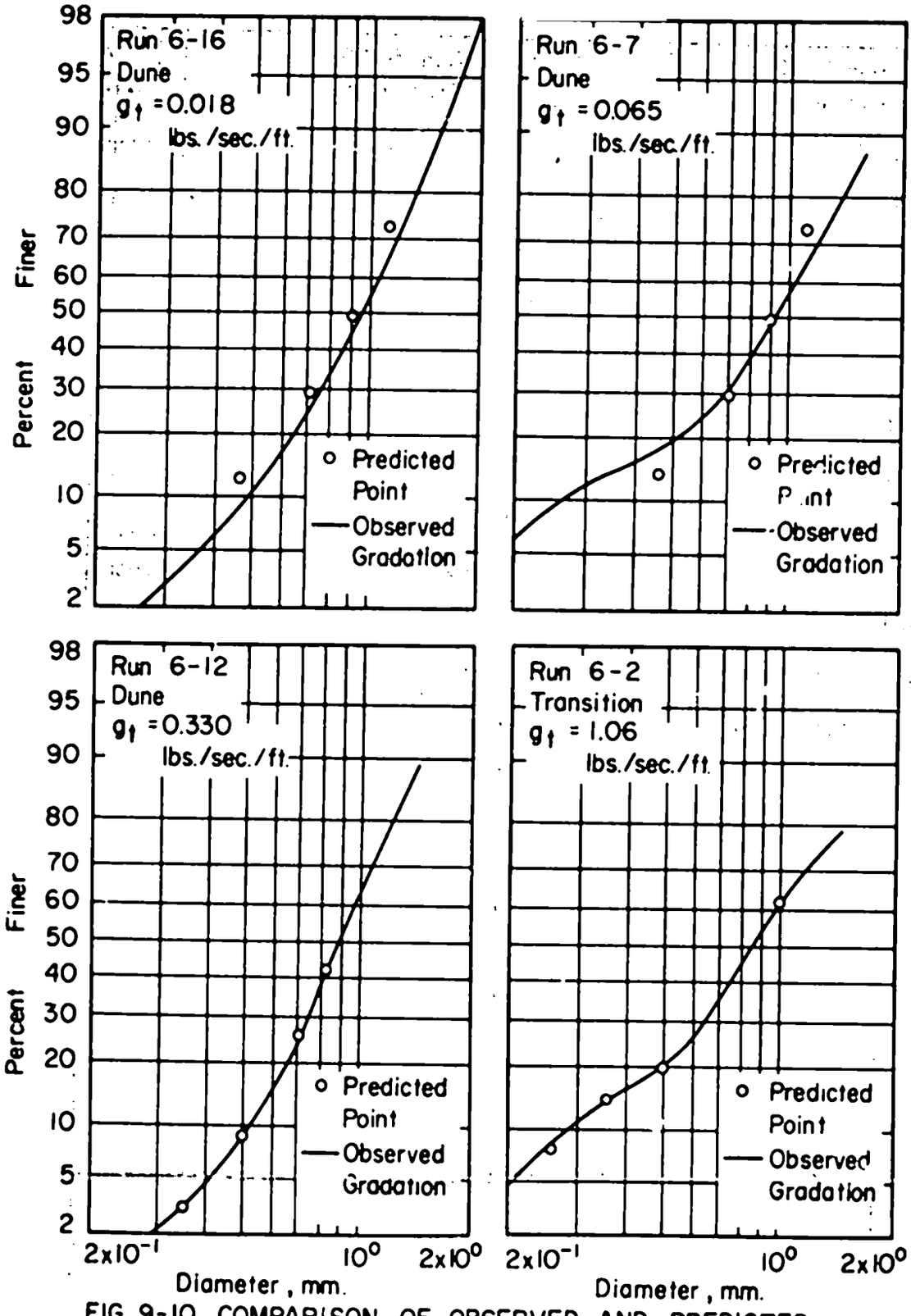

FIG. 9-10 COMPARISON OF OBSERVED AND PREDICTED GRADATION OF TOTAL BED-MATERIAL LOAD
(Bed Material D_{50} = 0.93 mm., σ = 1.54)

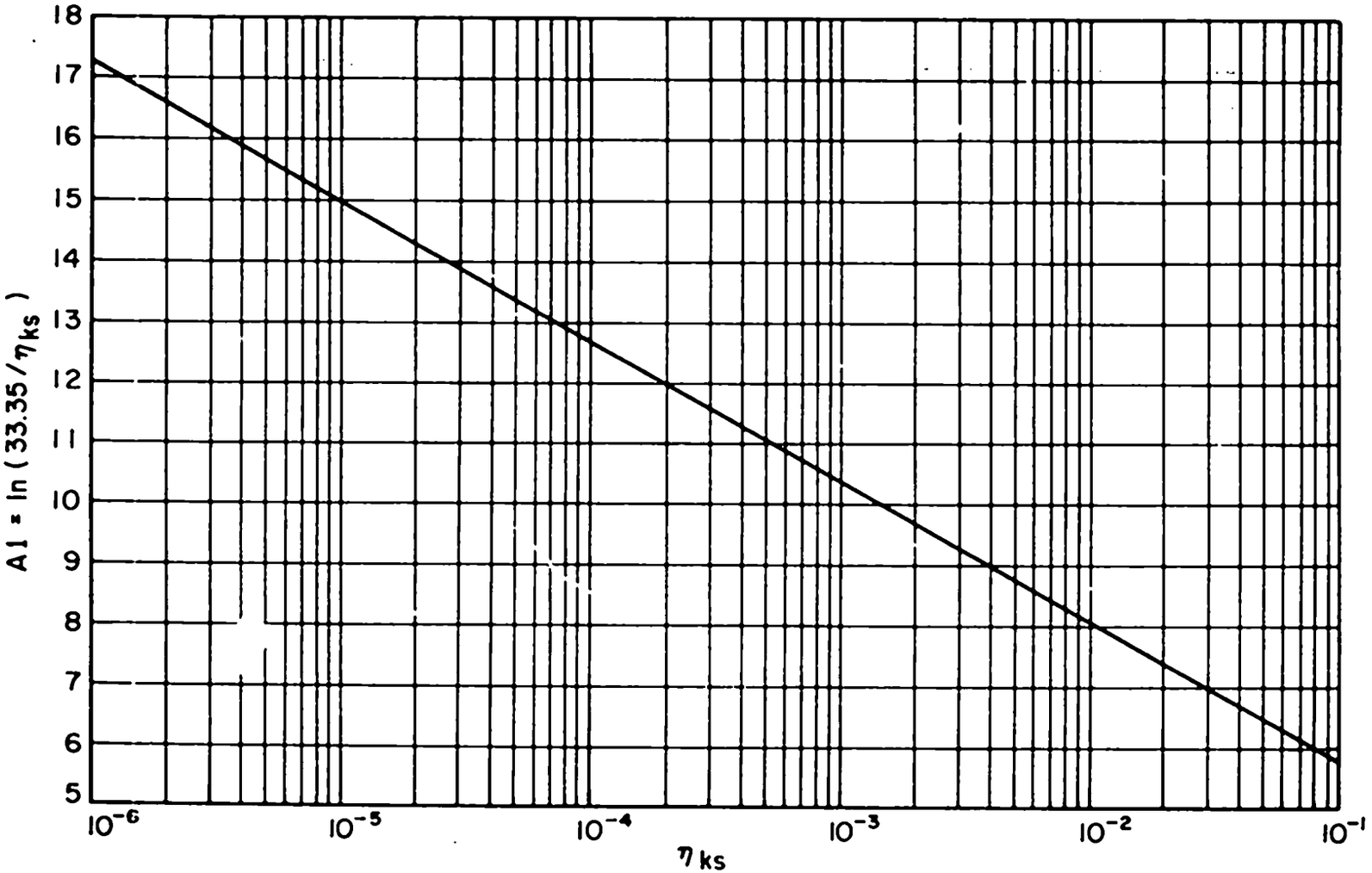

FIG. 10-1 A1 VERSUS η_{ks}

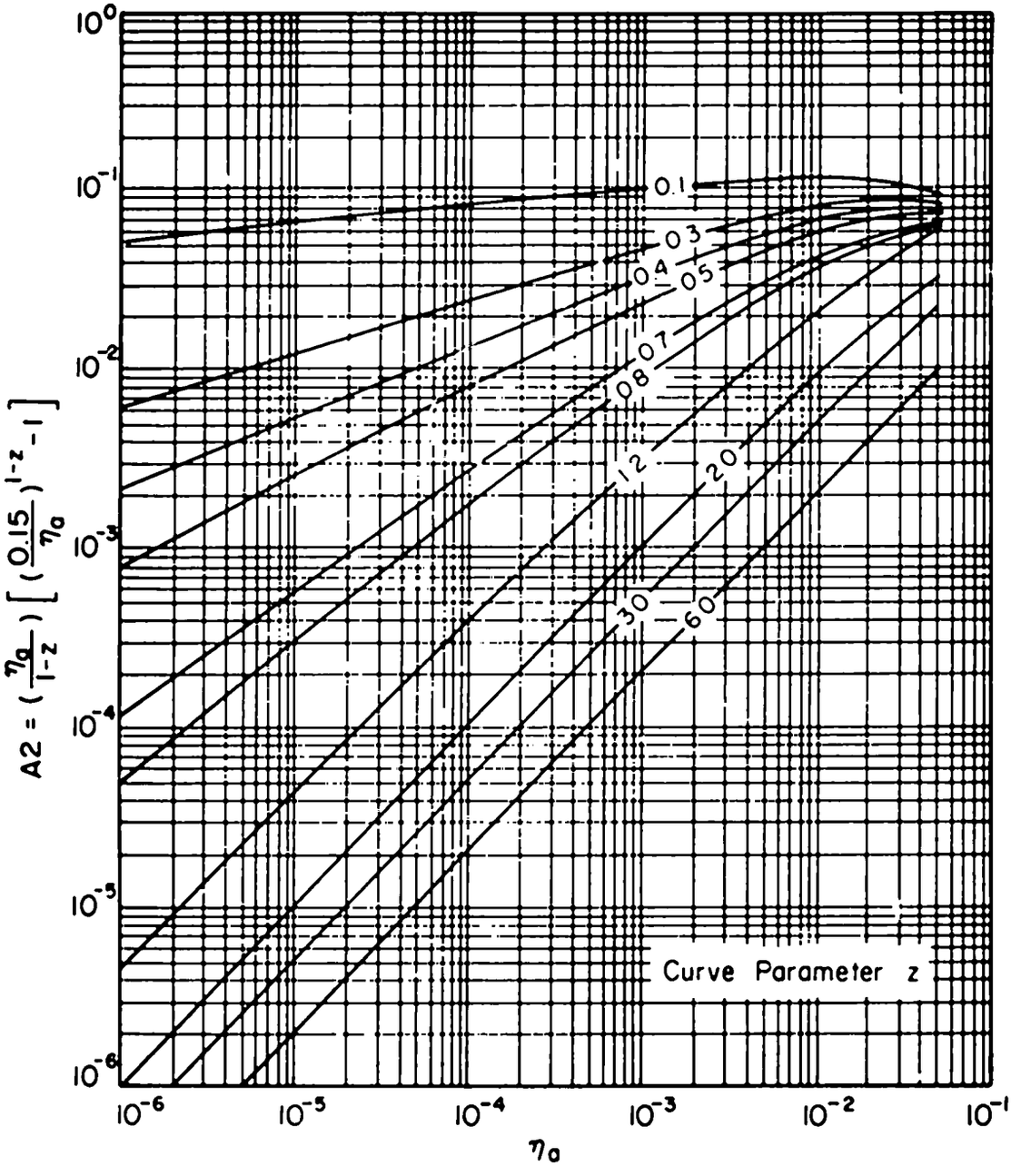

FIG. 10-2 A2 VERSUS η_a FOR DIFFERENT z VALUES

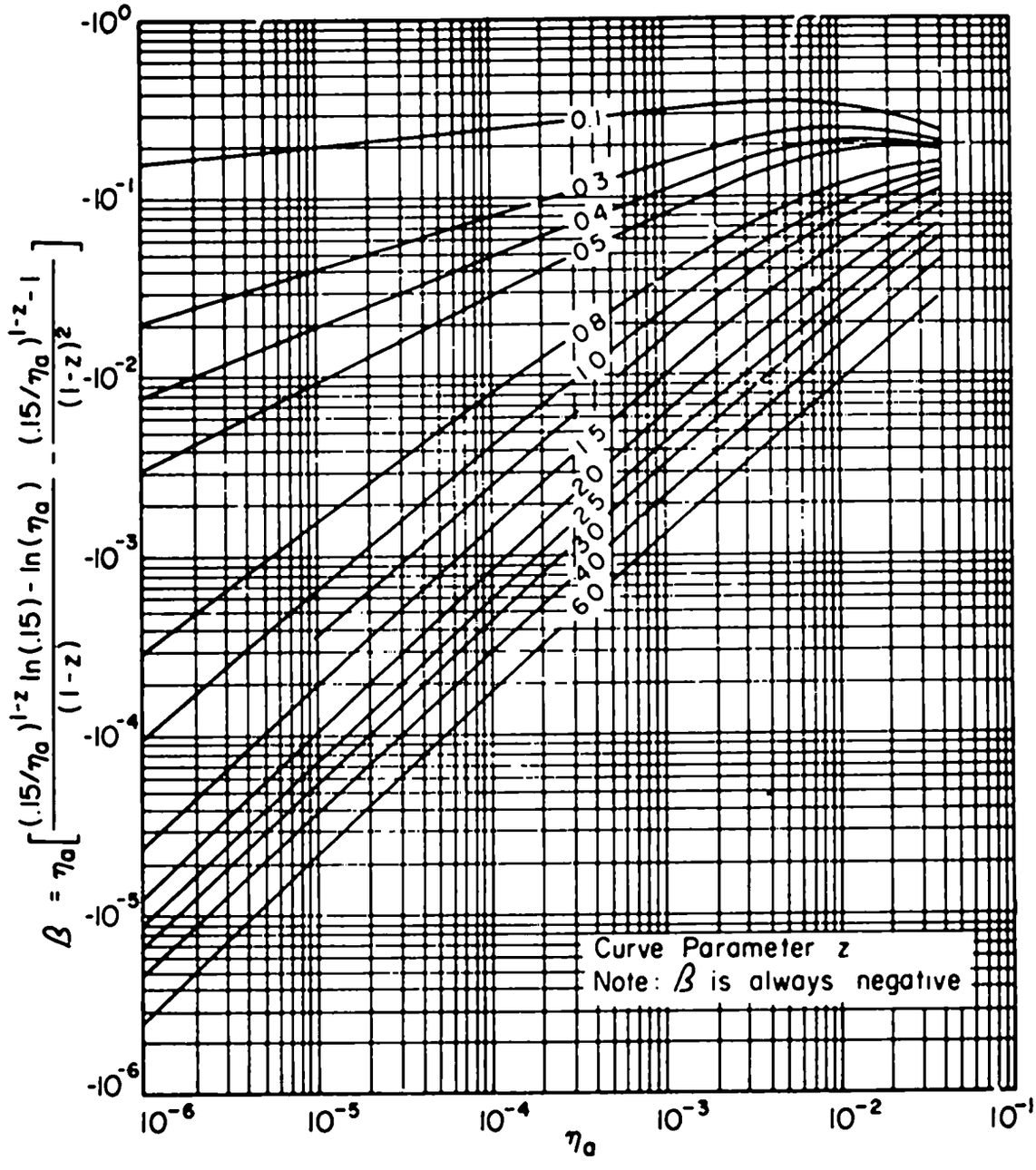

FIG. 10-3 β VERSUS η_a FOR DIFFERENT z VALUES

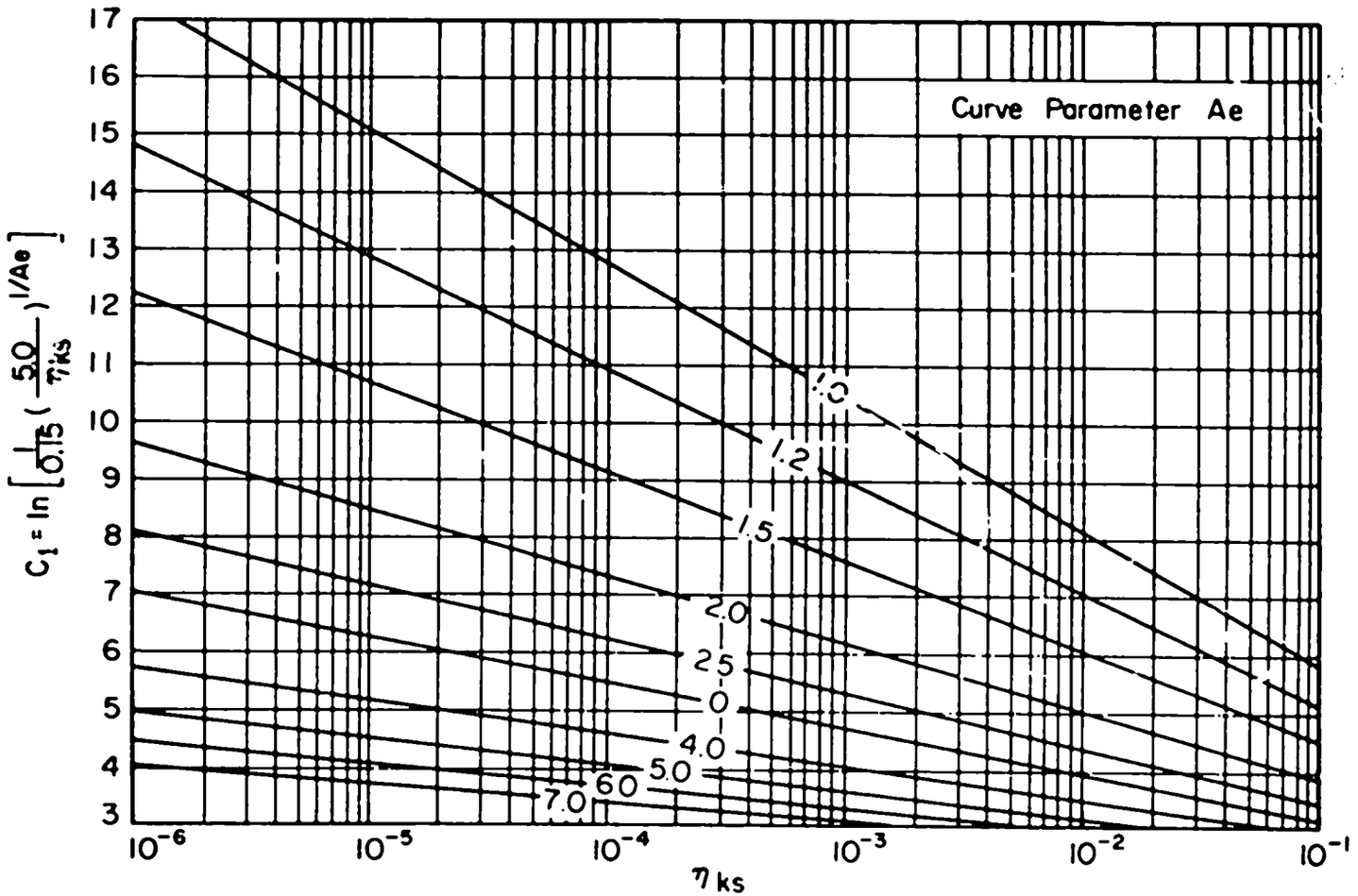

FIG. 10-4 C_1 VERSUS η_{ks} FOR DIFFERENT Ae VALUES

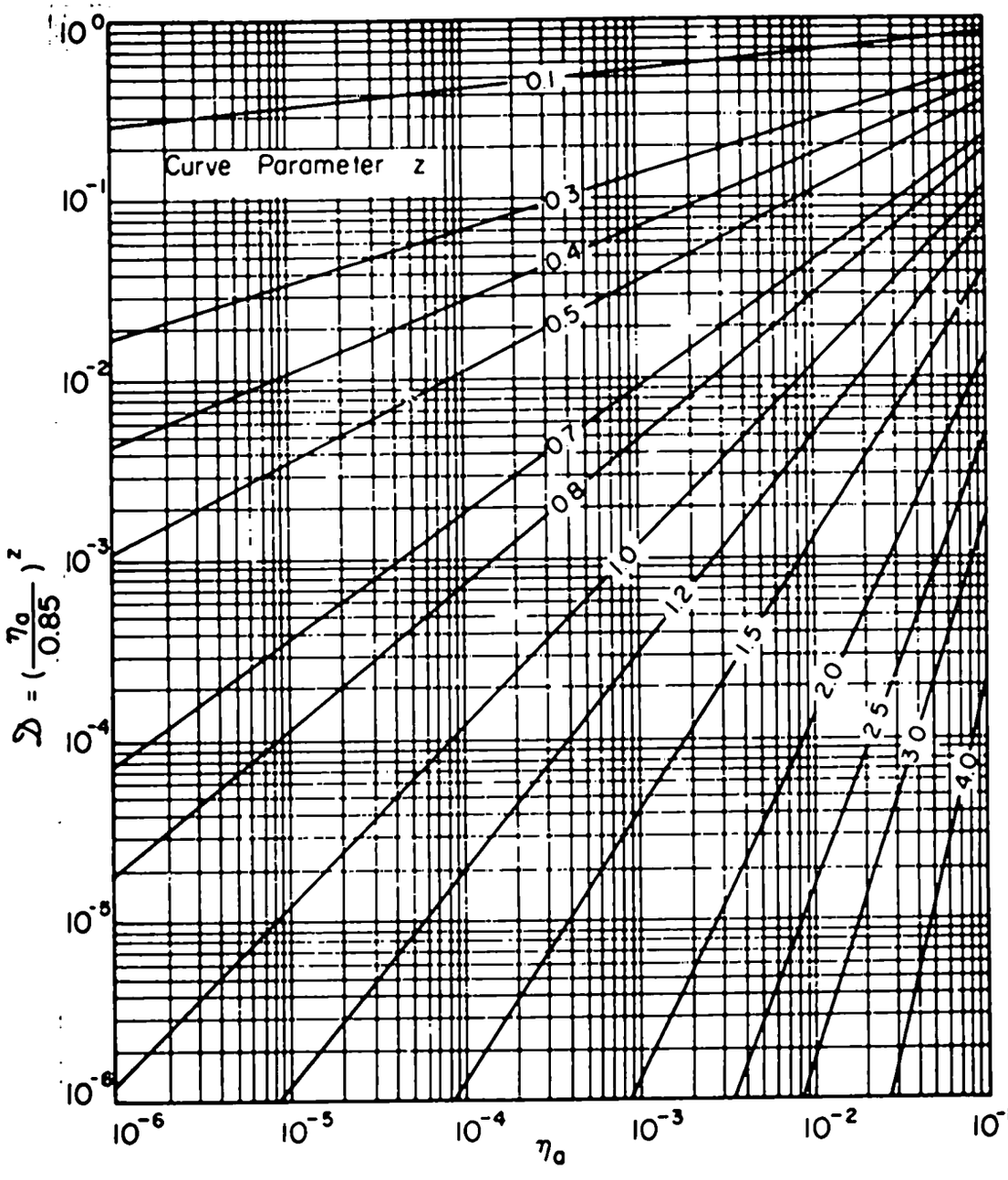

FIG. 10-5 $\mathcal{D}$ VERSUS η_a FOR DIFFERENT z VALUES

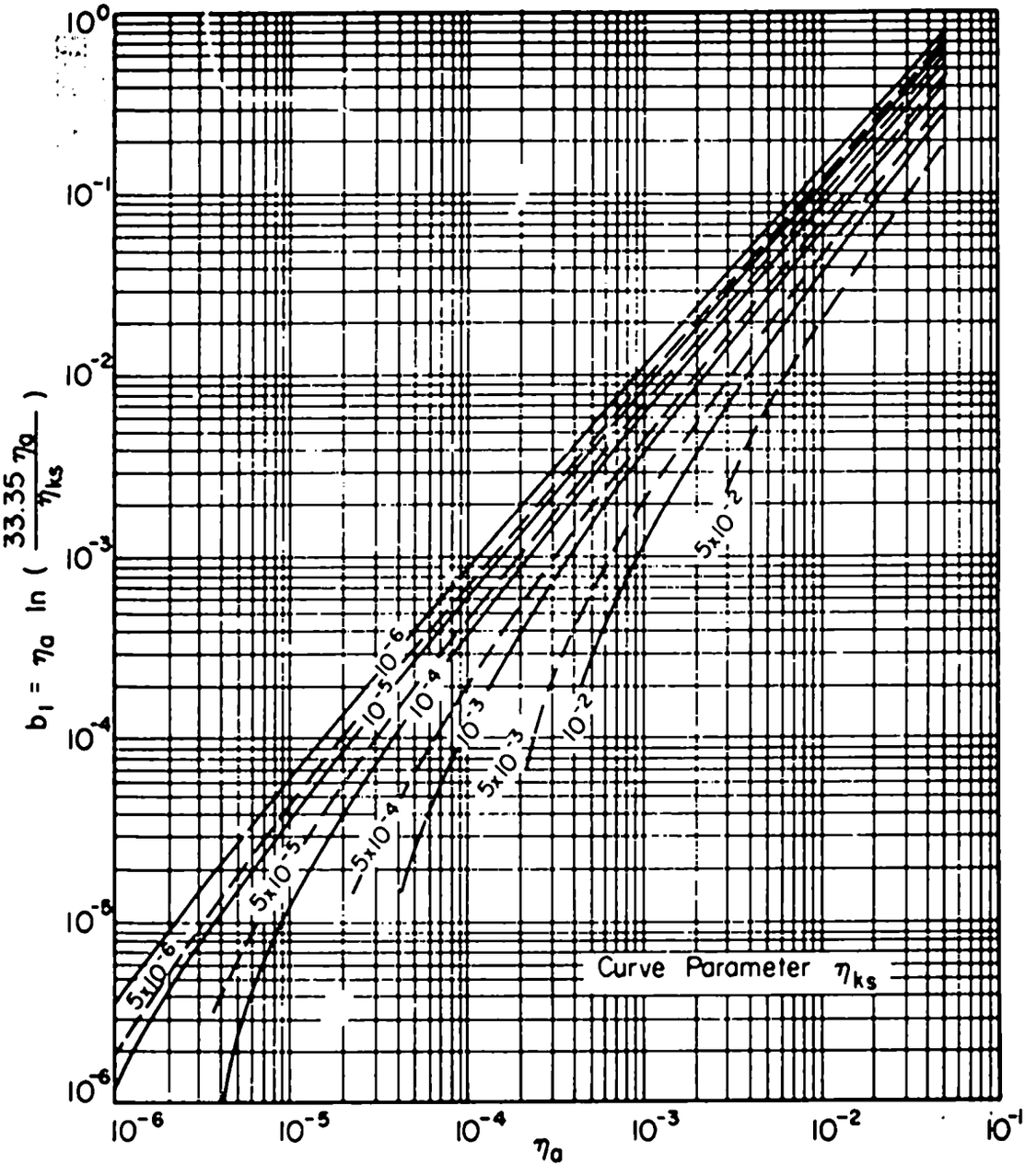

FIG. 10-6 b_1 VERSUS η_a FOR DIFFERENT VALUES OF η_{ks}

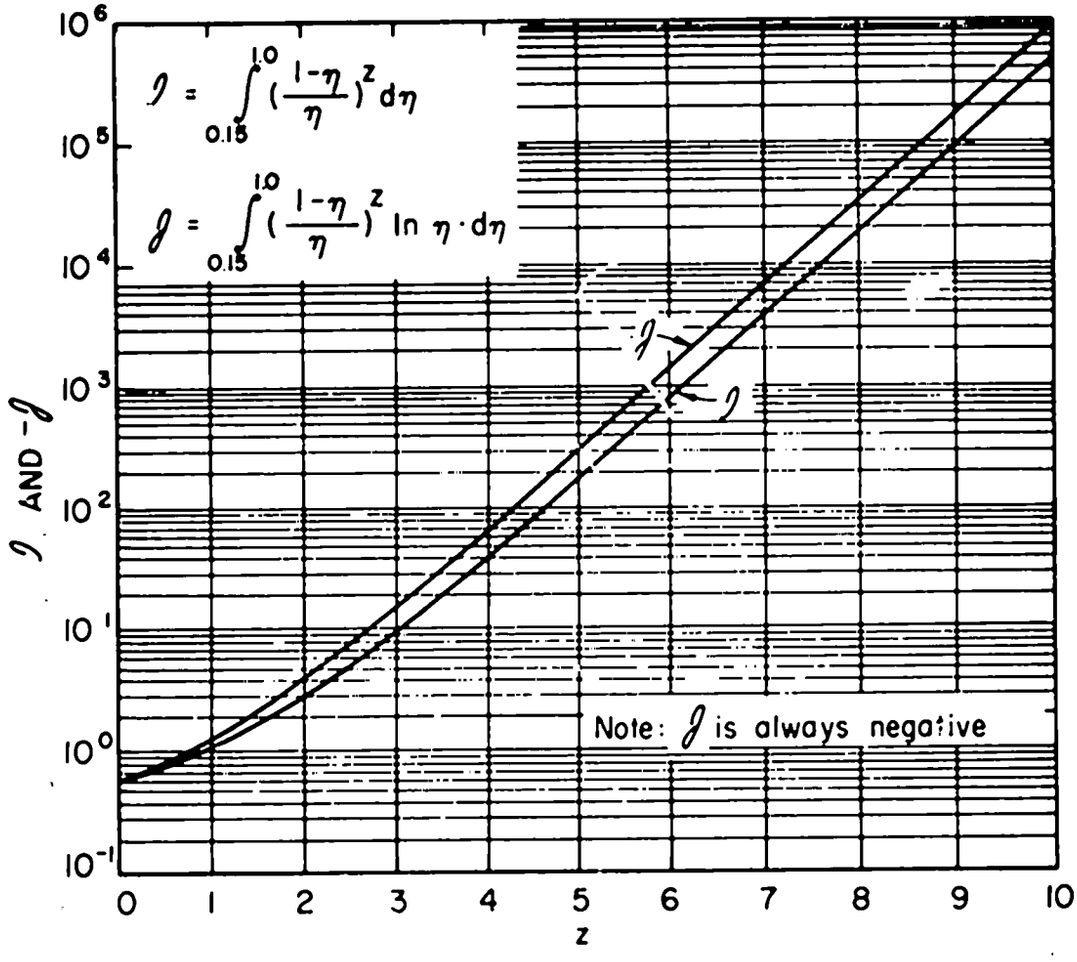

FIG. 10-7 INTEGRALS $\mathcal{I}$ AND $\mathcal{J}$ VERSUS z

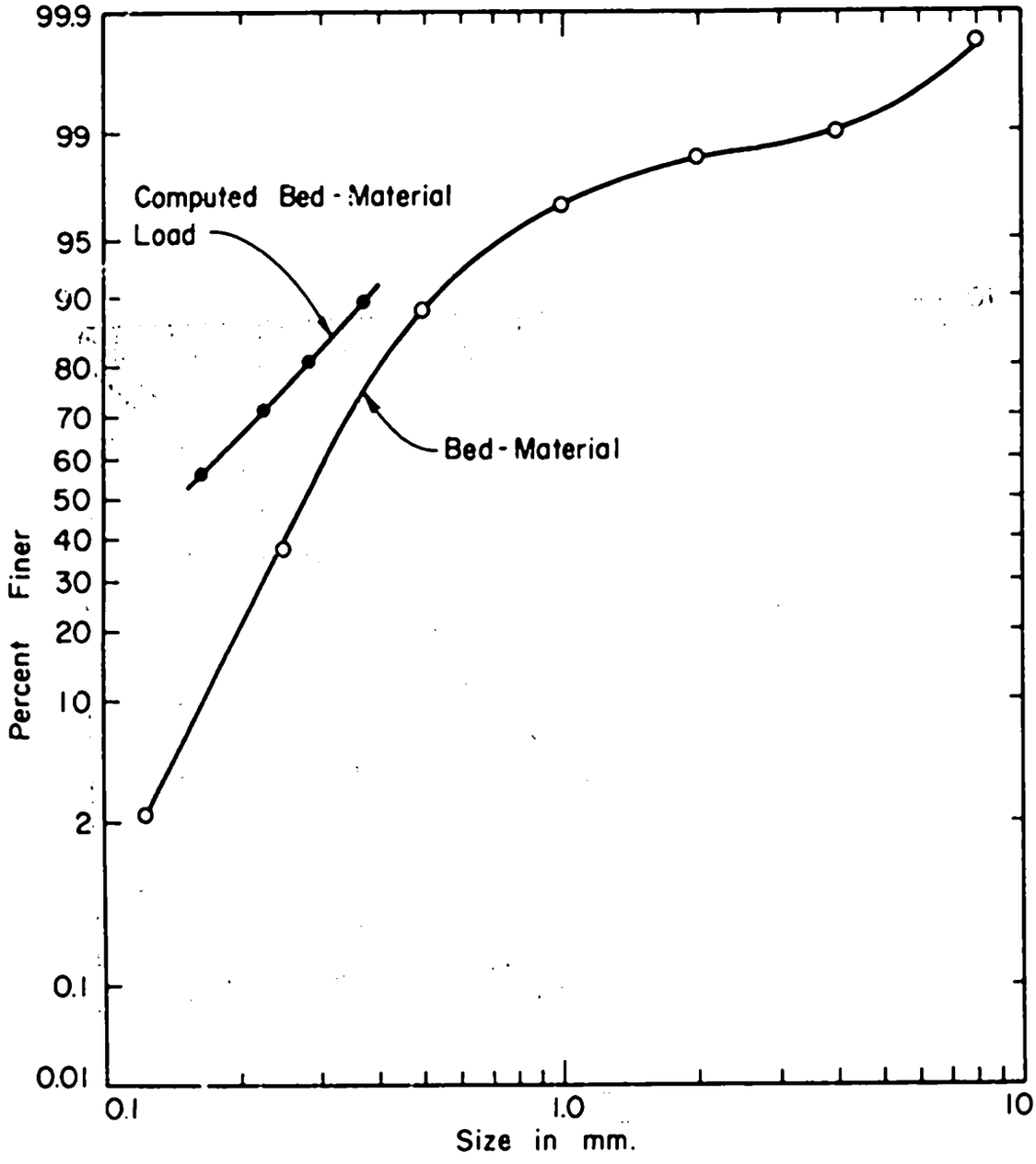

FIG. 10-8 BED-MATERIAL AND BED-MATERIAL LOAD SIZE DISTRIBUTION FOR RIO GRANDE AT ALBUQUERQUE, N.M. (OBSERVATION DATED MARCH 26, 1954)

TABLES

TABLE 3-1 WEST PAKISTAN CANALS[1]

	Canal[2]	Reduced Distance[3]	Date of Observation	Discharge cfs	X-Sectional Area ft²	Average Velocity, fps	Surface Width ft	Average Depth ft	1/Slope	Hydraulic Radius ft	Kin. Viscosity $\times 10^5$ ft²/sec.	Bed Material D_{50} mm	ϕ
1	LCC	147	Nov. 11, '62	5040	1640	3.00	304	5.00	4040	7.00	1.170	.360	1.426
2	LCC	147	Dec. 4, '62	4170	1407	2.50	305	7.00	5360	7.70	1.095	.300	1.250
3	LCC	147	Jan. 23, '63	4000	1362	3.13	307	7.60	5600	7.40	1.365	.295	1.300
4	LCC	147	Feb. 8, '63	1570	903	1.74	107	4.60	7730	4.56	1.210	.325	1.314
5	LCC	147	Apr. 13, '63	4910	1624	3.02	303	8.00	5670	7.90	1.050	.290	1.343
6	LCC	147	May 15, '63	5150	1713	3.00	305	8.40	5600	8.30	1.060	.278	1.306
7	LCC	147	Jun. 10, '63	5630	1761	3.19	306	8.60	5400	8.40	1.000	.268	1.362
8	LCC	147	Jul. 12, '63	5600	1795	3.12	304	8.80	5060	8.60	0.975	.265	1.316
9	LCC	147	Sep 9, '63	5710	1846	3.09	304	9.10	5440	8.80	0.917	.257	1.305
10	LCC	147	Oct 14, '63	3930	1460	2.69	306	7.30	6330	7.30	1.060	.230	1.263
11	LCC	176	Apr. 12, '63	5370	1663	3.17	212	7.85	6130	7.70	0.965	.300	1.247
12	LCC	176	May 16, '63	5160	1792	2.86	210	8.30	5060	8.30	1.060	.250	1.293
13	LCC	176	Jun. 11, '63	5700	1700	3.30	212	8.00	5400	8.00	1.000	.260	1.453
14	LCC	176	Jul. 17, '63	6300	1821	3.46	215	8.40	5100	8.30	1.095	.250	1.306
15	LCC	176	Sep. 10, '63	5750	1854	3.10	214	8.70	4800	8.40	0.940	.270	1.456
16	LCC	176	Oct. 15, '63	4350	1504	2.73	213	7.30	5520	7.30	1.060	.325	1.362
17	UCB	42	Nov. 7, '62	5070	1665	3.06	215	7.80	6300	7.70	1.140	.250	1.423
18	UCB	42	Dec. 6, '62	4800	1604	3.06	214	7.50	6220	7.30	1.400	.300	1.373
19	UCB	42	Jan. 10, '63	4450	1516	2.94	217	7.00	7540	6.90	1.300	.245	1.423
20	UCB	42	Feb. 5, '63	725	475	1.55	193	2.50	7140	2.50	1.170	.091	1.290
21	UCB	42	Mar. 7, '63	5150	1600	3.03	217	7.80	6000	7.60	1.155	340	1.456
22	UCB	42	Apr. 17, '63	4800	1667	2.88	218	7.60	5030	7.50	1.092	.080	1.274
23	UCB	42	May 31, '63	4770	1630	2.91	212	7.70	5010	7.60	0.900	130	1.500
24	UCB	42	Jun. 22, '63	5200	1713	3.00	218	7.80	5000	7.60	1.065	.142	1.276
25	UCB	42	Jul. 24, '63	5420	1724	3.14	215	8.00	5040	7.90	0.900	.256	1.375
26	UCB	42	Aug. 31, '63	5070	1070	3.19	216	8.60	5050	8.50	0.975	260	1.530
27	UCB	42	Sep. 18, '63	6170	1806	3.34	218	8.70	5710	8.40	0.975	260	1.523
28	UCB	42	Oct 22, '63	4750	1700	2.78	215	8.00	5010	7.80	1.050	.275	1.315
29	UCB	106	Nov 6, '62	4610	1513	3.18	160	9.00	6200	8.70	1.130	.256	1.375
30	UCB	106	Dec. 7, '62	4500	1455	3.15	160	8.60	6360	8.30	1.365	.270	1.422
31	UCB	106	Feb 4, '63	724	560	1.27	152	3.70	9030	3.70	1.106	200	1.265
32	UCB	106	Mar. 6, '63	4770	1466	3.25	167	8.80	6360	8.60	1.154	260	1.554
33	UCB	106	Apr 17, '63	4270	1456	2.93	160	8.70	5000	8.60	1.077	005	1.300
34	UCB	106	May 22, '63	4610	1504	3.07	171	8.80	4700	8.50	1.036	.085	1.530
35	UCB	106	Jun. 21, '63	4000	1456	3.35	166	8.70	6670	8.60	1.025	.235	1.406
36	UCB	106	Jul. 25, '63	5500	1525	3.53	166	9.10	6600	8.70	0.975	.230	1.306
37	UCB	106	Aug. 31, '63	5340	1630	3.15	172	9.60	5510	9.30	0.940	.200	1.334
38	UCB	136	Sep. 17, '63	5630	1730	3.20	170	10.10	5000	9.60	-	.212	1.310
39	UCB	136	Oct. 22, '63	4630	1522	3.04	171	9.00	5100	8.60	1.036	.270	1.303
40	LBD	35	Sep 27, '63	7300	3444	2.02	232	10.50	7050	10.20	1.025	.305	1.433
41	LBD	35	Jul 31, '63	7170	3410	2.07	236	10.30	11700	10.00	0.905	.174	1.417
42	LBD	75	Aug 17, '63	7400	3413	2.07	235	10.30	12700	10.10	0.875	.235	1.345
43	LBD	35	Sep 13, '63	7130	2521	2.82	230	10.60	10000	10.30	0.905	.170	1.310

1. Data selected from Canal and Headworks Program, 1962-63 Data Tabulation, Part II, West Pakistan Water and Power Development Authority, Lahore, Pakistan.

2. LCC Lower Chenab Canal

   UCB Upper Ongore Branch Canal

   LBD Lower Bari Doab Canal

3. Reduced distance is 1,000 ft from canal headworks.

TABLE 7-1 VALUES OF FRICTION FACTOR f VERSUS R/f
BASED ON TRACY AND LESTER (1961)

f	R/f	f	R/f
.012	.104E+09	.047	.803E+05
.013	.617E+8	.048	.736E+05
.014	.384E+08	.049	.677E+05
.015	.250E+08	.050	.624E+05
.016	.169E+08	.051	.576E+05
.017	.118E+08	.052	.533E+05
.018	.850E+07	.053	.494E+05
.019	.625E+07	.054	.459E+05
.020	.470E+07	.055	.427E+05
.021	.360E+07	.056	.398E+05
.022	.281E+07	.057	.371E+05
.023	.222E+07	.058	.347E+05
.024	.178E+07	.059	.325E+05
.025	.144E+07	.060	.305E+05
.026	.118E+07	.061	.286E+05
.027	.980E+06	.062	.269E+05
.028	.820E+06	.063	.254E+05
.029	.691E+06	.064	.239E+05
.030	.587E+06	.065	.226E+05
.031	.503E+06	.066	.213E+05
.032	.433E+06	.067	.202E+05
.033	.375E+06	.068	.191E+05
.034	.327E+06	.069	.181E+05
.035	.287E+06	.070	.172E+05
.036	.252E+06	.071	.163E+05
.037	.223E+06	.072	.155E+05
.038	.198E+06	.073	.147E+05
.039	.177E+06	.074	.140E+05
.040	.159E+06	.075	.134E+05
.041	.143E+06	.076	.128E+05
.042	.129E+06	.077	.122E+05
.043	.116E+06	.078	.116E+05
.044	.106E+06	.079	.111E+05
.045	.961E+05	.080	.107E+05
.046	.877E+05	.081	.102E+05

TABLE 7-2 SIZE DISTRIBUTION OF SANDS

Ref Table No USGS P.P. 462-I	Median size mm	Geometric standard deviation
2	0.19	1.30
3	0.27	1.56
4	0.28	1.67
5	0.45	1.60
6	0.93	1.54
7	0.32	1.57
8	0.33	1.25
9	0.33	2.07
10	0.47	1.54
11	0.54	1.52
Barton and Lin (1955)	0.18	1.25

TABLE 7-3 VARIATION OF (WITH REYNOLDS NUMBER R_{x_0}, FOR PLANE-RED RUNS

Equivalent Roughness	With Hull Correction (Mean	Std. Dev.	Co. Variance	Correlation Coeff.	Student's T	Null Hypothesis	Without Hull Correction (Mean	Std. Dev.	Co. Variance	Correlation Coeff.	Student's T	Null Hypothesis
0_{90}	12.756	11.712	.918	.007	.105	True	2.433	1.594	.655	-.070	-.430	True
0_{84}	11.497	10.616	.923	.060	.412	True	2.102	1.667	.660	-.103	-.633	True
0_{67}	9.373	8.872	.947	.032	.191	True	1.753	1.257	.795	-.155	-.940	True
0_{64}	9.219	8.750	.949	.030	.170	True	1.753	1.242	.790	-.156	-.950	True
0_{50}	8.050	7.843	.975	.020	.121	True	1.520	1.128	.750	-.180	-1.090	True
0_{33}	7.064	7.078	1.002	.023	.130	True	1.336	1.030	.771	-.193	-1.176	True
0_{13}	6.952	6.992	1.006	.024	.143	True	1.315	1.019	.775	-.194	-1.185	True

TABLE 7-4 VARIATION OF (WITH ASPECT RATIO, FOR PLANE-RED RUNS

Equivalent Roughness	With Hull Correction (Mean	Std. Dev.	Co. Variance	Correlation Coeff.	Student's T	Null Hypothesis	Without Hull Correction (Mean	Std. Dev.	Co. Variance	Correlation Coeff.	Student's T	Null Hypothesis
0_{90}	12.756	11.712	.918	-.544	-3.091	False	2.433	1.594	.655	.276	1.725	True
0_{84}	11.497	10.616	.923	-.546	-3.011	False	2.102	1.667	.660	.255	1.581	True
0_{67}	9.373	8.872	.947	-.544	-3.006	False	1.753	1.257	.795	.219	1.387	True
0_{64}	9.219	8.750	.947	-.543	-3.001	False	1.753	1.242	.708	.206	1.263	True
0_{50}	8.050	7.843	.975	-.530	-3.030	False	1.520	1.128	.750	.176	1.079	True
0_{33}	7.064	7.078	1.002	-.530	-3.754	False	1.336	1.030	.771	.146	.886	True
0_{13}	6.952	6.992	1.006	-.529	-3.744	False	1.315	1.019	.775	.143	.864	True

TABLE 7-5 SUMMARY OF ζ VALUES AND RELATED PARAMETERS FOR PLANE BED RUNS

$(D_s = D_{84})$

S.No.	Run	Depth d(ft)	Velocity V(fps)	Slope $S \times 10^3$	Flume Width (ft)	$k_s \times 10^3$ (ft)	Without wall correction: f	ζ	R_{s0}	Aspect Ratio	$Z \times 10^{-6}$	With wall correction: ζ	R_{s0}	Aspect Ratio	$Z \times 10^{-6}$
1	3-229	.43	.87	.016	8.0	.81	.023	3.15	3.3	18.6	.130	9.32	5.1	30.8	.116
2	3-15	.79	3.46	.112	8.0	.81	.019	3.77	12.4	10.1	.904	11.00	11.2	12.5	.804
3	3-10	.81	3.00	.170	8.0	.81	.027	1.53	13.2	15.7	.536	3.25	11.2	18.8	.445
4	3-46	.74	3.66	.167	8.0	1.30	.023	3.10	34.5	10.8	.073	9.32	22.0	13.6	.775
5	6-21	.60	3.11	.153	8.0	1.53	.034	3.60	30.1	13.3	.570	8.72	18.4	16.0	.676
6	6-25	.72	3.79	.190	8.0	1.53	.036	2.90	36.6	11.1	.000	7.90	23.7	14.0	.700
7	6-28	.58	3.57	.220	8.0	1.53	.025	3.46	35.1	14.5	.630	7.79	23.0	17.3	.630
8	6-30	.53	3.77	.270	8.0	1.53	.036	3.33	37.1	15.4	.643	7.15	34.9	18.2	.543
9	6-27	1.04	1.47	.030	8.0	4.70	.013	2.30	43.7	7.9	.562	9.61	37.2	11.1	.617
10	6-30	1.03	1.32	.030	8.0	4.70	.043	1.07	41.0	7.6	.490	4.82	34.6	11.2	.546
11	6-31	1.01	1.40	.030	8.0	4.70	.036	2.07	43.0	7.9	.563	8.44	36.6	11.1	.601
12	6-31	.50	1.35	.054	8.0	4.70	.037	3.31	37.0	16.0	.231	6.57	34.0	19.0	.194
13	6-32	.52	1.50	.064	8.0	4.70	.038	3.11	41.0	15.4	.264	6.30	37.6	18.5	.220
14	6-34	.40	1.46	.064	8.0	4.70	.041	2.67	44.4	16.3	.260	5.44	40.5	19.5	.218
15	10-60	.62	4.30	.42	8.0	2.37	.030	2.75	52.5	12.9	.000	7.09	47.2	16.0	.736
16	10-61	.61	4.36	.365	8.0	2.37	.030	2.93	52.2	13.1	.007	7.40	47.0	16.2	.719
17	10-71	.32	3.71	.531	8.0	2.37	.043	1.83	47.1	25.0	.346	2.90	44.3	28.2	.308
18	10-72	.32	3.36	.550	8.0	2.37	.043	1.80	43.1	25.0	.319	2.86	40.5	28.2	.302
19	10-70	.30	3.41	.640	8.0	2.37	.043	1.92	40.3	26.7	.341	2.90	46.5	29.9	.304
20	10-100	.51	5.30	.790	8.0	2.37	.037	1.67	66.2	15.7	.035	3.63	60.2	19.0	.000
21	9-10	.56	4.16	.417	1.97	1.65	.034	1.27	50.0	3.5	1.040	20.50	36.0	6.02	.536
22	9-12	.67	4.03	.436	1.97	1.65	.040	.42	34.3	2.9	.715	16.60	22.2	7.00	300
23	9-01	.51	4.02	.290	1.97	1.35	.021	4.32	27.3	3.9	.750	44.70	21.8	6.1	.483
24	9-13	.51	4.34	.350	1.97	1.35	.026	3.17	30.1	3.9	.801	36.00	23.5	6.3	480
25	9-04	.51	4.00	4.33	1.97	3.34	.036	1.79	57.5	3.9	.705	29.00	42.2	7.1	.434
26	11-140	.70	3.51	.330	1.97	3.60	.060	.62	30.0	3.0	.400	21.50	30.2	6.6	.175
27	11-10	.64	4.30	.445	1.97	3.60	.043	1.00	79.3	3.1	1.030	35.70	52.7	7.0	.453
28	8L-18	.60	2.04	.156	4.0	.74	.034	.52	13.4	5.8	.776	3.50	10.0	9.1	.407
29	8L-19	.75	3.17	.167	4.0	.74	.032	.55	16.4	5.3	.933	4.60	11.4	8.5	.575
30	8L-20	.61	2.07	.166	4.0	.74	.030	.90	13.0	6.6	.710	4.96	10.8	8.5	.400
31	8L-22	.76	3.27	.170	4.0	.74	.032	.53	16.3	5.3	.930	5.10	11.1	8.4	.583
32	8L-23	.65	3.18	.196	4.0	.74	.030	.76	15.4	6.2	.800	4.90	12.5	9.3	.586
33	8L-25	.76	3.77	.134	4.0	.74	.032	.52	13.4	5.1	.801	4.66	10.5	8.3	540
34	8L-26	.60	3.71	.125	4.0	.74	.030	.74	12.6	5.8	.771	5.06	10.3	8.8	.507
35	8L-30	.60	3.54	.121	4.0	.74	.030	.96	11.0	6.7	.636	5.15	9.8	9.6	.443
36	8L-31	.42	3.71	.123	4.0	.74	.010	0.01	13.1	9.5	.404	23.6	9.2	11.5	.400
37	8L-35	.56	3.34	.160	4.0	.74	.021	3.68	13.2	7.1	.750	15.6	11.4	9.5	.502
38	8L-36	.53	3.76	.210	4.0	.74	.025	1.90	16.5	7.6	.853	17.5	13.0	9.9	.651

1. Equivalent roughness $k_s = D_{84} = D_{50} \times \sigma$
2. ζ is defined by $\frac{1}{\sqrt{f}} = 2.03 \log(\zeta \frac{R}{k_s})$.
3. For values without wall correction hydraulic radius $R = d$, $Z = \frac{dSV}{\nu}$, $R_{s0} = \frac{V_* D_{84}}{\nu}$ and Aspect Ratio $= \frac{W}{d}$
4. Wall correction based on Tracy-Lester smooth flume, subcritical flow equation (Reduce to Equation 7-9).
5. For values with wall correction, R = hydraulic radius associated with bed, R_b.
6. S No. 25-38 are from Barton-Lin data (Chapter II).

TABLE 7-4 COMPARISON OF OBSERVED AND PREDICTED VALUES OF f FOR PLANE-BED RUNS

S.No.	Run	f_o	f_p	C_t=30[4]	f_o-f_p	Run	Run	f_o	f_p	C_t	f_o-f_p
1	3-230	.025	.025	0.2	.002	16	10-61	.030	.031	3300	.002
2	3-15	.019	.021	3000	.002	17	10-71	.042	.030	3250	-.003
3	3-10	.027	.034	3400	-.005	18	10-72	.043	.030	5600	-.004
4	3-06	.023	.025	1670	.002	19	10-70	.043	.030	6310	-.004
5	6-22	.034	.027	1540	.003	20	10-100	037	.033	8440	-.004
6	6-25	.036	.027	2710	.001	21	7-19	.034	.020	4540	-.025
7	6-26	.025	.030	2760	.003	22	7-13	.040	.027	2060	-.022
8	6-29	.036	.030	3130	.003	23	8-01	.023	026	3000	005
9	6-27	.033	.033	2.0	.000	24	8-13	.036	.030	3260	.002
10	6-30	.043	.033	0.4	-.010	25	9-04	.036	033	5100	-.004
11	6-21	.035	.033	0.4	-.002	26	11-140	.050	.031	3060	-.019
12	6-31	.037	.043	4.3	.006	27	11-10	.043	033	3600	-.041
13	6-32	.036	.041	30.0	.003						
14	6-24	041	.043	15.0	.001						
15	10-60	.030	.031	3250	.001						

1. f_o is observed value of friction factor f
2. f_p is predicted value of f, from $\frac{1}{\sqrt{f}} = 2.03 \log(3.4 \frac{d}{d_{84}})$ without using wall correction
3. For other data about these runs, refer to TABLE 7-1
4. C_t is concentration by weight of total load.

TABLE 8-1 SEPARATION OF BED FORMS FOR THE FLUME DATA

Ref. Table No. (1)	Median Fall Dia. $D_{50} \times 10^3$ ft	Standard Deviation σ	$D_{84} \times 10^3$ ft (2)	Maximum Stream Power P_{max} (3) ft-lb/sec/sq. ft: Upper Limit for Lower Regime	Intermediate range	Lower Limit for Upper Regime
2	.625	1.30	.810	.202	.202 - .412	.412
3	.885	1.56	1.380	.312	.312 - .555	.555
4	.918	1.67	1.532	.207	.207 - .421	.421
5	1.475	1.60	2.360	.275(4)	.275 - .889	.889
6	3.049	1	4.700	1.010(5)	1.010 -1.660	1.660
7	1.049	1.57	1.648	.258	.258 - .409	.409
8	1.082	1.25	1.351	.358	.358 - .508	.508
9	1.082	2.07	2.240	.179	-	.215
10	1.541	1.54	2.365	.460	.460 - .863	.863
11	1.770	1.52	2.690	.386	.386 -1.070	1.070

Notes:
1. Table number referred to is from USGS Profesional Paper No. 462-I, 1966.
2. D_{84} based on lognormal distribution $= D_{50} \times \sigma$.
3. Maximum possible stream power based on $h_s = D_{84}$ and Keulegan's velocity Equation (8-12). Upper limit for lower regime refers to the value of P_{max} which resulted in lower regime bed forms only. Lower limit for upper regime similarly refers to value of P_{max} which resulted in upper regime bed forms only. In the intermediate range of P_{max} both upper and lower regime bed forms resulted in the flumes.
4. Excluding run 5-26.
5. Excluding plane-bed runs before dunes, which are part of lower regime.

TABLE 8-2 COORDIATES OF STRAIGHT SEGMENTS (ON LOG-LOG PAPER) OF RESISTANCE CURVES

RANGE OF $(P_{max} \cdot D_{50})$ *	UPPER		UPPER-INTERMEDIATE		LOWER-INTERMEDIATE		LOWER	
	1/S	$V/\Delta U_{*o}$	1/S	$V/\Delta U_{*o}$	1/S	$V/\Delta U_{*o}$	1/S	$V/\Delta U_{*o}$
	.9	5.0	1.2	35.0	1.1	33.0	5.0	13.0
	1.1	15.0	1.5	35.0	1.7	20.0	6.6	13.0
	1.3	20.0	2.5	28.0	3.0	15.0	11.0	11.0
	1.5	22.0	5.0	15.2	6.0	11.0	20.0	11.0
	2.0	20.0	10.0	17.0	10.0	10.0	30.0	12.0
	4.0	15.0	15.0	17.0	13.0	10.0	40.0	16.0
	10.0	17.0			25.0	11.0	50.0	22.0
	15.0	17.0			30.0	11.0	55.0	22.0

Notes:
1. S is Shield's Parameter $\frac{\rho U_{*oo}^2}{(\gamma_s - \gamma_f) D_{50}}$.
2. For plotted curves refer to Figures 8-9 and 8-10.
3. For $P_{max} \cdot D_{50}$ range refer to Figure 8-3.

TABLE 9-1 VARIATION OF RELATIVE CONCENTRATION C_a/C_{a_0}

η	C_a/C_{a_0} $\epsilon = 0.3$ (1)	(2)	C_a/C_{a_0} $\epsilon = 0.6$ (1)	(2)	C_a/C_{a_0} $\epsilon = 1.0$ (1)	(2)	C_a/C_{a_0} $\epsilon = 3.0$ (1)	(2)	C_a/C_{a_0} $\epsilon = 5.0$ (1)	(2)
.001	[illegible]	[illegible]	[illegible]	[illegible]	[illegible]	[illegible]	[illegible]	[illegible]	[illegible]	[illegible]
.005	.6175+00	.6164+00	.5615+00	.5630+00	.3002+00	.1904+00	.0305+02	.7904+02	.3300+03	.3142+03
.010	.5611+00	.5000+00	.2511+00	.2520+00	.1002+00	.0912+01	.1302+02	.9736+03	.1000+04	.9564+05
.020	.4375+00	.4054+00	.1662+00	.1600+00	.5002+01	.5400+01	.1351+03	.1100+03	.3170+05	.2042+05
.050	.3004+00	.3054+00	.9562+01	.9700+01	.3000+01	.1900+01	.0000+05	.6000+05	.3790+06	.2090+06
.100	.2510+00	.2430+00	.6310+01	.5930+01	.1300+01	.9010+02	.1300+05	.7310+06	.1000+00	.5930+10
.130	.2300+00	.2704+00	.5662+01	.5242+01	.0530+02	.7542+02	.5790+06	.3062+06	.6030+10	.3130+10
.150	.720+00	.2130+00	.4954+01	.4490+01	.6675+02	.5675+02	.2062+06	.1030+06	.1375+10	.5075+11
.300	.3002+00	.1910+00	.4010+01	.3641+01	.4710+02	.4002+02	.1342+06	.6420+07	.2310+11	.1034+11
.500	.1752+00	.1430+00	.2900+01	.3644+01	.2750+02	.2342+02	.3075+07	.1275+07	.1546+12	.6054+13
.620	.1490+00	.1420+00	.2230+01	.2675+01	.1754+02	.1500+02	.5600+08	.3900+08	.1710+13	.7630+14
.500	.1320+00	[illegible]	.1750+01	.1500+01	.1100+02	.1000+02	.1630+08	.1000+08	.3750+14	.1610+14
.600	.1170+00	.1120+00	.1370+01	.1200+01	.7500+03	.6675+03	.4075+09	.2975+09	.2975+15	.1325+15
.700	.1030+00	.0975+01	.1062+01	.9540+02	.5040+03	.4290+03	.1700+00	.7900+10	.3750+16	.1450+16
.800	.0725+01	.0310+01	.7610+02	.6000+02	.2900+03	.2560+03	.2540+10	.1570+10	.2300+17	.9010+16
.900	.0640+01	.0510+01	.6400+02	.4240+02	.1310+03	.1110+03	.2230+11	.1300+11	.3070+19	.170 +19
.990	.3530+01	.3170+01	.1110+02	.1910+02	.1190+04	.1910+04	.1602+16	.1234+16	.2370+20	.4062+20

1. Computed with Equation (9-11) in inner layer (ϵ_w = linear) and Equation (9-9) in outer layer
2. Computed with Equation (9-9) (vertical distribution of ϵ_w = parabolic) throughout the vertical.
3. Inner layer $\eta \leq 0.15$, outer layer $0.15 < \eta \leq 1.0$

TABLE 10-1 VALUES OF $A1 = \ln(\frac{33.35}{\eta_{ks}})$

SNO	η_{ks}	A1
1	10^{-6}	17.3
2	5×10^{-6}	15.7
3	10^{-5}	15.0
4	5×10^{-5}	13.4
5	10^{-4}	12.7
6	5×10^{-4}	11.1
7	10^{-3}	10.4
8	5×10^{-3}	8.8
9	10^{-2}	8.1
10	5×10^{-2}	6.5

TABLE 10-2 VALUES OF $AJ = \left(\frac{\epsilon_0}{1-\epsilon}\right)\left(\left(\frac{.15}{\epsilon_0}\right)^{1-\epsilon} - 1\right)$

S.No.	ϵ	ϵ_0 = 10^{-6}	5×10^{-6}	10^{-5}	5×10^{-5}	10^{-4}	5×10^{-4}	10^{-3}	5×10^{-3}	10^{-2}	5×10^{-2}
1	0.10	.3066E-01	.3046E-01	.6375E-01	.7400E-01	.8812E-01	.9375E-01	.0090E-01	.1136E+00	.1164E+00	9300E-01
2	0.20	.6000E-02	.9730E-02	.1300E-01	.1930E-01	.2375E-01	.3000E-01	.4630E-01	.7910E-01	8000E-01	8275E-01
3	0.30	.2130E-02	.6000E-02	.5530E-02	.1010E-01	.1130E	.3475E-01	.3300E-01	.5500E-01	.6000E 01	7700E-01
4	0.40	.7730E-03	.1732E-02	.3430E-02	.5300E-02	.7510E-02	.1630E-01	.2250E-01	.4400E-01	.5750E-01	.7325E-01
5	0.50	.1160E-03	.3510E-03	.5630E-03	.1675E-02	.3060E-02	.7560E-02	.1175E-01	.2060E-01	4100E-01	.6510E-01
6	0.60	.4930E-04	.1730E-03	.3930E-03	.0000E-03	.1600E-02	.5330E-02	.0625E-02	.3440E-01	.3590E-01	6140E-01
7	0.70	.1630E-04	.6740E-04	.1330E-03	.4030E-03	.8630E-03	.3300E-02	5600E-02	.1830E-01	.2900E-01	5650E-01
8	1.00	.0900E-05	.4030E-04	.7630E-04	.3300E-03	.6130E-03	.2400E-02	.4430E-02	.1560E-01	.2530E 01	.5300E-01
9	1.20	.4540E-05	.2100E-04	.4270E-04	.2000E-03	.3640E-03	.1700E-02	.3100E-02	.1230E-01	.2000E-01	4030E-01
10	1.50	.1990E-05	.9040E-05	.1900E-04	.9430E-04	.1950E-03	.9430E-03	.1860E-02	8170E-02	.1400E-01	4230E-01
11	2.00	1000E-05	.5000E-05	.1000E-04	.5000E-04	.0000E-04	.4900E-03	.9030E-03	4630E-02	.0130E-02	.3130E-01
12	2.50	.6670E-06	.3330E-05	.6670E-05	.3330E-04	.6670E-04	.3330E-03	.6660E-03	3330E-02	6530E-02	.2600E-01
13	3.00	.5000E-06	.2500E-05	.5000E-05	.2500E-04	.5000E-04	.2500E-03	.5000E-03	2500 02	4900E-02	2230E-01
14	3.50	.4000E-06	2000E-05	.4000E-05	.2000E-04	.4000E-04	.2000E-03	4000E-03	.2000E-02	.4000E-02	.1870E-01
15	4.00	.3330E-06	.1670E-05	.3330E-05	.1670E-04	.3330E-04	.1670E-03	.3330E-03	1670E-02	3330E-02	1600E-01
16	5.00	.2500E-06	.1250E-05	.2500E-05	.1250E-04	.2500E-04	.1250E-03	.2500E-03	.1250E-02	.2500E-02	.1230E-01
17	6.00	.2000E-06	1000E 05	.2000E-05	.1000E-04	.2000E-04	.1000E-03	.2000E-03	.1000E-02	.2000E-02	.9960E-02

TABLE 10-3 VALUES OF $B = \epsilon_0 \left(\frac{\left(\frac{.15}{\epsilon_0}\right)^{1-\epsilon} \ln(.15) - \ln(\epsilon_0)}{(1-\epsilon)} - \frac{\left(\frac{.15}{\epsilon_0}\right)^{1-\epsilon} - 1}{(1-\epsilon)^2} \right)$

S.No.	ϵ	ϵ_0 = 10^{-6}	5×10^{-6}	10^{-5}	5×10^{-5}	10^{-4}	5×10^{-4}	10^{-3}	5×10^{-3}	10^{-2}	5×10^{-2}
1	0.10	-.1520E+00	-.1790E+00	-.1930E+00	-.2250E+00	-.2400E+00	-.2790E+00	-.2950E+00	-.3210E+00	-.3190E+00	-.2210E+00
2	0.20	-.1090E-01	-.3220E-01	-.3060E-01	-.6370E-01	-.7700E-01	-.1270E+00	-.1470E+00	-.2000E+00	-.2300E+00	-.1970E+00
3	0.40	-.7510E-02	-.1430E-01	-.1600E-01	-.5530E-01	-.6430E-01	-.0530E-01	-.1060E+00	-.1710E+00	-.1970E+00	-.1860E+00
4	0.50	-.2090E-02	-.6110E-02	-.9280E-02	-.3020E-01	-.2790E-01	-.5790E-01	-.7560E-01	-.1430E+00	-.1750E+00	-.1750E+00
5	0.70	-.5650E-03	-.1660E-02	-.3630E-02	-.7470E-02	-.1150E-01	-.3000E-01	-.4450E-01	-.9030E-01	-.1200E+00	-.1570E+00
6	0.80	-.2000E-03	-.0250E-03	-.1530E-02	-.4430E-02	-.7700E-02	-.2250E-01	-.5460E-01	-.0900E-01	-.1170E+00	-.1400E+00
7	0.90	-.1100E-03	-.6460E-03	-.7000E-03	-.2770E-02	-.4710E-02	-.1520E-01	-.2450E-01	-.6560E-01	-.0360E-01	-.1360E+00
8	1.00	-.9360E-04	-.3630E-03	-.6450E-03	-.2360E-03	-.4060E-02	-.1350E-01	-.2210E-01	-.6170E-01	-.0000E-01	-.1340E+00
9	1.05	-.7500E-04	-.3020E-03	-.5410E-03	-.2030E-02	-.3540E-02	-.1210E-01	-.2000E-01	-.5700E-01	-.0310E-01	-.1310E+00
10	1.20	-.6550E-04	-.1900E-03	-.3400E-03	-.1300E-02	-.2060E-02	-.0900E-02	-.1520E-01	-.4670E-01	-.7950E-01	1230E-00
11	1.50	-.2360E-04	-.1220E-03	-.1900E-03	-.7910E-03	-.1440E-02	-.5410E-02	-.9030E-02	-.3370E-01	-.5360E-01	-.1060E+00
12	2.00	-.1700E-04	-.5600E-04	-.1050E-03	-.4450E-03	-.0310E-03	-.3300E-02	-.5900E-02	-.2130E-01	-.1550E-01	-.0400E-01
13	2.50	-.0770E-05	-.3050E-04	-.7230E-04	-.3000E-03	-.5700E-03	-.3310E-02	-.4160E-02	-.1540E-01	-.3610E-01	-.0070E-01
14	3.00	-.6440E-05	-.2930E-04	-.5510E-04	-.2350E-03	-.4360E-03	-.1700E-02	-.3200E-02	-.1290E-01	-.3060E 01	-.5050E-01
15	3.50	-.5370E-05	-.2360E-04	-.4450E-04	-.1900E-03	-.3520E-03	-.1441E-02	-.3600E-02	-.9000E-02	-.1600E-01	-.5000E-01
16	4.00	-.4490E-05	-.1960E-04	-.3730E-04	-.1600E-03	-.2960E-03	-.1210E-02	-.2190E-02	-.8270E-02	-.1420E-01	-.4340E-01
17	5.00	-.3300E-05	-.1490E-04	-.2920E-04	-.1210E-03	-.2340E-03	-.0190E-03	-.1660E-02	-.6310E-02	-.1090E-01	-.3410E-01
18	6.00	-.2720E-05	-.1300E-04	-.2360E-04	-.0900E-04	-.1800E-03	-.7400E-03	-.1340E-02	-.5130E-02	-.0810E-01	-.2790E-01

TABLE 10-4 VALUES OF $C_1 = \ln\left[\frac{1}{.15}\left(\frac{\delta_{L0}}{\delta_{L0}}\right)^{\frac{1}{\alpha}}\right]$

S.No.	A_0	δ_{L0}									
		10^{-6}	5×10^{-5}	10^{-5}	5×10^{-5}	10^{-4}	5×10^{-4}	10^{-3}	5×10^{-3}	10^{-2}	5×10^{-2}
1	1.00	.1732+02	.1572+02	.1502+02	.1340+02	.1270+02	.1110+02	.1040+02	.8812+01	.8112+01	.6532+01
2	1.20	.1440+02	.1342+02	.1302+02	.1150+02	.1090+02	.9670+01	.9080+01	.7630+01	.7060+01	.5742+01
3	1.40	.1300+02	1163+02	.1120+02	.1010+02	.9630+01	.8480+01	.7900+01	.6630+01	.6342+01	.5190+01
4	1.60	1220+02	1110+02	.1060+02	.9570+01	.9110+01	.8040+01	.7500+01	.6500+01	.6041+01	.4977+01
5	1.80	.1152+02	.1052+02	1010+02	.9090+01	.8660+01	.7650+01	.7220+01	.6210+01	.5790+01	.4784+01
6	2.00	1092+02	9971+01	9590+01	.8700+01	.7940+01	.7010+01	.6630+01	.5742+01	.5350+01	.4462+01
7	2.20	.9812+01	.8912+01	8460+01	.7650+01	.7310+01	.6500+01	.6160+01	.5350+01	.5000+01	.4302+01
8	2.40	.8910+01	.8180+01	.7860+01	.7130+01	.6830+01	.6080+01	.5770+01	.5040+01	.4770+01	.3990+01
9	2.60	.8330+01	7650+01	.7370+01	.6690+01	.6410+01	.5740+01	.5450+01	.4780+01	.4500+01	.3825+01
10	2.80	.8070+01	.7470+01	7150+01	.6500+01	.6230+01	.5580+01	.5300+01	.4660+01	.4300+01	.3742+01
11	3.00	.7630+01	7110+01	.6900+01	6330+01	.6060+01	.5440+01	.5170+01	.4550+01	.4290+01	.3672+01
12	3.20	.7410+01	6830+01	.6500+01	.6010+01	.5760+01	.5190+01	.4900+01	.4360+01	.4130+01	.3540+01
13	3.40	.7042+01	6500+01	6270+01	.5730+01	.5500+01	.4970+01	.4720+01	.4300+01	.3970+01	.3410+01
14	3.60	.6730+01	6310+01	6090+01	.5500+01	.5300+01	.4700+01	.4560+01	.4060+01	.3800+01	.3300+01
15	3.80	.6300+01	.5600+01	.5610+01	.5190+01	.4900+01	.4530+01	.4330+01	.3970+01	.3670+01	.3210+01
16	4.00	.5960+01	.5530+01	.5350+01	.4930+01	.4740+01	.4330+01	.4140+01	.3730+01	.3530+01	.3110+01
17	4.20	.5750+01	.5350+01	.5170+01	.4780+01	.4600+01	.4200+01	.4030+01	.3630+01	.3450+01	.3060+01
18	4.40	.5530+01	.4970+01	.4810+01	.4460+01	.4300+01	.3940+01	.3790+01	.3430+01	.3280+01	.2920+01
19	4.60	.4900+01	.4660+01	.4530+01	.4300+01	.4060+01	.3740+01	.3600+01	.3300+01	.3160+01	.2830+01
20	4.80	.4700+01	.4410+01	.4280+01	.3990+01	.3850+01	.3570+01	.3450+01	.3150+01	.3030+01	.2730+01
21	5.00	.4470+01	.4300+01	.4000+01	.3820+01	.3700+01	.3430+01	.3320+01	.3050+01	.2930+01	.2660+01
22	5.00	.4100+01	.3870+01	.3770+01	.3540+01	.3440+01	.3210+01	.3110+01	2900+01	.2790+01	.2560+01

TABLE 10-5 VALUES OF $\theta = \left(\frac{\delta_0}{.15}\right)^{\alpha}$

S.No	α	δ_0									
		10^{-6}	5×10^{-6}	10^{-5}	5×10^{-5}	10^{-4}	5×10^{-4}	10^{-3}	5×10^{-3}	10^{-2}	5×10^{-2}
1	0.10	.2510+00	.3000+00	.3210+00	.3700+00	.4050+00	.4750+00	.5000+00	.5900+00	.6410+00	.7530+00
2	0.20	.1660+01	.2720+01	.3130+01	.5300+01	.6620+01	.1970+00	.1320+00	.2140+00	.3040+00	.4270+00
3	0.40	.4250+02	.8000+02	1270+01	2930+01	.7400+01	.5100+01	.6730+01	.1200+00	.1690+00	.3270+00
4	0.50	.1000+03	.2430+03	5430+03	.7670+03	.1300+01	.3430+01	.5430+01	.7670+01	.1300+00	.3430+00
5	0.70	.7070+04	.3160+03	5540+03	.1000+02	.1700+02	5400+02	.8000+02	.2750+01	6440+01	1300+00
6	0.80	.1000+04	.6310+04	1140+03	.6130+03	.7190+03	.3000+02	.6530+02	.1640+01	2040+01	1040+00
7	0.95	.3330+05	.1070+04	.2000+04	.9770+04	.1640+03	.8530+03	.1650+02	.7600+02	1470+01	6700+01
8	1.00	.1100+05	5000+05	.1100+04	5400+04	.1100+03	.5000+03	.1100+02	.5000+02	.1100+01	5000+01
9	1.05	.3040+06	.1320+05	.6670+05	.3610+04	.7400+04	.4060+03	.8000+03	.4550+02	.9470+02	5110+01
10	1.30	.7070+07	.5790+06	.1220+05	.8300+05	.1930+04	.1330+03	.3040+03	.2110+02	4840+02	3340+01
11	1.50	.1300+08	.1430+07	.4040+07	.4510+06	.1300+06	.1430+04	.4040+04	.4120+03	1790+02	1430+01
12	2.00	*	.3460+10	.1300+09	.3460+08	.1300+07	.3460+06	.1300+05	.3460+04	.1300+03	3460+02
13	2.50	*	*	*	.3460+10	.1300+09	.8300+08	.4730+07	.3630+05	1500+04	.8300+03
14	3.00	*	*	*	*	*	.3040+09	.1630+08	.7940+06	.1630+05	.3040+03
15	3.50	*	*	*	*	*	*	.5500+13	1560+07	1770+06	6940+04
16	4.00	*	*	*	*	*	*	*	1300+06	.1930+07	.1300+04
17	5.00	*	*	*	*	*	*	*	*	.2750+09	.7040+06
18	6.00	*	*	*	*	*	*	*	*	*	.6140+07

Note: * Value less than 10^{-10}

TABLE 10-6 VALUES OF $b_1 = \eta_a \ln\left(\frac{33.35\eta_a}{\eta_{ks}}\right)$

S.No.	η_{ks}	η_a 10^{-6}	5×10^{-6}	10^{-5}	5×10^{-5}	10^{-4}	5×10^{-4}	10^{-3}	5×10^{-3}	10^{-2}	5×10^{-2}
1	10^{-6}	.351E-05	.256E-04	.581E-04	.371E-03	.811E-03	.486E-03	.104E-01	.601E-01	.127E+00	.716E+00
2	5×10^{-6}	.190E-05	.175E-04	.420E-04	.290E-03	.650E-03	.406E-02	.881E-02	.521E-02	.111E-01	.636E+00
3	10^{-5}	.120E-05	.141E-04	.351E-04	.256E-03	.581E-03	.371E-02	.811E-02	.486E-01	.104E+00	.601E+00
4	5×10^{-5}		.602E-05	.190E-04	.175E-03	.420E-03	.290E-02	.650E-02	.406E-01	.881E-01	.521E+00
5	10^{-4}		.256E-05	.120E-04	.141E-03	.351E-03	.256E-02	.581E-02	.371E-01	.811E-01	.486E+00
6	5×10^{-4}				.602E-04	.190E-03	.175E-02	.420E-02	.290E-01	.650E-01	.406E+00
7	10^{-3}				.256E-04	.120E-03	.141E-02	.351E-02	.256E-01	.581E-01	.371E+00
8	5×10^{-3}						.602E-03	.190E-02	.175E-01	.420E-01	.290E+00
9	10^{-2}						.256E-03	.120E-02	.141E-01	.351E-01	.256E+00
10	5×10^{-2}								.602E-02	.190E-01	.175E+00

TABLE 10-7 VALUES OF $I = \int_{.15} \left(\frac{1-\eta}{\eta}\right)^z d\eta$ AND $J = \int_{.15} \left(\frac{1-\eta}{\eta}\right)^z \ln[\eta] d\eta$

S.No.	z	I	J
1	.05	.8301E+00	-.5794E+00
2	.10	.8159E+00	-.5948E+00
3	.15	.8054E+00	-.6118E+00
4	.20	.7984E+00	-.6304E+00
5	.30	.7935E+00	-.6728E+00
6	.40	.7996E+00	-.7225E+00
7	.50	.8160E+00	-.7804E+00
8	.60	.8421E+00	-.8475E+00
9	.70	.8779E+00	-.9249E+00
10	.80	.9236E+00	-.1014E+01
11	1.00	.1047E+01	-.1234E+01
12	1.20	.1220E+01	-.1524E+01
13	1.40	.1454E+01	-.1905E+01
14	1.60	.1766E+01	-.2407E+01
15	1.80	.2178E+01	-.3070E+01
16	2.00	.2722E+01	-.3947E+01
17	2.50	.4979E+01	-.7618E+01
18	3.00	.9564E+01	-.1519E+02
19	3.50	.1902E+02	-.3103E+02
20	4.00	.3880E+02	-.6462E+02
21	5.00	.1706E+03	-.2923E+03
22	6.00	.7886E+03	-.1376E+04
23	7.00	.3770E+04	-.6665E+04
24	10.00	.4667E+06	-.8437E+06

TABLE 10-8 COMPUTATION OF TRANSPORT PARAMETER G FOR RIO GRANDE AT ALBUQUERQUE, N.M.

OBSERVATION DATED MARCH 26, 1954

Line No.	Quantity	Fraction No. 1	2	3	4	5
1.	Geometric Mean Size, D_i, $\times 10^3$ ft	1.78	1.22	0.948	0.744	0.554
2.	Fall Velocity w_i, ft/sec	0.206	0.147	0.112	0.082	0.052
3.	z_i	2.61	1.86	1.42	1.04	0.664
4.	Critical Shear $\tau_{ci} \times 10^2$ lb/ft^2	0.573	0.451	0.384	0.355	0.330
5.	$\frac{\tau_o - \tau_{ci}}{\tau_o}$	0.924	0.941	0.950	0.954	0.957
6.	$\eta_{si} \times 10^1$	3.24	2.22	1.72	1.35	1.01
7.	$A2_i \times 10^3$	2.0	2.4	3.3	6.0	14.0
8.	$A_i \times 10^3$	20.2	24.2	33.3	61.2	141.4
9.	$B_i \times 10^3$	-10.0	-10.15	-15.5	-25.5	-45.0
10.	$\frac{1}{\lambda_o}(A_i + B_i) \times 10^3$	3.37	4.64	5.89	11.80	31.80
11.	I_i	5.50	2.50	1.50	1.05	0.80
12.	J_i	-8.00	-3.80	-2.00	-1.30	-0.80
13.	$D_i \times 10^5$	0.00	1.2	14.0	120.0	1200.
14.	$C_i \times 10^5$	0.00	5.51	64.4	551.	5510.
15.	$(C_i I_i + D_i J_i) \times 10^5$	0.0	9.2	68.6	423.0	3450.
16.	$(\frac{1}{\lambda_o}(A_i + B_i) + C_i I_i + D_i J_i) \times 10^3$	3.37	4.73	6.58	16.03	66.30
17.	$(\frac{g_{si}}{2.5U_{*o}\, C_b}) \times 10^3$	3.42	4.90	6.88	16.83	69.74
18.	$\frac{d}{\lambda_o} \times b_{1i}$	4.00	2.40	1.63	1.20	0.84
19.	$(\frac{g_{bi}}{2.5U_{*o}\, C_b}) \times 10^3$	3.70	2.26	1.55	1.14	0.81
20.	$(\frac{g_{ti}}{2.5U_{*o}\, C_b}) \times 10^3$	7.12	7.16	8.43	17.97	70.55
21.	f_{gi}	6.4	6.5	7.6	16.1	63.4

22. $$G = \gamma_s\, S^{3/4} \left(\frac{w_{50}}{U_{*oo}}\right) \frac{2.5U_{*o}}{S} \sum_{i=1}^{5} \left(\frac{g_{ti}}{2.5U_{*o}\, C_b}\right)$$

$$= 2.65 \times 62.4 \times 0.156 \times 1.722 \times 0.099 \times 111.2 \times 10^{-3}$$

$$= 0.486 \text{ lbs per sec per ft.}$$

(Mrs.) Betty Hutcheson
Rt. 3 Box 691
Fort Collins, Colorado 80521